S-N/99205--058

STOLLER-NAVARRO

Unclassified Source Term and Radionuclide Data for Corrective Action Unit 98: Frenchman Flat Nevada Test Site, Nevada

Revision No.: 0

September 2005

Approved for public release; further dissemination unlimited.

Available for sale to the public from:

U.S. Department of Commerce
National Technical Information Service
5285 Port Royal Road
Springfield, VA 22161
Phone: 800.553.6847
Fax: 703.605.6900
Email: *orders@ntis.gov*
Online ordering: *http://www.ntis.gov/ordering.htm*

Available electronically at *http://www.osti.gov/bridge*

Available for a processing fee to U.S. Department of Energy and its contractors, in paper, from:

U.S. Department of Energy
Office of Scientific and Technical Information
P.O. Box 62
Oak Ridge, TN 37831-0062
Phone: 865.576.8401
Fax: 865.576.5728
Email: *reports@adonis.osti.gov*

S-N/99205--058

UNCLASSIFIED SOURCE TERM AND RADIONUCLIDE DATA FOR CORRECTIVE ACTION UNIT 98: FRENCHMAN FLAT, NEVADA TEST SITE, NEVADA

Revision No.: 0

September 2005

Stoller-Navarro Joint Venture
7710 W. Cheyenne, Bldg 3
Las Vegas, NV 89129

UNCLASSIFIED SOURCE TERM AND RADIONUCLIDE DATA FOR CORRECTIVE ACTION UNIT 98: FRENCHMAN FLAT, NEVADA TEST SITE, NEVADA

Approved by: Approved Signature Date: 9-14-05

John McCord, UGTA Project Manager
Stoller-Navarro Joint Venture

Table of Contents

Table of Contents *(Continued)*

Table of Contents *(Continued)*

List of Figures

List of Figures *(Continued)*

List of Figures *(Continued)*

List of Figures *(Continued)*

List of Tables

List of Acronyms and Abbreviations

Al	Aluminum
Am	Americium
Ar	Argon
Bq	Becquerel
BN	Bechtel Nevada
C	Carbon
°C	Degrees Celsius
Ca	Calcium
CADD	Corrective Action Decision Document
CAI	Corrective Action Investigation
Cal	Calorie
CAIP	Corrective Action Investigation Plan
CAP	Corrective Action Plan
CAS	Corrective Action Site
CAU	Corrective Action Unit
CAV	Cavity
Cd	Cadmium
Ce	Cerium
CHM	Chimney
Cl	Chlorine
Cm	Curium
Co	Cobalt
CR	Closure Report
Cs	Cesium
CT	Contaminant Transport
CZ	Compressed zone
DoD	U.S. Department of Defense
DOE	U.S. Department of Energy
DRI	Desert Research Institute
EPA	U.S. Environmental Protection Agency
Eu	Europium
EV	Exchange volume

FFACO	*Federal Facility Agreement and Consent Order*
ft	Foot (feet)
FY	Fiscal year
g	Gram
g/cm^3	Grams per cubic centimeter
Gd	Gadolinium
gpm	Gallons per minute
^3H	Tritium
HGU	Hydrogeologic unit
Ho	Holmium
HST	Hydrologic source term
HSU	Hydrostratigraphic Unit
I	Iodine
IT	IT Corporation
IAEA	International Atomic Energy Agency
K	Hydraulic conductivity
K	Potassium
K_d	Linear distribution (partitioning) coefficient
kcal	Kilocalorie
kg	Kilogram
Kr	Krypton
kt	Kiloton
LANL	Los Alamos National Laboratory
LLNL	Lawrence Livermore National Laboratory
LTCU	Lower Tuff Confining Unit
m	Meter
m^2	Square meters
m^2/g	Square meters per gram
m^3	Cubic meters
m/yr	Meters per year
MDA	Minimum detectable activity
MGZ	Melt glass zone
mg/L	Milligrams per liter

mL/g	Milliliters per gram
Mn	Manganese
mol	Mole
Mt	Megaton
MWAT	Multi-well aquifer test
Na	Sodium
Nb	Niobium
NDEP	Nevada Division of Environmental Protection
Ni	Nickel
NNSA/NSO	U.S. Department of Energy, National Nuclear Security Administration Nevada Site Office
Np	Neptunium
NTS	Nevada Test Site
NUFT	Nonisothermal Unsaturated-Saturated Flow and Transport
OAA	Older alluvial aquifer
pCi/L	Picocuries per liter
Pb	Lead
Pd	Palladium
psi	Pounds per square inch
Pu	Plutonium
R	Retardation Coefficients
Ra	Radium
Rb	Rubidium
R_c	Cavity Radius
RNM	Radionuclide migration
RREMP	Routine Radiological Environmental Monitoring Program
RST	Radiologic Source Term
Ru	Ruthenium
Sb	Antimony
SEM	Scanning electron microscope
Sm	Samarium
Sn	Tin
SNJV	Stoller-Navarro Joint Venture
Sr	Strontium

SSM	Simplified source term model
SST	Simplified source term
t_0	Time of nuclear test
Tc	Technetium
Th	Thorium
TM-LVTA	Timber Mountain-Lower Vitric Tuff Aquifer
TM-WTA	Timber Mountain-Welded Tuff Aquifer
TNT	Trinitrotoluene
TWG	Technical Working Group
U	Uranium
UGTA	Underground Test Area
USGS	U.S. Geological Survey
XRD	X-ray diffraction
Zr	Zirconium
1-D	One-dimensional
3-D	Three-dimensional
μm	Micrometer
δ	Delta

1.0 Introduction

Frenchman Flat is one of several areas of the Nevada Test Site (NTS) used for underground nuclear testing (Figure 1-1). These nuclear tests resulted in groundwater contamination in the vicinity of the underground test areas. As a result, the U.S. Department of Energy (DOE), National Nuclear Security Administration Nevada Site Office (NNSA/NSO) is currently conducting a corrective action investigation (CAI) of the Frenchman Flat underground test areas.

Since 1996, the Nevada Division of Environmental Protection (NDEP) has regulated NNSA/NSO corrective actions through the *Federal Facility Agreement and Consent Order* ([FFACO], 1996). Appendix VI of the FFACO agreement, "Corrective Action Strategy," was revised on December 7, 2000, and describes the processes that will be used to complete corrective actions, including those in the Underground Test Area (UGTA) Project. The individual locations covered by the agreement are known as corrective action sites (CASs), which are grouped into corrective action units (CAUs). The UGTA CASs are grouped geographically into five CAUs: Frenchman Flat, Central Pahute Mesa, Western Pahute Mesa, Yucca Flat/Climax Mine, and Rainier Mesa/Shoshone Mountain (Figure 1-1). These CAUs have distinctly different contaminant source, geologic, and hydrogeologic characteristics related to their location (FFACO, 1996). The Frenchman Flat CAU consists of 10 CASs located in the northern part of Area 5 and the southern part of Area 11 (Figure 1-1).

This report documents the evaluation of the information and data available on the unclassified source term and radionuclide contamination for Frenchman Flat, CAU 98. The methodology used to estimate hydrologic source terms (HSTs) for the Frenchman Flat CAU is also documented. The HST of an underground nuclear test is the portion of the total inventory of radionuclides that is released over time into the groundwater following the test. The total residual inventory of radionuclides associated with one or more tests is known as the radiologic source term (RST). The RST is comprised of radionuclides in water, glass, or other phases or mineralogic forms.

This evaluation was conducted in support of the development of a CAU contaminant transport model for the Frenchman Flat CAU.

1.1 Purpose and Scope

The purpose of this evaluation is to contribute to the analysis of available information regarding the unclassified HST and radionuclide data relevant to the

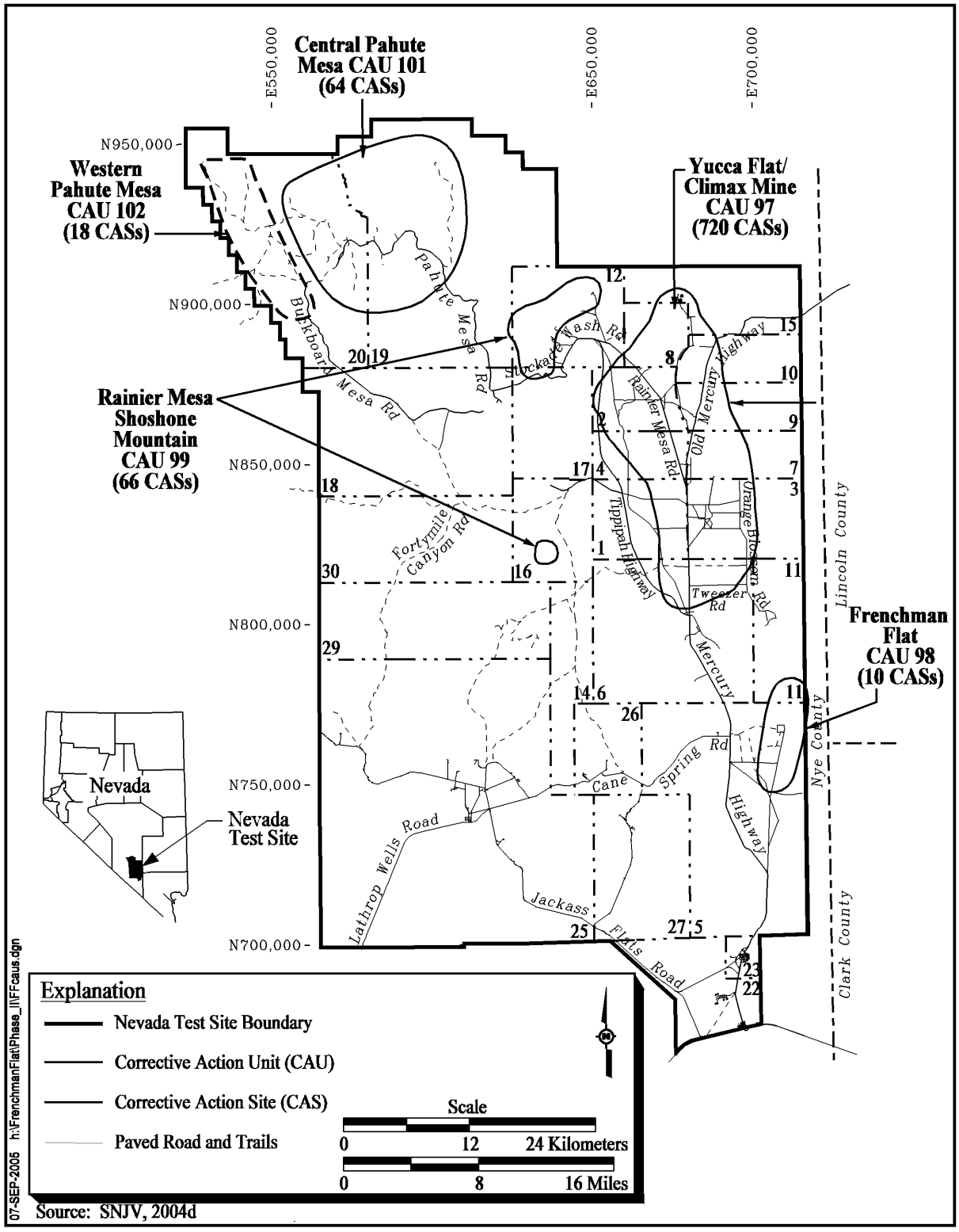

Figure 1-1
Location of the Frenchman Flat Corrective Action Unit

Frenchman Flat CAU. This work builds on the unclassified HST process models developed by Lawrence Livermore National Laboratory (LLNL). Specifically, the detailed HST process model currently being developed by LLNL for CAMBRIC (Tompson et al., 2005) is used to develop, calibrate, and test a simplified version of the HST model. Simplified source term models (SSMs) will then be used to estimate the HST for the other nine underground tests in Frenchman Flat for which HST process models do not exist. Neither sufficient data nor resources are available to support the development of HST process models for all tests within Frenchman Flat; thus, SSMs are required to estimate each HST for these tests.

Specific objectives include:

- Compiling and reviewing available information and data relating to the unclassified source term and radionuclide contamination within the Frenchman Flat CAU.
- Developing a simplification of the detailed HST process model developed by LLNL for the CAMBRIC test.
- Calibrating and testing the SSM to the LLNL CAMBRIC HST model.
- Developing SSMs for the nine other underground nuclear tests conducted in Frenchman Flat.

Data of interest include observed radionuclide activities at various wells in Frenchman Flat and vicinity. Other information of interest includes studies relating to the groundwater radionuclides migrating away from the nuclear test locations. The area of investigation, as described in DOE/NV (2001), was selected to encompass the Frenchman Flat CAU and immediately downgradient areas that may be impacted. The investigation area is in the southeastern portion of the NTS and extends from southern Yucca Flat to the southern NTS area including Mercury (Figure 1-2).

Information regarding the unclassified HST consists primarily of that obtained from the LLNL unclassified HST models (Tompson et al., 1999; Pawloski et al., 2001; and Tompson et al., 2005) and from activities performed in support of their development. These multi-dimensional process-level models simulate the thermal, hydrological, and chemical processes that govern the radionuclides in groundwater migrating away from underground test cavities through the immediate area around the test. An SSM is developed to capture the important processes and uncertainties of the HST in an efficient computational methodology. The SSMs are guided and calibrated by the results from the HST process models and can be used to estimate the HST associated with other tests for which process models do not exist.

The scope of this work includes the following: literature search, information and data compilation, data analysis including estimating the uncertainty associated with the available information, development and application of SSMs for all underground tests in the Frenchman Flat CAU.

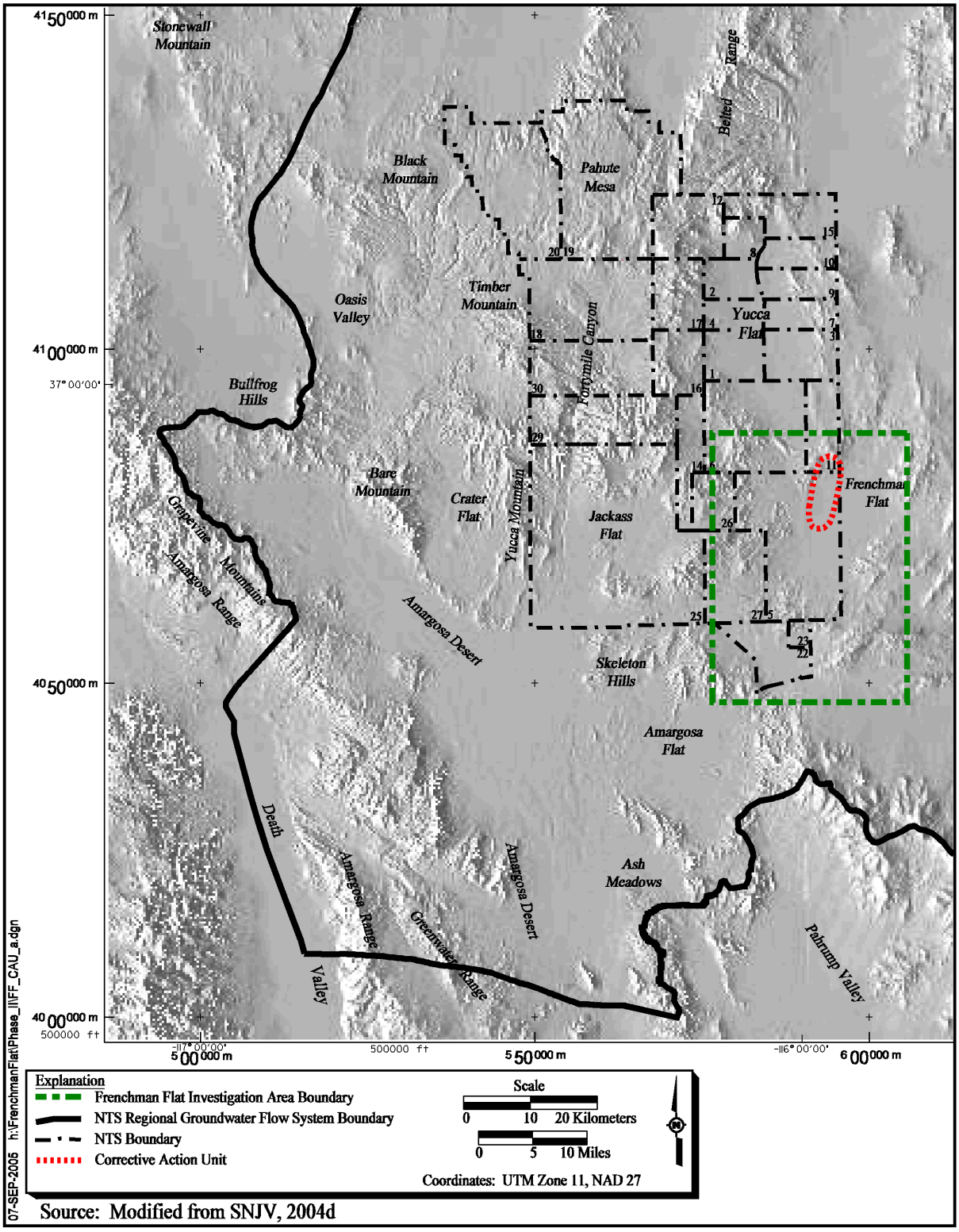

Figure 1-2
Investigation Area for the Frenchman Flat Corrective Action Unit

1.2 Project Background

Frenchman Flat is an area within the NTS that was used by the DOE and the U.S. Department of Defense (DoD) for underground nuclear testing over a seven year period (Figure 1-1). Underground nuclear testing on Frenchman Flat began with Operation Whetstone and ended with Operation Grommet (DOE/NV, 2000b). The first test in Frenchman Flat, WISHBONE, was conducted on February 18, 1965 and the final test, DIAGONAL LINE, was conducted on November 24, 1971 (DOE/NV, 2000b). Figure 1-3 shows the location of the nuclear tests conducted at Frenchman Flat. These tests were detonated in deep vertical shafts or drillholes in alluvial and volcanic rock. Table 1-1 presents information relative to the ten underground nuclear tests that were conducted in Frenchman Flat. Five tests were detonated in Area 5 as well as in Area 11 of the NTS. All underground nuclear tests conducted in Frenchman Flat, except two, (CAMBRIC-750 tons; DERRINGER-7.8 kilotons [kt]) have unclassified yields specified as "less than 20 kt" (DOE/NV, 2000b, Bowen et al., 2001).

Transport in groundwater is the primary mechanism for the subsurface contamination migrating away from the Frenchman Flat underground nuclear tests. All tests on Frenchman Flat were conducted within 100 meters (m) of the water table and will be modeled as saturated source areas, which is considered a conservative assumption. Detonations within a distance of 100 m above the water table are assumed to have impacted the water table (DOE/NV, 1997b).

To address the issue of this groundwater contamination and ensure the protection of the public and the environment, the DOE NNSA/NSO implemented a CAI of Frenchman Flat. In addition, the NNSA/NSO has established a long-term program, the Routine Radiological Environmental Monitoring Program (RREMP), to monitor groundwater for the presence of radionuclides (BN, 2003).

For the UGTA Project, the corrective action strategy includes two major phases: a regional evaluation addressing all CAUs and a CAI process for each of the individual CAUs. The first major phase was completed with the development of the *Regional Groundwater Flow and Tritium Transport Modeling and Risk Assessment of the Underground Test Area, Nevada Test Site, Nevada* (DOE/NV, 1997a). The flow and transport model (DOE/NV, 1997a) provided the initial basis for determining the magnitude of risk from the source areas on the NTS to potential receptors and a regional context for future individual CAU investigations. The second phase of the CAI process focuses on refining the results of the regional-scale modeling, through acquisition and analysis of CAU-specific data, and development of CAU-scale flow and transport models. The CAU-specific objectives are to estimate movement of contaminants utilizing CAU-specific hydrogeologic and transport parameter data and to define boundaries that encompass the extent of contamination.

Figure 1-4 shows the process flow diagram for implementing the corrective action strategy for the individual UGTA CAUs. The CAU-specific corrective action process includes six major elements: Corrective Action Investigation Plan (CAIP),

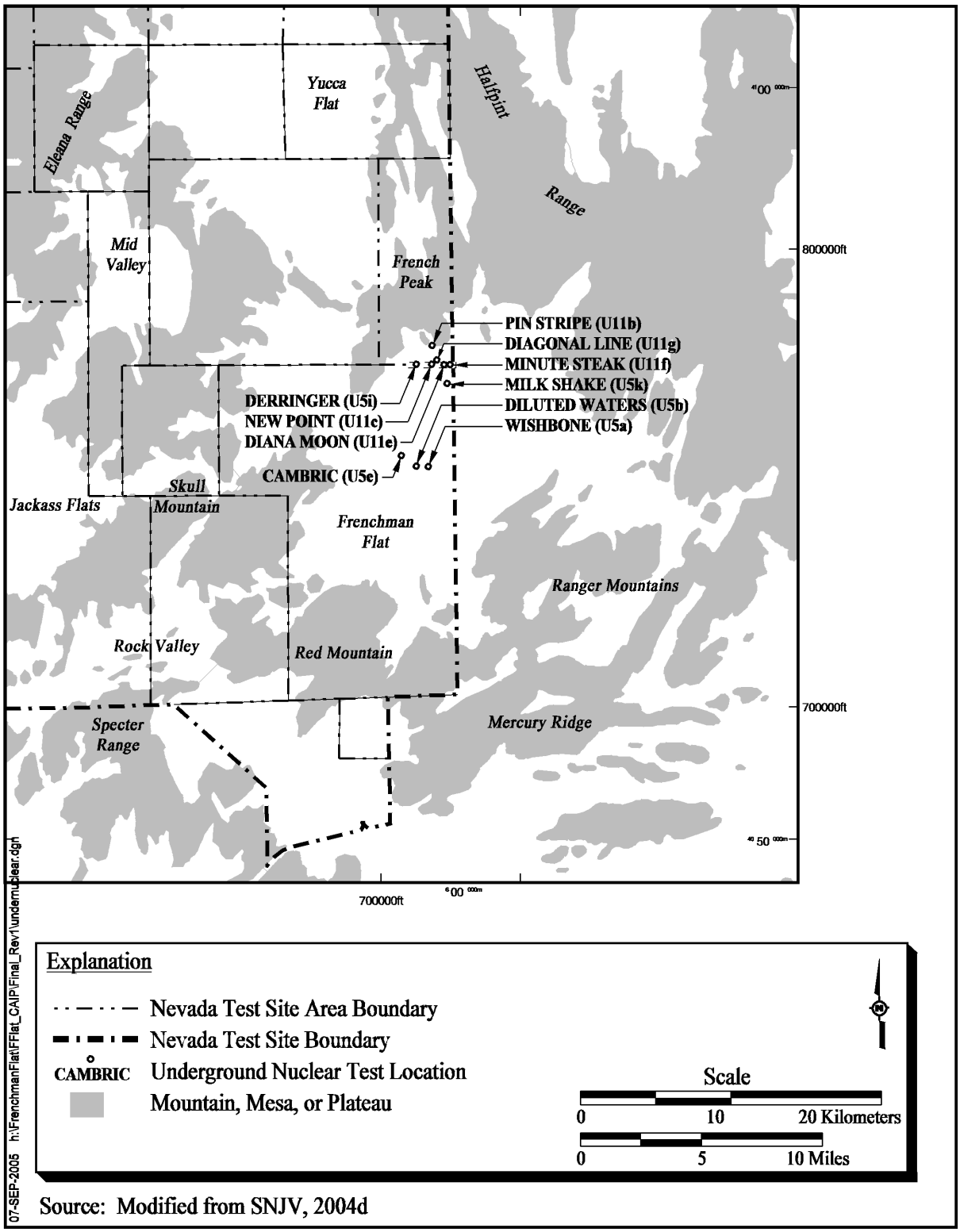

Figure 1-3
Location of Underground Nuclear Tests in Frenchman Flat

Table 1-1
Corrective Action Sites in the Frenchman Flat Corrective Action Unit

Test Name	Hole Name	CAS Number	Test Date	UTM Zone 11, NAD 27 (m)	Yield Range (kt)	Surface Elevation (m amsl)	Bottom of Hole Elevation (m amsl)	Working Point Depth (m)	Working Point HSU	Working Point HGU
CAMBRIC	U5e	05-57-003	05/14/1965	E 592142.7 N 4075575.4	0.75	956	651	295	AA	AA
DERRINGER	U5i	05-57-004	09/12/1966	E 593518.3 N 4081415.4	7.8	1,040	392	255	OAA	AA
DIAGONAL LINE	U11g	11-57-005	11/24/1971	E 594939.1 N 4081801.6	<20	1,038	761	264	OAA	AA
DIANA MOON	U11e	11-57-003	08/27/1968	E 595265.3 N 4081581.8	<20	1,032	777	242	OAA	AA
DILUTED WATERS	U5b	05-57-002	06/16/1965	E 593110.1 N 4074994.0	<20	943	737	193	AA	AA
MILK SHAKE	U5k	05-57-005	03/25/1968	E 595267.2 N 4080972.3	<20	1,021	745	265	OAA	AA
MINUTE STEAK	U11f	11-57-004	09/12/1969	E 595494.8 N 4081584.4	<20	1,034	757	265	OAA	AA
NEW POINT	U11c	11-57-002	12/13/1966	E 594655.9 N 4081579.7	<20	1,030	775	239	OAA	AA
PIN STRIPE	U11b	11-57-001	04/25/1966	E 594386.2 N 4082708.0	<20	1,093	794	296	TM-LTVA	VTA
WISHBONE	U5a	05-57-001	02/18/1965	E 593719.6 N 4074996.1	<20	941	750	175	AA	AA

Sources: BN (2004a); DOE/NV (2000a); DOE/NV (1997b); FFACO (1996)

AA = Alluvial aquifer
amsl = Above mean sea level
HGU = Hydrogeologic unit
HSU = Hydrostratigraphic unit
kt - Kiloton
m = Meters
OAA = Older Alluvial Aquifer
TM-LVTA = Timber Mountain Lower Vitric Tuff Aquifer
VTA = Vitric Tuff Aquifer

CAI, Corrective Action Decision Document (CADD), Corrective Action Plan (CAP), Closure Report (CR), and long-term monitoring.

- The CAI planning is documented in the CAIP, an FFACO-required document that provides or references all specific information for planning investigation activities associated with CAUs or CASs.

- The CAI includes the collection of new data, evaluation of new and existing data, and development and use of CAU-specific groundwater flow and transport model(s).

- The CADD is a required report that documents the CAI. It describes the results of the CAI, corrective action alternatives considered, results of their comparative evaluation, selected corrective actions, and rationale for its selection.

- The CAP is prepared to describe how the selected remedial alternative is to be implemented. The CAP will contain the engineering design and all specifications that are necessary to implement the selected remedial alternative.

- The UGTA strategy has provisions for CAU closure only if the long-term-monitoring alternative is selected. Closure activities include the preparation of a CR, review of the CR by NDEP, and long-term closure monitoring by DOE. The long-term, post-closure monitoring is designed to ensure the compliance boundary is not violated.

The CAI process may be iterative, resulting in several phases of data collection, analysis, and modeling, with assessment of confidence in the results at the completion of each phase. If further data collection, analysis, and modeling are required, a CAIP addendum will be issued to direct the new phase of activities.

The CAI for Frenchman Flat including hydrologic and transport data compilation, analysis, and model development was completed in 1999. Following the completion and documentation of the work, comprehensive internal and external peer reviews were conducted. Based on the outcome from the external and internal peer reviews, the need for additional work scope (including new data collection and modeling activities) was identified and an addendum to the Frenchman Flat CAIP was developed. This addendum, *Addendum to Revision 1 of the Corrective Action Investigation Plan for Corrective Action Unit 98: Frenchman Flat, Nevada Test Site, Nevada* (DOE/NV, 2001), details the new data collection and modeling activities to address the documented deficiencies in the Frenchman Flat CAI. The new data collection activities identified in the addendum (DOE/NV, 2001) have now been completed.

1.3 Corrective Action Investigation Documentation

The Frenchman Flat CAI activities are documented in various reports describing the results of the characterization activities and a series of reports describing the

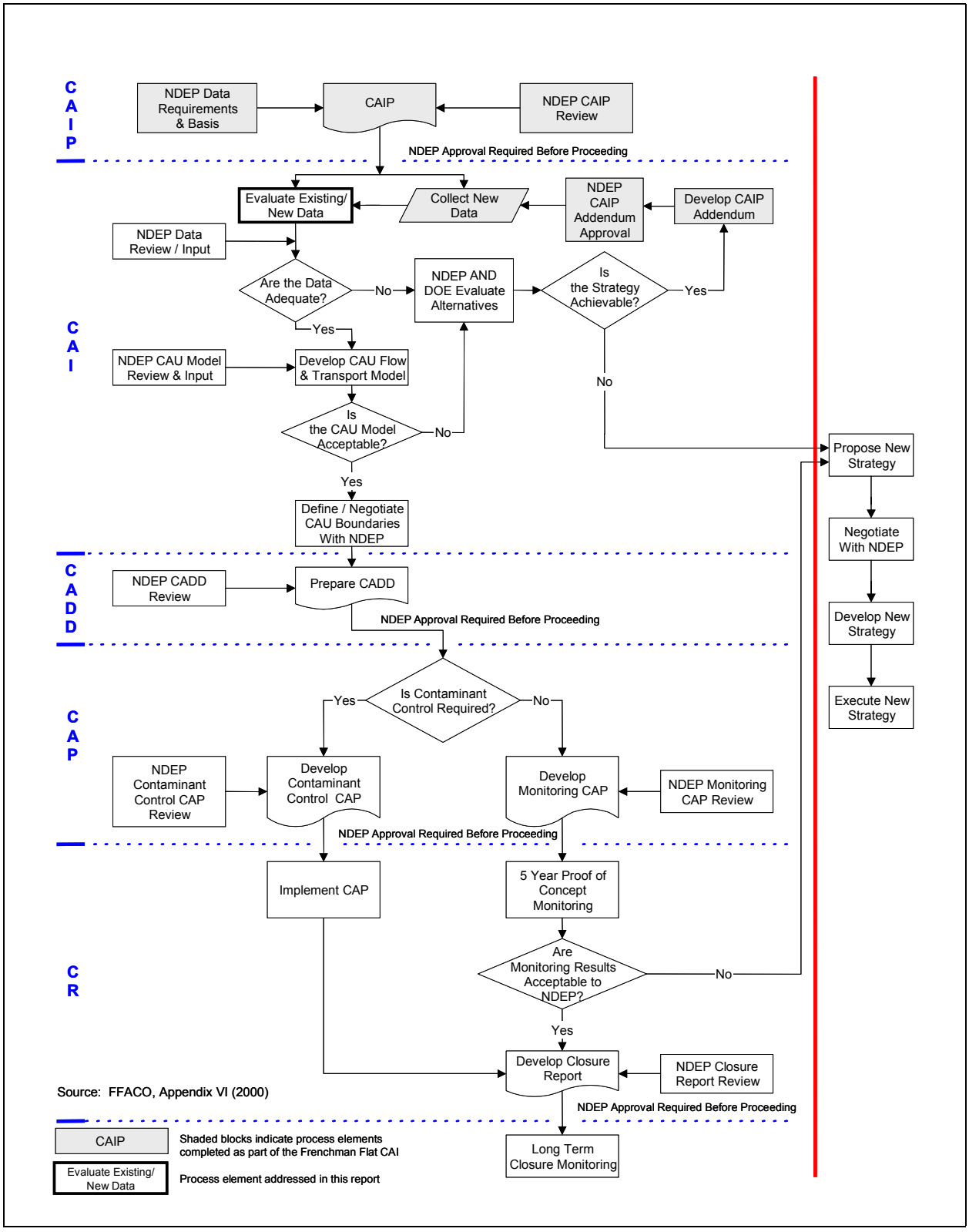

Figure 1-4
Process Flow Diagram for the Underground Test Area Corrective Action Units

CAU model, associated data, and results. The CAU model documentation for activities consists of the following reports:

- *Corrective Action Investigation Plan for Corrective Action Unit 98: Frenchman Flat, Nevada Test Site, Nevada* (DOE/NV, 1999).

- *Underground Test Area Subproject Corrective Action Unit 98: Frenchman Flat Data Analysis Task, Volume I - Hydrostratigraphic Model Documentation Package* (IT, 1998). This volume documents the development of the three-dimensional (3-D) hydrostratigraphic framework model for the Frenchman Flat CAU.

- *Underground Test Area Project Corrective Action Unit 98: Frenchman Flat, Volume II - Groundwater Data Documentation Package* (IT, 1999b). This volume presents the groundwater data incorporated into the groundwater flow and contaminant transport model for the Frenchman Flat CAU.

- *Underground Test Area Project Corrective Action Unit 98: Frenchman Flat Data Analysis Task, Volume III - Groundwater Flow and Contaminant Transport Model Documentation Package* (IT, 1999c). This volume presents the groundwater flow and transport model for the Frenchman Flat CAU.

- *External Peer Review Group Report on Frenchman Flat Data Analysis and Modeling Task, Underground Test Area Project, Revision No. 0* (IT, 1999a). This document identifies deficiencies in the CAI. Specific recommendations related to data sufficiency and uncertainty analysis are addressed.

- *Lessons Learned from the Frenchman Flat Corrective Action Groundwater Flow and Radionuclide Transport Model* (IT, 2000a). This document identifies lessons learned during the CAI. Specific recommendations related to data sufficiency and uncertainty analysis are addressed.

After the CAI was completed and evaluated, the decision was made to undertake a second phase of CAI activities to address deficiencies in data, modeling, and documentation. This second phase of CAI activities is currently underway. The primary CAU model documentation for activities that have been completed to date consists of the following reports:

- *Addendum to Revision 1 of the Corrective Action Investigation Plan for Corrective Action Unit 98: Frenchman Flat, Nevada Test Site, Nevada* (DOE/NV, 2001)

- A report describing the assessment of geologic data and the resulting hydrostratigraphic model titled *A Hydrostratigraphic Model for the Groundwater Flow and Contaminant Transport Model of Corrective*

Action Unit 98: Frenchman Flat, Clark, Lincoln, and Nye Counties, Nevada (BN, 2004a).

- A report describing the analysis of hydrologic data in support of the CAU groundwater flow model titled *Phase II Hydrologic Data for the Groundwater Flow and Contaminant Transport Model of Corrective Action Unit 98: Frenchman Flat, Nye County, Nevada* (SNJV, 2004d).

- A report describing the analysis of contaminant transport parameter data titled *Phase II Contaminant Transport Parameters Data for the Groundwater Flow and Contaminant Transport Model of Corrective Action Unit 98: Frenchman Flat, Nye County, Nevada* (SNJV, 2005).

Activities performed during the second phase of the CAI activities are summarized within these primary documents. Additional documents including this unclassified source term and radionuclide data report will be completed in preparation for the prediction of a contaminant boundary for the CAU. These include:

- A report describing the groundwater flow model developed for the Frenchman Flat area.

- A report describing the radionuclide transport model developed for the Frenchman Flat area.

- A report summarizing all data analysis and modeling activities. This report will include a summary of the information presented in the documents listed above.

1.4 Hydrologic Source Term Modeling and Radionuclide Data Documentation

Numerous analyses and reports were used to support the development of the SSMs. Some of the important sources of information regarding the CAMBRIC radionuclide migration (RNM) experiment, evaluations related to the CAMBRIC HST, and Frenchman Flat radionuclide data include the following:

- A report describing the updated CAMBRIC HST steady state model titled *Evaluation of the Non-Transient Hydrologic Source Term from the CAMBRIC Underground Nuclear Test in Frenchman Flat, Nevada Test Site* (Tompson et al., 2005). This document summarizes the development and preliminary results of the LLNL steady state HST model that provides the basis for the development of the SSMs.

- A report documenting an analysis of potential radionuclide transport pathways in groundwater beneath northern Frenchman Flat titled *Assessment of Radionuclide Migration from Underground Nuclear Tests in Northern Frenchman Flat, Nevada Test Site* (SNJV, 2004a).

- A report documenting the analysis of the hydraulic data collected for Wells ER-5-3, ER-5-3#2, and ER-5-3#3 titled *Interpretation of Hydraulic Test and Multiple-Well Aquifer Test Data at Frenchman Flat Well Cluster ER-5-3* (SNJV, 2004c).

- Two reports presenting analysis of the mineral abundance within the Frenchman Flat alluvium titled *Alluvial Layering and Distribution of Reactive Phases within Drill Holes ER-5-4 and UE-5n of Frenchman Flat* (Warren et al., 2002) and *Geostatistical Analysis of Spatial Variability of Mineral Abundance and K_d in Frenchman Flat, NTS, Alluvium* (Carle et al., 2002).

- A report presenting the analysis and interpretation of hydraulic data from the Well ER-5-4 single-well test, the Well ER-5-4 #2 single-well test, and the well cluster RNM-2S multiple-well aquifer test, which included the ER-5-4 wells and others titled *Integrated Analysis Report for Single- and Multiple-Well Aquifer Testing at Frenchman Flat Well Cluster RNM-2S* (SNJV, 2004b).

- A description of an approach for the development of an unclassified SSM for Frenchman Flat (Phase I) titled *Method for Calculating a Simplified Hydrologic Source Term for Frenchman Flat Sensitivity Studies of Radionuclide Transport Away from Underground Nuclear Tests* (Tompson et al., 2004).

- A description of the estimated radionuclide inventories for each UGTA CAU and the uncertainties associated with the inventories titled *Nevada Test Site Radionuclide Inventory, 1951 - 1992* (Bowen et al., 2001).

- A comprehensive description of the development of the initial unclassified HST for the CAMBRIC test titled *Evaluation of the Hydrologic Source Term from Underground Nuclear Tests in Frenchman Flat at the Nevada Test Site: The CAMBRIC Test* (Tompson et al., 1999).

- Reports providing an explanation of the experiments conducted at CAMBRIC, such as *Radioactivity in the Underground Environment of the Cambric Nuclear Explosion at the Nevada Test* (Hoffman et al., 1977) and *The Cambric Migration Experiment: A Summary Report* (Bryant, 1992).

- Annual progress reports by LLNL and LANL for the RNM and UGTA Projects. These reports provide information regarding transport of radionuclides specific to the CAMBRIC RNM experiment as well as radionuclide data and evaluations relevant to the Frenchman Flat investigation area. Information from numerous annual reports are included and referenced accordingly.

- Radiochemistry data provided by LLNL, LANL, Stoller-Navarro Joint Venture (SNJV), the Desert Research Institute (DRI), U.S. Geological Survey (USGS), IT Corporation, Shaw Environmental, and Bechtel Nevada (BN) are contained in the UGTA comprehensive water quality

database for groundwater in the vicinity of the NTS, *GEOCHEM*. A brief description of the *GEOCHEM* database is provided in Appendix C.

1.5 Document Organization

This document consists of seven sections and six appendices. Summaries of the section contents follow:

- Section 1.0 provides a description of the project background, the purpose and scope of this data analysis task, and this summary of the document.
- Section 2.0 provides a summary description of the modeling approach proposed for the Frenchman Flat CAU.
- Section 3.0 provides background information regarding the HST for Frenchman Flat including a description of the LLNL steady state HST model for CAMBRIC. This section also includes summary descriptions of the information available on radionuclide contamination sources and extent for the Frenchman Flat CAU. This includes radionuclide data, available to date, and a discussion on the nature and extent of radionuclide contamination originating from the Frenchman Flat CAU.
- Section 4.0 presents the approach used to simplify the CAMBRIC HST process model.
- Section 5.0 describes the process used to quantify the HST and associated uncertainties for the Frenchman Flat underground tests.
- Section 6.0 provides a summary and describes the limitations associated with the information presented in this document.
- Section 7.0 provides a list of references used in this document.
- Appendix A contains a description of the Frenchman Flat hydrostratigraphic unit model layers.
- Appendix B contains a description of the GoldSim® software package used to develop the simplified source term model.
- Appendix C contains a description of the *GEOCHEM* database that includes radionuclide data for the Frenchman Flat CAU.
- Appendix D provides comparisons of mass fluxes from the simplified source term model and the CAMBRIC process model.
- Appendix E provides the mass fluxes for a groundwater tracer, a melt glass tracer, and a sorbing radionuclide from SSMs for nine tests in Frenchman Flat.

- Appendix F provides electronic files that contain mass fluxes for thirty-six radionuclides generated from SSMs for nine tests in Frenchman Flat.

2.0 Corrective Action Unit Modeling Approach

This section presents an overview of the CAU modeling approach and data requirements. This information provides a basis for understanding the importance of the HST, the contamination data and various other groundwater flow and transport parameters, and their use in the CAU models.

2.1 Overview of CAU Modeling Approach

Underground nuclear testing at the NTS included a total of 908 detonations in shafts and tunnels with approximately one-third of these tests conducted near or below the water table (DOE/NV, 1997b). Groundwater flow through these sources occurs through diverse and structurally complex rocks (Laczniak et al., 1996). Given the complexity of the system, contamination sources, and processes controlling transport, numerical models are required to meet the objectives of the FFACO strategy. The modeling approach, therefore, utilizes an integrated 3-D model for flow and transport.

The CAU flow and transport model will include a saturated zone groundwater flow model, a radionuclide transport model, based upon the flow model, and a series of component sub-models or parameterizations built into the models that serve to define initial or boundary or auxiliary source conditions (HST models are such an example) or simplify smaller scale processes. The integrating numerical model will be a 3-D finite-element flow and transport simulator that captures the complex geologic structure including units of variable thickness, faults, and offsets, as well as complex transport processes associated with reactive solutes and fractured rock. The CAU groundwater flow model component requires two other component models: the NTS regional groundwater flow model and the recharge model. The CAU contaminant transport model component requires the HST models. Essential aspects of the processes described by the detailed models must be accurately represented in the CAU model. This representation must include the uncertainty associated with the process or parameters.

2.1.1 Data Requirements

The UGTA quality assurance requirements associated with data collection and analysis activities are described in DOE/NV (2000a). Data requirements for the CAU model fall into the following categories:

Groundwater Flow

Data types required for the groundwater flow model include permeability (or hydraulic conductivity), storage parameters, precipitation recharge, lateral boundary fluxes, hydraulic heads, and groundwater chemistry. These data types are the subject of the hydrologic data report for Frenchman Flat (SNJV, 2004d).

Transport Parameters

Major transport data types of interest include effective porosity, dispersivity, matrix porosity, matrix diffusion, sorption coefficients, and colloid-facilitated transport parameters. Note that sorption coefficients are a parameterization used to simplify more complicated ion exchange or surface complexation processes. For the purpose of modeling, effective porosity and matrix porosity are considered to be transport parameters rather than hydrologic parameters as they are required input variables in the contaminant transport model. Details of these parameters are the subject of SNJV (2005).

Contamination Sources and Extent

Contaminants are currently located in the 10 test locations and possibly downgradient areas. Information on the unclassified HST and the radionuclide data for Frenchman Flat is the subject of this report.

Hydrologic Source Term

The HST refers to the fraction of the total radionuclide inventory in the subsurface that is available for transport by groundwater, and consequently available for near- and far-field transport (Kersting, 1996). The HST consists of radionuclides that are present as dissolved, colloidal, coprecipitated, sorbed, glass-associated, or any other forms that are released into the groundwater following the test. The HST is estimated using a detailed HST model that describes processes that occur in the near-field environment of the underground nuclear test. The near-field environment generally encompasses a volume with a diameter of approximately four to eight times the radius of the test cavity (Tompson et al., 1999).

The focus of these models is on processes that occur well after the nuclear test, as opposed to the more dynamic processes that take place immediately after detonation (Tompson et al., 1999). These processes include decay and ingrowth of radionuclides; partitioning of the radionuclides between the melt glass, rubble, gas, and water fractions of the cavity/chimney region; release of radionuclides as a function of melt glass dissolution; and chemical reactions including aqueous complexation, surface complexation, ion exchange, precipitation, and dissolution.

Unclassified and classified estimates of the HST will be made for Frenchman Flat. The unclassified HST will be derived from the unclassified version of the total radionuclide inventory for Frenchman Flat (Bowen et al., 2001). Two unclassified HST models for CAMBRIC are being developed by LLNL: a transient and a steady-state. The transient HST model includes the impact of twenty years of pumping at RMN-2S (Tompson et al., 2005). CAMBRIC was selected for HST modeling since there is a relatively large amount of unclassified hydrologic and radionuclide inventory data available, both inside and outside of the test cavity. The HST model is then used for the development and testing of SSMs to estimate

the HST for other underground tests for which lesser amounts of data are available. The mass of radionuclides for the CAU transport model will be derived from the release functions calculated using the SSM. These will be in the form of mass flux versus time at the intersection of SSM and the CAU transport model. The unclassified HST model abstraction process and the mass flux versus time results for each of the Frenchman Flat tests are the subject of this document and are, therefore, described in detail in Section 3.0 through Section 5.0. Details describing the integration of the CAMBRIC HST model and the SSMs into the CAU contaminant transport model will be described in the corresponding Frenchman Flat contaminant transport modeling report.

The classified version of the HST will be based on classified information from individual tests and will be used to calculate the final location of the contaminant boundary.

Radionuclide Data

Measurements of radionuclide concentrations in groundwater samples are essential for evaluating the CAU-model predictions. These data may be used to constrain or calibrate transport models; thus, providing further confidence in the simulations. Evidence of radionuclide migration away from test locations, as observed during the CAMBRIC pumping test (Hoffman et al., 1977; Bryant, 1992), could be compared with simulated results of the CAU model. The direct measurement of radionuclide concentrations in cavity water samples is used to constrain and validate HST model predictions. Additionally, the time series of radionuclide concentrations from cavity samples may be of sufficient quality to compare with simulated concentration declines at the same locations. A summary of the available information relating to the extent of radionuclide contamination within Frenchman Flat, and radionuclide migration during the CAMBRIC pumping experiment, are presented in Section 3.0 of this report.

3.0 Review of Available Information

Modeling the release of radionuclides from the RST and their migration within the Frenchman Flat groundwater system requires an understanding of the sources of radionuclides and the processes involved in their near-field environment. Currently, available information on the sources of radionuclide contamination includes underground nuclear test data, the phenomenology of underground nuclear tests, the unclassified radionuclide inventory, and radionuclide distribution in the nuclear test cavities and vicinity.

To better understand and quantify the processes involved in the release and migration of radionuclides within the near-field, LLNL developed near-field HST models for Frenchman Flat and Pahute Mesa. Lawrence Livermore National Laboratory defines the near-field as the subsurface environment located within several cavity radii of the test. Specifically, these models include the Phase I CAMBRIC HST model (Tompson et al., 1999), the Phase I Frenchman Flat Simplified HST model (Tompson et al., 2004), and the CHESHIRE HST Model (Pawloski et al., 2001). In addition, LLNL is currently developing two Phase II HST models (transient and steady-state) for CAMBRIC (Tompson et al., 2005). The Phase II CAMBRIC HST analyses are available to help understand the processes involved to quantitatively forecast the HST within the near-field environment of the CAMBRIC test (Tompson et al., 2005). The steady-state CAMBRIC HST provides the basis for developing, calibrating, and testing the SSMs for the Frenchman Flat CAU. A description of this HST model is presented in this section. Available radionuclide data for the groundwaters of the Frenchman Flat CAU are also described in this section.

3.1 Underground Nuclear Test Data

A total of ten shaft nuclear tests were conducted in Frenchman Flat. Shaft nuclear devices were exploded in drilled or mined vertical holes. The locations of the underground nuclear tests are shown in Figure 1-3. The test name, emplacement hole name, CAS number, test coordinates, test date, yield range, land surface elevation, and working point information for each of the tests in Frenchman Flat are listed in Table 1-1. In addition, an illustration of the ten Frenchman Flat emplacement holes is provided in Figure 3-1. The estimated elevations of the working point, water table, and HSUs as well as the calculated cavity radius for each test is included in Figure 3-1. Further information regarding the calculation of the cavity radius is provided in Section 5.1.2.1.

The term "yield" refers to the total effective energy released in a nuclear explosion and is usually expressed in terms of the equivalent tonnage of trinitrotoluene

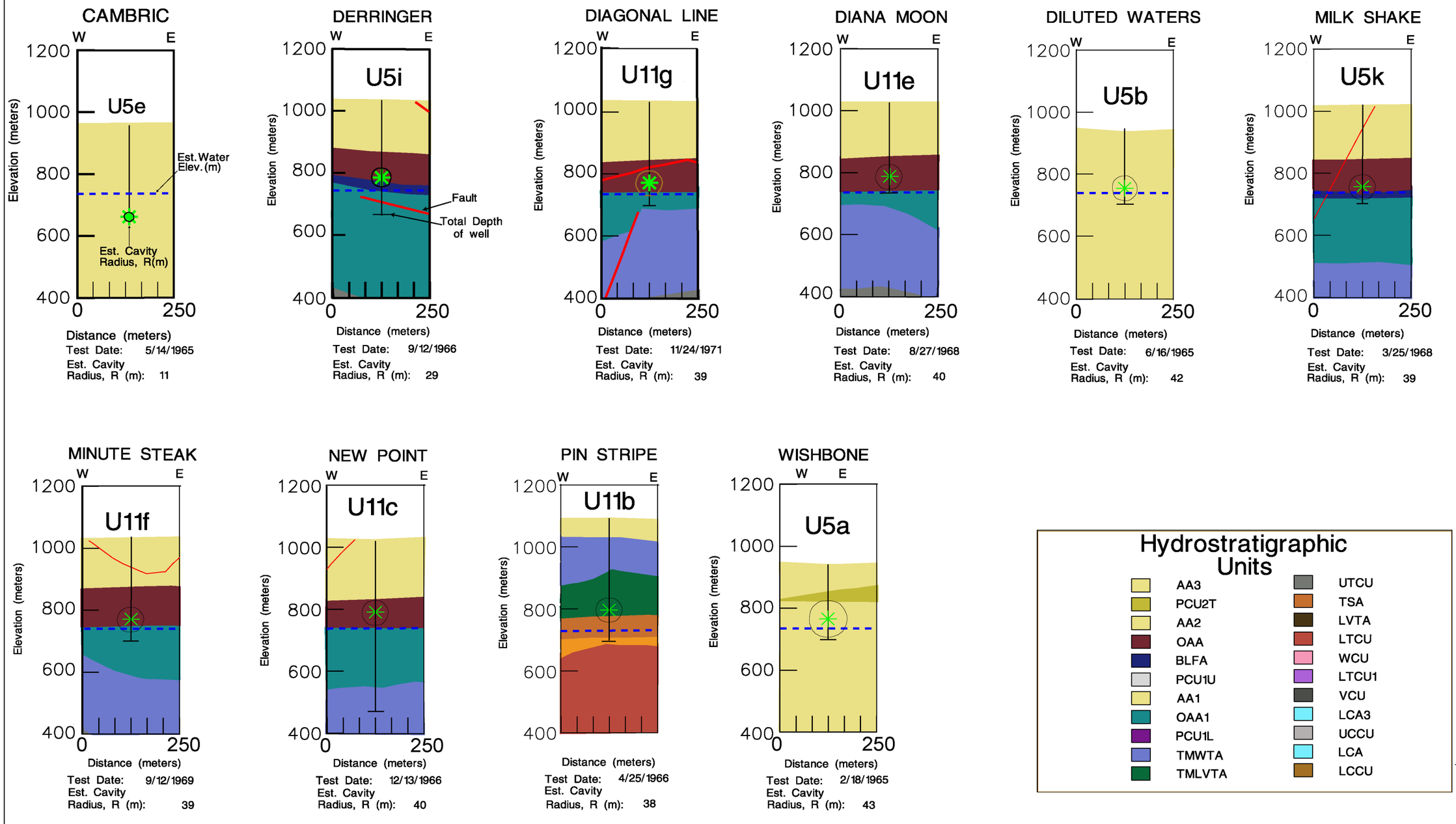

Figure 3-1
Hydrostrategraphic Cross Sections Showing Each Underground Nuclear Test Conducted in Frenchman Flat Area

(TNT) required to produce the same energy release in an explosion. A one kt yield represents the energy of a nuclear explosion that is equivalent to the explosive power of one thousand tons of TNT (DOE/NV, 2000b). An announced yield is available for two tests, CAMBRIC and DERRINGER (Table 1-1). Only the upper limit of the yield range is reported for eight of the ten tests (Table 1-1). The PIN STRIPE test was the only test detonated in a volcanic tuff formation; all of the other Frenchman Flat tests were detonated in alluvium (Table 1-1, Figure 3-1). CAMBRIC was conducted below the water table and the remaining nine tests were detonated from 15 to 62 m above the water table. Thus, all tests within Frenchman Flat were conducted within 100 m of the water table (Table 1-1, Figure 3-1). Detonations within a distance of 100 m above the water table are assumed to have impacted the water table (DOE/NV, 1997b).

3.2 Phenomenology of an Underground Nuclear Explosion

Phenomenology describes the effects of a nuclear explosion on the host media as a function of time. Phenomenological models describe the impact to the media resulting from the explosion. This section includes an overview of the phenomenology of an underground nuclear explosion followed by a description of the resulting distribution of materials introduced to the subsurface.

3.2.1 Phenomenology Overview

The testing of an underground nuclear explosion results in successive, physical phenomena that occur within measured time frames. The following describes the time frames and corresponding phenomena based on a report prepared by the U.S. Congress, Office of Technology Assessment (1989):

Within microseconds, billions of atoms release their energy. Temperatures increase as high as several hundred million degrees Celsius (°C) and pressures of several million pounds per square inch (psi) are created. This results in the creation of a powerful shock wave that spreads outward from the point of origin.

- Within tens of milliseconds, the shock wave expands and the surrounding rock is crushed, melted, and vaporized, creating an expanding cavity. It is estimated that the shock wave vaporizes approximately 70 metric tons and melts 700 metric tons of rock for each kt of explosive yield (Olson, 1967; Bowen et al., 2001).

- Within tenths of a second, the cavity reaches its fullest potential in terms of growth. The shock wave generated by the explosion fractures and crushes the rock as it extends outward from the cavity. The shock wave eventually loses its strength and momentum and becomes too weak to continue to crush rock. Thus, the crushed rock is characterized by a compression and relaxation phase that results in seismic waves.

- Within a few seconds, molten rock collects, solidifies, and forms at the bottom of the cavity. Cooling results in a decrease in the gas pressure of the cavity.

- Within minutes or up to days, cavity collapse occurs because of the decreased gas pressure, which causes the overlying rock that supports the cavity to weaken. A process referred to as "chimneying" is a result of rock debris and loose rubble falling into the cavity causing the void area to move upward. "Chimneying" is continuous until one of the following occurs to the void region: the void becomes completely filled with loose rubble, the shape of the void in conjunction with the stability of the rock can sustain the overburden material, or the chimney approaches ground surface.

Other phenomena related to underground nuclear testing may occur, including hydrofracturing, prompt injection of radionuclides, groundwater effects (e.g., mounding and pressurization), and movement of preexisting structural features (e.g., faults). These may affect cavity growth, residual stress, collapse, and crater formation.

3.2.2 Distribution of Materials Related to Testing

The nuclear explosion phenomena described above are responsible for the observed distribution of materials that were introduced into the subsurface during testing. Radioactive elements are not uniformly distributed in the cavity/chimney region but are partitioned based on their physical and chemical characteristics.

Smith (1993) indicates that the partitioning can be described in terms of a three- stage condensation process. The refractory radionuclides (e.g., actinides), whose melting points are significantly greater than the melting temperature of the adjacent geologic media, are scavenged by the molten material that lines the cavity. These radionuclides are deposited within the melt glass. Further condensation occurs as cavity gas moves into the crushed rubble and fractured material surrounding the working point. During this stage, the radioisotopes of intermediate volatility, often with gaseous precursors (e.g., cesium-137 [^{137}Cs]), condense and deposit on rubble and fracture surfaces. Final condensation occurs as residual gas ascends toward the ground surface. Condensation during this stage also occurs on surfaces. The above process leads to a distribution of radionuclides that is fractionated, with heavier refractory radionuclides concentrated within the melt glass and lighter and volatile radionuclides concentrated higher in the chimney (Smith, 1993). Tritium initially is distributed in the gas phase and later as molecular tritium oxide in steam (Smith, 1995a).

During tests conducted at or below the water table, groundwater is evacuated from the test cavity and then slowly seeps back into the cavity after the detonation (Borg et al., 1976). Where detonations are near or below the static water level, groundwater is possibly impacted due to the prompt injection of radionuclides into surrounding fractures or the leaching of radionuclides as water seeps back into the test cavity and rubble chimney.

The distribution of radionuclides in the cavity/chimney region greatly influences the availability of potential contaminants for transport by groundwater. Radionuclides incorporated in the melt glass matrix are accessible to groundwater only through slow processes such as melt glass dissolution. Other radionuclides are predominantly associated with surfaces and are accessible to groundwater through relatively fast processes such as ion exchange (Smith, 1995b).

3.3 Unclassified Radionuclide Inventory

A comprehensive unclassified inventory of the radionuclide source term for the NTS is found in the report, "Nevada Test Site Radionuclide Inventory, 1951-1992" (Bowen et al., 2001). This inventory provides an estimate of radioactivity remaining underground at the NTS after nuclear testing. The inventory was subdivided into five areas roughly corresponding to the UGTA CAUs. The inventory for Yucca Flat was further subdivided by tests based on the depth of the working point relative to that of the water table. The inventory for Pahute Mesa was subdivided by NTS area. The inventory includes tritium, fission products, unspent fuel materials, and activation products.

The total radionuclide inventory for Frenchman Flat (Areas 5 and 11) is provided in Table 3-1. This list includes 44 radiological contaminants that have half-lives greater than 10 years (with the exception of europium-154 [^{154}Eu]). Criteria for inclusion of radionuclides in the inventory are discussed in the Bowen et al. (2001) report. This inventory also includes naturally occurring radioactive isotopes (^{40}K, ^{232}Th, ^{234}U, ^{235}U, and ^{238}U) and represents the amount in the rock that was melted during the detonation (700 tons/kt yield). The source of ^{40}K is natural, whereas the others (^{232}Th, ^{234}U, ^{235}U, and ^{238}U) are naturally occurring as well as a device component (Bowen et. al., 2001). This inventory has been decay-corrected to September 23, 1992, the date of the last underground nuclear test. Table 3-2 lists the estimated accuracies of this inventory for various groups of radionuclides, as reported by Bowen et al. (2001). Further discussion of the reported accuracies is provided in Section 5.1.1.

The list of radionuclides provided in Table 3-1 is the preliminary list of potential contaminants for the Frenchman Flat CAU. This lists supersedes the list of potential contaminants presented in the Frenchman Flat CAIP (DOE/NV, 1999). Note that lead (^{205}Pb and ^{210}Pb) had previously been included in the list of potential contaminants for the CAU, because it is known to have been used in significant quantities in underground nuclear tests (DOE/NV, 1999). Lead has since been deleted from the list, because it has not been found in groundwater samples.

3.4 Radionuclide Distribution in the Subsurface

Information available on radionuclide distribution within the subsurface includes the observed radionuclide activities from analysis of groundwater samples and various reports containing evaluations of the sampling data. The groundwater sampling data and the findings of several reports that are pertinent to the HST are

Table 3-1
Total Radionuclide Inventory for Frenchman Flat of the Nevada Test Site

Radionuclide	Radionuclide Abbreviation	Atomic Weight (g/mol)	Curies[a]	Atoms[a]	Moles[b]	Mass[c] (g)
Tritium	^{3}H	3.0160	1.74E+05	3.62E+24	6.01E+00	1.81E+01
Carbon-14	^{14}C	14.0032	6.65E+01	6.41E+23	1.06E+00	1.49E+01
Aluminum-26	^{26}Al	25.9869	7.04E-03	8.41E+21	1.40E-02	3.63E-01
Chlorine-36	^{36}Cl	35.9683	8.91E+00	4.52E+24	7.50E+00	2.70E+02
Argon-39	^{39}Ar	38.9643	6.17E+00	2.79E+21	4.64E-03	1.81E-01
Potassium-40	^{40}K	39.9640	1.65E+00	3.53E+27	5.86E+03	2.34E+05
Calcium-41	^{41}Ca	40.9623	6.54E+01	1.14E+25	1.88E+01	7.72E+02
Nickel-59	^{59}Ni	58.9344	1.63E+00	2.09E+23	3.47E-01	2.05E+01
Nickel-63	^{63}Ni	62.9297	1.68E+02	2.83E+22	4.70E-02	2.96E+00
Krypton-85	^{85}Kr	84.9125	1.29E+02	2.33E+21	3.87E-03	3.29E-01
Strontium-90	^{90}Sr	89.9077	1.88E+03	9.11E+22	1.51E-01	1.36E+01
Zirconium-93	^{93}Zr	92.9065	1.12E-01	2.83E+23	4.69E-01	4.37E+01
Niobium-93	^{93m}Nb	92.9064	0.00E+00	0.00E+00	0.00E+00	0.00E+00
Niobium-94	^{94}Nb	93.9073	6.97E-01	2.35E+22	3.90E-02	3.66E+00
Technetium-99	^{99}Tc	98.9063	1.17E+00	4.19E+23	6.96E-01	6.88E+01
Palladium-107	^{107}Pd	106.9051	1.95E-02	2.14E+23	3.55E-01	3.80E+01
Cadmium-113	^{113m}Cd	112.9044	2.99E+00	7.10E+19	1.18E-04	1.33E-02
Tin-121	^{121m}Sn	120.9042	1.65E+01	1.53E+21	2.53E-03	3.07E-01
Tin-126	^{126}Sn	125.9077	8.19E-02	3.45E+22	5.73E-02	7.21E+00
Iodine-129	^{129}I	128.9050	4.54E-03	1.20E+23	1.99E-01	2.57E+01
Cesium-135	^{135}Cs	134.9060	1.36E-01	5.28E+23	8.76E-01	1.18E+02
Cesium-137	^{137}Cs	136.9071	5.04E+03	2.56E+23	4.24E-01	5.82E+01
Samarium-151	^{151}Sm	150.9199	2.95E+02	4.47E+22	7.42E-02	1.12E+01
Europium-150	^{150}Eu	149.9197	9.86E-03	5.98E+17	9.93E-07	1.49E-04
Europium-152	^{152}Eu	151.9217	7.57E+02	1.73E+22	2.87E-02	4.36E+00
Europium-154	^{154}Eu	153.9230	2.62E+02	3.80E+21	6.30E-03	9.70E-01
Holmium-166	^{166m}Ho	165.9323	2.02E+00	4.09E+21	6.80E-03	1.13E+00
Thorium-232	^{232}Th	232.0381	1.20E-01	2.82E+27	4.68E+03	1.09E+06
Uranium-232	^{232}U	232.0371	1.03E-02	1.21E+18	2.01E-06	4.66E-04
Uranium-233	^{233}U	233.0396	1.33E-03	3.58E+20	5.94E-04	1.39E-01
Uranium-234	^{234}U	234.0409	4.32E-01	1.79E+23	2.97E-01	6.96E+01
Uranium-235	^{235}U	235.0439	8.57E-03	1.02E+25	1.69E+01	3.98E+03
Uranium-236	^{236}U	236.0456	3.00E-03	1.18E+23	1.96E-01	4.63E+01
Uranium-238	^{238}U	238.0508	9.51E-02	7.16E+26	1.19E+03	2.83E+05
Neptunium-237	^{237}Np	237.0482	1.38E-02	4.97E+22	8.25E-02	1.96E+01
Plutonium-238	^{238}Pu	238.0496	3.23E+02	4.78E+22	7.93E-02	1.89E+01
Plutonium-239	^{239}Pu	239.0522	1.42E+03	5.74E+25	9.54E+01	2.28E+04
Plutonium-240	^{240}Pu	240.0538	3.49E+02	3.86E+24	6.40E+00	1.54E+03
Plutonium-241	^{241}Pu	241.0568	4.41E+03	1.07E+23	1.78E-01	4.28E+01
Plutonium-242	^{242}Pu	242.0587	2.88E-02	1.82E+22	3.02E-02	7.32E+00
Americium-241	^{241}Am	241.0568	5.02E+02	3.66E+23	6.08E-01	1.47E+02
Americium-243	^{243}Am	243.0614	0.00E+00	0.00E+00	0.00E+00	0.00E+00
Curium-244	^{244}Cm	244.0627	0.00E+00	0.00E+00	0.00E+00	0.00E+00
Total			1.90E+05	7.16E+27	1.19E+04	1.63E+06

[a]Total inventory in atoms and curies from Bowen et al. (2001)

[b]Total Inventory in moles calculated by dividing the total inventory in atoms by 6.022×10^{23} atoms/mole

[c]Total Inventory in grams calculated by multiplying the total inventory in moles by the atomic weight

Table 3-2
Estimated Accuracies for Various Groups of Radionuclides

Radionuclide Group	Accuracy
Fission Products	~10 to 30 percent
Unspent Fuel Materials	~ 20 percent or better
Fuel Activation Products	~ 50 percent or better
Residual Tritium	~ 300 percent or better
Activation Products	~ a factor of 10

Source: Bowen et al., 2001

discussed in this section. Reports containing results of evaluations of the radiochemistry of near-field water and groundwater samples are also summarized in this section.

3.4.1 Radiochemistry of Near-Field Water

Smith (2002) conducted an evaluation of the radiochemistry of near-field water samples at the NTS. Smith (2002) defined "near-field" as including "the area extending radially approximately 300 meters from surface ground zero (the firing point of an underground nuclear test projected upwards to the earth's surface)." The purpose of this evaluation was to summarize historical near-field data collection activities at the NTS, to describe the hydrogeologic and radiochemical environment of near-field sampling locations, to assemble a representative set of near-field radiochemical data, to review prior analyses of the data, and to assess the usability of the data in the development of a HST.

Of the sixteen near-field study sites where water has been produced, only five (ALMENDRO, CAMBRIC, CHANCELLOR, CHESHIRE, and DALHART) produce water from the cavity region. The evaluation performed by Smith (2002) focussed on three near-field sites (ALMENDRO, CAMBRIC, and CHESHIRE). The U-19ad PS1A post-shot hole was completed in the CHANCELLOR cavity in 2004 and thus preceded the evaluation. The results from the limited sampling events have provided valuable information. Conclusions of the evaluation performed by Smith (2002) are as follows:

- Widespread groundwater contamination from the underground nuclear tests is unlikely. Relative to the RST, only a small fraction of the actinides, fission products, and activation products are measured in near-field groundwaters.

- Soluble radionuclides – tritium, ^{14}C, ^{36}Cl, ^{85}Kr, ^{99}Tc, and ^{129}I are found as dissolved species and scale proportionately to the activities of tritium. Although found in cavity and chimney waters, radionuclides– ^{90}Sr, ^{137}Cs, ^{152}Eu, ^{154}Eu, and ^{239}Pu are not readily transported outside of the cavity or chimney to this immediate environment.

- Because of their lower hydraulic gradients, Frenchman Flat and Yucca Flat have a lower potential than Pahute Mesa for lateral migration of radionuclides in groundwater.

- Time-series analyses of radionuclide concentration data provide information on processes that control radionuclide migration in groundwater, which include dilution, dispersion, leaching, and precipitation.

- Plutonium and other relatively insoluble radionuclides may be transported at ambient groundwater velocities through sorption to clay and zeolite colloids suspended in fractured rock aquifers.

- Depending on the working point location in the rock, soluble species may ascend to more transmissive aquifers due to the residual heat from underground nuclear tests. Other tests remain isolated for decades after the detonation.

- Radionuclides may be mobilized by prompt processes along specific and narrow passages related to rock strength and geologic structure. Volatile radionuclides may migrate to shallower intervals of the nuclear chimney through gas phase transport (Smith, 2002).

Based on the findings of Smith (2002), analytical results from near-field water samples provide useful information for HST modeling. However, with the small number of sampling locations, translating the information to a larger area poses significant challenges.

3.4.2 Radionuclide Distribution Outside the Cavity Region

Nimz and Thompson (1992) present data and analyses to support the hypothesis of prompt fracture injection as a mechanism to transport radionuclides some distance away from an underground test cavity. On the basis of data from samples collected from several locations in Yucca Flat (i.e., U-3cn#5, UE-4g#2, U-9 ITS U-29, U-3kz, and UE-2ce), the transport of radionuclides over distances of 60 to perhaps 300 m may be attributable to prompt injection into fractures. The Nimz and Thompson (1992) report also includes an interpretation of earlier data from Thompson and Gilmore (1991) that showed radionuclides had migrated 350 m from an underground test through volcanic tuff.

Smith et al. (1996) suggest late time gaseous transport may also contribute to rapid migration of some radionuclides a short distance away from the cavities based on analyses from near the INGOT test in Yucca Flat.

Rose et al. (2000) used secondary ion mass spectrometry to analyze geologic samples from the near field of the BULLION and TYBO tests in Pahute Mesa. The results show correlated ^{22}Na and ^{235}U enrichments in the vadose zone at a distance of several hundred meters from the working point of the BULLION test. These results were interpreted as evidence for prompt injection.

These studies suggest that the initial distribution of radionuclides may extend beyond the edge of the cavity perhaps as much as several hundred meters.

3.4.3 Groundwater Sampling Data

Observed radionuclide concentrations in groundwater samples may be used to constrain or validate predictions made by transport models. Groundwater sampling data for the NTS and vicinity are available from various programs sponsored by NNSA/NSO and other organizations. Groundwater sample analysis results are stored and maintained in a centralized and comprehensive water chemistry database, *GEOCHEM*. This database was developed under the UGTA Project to support the environmental restoration activities of the underground test areas of the NTS. A brief description of the *GEOCHEM* database is provided in Appendix C. Details may be found in the *GEOCHEM* database User's Guide (SNJV, 2004e).

Available radionuclide data from wells within the Frenchman Flat CAU were compiled from the *GEOCHEM* database. The sampling locations, and their proximity to the tests, are shown in Figure 3-2. The investigation area shown in Figure 3-2 is consistent with that identified in Figure 1-2. The data set compiled for this study area includes radionuclide activity measurements generated during 1,505 recorded sampling events at 20 different wells. A sampling event is defined as a particular date of sampling with the earliest event reported within the data set dated 1957. The primary agencies providing data to the database include SNJV, LLNL, LANL, USGS, DRI, BN, IT Corporation, and Shaw Environmental. Each agency typically analyzes for a different suite of radionuclides. Tritium activities are generally reported by all agencies. Only three of the sampling well locations shown in Figure 3-2 (RNM-1, RNM-2S, and UE-5n) contain radionuclides that can be unequivocally linked to underground testing. All other wells produce groundwater containing natural environmental levels of radionuclides as discussed in Section 3.4.4.

This discussion of radionuclides in groundwater is divided into data related to the CAMBRIC RNM project and data from wells unrelated to the CAMBRIC RNM experiment. All activity concentration data given in the following sections are presented as the concentration at the time of sampling; no data were decay-corrected to the time of detonation.

3.4.3.1 CAMBRIC RNM Project

The CAMBRIC RNM project was initiated in 1974 to provide data on the radionuclides migration away from the site of the CAMBRIC underground nuclear test. One well, RNM-1, was slant-drilled through the radioactive debris and cavity formed by the CAMBRIC test. Another well, RNM-2S, was installed 91 m south of the center of the CAMBRIC detonation point. Groundwater flow from the detonation point to well RNM-2S was induced by pumping well RNM-2S from October 1975 to August 1991 (Bryant, 1992). Pumping was nearly continuous,

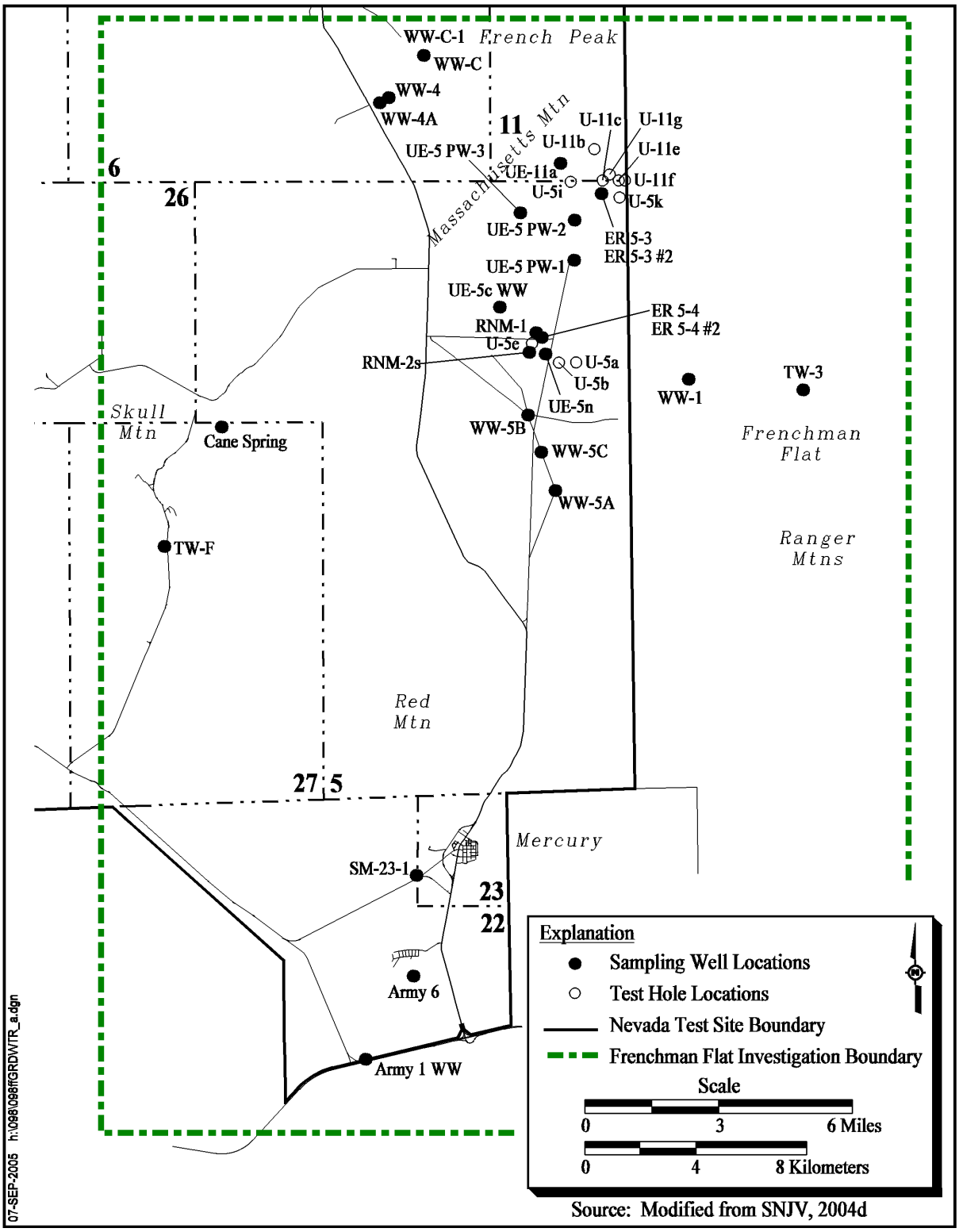

Figure 3-2
Groundwater Sampling and Test Hole Locations within the Frenchman Flat Area

first at 300 gallons per minute (gpm) and then at 600 gpm. Pumping was necessary to produce an artificial gradient so that water would move to well RNM-2S in a reasonable amount of time. Approximately 1.7 x 10^7 cubic meters (m^3) of water were discharged during this RNM experiment (Finnegan and Thompson, 2002) into an unlined discharge ditch that was used to transport the water pumped from Wells RNM-1 and RNM-2S to Frenchman Lake.

A multi-well aquifer test (MWAT) was later conducted (April 26, 2003 to July 10, 2003) in order to acquire data for use in estimating hydraulic properties of the alluvium in the vicinity of RNM-2S (SNJV, 2004b). RNM-2S was pumped continuously for a period of 75 days at an average rate of 595.5 gpm. Groundwater characterization samples were collected from well RNM-2S by SNJV, LLNL, and LANL at the beginning, and again at the end, of the test. Details regarding the RNM-2S MWAT, including the analysis and interpretation of the hydraulic data collected, are presented in SNJV, 2004b.

3.4.3.2 Well RNM-1

Groundwater samples were periodically collected from five isolated zones within well RNM-1 during 1974 and 1975, approximately ten years after the CAMBRIC detonation. The zones were 50 m below the bottom of the cavity (Zone 1), lower cavity (Zone 2), upper cavity (Zone 3), chimney area (Zone 4), and periphery of chimney (Zone 5). Table 3-3 presents average radionuclide concentrations in groundwater from these sampling zones. Bryant (1992) reported that no radioactive constituents were detected in groundwater below the bottom of the cavity (Zone 1) suggesting limited vertical migration during the ten year period following the detonation. Radionuclide concentrations in cavity groundwater (Zones 2 and 3) were substantially elevated (Table 3-3). Concentrations of ^{137}Cs, ^{85}Kr, ^{90}Sr, and tritium were also elevated in groundwater samples from the chimney area and periphery of the chimney (Zones 4 and 5). Although elevated, concentrations in the chimney area and periphery were lower compared with concentrations found in the cavity. Antimony-125 (^{125}Sb), ^{239}Pu, and ruthenium-106 (^{106}Ru) activities were below detection in groundwater samples from the chimney and periphery (Table 3-3).

Radionuclide data, provided to the *GEOCHEM* database by LANL, are presented in Figure 3-3. Figure 3-3 shows the temporal change of radionuclide concentrations in Well RNM-1 groundwater samples from the chimney and periphery zones (Zones 4 and 5) during the pumping of RNM-2S. Except for the first sample (from 1975), which was from Zone 4 only, samples were composites of both zones. Tritium and ^{85}Kr concentrations decreased several orders of magnitude over the period of pumping (1975 to 1991); and to a lesser extent, ^{137}Cs and ^{90}Sr concentrations also decreased (Figure 3-3). Only small changes in concentrations were observed at RNM-1 once the pump in RNM-2S was stopped. At that time, the tritium and ^{85}Kr concentrations were near the analytical detection limits (Finnegan and Thompson, 2001).

Table 3-3
Radionuclide Concentrations in Groundwater at Well RNM-1

Water Source	Sample Date(s)[a]	Antimony-125 (pCi/L)[b]	Cesium-137 (pCi/L)	Iodine-129 (pCi/L)	Krypton-85 (pCi/L)	Ruthenium-106 (pCi/L)	Strontium-90 (pCi/L)	Plutonium-239 (pCi/L)	Tritium (pCi/L)
Below Cavity (Zone 1)	7/10/1974	ND	ND	no data	ND[d]	ND	ND	ND	ND
Lower Cavity (Zone 2)	9/6/1974	$2.2 \times 10^{+3}$ filtered[c]	$5.9 \times 10^{+2}$ filtered[c]	5.3[d, e]	no data	$3.6 \times 10^{+3}$ filtered[c]	no data	6.3[d, e]	$1.9 \times 10^{+9}$ [d]
	9/6/1974	$1.4 \times 10^{+3}$ unfiltered	$6.1 \times 10^{+2}$ unfiltered		no data	$4.0 \times 10^{+3}$ unfiltered	$4.0 \times 10^{+3}$ unfiltered		
	11/5/1974	$4.2 \times 10^{+3}$	$6.7 \times 10^{+2}$	8.1[d]	$1.6 \times 10^{+5}$ [d]	$4.0 \times 10^{+3}$	$2.9 \times 10^{+3}$	1.3[d]	$5.3 \times 10^{+9}$
Upper Cavity (Zone 3)	4/29/1975	$9.8 \times 10^{+2}$	$1.5 \times 10^{+3}$	2.9[d]	$2.3 \times 10^{+5}$ [d]	$1.9 \times 10^{+3}$	$2.6 \times 10^{+3}$	1.2[d]	$3.7 \times 10^{+9}$
Chimney Area (Zone 4)	8/7/1975 - 8/8/1975	ND[d]	$3.7 \times 10^{+2}$	4.6×10^{-3} [d]	$1.6 \times 10^{+4}$	ND[d]	$1.8 \times 10^{+3}$	ND[d]	$7.5 \times 10^{+7}$
Periphery of Chimney (Zone 5)	8/14/1975	ND[d]	$8.2 \times 10^{+1}$	1.6×10^{-3} [d]	$3.1 \times 10^{+3}$	ND[d]	$8.2 \times 10^{+1}$	ND[d]	$2.8 \times 10^{+7}$

[a]Data source is Hoffman et al. (1977) unless otherwise noted
[b]Picocuries per liter
[c]Filtered through a 1-micrometer filter in the field (Hoffman et al., 1977)
[d]Information reported in Bryant (1992)
[e]Data from 9/5/1974 to 9/6/1974 Zone 2 samples not differentiated into filtered and unfiltered
ND = No radioactivity above background detected

3.4.3.3 Well RNM-2S

Figure 3-4 shows radionuclide concentrations in groundwater at Well RNM-2S as a function of time. Tritium, ^{85}Kr, ^{36}Cl, ^{106}Ru, and ^{129}I were transported in groundwater from the CAMBRIC test area. These radionuclides are all known to be relatively mobile in the groundwater environment. Typically, 99.9 percent of the tritium occurs as tritiated water (Smith, 1995a) and should, therefore, move at the same velocity as groundwater. Krypton is a dissolved gas, and the other radionuclides are generally present in groundwater as anionic constituents.

Maximum tritium concentrations were observed at well RNM-2S in 1979, and peak ^{85}Kr concentrations were observed in mid-1981 to 1982. The breakthrough, as well as the maximum concentration of ^{36}Cl in RNM-2S are reported to have occurred before that of tritium (Ogard et. al., 1988). This early arrival may be attributed to anion exclusion, which effectively prevents anionic constituents from entering into dead-end pore spaces, and the intragranular porosity of aquifer materials (Ogard et al., 1988). Anion exclusion also keeps the anions more in the center of pores where groundwater velocities are greater. The early arrival of ^{36}Cl may also be attributed to differences in the initial distributions of ^{36}Cl and tritium within the test cavity and near-field environment following detonation of the test (Tompson et al., 2002). Burbey and Wheatcraft (1986) suggested slight

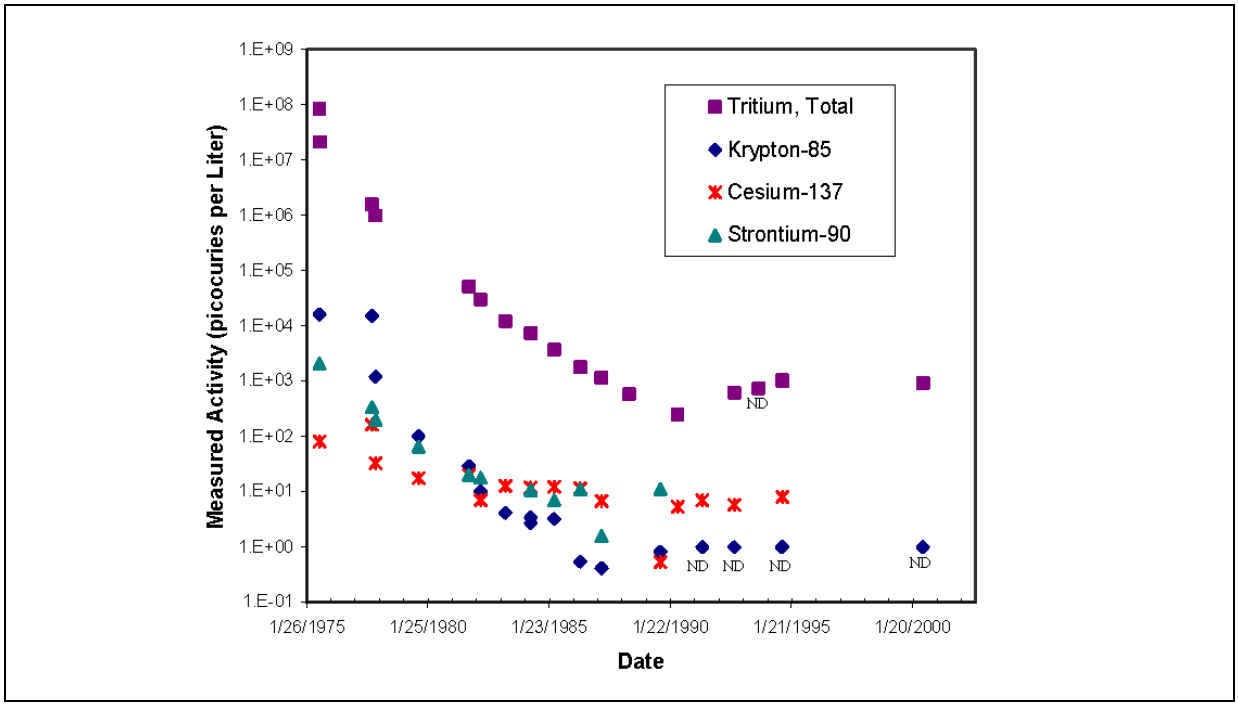

Figure 3-3
Radionuclide Concentrations in Groundwater at Well RNM-1

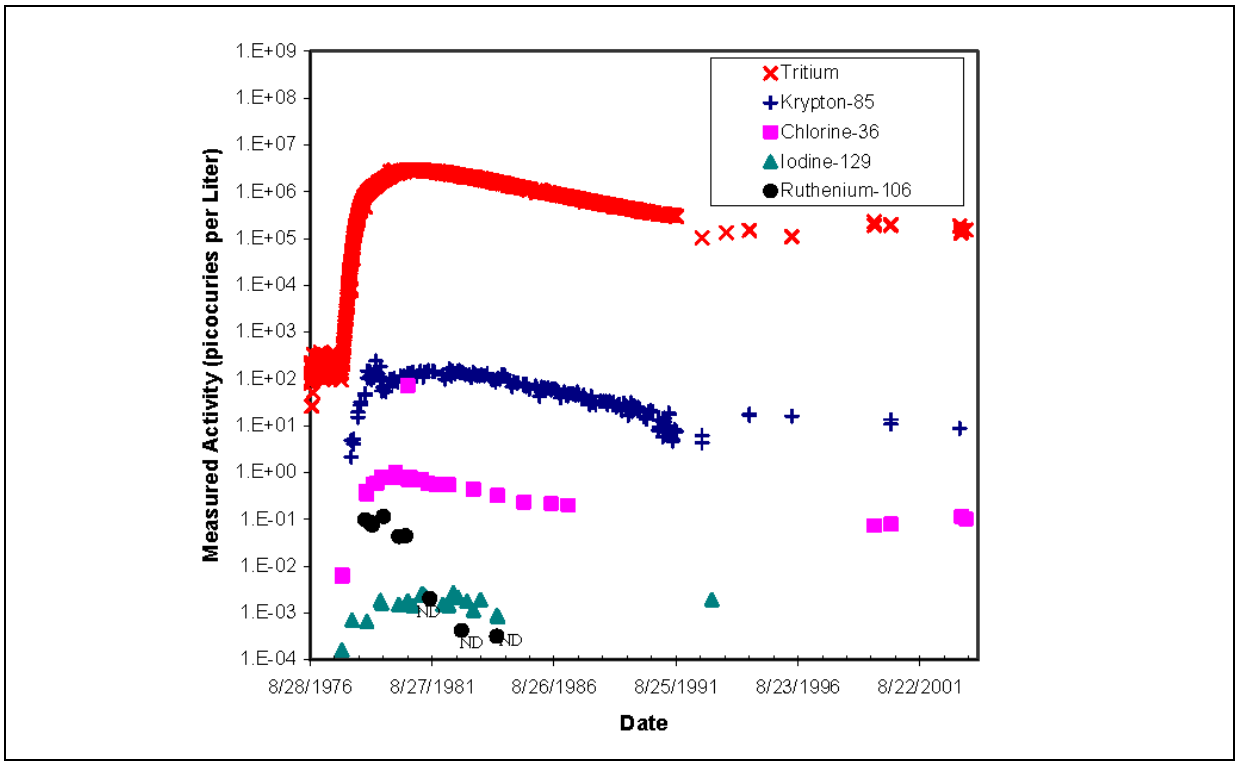

Figure 3-4
Radionuclide Concentrations in Groundwater at Well RNM-2S

retardation of tritium, although the physical mechanism for the retardation was not identified. The relative breakthrough of ^{106}Ru is difficult to assess based on the small number of data points available (Figure 3-4). The dominant aqueous ionic form of ^{106}Ru, RuO_4^-, is anionic and, therefore, likely to migrate in groundwater (Buddemeir and Isherwood, 1985). The ratios of ^{106}Ru to tritium were reported to be nearly the same for samples collected at both RNM-1 and RNM-2S, which suggests that ^{106}Ru and tritium traveled at the same rate from the CAMBRIC cavity to RNM-2S (Bryant, 1992).

The radionuclides ^{137}Cs, ^{239}Pu, ^{125}Sb, and ^{90}Sr were not detected in Well RNM-2S groundwater, although these radionuclides were present in groundwater samples from the CAMBRIC cavity (Table 3-4). This indicates limited migration of these radionuclides in the groundwater over this period of time. Relatively high retardation is expected for Cs and Sr due to their strong affinities for mica, clay, and zeolite ion exchange sites. Plutonium is typically very insoluble in groundwater (Bryant, 1992).

Water and radionuclides discharged into the unlined CAMBRIC ditch, during the 16-year pumping study, were thought to have infiltrated through the unsaturated zone and back into the groundwater. Tompson et al. (2002) utilized pumping and effluent data in conjunction with geologic data, radionuclide measurements, isotopic age-dating estimates, and vadose zone flow and transport models to better understand the movement of radionuclides between the CAMBRIC ditch and the water table. The results of this investigation suggested that the transport of tritium, ^{36}Cl, ^{99}Tc, and ^{129}I through the 200 m vadose zone was relatively fast (3 to 5 years) under flowing conditions of the ditch. Longer residence times in the draining system were observed following ditch shutoff (Tompson et al., 2002). This study also suggested that 15 to 20 percent of the tritium, and other mobile radionuclides, pumped from RNM-2S during the initial sixteen year test were recycled from the ditch and not entirely attributable to the CAMBRIC test (Tompson et al., 2002; Rose et al., 2004).

3.4.3.4 Well UE-5n

Well UE-5n, an exploratory hole, was drilled approximately 560 m southeast of the RNM-1 hole in March 1976. Although not part of the CAMBRIC RNM experiment, Well UE-5n is located within 100 m of the CAMBRIC ditch. Radionuclides were not detected in UE-5n waters until 1989 and are thought to reflect infiltration of water from the CAMBRIC ditch (Rose et al., 2003). Tritium activities of 1.41×10^5 and 1.35×10^5 picocuries per liter (pCi/L) were measured in samples collected from UE-5n in September 1999 and April 2001, respectively. If the April 2001 samples are decay-corrected to the time of the September 1999 sampling date, an average activity of 1.49×10^5 pCi/L is obtained. This indicates a slight increase in activity over the period between sampling times (Finnegan and Thompson, 2002). In addition, ^{36}Cl, ^{129}I, and ^{99}Tc were detected in UE-5n waters suggesting infiltration of these radionuclides from the CAMBRIC ditch as well. No ^{85}Kr or ^{14}C activity, and very low levels (82 to 84 parts per quadrillion) of ^{237}Np were detected in UE-5n groundwaters (Finnegan and Thompson, 2002; Tompson et al., 2005b). This suggests that ^{14}C may have interacted chemically

with the calcite in the alluvium, while ^{85}Kr may have partitioned into the atmosphere and soil gases during flow in the ditch (Tompson et al., 2002). The isotopic composition of dissolved uranium in UE-5n groundwaters is consistent with natural abundances (Rose et al., 2003).

3.4.4 Non-CAMBRIC Radionuclide Data

In general, groundwater radionuclide concentrations are low (most likely background) at well locations other than those associated with the CAMBRIC RNM project. Much of the radionuclide data for wells within Frenchman Flat are generated from the Routine Radiological Environmental Monitoring Program ([RREMP]; BN, 2003). The following wells within the study area (Figure 3-2) are monitored for this program: Army WW#1, WW-C1, WW-4, WW-4A, WW-5B, WW-5C, UE-5C WW, UE-5 PW-1, UE-5 PW-2, and UE-5 PW-3. The radionuclides measured for the RREMP include:

- Tritium
- ^{241}Am
- Cerium-144 (^{144}Ce)
- Cobalt-60 (^{60}Co)
- ^{134}Cs and ^{137}Cs
- ^{152}Eu, ^{154}Eu, and ^{155}Eu
- ^{40}K
- Lead-212 (^{212}Pb)
- ^{238}Pu and $^{238+239}Pu$
- Radium-226 (^{226}Ra) and ^{228}Ra
- ^{106}Ru
- ^{125}Sb
- ^{90}Sr

Although measured values for radionuclide activities are reported in some cases in the compiled data set, the values are typically less than the minimum detectable activity (MDA) and/or the measurement error reported as 2 sigma (2 times the standard deviation). Many of the reported data are notably low, but no MDA is reported. All tritium measurements were reported as less than the MDA of approximately 20 pCi/L during the 2003 monitoring events (BN, 2004b). A general lack of human-made alpha, beta, and gamma emitting radionuclides in groundwater samples collected from the Frenchman Flat monitoring wells during the 2003 monitoring events is reported by BN (2004b). Although very low yet detectable concentrations of naturally occurring ^{226}Ra and ^{228}Ra were observed, the levels did not exceed U.S. Environmental Protection Agency (EPA) levels of concern or their established maximum contaminant levels for drinking water (BN, 2004b) and were consistent with natural abundances.

In addition to the routine radiological monitoring performed by BN, multiple agencies (SNJV, LLNL, LANL, DRI, USGS, and BN) collected and analyzed groundwater samples from the newly drilled wells ER-5-3, ER-5-3#2, ER-5-4, and ER-5-4#2. All resulting data are contained in the *GEOCHEM* database.

3.4.4.1 ER-5-3

Well ER-5-3 was drilled and completed during fiscal year (FY) 2000 and primarily produces water originating from the Timber Mountain - Welded Tuff Aquifer (TM-WTA), (IT, 2000b; IT, 2001a). Groundwater characterization samples were collected from ER-5-3 in March 2001. No radionuclide activity attributed to nuclear testing was detected in this well (Finnegan and Thompson, 2002; Rose, 2003a, b).

3.4.4.2 ER-5-3#2

Well ER-5-3#2 located about 30 m east of ER-5-3, was drilled and completed in FY 2000 and then recompleted in FY 2001. ER-5-3#2 has a single completion zone in the lower carbonate aquifer. Groundwater characterization samples were collected from ER-5-3#2 in May 2001. No radionuclide activity attributed to nuclear testing was detected in this well (Finnegan and Thompson, 2002; Rose, 2003a, b).

3.4.4.3 ER-5-4

Well ER-5-4 was drilled and completed to a total depth of 1,137.5 m in FY 2001 and produces water primarily from the alluvial aquifer (IT, 2001b). ER-5-4 is located in the central portion of Frenchman Flat, approximately 350 m northeast of the emplacement hole for the CAMBRIC test. During drilling, tritium was detected at a depth of approximately 305 m with activities ranging from 4,300 to 5,400 pCi/L (Finnegan and Thompson, 2002). No other fission products or other weapon related radionuclides were observed during this time (Finnegan and Thompson, 2002). Notably, the tritium was found at a depth equivalent to the depth of the CAMBRIC test. Characterization samples were collected in July 2001 and analyzed by multiple agencies. Although the interval containing tritium activities was cased off during completion, a detectable amount of tritium (2.5 pCi/L) was measured by LLNL (Rose, 2003c). The ^{3}He in-growth method for tritium analysis used by LLNL has an associated detection limit of approximately 1 pCi/L. No other activity was detected in these samples other than background gamma activity of ^{238}U, ^{235}U, ^{232}Th (and their daughters), and ^{40}K (Finnegan and Thompson, 2002; Rose, 2003c).

3.4.4.4 ER-5-4#2

Well ER-5-4#2 was drilled and completed in FY 2002 approximately 30 m south of ER-5-4 (Shaw, 2003). ER-5-4#2 was completed to a total depth of 2,133.6 m and produces water primarily from the lower tuff confining unit (LTCU). Groundwater characterization samples were collected in November 2002. A tritium activity of 156.8 pCi/L was reported by LLNL but problems with low-level measurements of tritium were experienced in their laboratory during this time. The measured activity in this sample may have been due to post-sampling

cross-contamination (Rose, 2003d). No activity in these samples other than background gamma activity of ^{238}U, ^{235}U, ^{232}Th and their daughters, and ^{40}K were detected by the other agencies (Finnegan and Thompson, 2004).

3.5 CAMBRIC Hydrologic Source Term

In support of the Frenchman Flat CAU model, Tompson et al. (1999) developed a process model for the unclassified CAMBRIC HST. The objective of this model was to provide a modeling framework to quantitatively forecast the HST within the near-field environment of an underground nuclear test. Near-field in this case was loosely defined as four to eight cavity radii centered on the working point of the CAMBRIC test. The radionuclides tritium, ^{90}Sr, ^{137}Cs, ^{155}Eu, ^{239}Pu, and ^{241}Am were selected for the CAMBRIC source-term modeling effort because their inventories were unclassified and available at the time of model development. These radionuclides have a varied initial distribution in the melt glass, chimney, and cavity areas, and are considered to represent a cross section of geochemical behavior in the subsurface environment. A melt glass dissolution model was included to predict the release of potential contaminants from the melt glass. Geochemical reactions (e.g., aqueous and surface complexation, ion exchange, and precipitation/ dissolution) were modeled to assess the influence of these reactions on release rates (Tompson et al., 1999).

Due to certain data limitations and a perceived need to generalize the results of this initial HST model, some of the calculations were simplified (Tompson et al., 1999). The following lists some of these limitations and simplifications as described in Tompson et al. (2005):

- Transient effects arising from 16 years of pumping at RNM-2S during the RNM experiment were not incorporated.
- Infiltration of radionuclides from the CAMBRIC drainage ditch was not addressed.
- Background data on the ambient groundwater flow direction were not represented.
- Hydrothermal effects arising from residual test heat were not considered.
- Only a small number of radionuclides and geochemical reactions were incorporated.

Excluding transient effects in the CAMBRIC HST calculation (Tompson et al., 1999), arising from 16 years of pumping at RNM-2S, results in neglecting the displacement of the radionuclides toward the pumping well over the period of pumping, the immediate loss of some radionuclides from the groundwater as a result of pumping, the introduction of some radionuclides into the vadose zone and their reintroduction in groundwater underlying the ditch, and the introduction of some or all of the radionuclides into Frenchman Lake. This was justified since the goal of the original CAMBRIC HST model was to develop

a model for the basic release mechanisms without the complications of the transient effects.

As part of the Phase II Frenchman Flat CAU flow and transport modeling effort, LLNL initiated a task to update the CAMBRIC HST. Source term calculations performed by LLNL include a transient CAMBRIC source term that addresses each of the limitations described above and also includes improvements in data sources and modeling approaches, and a steady-state (non-transient) source term that is a generic release model, generated under steady-state flow conditions, and does not include the transient effects resulting from pumping during the RNM experiment, and from residual test heat nor the infiltration of radionuclides from the drainage ditch (Tompson et al., 2005). The steady-state HST model described by Tompson et al., (2005) provides the basis for developing an SSM abstraction, that is appropriate for the other nine tests in Frenchman Flat, where the HST was not impacted by pumping nor radionuclide infiltration from the drainage ditch.

The following section is dedicated to summarizing the development of the CAMBRIC steady-state HST model. The abstraction of this model for the development of the CAMBRIC SSM is described in Section 4.0.

3.5.1 Phase II CAMBRIC Steady-State Hydrologic Source Term Model

The general approach used by LLNL to develop the CAMBRIC steady-state HST model includes the following tasks:

1. Estimate the abundance, spatial distribution, and chemical state of radionuclide contamination immediately after the test.

2. Determine the mechanisms and rates of radionuclide release into the groundwater as a function of time. The rates of radionuclide release from the melt glass in the steady-state model were predicted from a model that included the influence of a cool-down temperature profile derived from the transient CAMBRIC groundwater flow model.

3. Forecast the rates of radionuclide movement away from the working point of the test for a 1,000-year period, as affected by groundwater flow and chemical reactions.

A conceptual model of the CAMBRIC near-field environment was first developed. The conceptual model includes a cavity zone, melt glass zone (MGZ), compressed zone, and three portions of the collapsed chimney (CHM1, CHM2, and CHM3). The cavity is assumed to be spherical and centered at the CAMBRIC working point. The compressed zone is assumed to be spherical, centered at the CAMBRIC working point, and excludes the volume occupied by the chimney, cavity, and the melt glass. The radius of the cavity (13.4 m) and the compressed zone (18 m) were determined using the original analyses of the drill back gamma-log survey performed immediately after the CAMBRIC test (Tompson et al., 2005). The MGZ is represented as a mixture of the nuclear melt glass and collapsed alluvium in the lower hemisphere of the cavity (i.e., the lower

7.4 m portion of the CAMBRIC cavity). This is also based on the results of the gamma log analyses (Tompson et al., 2005). The chimney is assumed to be cylindrical with a radius centered at the CAMBRIC working point. CHM1 extends 27 m upward from the top of the cavity, CHM2 extends from 27 m to 46 m, and CHM3 extends from 46 to 73 m above the CAMBRIC working point. A schematic demonstrating these regions is shown in Figure 3-5.

The geologic structure of the near-field environment in the CAMBRIC HST is consistent with the most recent HSU framework model (BN, 2004a; see also Appendix A). In addition, the CAMBRIC HST employs the mineralogic model developed by Warren et al. (2002) and the related interpretations described in Carle et al. (2002). Specifically, the AA2 unit is separated into seven alluvial layers that each have constant, effective-scale hydraulic medium properties (Tompson et al., 2005). The specific density of the alluvium is considered to be 2.5 grams per cubic centimeter (g/cm^3) in all layers. The elevations of the alluvial layers in the vicinity of the CAMBRIC test are shown in Figure 3-5.

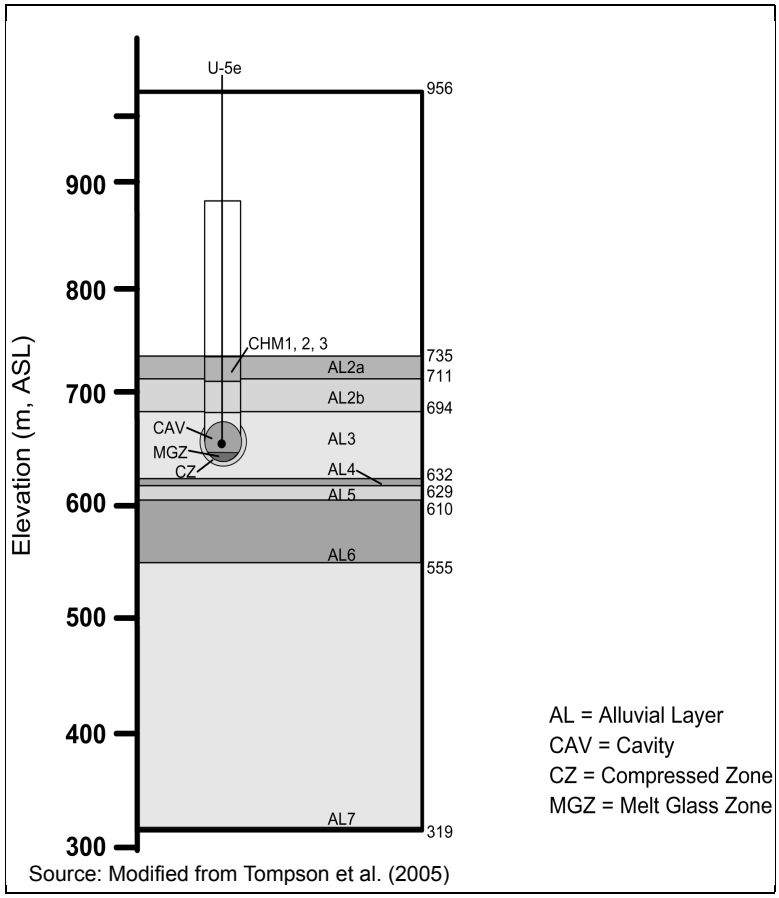

Figure 3-5
Diagram of the Cavity, Compressed Zone, and Chimney Region within the Alluvial Layers of the CAMBRIC HST

Thirty-six radionuclides were selected for incorporation into the unclassified CAMBRIC HST (Tompson et al., 2005, Table 3-4). The unclassified inventory used for the CAMBRIC model comes solely from the list reported in Bowen et al. (2001). Radionuclides were excluded from consideration either because no inventory existed, or if there was an inventory; none of the following criteria related to their abundance were satisfied (Pawloski et al., 2001):

1. The radionuclide must have a reported test-related inventory, as defined by the data in Smith (2001), and this inventory must equal or exceed any corresponding natural inventory in the rock.

2. For all alpha, beta, or electron capture/isomeric transition decay radionuclides, the ratio of the radionuclide activity (in Becquerels), or amount (in moles) to the activity; or amount for all alpha, beta, or electron capture/isomeric transition radionuclides exceeds a value of 0.1 percent of the total at some time during the 1,000-year period of interest.

3. The radionuclide has a reported concentration in groundwater taken from the cavity, chimney, or near the test.

The inventory, originally decay-corrected to September 23, 1992 (Bowen et al., 2001), is further decay-corrected to time zero (t_0) for CAMBRIC, May 14, 1965 (Table 3-4). This decay correction was particularly important for the decay chain ^{241}Pu -> ^{241}Am -> ^{237}Np since it results in a substantially lower initial mass of ^{241}Am than reported in Bowen et al. (2001).

The radiologic inventory used for the HST model were partitioned into solid melt glass in the MGZ and into groundwater in the cavity, the MGZ, the compressed zone, and the lower portion of the chimney (Tompson et al., 2005). The inventory was distributed into the melt glass, rubble, gas, and water based on the recommended values derived from the International Atomic Energy Agency ([IAEA], 1998; Table 3-4). The terms “glass,” “rubble,” “gas,” and “water” are interpreted as follows (Tompson et al., 2004):

- “Glass” refers to the solidified melt glass. Radionuclides in the glass are not released until glass dissolution mobilizes them for transport in the groundwater.

- “Rubble” refers to the rubblized zones, excluding the melt glass. During the cooling process after a test, vaporized radionuclides in the rubble are assumed to condense throughout the pore spaces of the disturbed zone (i.e., the exchange volume). These radionuclides are immediately available to dissolve and mobilize in the pore water when it returns after the test.

- “Water” refers to gaseous radionuclides in steam that would condense into liquid water as steam condensed. This condensation is assumed to occur in the pore spaces of the exchange volume and the melt glass zone. These radionuclides are immediately available to dissolve and mobilize in the pore water when it returns after the test.

Table 3-4
Average Unclassified Inventory and Radionuclide Distributions for CAMBRIC

Radionuclide	Half-Life (Years)	Initial Moles[a]	Distribution (Percent of Initial Moles)			
			Glass	Rubble	Gas	Water
^{3}H	1.23×10^{1}	2.81×10^{0}	0	0	2	98
^{14}C	5.73×10^{3}	1.07×10^{-1}	0	10	80	10
^{36}Cl	3.01×10^{5}	7.50×10^{-1}	50	40	0	10
^{39}Ar	2.69×10^{2}	4.98×10^{-4}	0	10	80	10
^{41}Ca	1.03×10^{5}	1.89×10^{0}	70	30	0	0
^{59}Ni	7.51×10^{4}	3.47×10^{-2}	95	5	0	0
^{63}Ni	1.00×10^{2}	5.68×10^{-3}	95	5	0	0
^{85}Kr	1.07×10^{1}	2.26×10^{-3}	0	10	80	10
^{90}Sr	2.91×10^{1}	2.90×10^{-2}	40	60	0	0
^{93}Zr	1.50×10^{6}	4.69×10^{-2}	95	5	0	0
^{94}Nb	2.03×10^{4}	3.90×10^{-3}	95	5	0	0
^{99}Tc	2.13×10^{5}	6.96×10^{-2}	80	20	0	0
^{107}Pd	6.50×10^{6}	3.55×10^{-2}	70	30	0	0
^{121}Sn	5.50×10^{1}	3.58×10^{-4}	60	40	0	0
^{126}Sn	1.00×10^{5}	5.73×10^{-3}	70	30	0	0
^{129}I	1.57×10^{7}	1.99×10^{-2}	50	40	0	10
^{135}Cs	2.30×10^{6}	8.76×10^{-2}	20	80	0	0
^{137}Cs	3.02×10^{1}	7.96×10^{-2}	20	80	0	0
^{151}Sm	9.00×10^{1}	9.17×10^{-3}	95	5	0	0
^{150}Eu	3.60×10^{1}	1.68×10^{-7}	95	5	0	0
^{152}Eu	1.35×10^{1}	1.17×10^{-2}	95	5	0	0
^{154}Eu	8.59×10^{0}	5.73×10^{-3}	95	5	0	0
^{166}Ho	1.20×10^{3}	6.90×10^{-4}	95	5	0	0
^{232}U	6.89×10^{1}	2.63×10^{-7}	90	10	0	0
^{233}U	1.59×10^{5}	5.94×10^{-5}	90	10	0	0
^{234}U	2.46×10^{5}	2.97×10^{-2}	90	10	0	0
^{235}U	7.04×10^{8}	1.69×10^{0}	90	10	0	0
^{236}U	2.34×10^{7}	1.96×10^{-2}	90	10	0	0
^{238}U	4.47×10^{9}	1.19×10^{2}	90	10	0	0
^{237}Np	2.14×10^{6}	6.37×10^{-3}	95	5	0	0
^{238}Pu	8.77×10^{1}	9.84×10^{-3}	95	5	0	0
^{239}Pu	2.41×10^{4}	9.55×10^{0}	95	5	0	0
^{240}Pu	6.56×10^{3}	6.42×10^{-1}	95	5	0	0
^{241}Pu	1.44×10^{1}	6.63×10^{-2}	95	5	0	0
^{242}Pu	3.75×10^{5}	3.02×10^{-3}	95	5	0	0
^{241}Am	4.33×10^{2}	1.42×10^{-2}	95	5	0	0

Source: Modified from Tompson et al., 2005

[a]Average Inventory, calculated from Bowen et al. (2001), is decay-corrected to CAMBRIC t_0

- "Gas" refers to noncondensible radionuclides that may exist as gases or coexist as bubbles in the pore fluids in the compressed zone, cavity zone, and melt glass zone at normal pressures and temperatures. Again, these radionuclides are immediately available to dissolve and mobilize in the pore water when it returns after the test.

To reduce the number of transport simulations, the radionuclides were segregated into 13 groups based on similarities in partitioning and chemical reactivity characteristics (Tompson et al., 2005). The results from these groups are then used to reconstruct the transport behavior of all radionuclides within the RST in a post processing step. The classes of radionuclides, along with the concentration of each group of radionuclides in both the melt glass and the aqueous phase, are shown in Table 3-5. An inventory of one mole was used for the two tracer classes (Tompson et al., 2005). The mass flux output from the HST is then corrected during post-processing to include the actual molar inventories and decay. Several of the sorbing radionuclides (Nb, Pd, Sn, and Zr) are treated as tracers primarily because sorption data are not available.

Table 3-5
Initial Concentrations of 13 Radionuclide Classes in the Aqueous Phase and Nuclear Melt Glass (Tompson et al., 2005, Table C3)

Component	Radionuclide Analogs	Glass	Water
		mole/g	mole/L
Tracer (rubble)	^{3}H, ^{14}C, ^{36}Cl, ^{39}Ar, ^{85}Kr, ^{99}Tc, ^{129}I, ^{93}Zr, ^{94}Nb, ^{107}Pd, ^{121}Sn, ^{126}Sn	0.00×10^{0}	1.39×10^{-7}
Tracer (glass)		1.90×10^{-9}	0.00×10^{0}
^{41}Ca		2.51×10^{-9}	7.84×10^{-8}
$^{59+63}Ni$		7.31×10^{-11}	2.80×10^{-10}
^{90}Sr		2.21×10^{-11}	2.41×10^{-9}
$^{135+137}Cs$		6.37×10^{-11}	1.85×10^{-8}
^{151}Sm		1.66×10^{-11}	6.35×10^{-11}
$^{150+152+154}Eu$	^{166}Ho	3.16×10^{-11}	1.21×10^{-10}
$^{232+233+234+235+236+238}U$		2.07×10^{-7}	1.67×10^{-6}
^{237}Np		1.15×10^{-11}	4.42×10^{-11}
$^{238+239+240+242}Pu$		1.85×10^{-8}	7.07×10^{-8}
^{241}Pu		1.20×10^{-10}	4.59×10^{-10}
^{241}Am		2.56×10^{-11}	9.81×10^{-11}

Source: Tompson et al., 2005
mole/g = Mole per gram
mole/L = Mole per liter

Note: Nb, Pd, Sn, and Zr are treated as tracers due to the lack of available surface complexation or ion exchange data.

The Nonisothermal Unsaturated-Saturated Flow and Transport (NUFT; Nitao, 1988) and Parflow groundwater flow models along with a combination of streamline and/or particle based transport models were used for the CAMBRIC steady-state and transient HST simulations (Tompson et al., 2005). The NUFT model is a numerical model that solves the continuum balance equations for the conservation of mass, momentum, and thermal energy. The NUFT model was used primarily in the transient simulations to study early (0- to 10-year) transient flow behavior under the effects of residual test heat. The NUFT model was also used to calibrate near-field alluvial layer permeabilities based on the RNM-2S MWAT test. The Parflow model was also used for the transient simulations to study later time (10- to 1,000-year) isothermal flow behavior under pumping and ditch recharge conditions (Tompson et al., 2005). The Parflow model was used in the steady-state simulations to provide a steady flow field (isothermal, no pumping, no ditch recharge) for the entire 1,000-year transport model simulation period (Tompson et al., 2005).

Transport simulations in the steady-state model were developed from a particle-based transport model (Pawloski et al., 2001). The temperature history of the melt glass was calculated from NUFT simulations of hydrothermal flow at early time. Temperature-dependent melt glass release functions were used to simulate the release of radionuclides from the melt glass (Tompson et al., 2005). The melt-glass release functions were developed based on the temperature history from NUFT simulations and geochemical modeling of the fluid evolution using Geochemist's Workbench (Bethke, 1996) and CRUNCH (Pawloski et al., 2001) codes. These functions will be described in more detail in Section 4.0. Surface complexation and ion exchange reactions between radionuclides and reactive minerals in the AA2 HSU were treated with a spatially variable sorption or partitioning model. Effective distribution coefficients (K_d) for each radionuclide class were developed for each mineralogically distinct alluvial layer (Table 3-6). Within each layer, uncorrelated spatial K_d heterogeneity was defined based on mineralogic variability with that layer. This variability is reported as a standard deviation of the logarithm of the mean K_d. The mean and the associated standard deviations of the log K_ds as reported in Tompson et al. (2005) are shown in Table 3-6.

Radionuclide fluxes were computed at three parallel breakthrough planes using the steady-state model. The planes are vertical and parallel to the CAMBRIC ditch and cross through wells RNM-1, RNM-2, and ER-5-4#2. They are 23, 93, and 269 m away from U-5e, respectively (Tompson et al., 2005, Figure 7).

3.6 Phase I Frenchman Flat Simplified Hydrologic Source Term

Tompson et al. (2004) developed an unclassified simplification of the HST for the 10 underground nuclear tests conducted in Frenchman Flat. This simplified HST was developed from the results of the CAMBRIC HST described in Tompson et al. (1999).

Table 3-6
Average and Standard Deviation of Log Distribution Coefficients (log Kd) for Each Alluvial Layer used in the Steady State Parflow Model (mL/g) (Tompson et al., 2005, Table E2)

	Ca	Cs	Sr	Ni	Am	Eu	Sm	Np	U	Pu
Layer AL2a, b; Chimney zones CHM 2,3										
Average	2.2	3.8	1.9	3.1	3.9	3.2	3.5	0.6	0.2	2.0
SD	0.1	0.2	0.1	0.1	0.1	0.1	0.2	0.1	0.1	0.1
Layer AL3; Chimney zones CHM 1										
Average	2.8	4.1	2.5	3.0	3.8	3.1	3.3	0.4	0.1	1.9
SD	0.2	0.1	0.2	0.1	0.1	0.1	0.2	0.1	0.2	0.1
Melt Glass Zone										
Average	2.7	4.0	2.5	3.0	3.7	3.0	3.2	0.4	0.1	1.9
SD	0.2	0.1	0.2	0.1	0.1	0.1	0.2	0.1	0.2	0.1
Layer AL4										
Average	2.7	4.1	2.5	3.1	3.9	3.1	3.3	0.5	0.2	2.0
SD	0.1	0.3	0.1	0.2	0.2	0.2	0.3	0.3	0.2	0.2
Layer AL5										
Average	2.6	4.2	2.4	3.0	3.8	3.1	3.3	0.5	0.1	1.9
SD	0.1	0.1	0.2	0.3	0.3	0.3	0.3	0.2	0.2	0.2
Layer AL6										
Average	2.1	4.0	1.8	3.1	3.9	3.2	3.4	0.5	0.2	2.0
SD	0.1	0.1	0.1	0.1	0.1	0.1	0.1	0.1	0.1	0.1
Layer AL7										
Average	2.1	4.0	1.8	3.1	3.9	3.2	3.5	0.6	0.3	2.1
SD	0.1	0.1	0.1	0.1	0.1	0.1	0.2	0.1	0.1	0.1

SD = Standard deviation

The basic elements of the simplified HST model are as follows:

- Estimated volume of geologic material impacted by the tests.
- Identities, quantities, and distribution of the radionuclides of importance.
- Simplified models of the release and retardation of these radionuclides in groundwater.

As stated by Tompson et al. (2004), the HST of a specific underground test represents the flux of test-related radionuclides into groundwater, away from the underground testing point. The HST is a function of the following:

- Radionuclide inventory.
- Spatial distribution of the radionuclide inventory around the working point of the test.
- Fractionation of the radionuclide inventory between melt glass and non-melt glass zones.
- Melt glass or other material dissolution or solubility.
- Rate of groundwater flow through the subsurface zones initially contaminated by the nuclear test.
- Chemical mobility of the radionuclide inventory in groundwater.
- Decay characteristics of the radionuclide inventory.

Many of these characteristics can be estimated from the yield, depth of burial, and knowledge of the unclassified radionuclide inventories. Only unclassified information on test yields and the total Frenchman Flat radionuclide inventory were presented in Tompson et al. (2004).

Principal assumptions include the following:

- Temperature is fixed (the impacts of residual test-related heat are not considered).
- Groundwater flow is in steady-state.
- Groundwater pH is constant.
- Radionuclide release from the melt glass occurs at a fixed rate.
- Chemical sorption (via ion exchange and surface complexation) is assumed to be described by retardation coefficients that are functions of the geologic medium and ambient groundwater chemistry.
- Radionuclide mineral precipitation/dissolution and formation of radionuclide-sorbing minerals in the melt glass elsewhere is ignored.

The results of the simplified HST were compared to those of the Phase I CAMBRIC HST. Tompson et al. (2004) acknowledges that the comparison was difficult because of several errors found in the Phase I CAMBRIC simulations and the limited understanding of the nature of the long-term simulated flux profiles. Based on the various examples of the simplified source term presented, it is concluded that the simplified HST appears to provide reasonable results for the

conditions under which it was derived. For example, the predicted release of ^{241}Am from the CAMBRIC test using the simplified HST model compare well with the results of the Phase I CAMBRIC HST model (Tompson et al., 1999).

3.7 Uncertainties in HST Definition

The HST may be estimated from measurements of radionuclide activities observed in the cavity water, or it may be derived from the radiologic source term. Uncertainties associated with the definition of the HST, in general, are related to the following sources:

1. Uncertainty in our knowledge of the RST inventory, its form, or its initial spatial distribution.

2. Uncertainty in our knowledge of the chemical processes that serve to release radionuclides as mobile (or immobile) species in groundwater.

3. Uncertainty in our knowledge of groundwater flow rates through the cavity and initially contaminated zone.

According to Smith et al. (1995), the definition of the HST is complicated by a number of factors. The main factors are as follows:

- Samples of cavity water are affected by drilling and completion activities.

- Radionuclides with half-lives shorter than 10 years are not accounted for in the RST radionuclide inventory.

- The transfer of radionuclides from the RST to the HST involves the processes of leaching and sorption. The relative importance of these two processes is not well understood.

- Little information exists on the factors affecting melt glass leaching. These factors include melt glass composition, its initial distribution of radionuclides, its available surface area, the leachate chemistry, and the cavity temperature.

- Information is lacking on the geochemical controls of radionuclide sorption. Geochemical controls include groundwater composition; the specific radionuclide in solution and its oxidation state; the fluid temperature; and the abundance, composition, and cation exchange capacity of the minerals present.

- Much more information on fracture systematics near test cavities is required. In addition, matrix diffusion coefficients are not available for all NTS lithologies.

- Extent of colloid loading in NTS is unknown. Colloid loading observed in well samples are affected by well construction, its development, and groundwater production during sampling.

Significant efforts to reduce these uncertainties have taken place over the past 10 years. Some of the more recent evaluations include: radionuclide sorption/ surface complexation investigations (Warren et al., 2002; Carle et al., 2002; Papelis and Um, 2003; Zavarin et al., 2004a, b, e); colloid transport investigations (Kersting and Reimus, 2003); nuclear melt glass dissolution and secondary mineral precipitation investigations (Zavarin et al., 2004c, d); and Frenchman Flat hydrological investigations (Tompson et al., 2002; SNJV, 2004b, c). New data generated during these investigations are presented in SNJV (2004d) and SNJV (2005). Uncertainties associated with the HST are discussed further in Section 5.0.

4.0 Source Term Process Model Simplifications

This section presents a description of an unclassified SSM developed to estimate radionuclide source inputs or HSTs for the Frenchman Flat radionuclide transport model. More specifically, this section describes the development and testing of an SSM that represents the near-field source term releases from the CAMBRIC test. The development of this SSM is based on steady state CAMBRIC flow and transport simulations described in Tompson et al. (2005). The steady-state CAMBRIC HST model and the CAMBRIC SSM were developed to provide the basis for the development of SSMs for the other nine tests in Frenchman Flat.

4.1 Simplified Source Term Model

As presented in Section 3.0, process HST models simulate the thermal, hydrological, and chemical processes that govern the migration of radionuclides from underground test cavities through an aquifer system. These multi-dimensional process models have the potential to simulate radionuclide release from a specific underground test, assuming that adequate site-specific data are available to support unclassified simulations. The disadvantage of the process model approach is the large amount of information required and the time-consuming process of performing multiple simulations to explore the potential range of releases from a given test. Given these limitations, it is impractical to use the process models to perform source calculations for all of the underground tests in Frenchman Flat. Therefore, SSMs are developed using the GoldSim® platform (Golder, 2002a, b) to generate cavity source flux terms for use in the CAU-scale radionuclide transport model of the Frenchman Flat area. A brief description of the GoldSim® platform is provided in Appendix B.

The objective of the SSMs is to provide an unclassified tool that captures the important processes and uncertainties of the process models in an efficient computational methodology. As such, the SSM is an alternate computational technique that provides insights into the range of potential radionuclide releases from individual underground tests. The SSM is not independent of the multi-dimensional process models because it is guided and calibrated by their results. In effect, the SSM is a parallel computational technique that can provide useful insights into the important processes and potential variability of the HST.

The initial step in developing the SSM for the Frenchman Flat tests has been the development of a SSM that simulates the process HST model for the CAMBRIC test (Tompson et al., 2005). The SSM for CAMBRIC captures the important hydrological and chemical processes in such a way that the range of output fluxes from the SSM will represent the range of fluxes from the detailed HST model. The

major stochastic parameters in the SSM are the groundwater flux through the exchange volume and the melt glass, as well as the K_ds in the melt glass, cavity, and compressed zones. The CAMBRIC SSM has constant values for the radionuclide inventory, yield, source parameters (i.e., volume, mass, and porosity), and for the distribution of inventory between the source volumes. The approach used to represent these parameters mirror that of the process CAMBRIC HST model. Modifications to the SSM will incorporate variability into some of these parameters for calculations of source terms for other underground tests in Frenchman Flat as described in Section 5.0.

4.1.1 Components of the Simplified Source Term Model

The SSM for CAMBRIC is comprised of a source region plus a small section of the surrounding near-field alluvium where the initial transport and mixing of waters flowing out of the source region takes place. The source region is divided into two subregions (Figure 4-1):

- The cavity which includes the "melt glass zone" at the bottom of the cavity consisting of the nuclear melt glass along with in-fallen alluvium, and the cavity zone consisting of the unconsolidated rubble from the collapsed chimney and the disturbed zone.

- The compressed zone which includes the lower compressed zone consisting of "intact" alluvium, and the upper compressed zone consisting of rubblized alluvium in the collapsed chimney directly above the cavity.

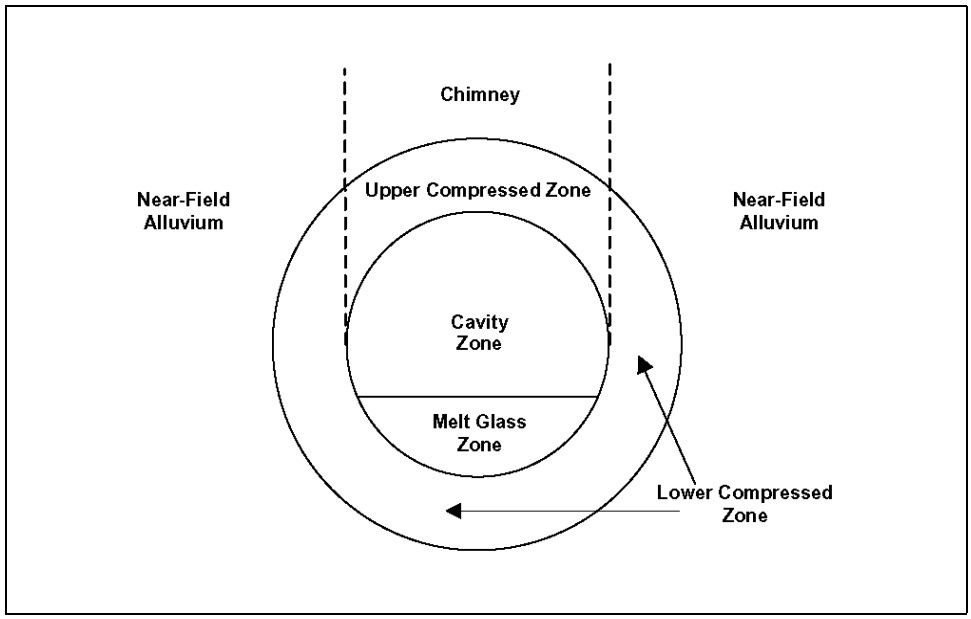

Figure 4-1
Schematic Diagram of the Source Term Regions in the CAMBRIC Process-Level Model and in the SSM

4.1.1.1 Dimensions of the Source Regions

For the SSM, the source is represented as two volumes: the melt glass zone and the exchange volume. The exchange volume consists of the cavity zone (i.e., the cavity excluding the melt glass zone) and the compressed zones immediately surrounding the cavity. The cavity and compressed zones are assumed to be spherical and centered on the working point. The radius of the cavity (13.4 m) and compressed zones (18.1 m) used for the SSM are consistent with those used for the process HST model (Tompson et al., 2005).

The mass of the nuclear melt glass is estimated on the basis of 700 metric tons (700,000 kilograms [kg]) of melt glass produced per kt of yield (Pawloski, 1999). This results in a total mass of 525 metric tons of glass for CAMBRIC, or 5.25×10^5 kg. The melt glass is assumed to be distributed evenly thoughout the melt glass zone, (i.e., the lower 7.4 m portion of the CAMBRIC cavity).

4.1.1.2 Volumes and Porosities of Initial Radionuclide Deposition

Based on the information in Section 4.1.1.1, Table 4-1 lists the volumes of the melt glass, cavity, lower compressed, and upper compressed zones for the CAMBRIC test. The porosity for each of these zones, as defined in Table B2 of Tompson et al. (2005), are also reported in Table 4-1. The pore volumes (Table 4-1) are based on constant porosity for the various regions. The saturated pores of these zones represent the volume in which the aqueous radionuclide fraction is initially distributed. Although the test will initially vaporize any water in the cavity and possibly the compressed zone, the pore volumes are fully saturated for the SSM, because the CAMBRIC cavity is below the water table, and the cavity is anticipated to rapidly refill with groundwater.

Table 4-1
Volume, Porosity, and Pore Volume of Source Regions

Zone	Volume (m^3)	Porosity[a]	Pore Volume (m^3)
Melt Glass Zone	1,881	0.29	545
Cavity Zone[b]	8,198	0.32	2,623
Lower Compressed Zone	11,153	0.27	3,011
Upper Compressed Zone[c]	3,607	0.36	1,299
Exchange Volume[d,e]	22,958	0.30	6,933

[a]Tompson et al. (2005)
[b]Cavity zone is the region within the cavity, excluding the melt glass
[c]Upper compressed zone is the lower portion of the chimney (CHM1; Tompson et al., 2005)
[d]Exchange Volume is the sum of the cavity zone and the compressed zone (upper and lower) volumes
[e]Porosity of the Exchange Volume is the effective porosity of its three component parts.

m^3 = cubic meters

The volumes and pore volumes in Table 4-1 do not exactly match the volumes in the HST model for CAMBRIC (Tompson et al., 2005, Table B-2). The values in Table 4-1 are geometrically exact, while the values in the HST model for CAMBRIC are adjusted for the finite size of the grid blocks in the model. The SSM uses the exact values in Table 4-1. The melt glass zone volumes are different by approximately 20 percent between the Parflow model and the SSM (see Tompson et al., 2005, Table B2). There is less than a 10 percent difference between the Parflow model and the SSM cavity and compressed zone volumes (Tompson et al., 2005).

4.1.2 Hydrologic Model

Groundwater will flow through the far-field alluvium with a flux determined by the effective permeability and far-field hydraulic head in the formation. When the groundwater reaches the underground test region, it will flow through the exchange volume and the melt glass zone at different rates, depending on the hydraulic conductivity of those two regions relative to each other and the hydraulic conductivity of the unaltered alluvium. The flowing groundwater removes radionuclides from the melt glass zone and exchange volume, and transports them through the near-field alluvium to the downgradient release boundary set at 23.03 m from the center of the cavity for the CAMBRIC SSM simulations. This boundary is envisioned as the location where the SSM intersects the Frenchman Flat CAU scale model and is referred to as the P1 plane.

The process HST model simulates the individual regions within the cavity and compressed zone. The mean value of horizontal permeability, denoted as k-h, and the porosity, ϕ, of the individual regions in the CAMBRIC HST model are defined in Figure 4-2 based on data in Table A2 of (Tompson et al., 2005). The HST model used a stochastic model to describe spatial variation in permeability and retardation distributions in the unaltered alluvium surrounding the altered zones of the CAMBRIC test. Distributions of breakthrough profiles for each radionuclide are developed for 50 separate realization of these distributions (with the properties inside the altered zone held constant for each realization). The CAMBRIC SSM captures this variability for the exchange volume through a distribution of flow rates, as well as the use of multiple transport pipes.

The groundwater flow system is represented in the SSM using four basic components: the exchange volume cell pathway, the melt glass zone cell pathway, multiple transport pathways for the exchange volume, and a transport pathway for the melt glass zone. It is reasonable within the context of the SSM to combine the cavity zone, the upper compressed zone, and the lower compressed zone into the exchange volume because the initial radionuclide inventory in the rubble and in the gas and water is distributed in the pore waters of the exchange volume. This inventory is available for immediate release and transport to the P1 plane. The mean horizontal permeabilities of the cavity zone, the upper compressed zone, and the lower compressed zone lie within a reasonably narrow range, so their representation as a single hydrologic source is reasonable. Although the mean horizontal permeabilities for the melt glass zone are also relatively similar to those of the cavity zone, a separate transport pipe is required for the melt glass zone.

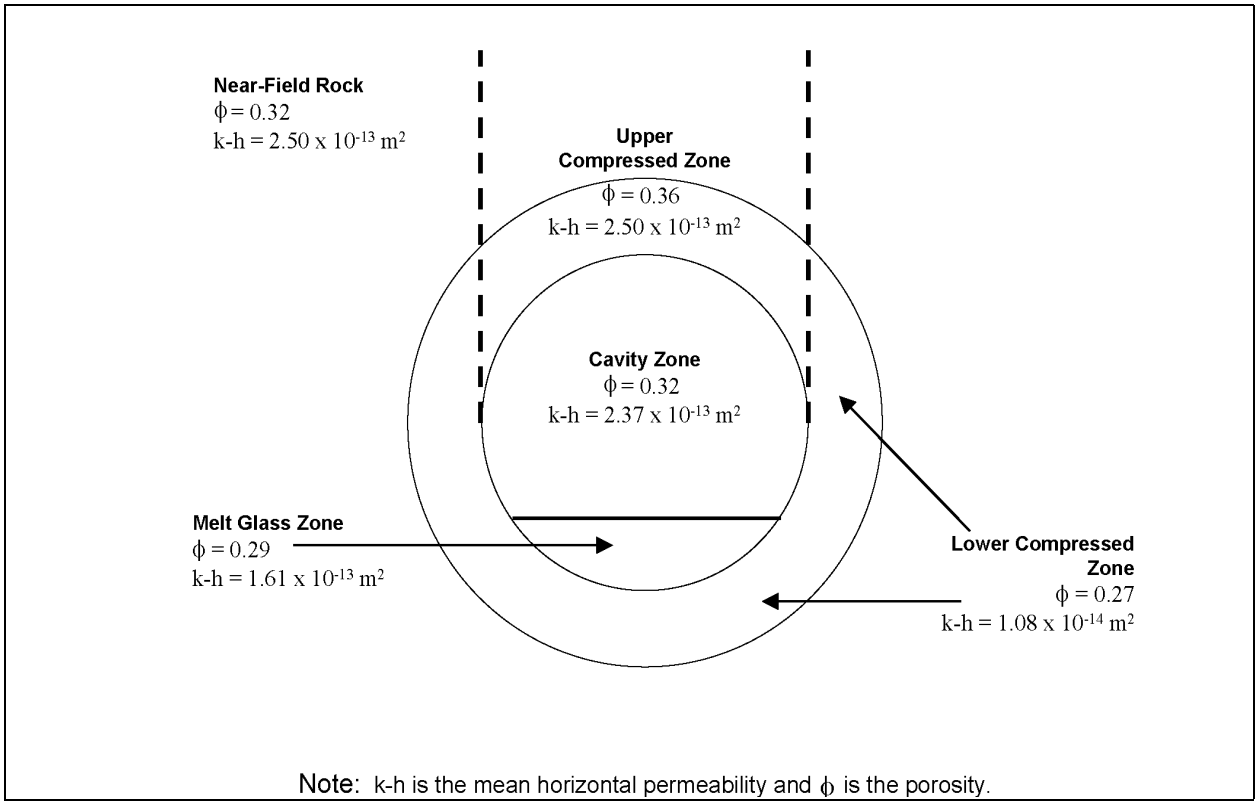

Figure 4-2
Hydrologic Properties for the Process Model of CAMBRIC (Tompson et al., 2005, Table C2)

Two sources of radionuclides are introduced into the melt glass zone: the inventory distributed into the pore waters of the melt glass zone, and the inventory distributed into the nuclear melt glass. The first source is available for immediate release and transport to the P1 plane whereas the radionuclide inventory in the nuclear melt glass is released over time as the glass dissolves, and is not immediately available for transport. Separate distribution coefficients are applied for the exchange volume and the melt glass zone (see Table 3-6).

Figure 4-3 illustrates the conceptual model for the SSM within the GoldSim® framework. The exchange volume is represented as four cell pathways and the melt glass zone is represented as a single cell pathway. The total volume and the porosity of the four exchange volume cell pathways are defined in Table 4-1. Similarly, the volume and porosity of the cell pathway for the melt glass zone is also defined in Table 4-1. The near-field alluvium and the alluvium in the cavity and compressed zones are represented as four exchange volume transport pipe pathways; one for each of the four cell pathways. The near-field alluvium as well as the alluvium and melt glass in the melt glass zone are represented as a single melt glass zone transport pipe pathway. Each of these pipe pathways is an independent, parallel flow pathway from the source volumes to the P1 release plane.

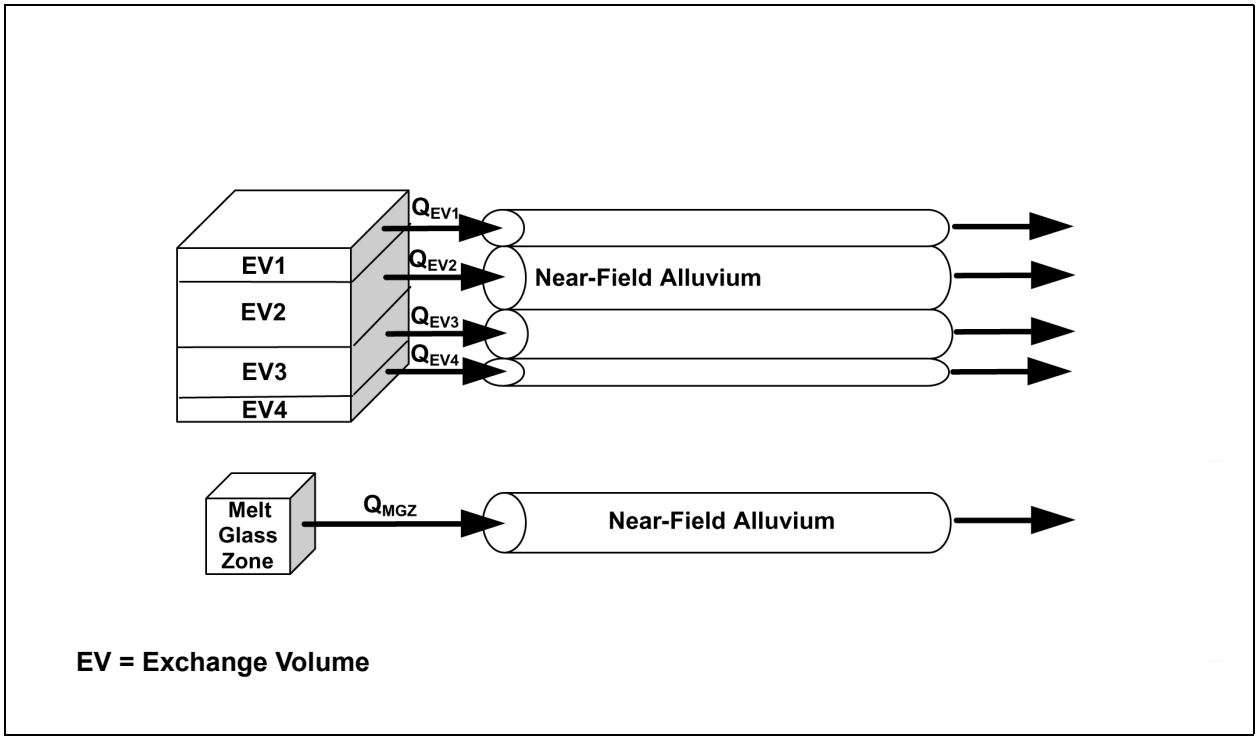

Figure 4-3
Schematic of the SSM Conceptual Model for the CAMBRIC Test

Each cell pathway is represented as a cubical volume. For a cube of volume V, the characteristic length of each cubical volume is given by $V^{1/3}$, or the length of an edge. The characteristic area of each face of the cube is given by $V^{2/3}$. Based on the data in Table 4-1, the characteristic area and characteristic length of the total exchange volume are 807.8 square meters (m^2) and 28.42 m, respectively, and the characteristic area and length of the melt glass zone are 152.37 m^2 and 12.34 m, respectively. The concentration within each cell pathway is based on homogeneous conditions in chemical equilibrium with the distribution coefficients for the various radionuclides. Solubility constraints are not defined in the SSM (or in the steady-state HST model) for CAMBRIC.

The fundamental output from the GoldSim® Contaminant Transport (CT) Module consists of the predicted mass fluxes for each radionuclide at specified locations within the hydrological system. The CT Module is a mass transport model, not a flow model, and does not directly solve for the movement of groundwater through the hydrological system. The fluxes between the exchange volumes and the transport pipe pathways, Q_{EV1}, Q_{EV2}, Q_{EV3}, and Q_{EV4}, and between the melt glass zone and the transport pipe pathway, Q_{MGZ}, must be defined in an appropriate manner. In a sense, the quantities Q_{EV} and Q_{MGZ} are the fundamental inputs to the SSM, rather than the permeability of the various hydrologic media. Section 4.2.4 explains how the values of Q_{EVi}, for i = 1, 2, 3, and 4 and Q_{MGZ} are determined for the CAMBRIC test.

The SSM conceptual model is clearly a simplification of the flow system in the source region and in the near-field. The HST model for CAMBRIC discretizes the individual source components (melt glass zone, cavity zone, and compressed zone) and the near-field alluvium, generating a complex, time dependent flow field near the test cavity. Similarly, the process HST model for CAMBRIC creates 50 realizations of near-field permeability and 50 realizations of the distribution coefficient for each radionuclide that can be sorbed. The 3-D permeability field results in complex 3-D flow pathways for the tracer (unretarded) radionuclides. Similarly, the randomly sampled field of distribution coefficients results in complex 3-D transport pathways that may differ from the flow pathways for the unretarded radionuclides.

The division of the exchange volume into four subvolumes, each with its own transport pathway, is motivated by the multiple transport pathways in the process level model and by the calibration of the SSM with the HST model. While a single cell for the exchange volume with a single transport pathway is adequate to describe the transport of the tracer radionuclides, a single transport pathway was not able to represent the transport of retarded radionuclides.

Thermal convection from the melt glass is not represented in the CAMBRIC SSM. The temperature of the melt glass drops rapidly after the test, because the yield of CAMBRIC is rather small. Cooling rates are also a function of the intrinsic thermal conductivity of the glass and alluvium, and more importantly the rate of groundwater moving through the region, both initially and over the month to year time frame, which serves to convect heat out of the system. The glass dissolution rate reduces to its ambient rate within a year or two after the test.

4.1.3 SSM Radionuclide Inventory and Its Partitioning

The unclassified radionuclide inventory for the SSM (and the HST) includes the 36 radionuclides identified by Tompson et al. (2005) as appropriate for inclusion in the process HST model (see Table 3-4). The initial mass of each of the 36 radionuclides in Table 3-4 is based on an average of the inventories of the ten underground nuclear tests detonated in Frenchman Flat (Bowen et al., 2001). This average inventory provides an unclassified inventory for the SSM that is representative of a range of underground tests, but does not represent the actual inventory for the CAMBRIC test. The inventory used for the HST and SSM was decay corrected to time zero for CAMBRIC, May 14, 1965 (Table 3-4).

Each of the radionuclides in Table 3-4 is represented as an individual radioisotope in the SSM, and the GoldSim® software automatically calculates decay and ingrowth. No post-processing is necessary. Radioisotopes with half-lives greater than 70,000 years are not set as radioactive in the SSM. A half-life greater than 70,000 years results in the decay of less than one percent of the initial inventory after 1,000 years. This change affects ^{36}Cl, ^{41}Ca, ^{59}Ni, ^{93}Zr, ^{99}Tc, ^{107}Pd, ^{126}Sn, ^{129}I, ^{135}Cs, ^{233}U, ^{234}U, ^{235}U, ^{236}U, ^{238}U, ^{237}Np, and ^{242}Pu in the SSM. All other radionuclides are set to decay according to the half lives presented in Table 3-4.

The SSM inventory also represents decay and ingrowth for two radionuclide decay chains:

$$^{241}\text{Pu} \rightarrow {}^{241}\text{Am} \rightarrow {}^{237}\text{Np} \quad (4\text{-}1)$$

$$^{238}\text{Pu} \rightarrow {}^{234}\text{U} \quad (4\text{-}2)$$

Although the process HST model does not represent the second chain, both chains are represented in the SSM. This is because there is no significant computational penalty from maintaining the two decay chains in the SSM inventory and because some site-specific inventories may have significant abundances of the parent relative to its daughter.

The total inventory of each radionuclide is partitioned between the exchange volume and the melt glass zone following the distribution of radionuclides into the glass, rubble, gas, and water presented in Table 3-4. The radionuclide mass in the glass is distributed into the melt glass zone. The radionuclide mass in the rubble, gas, and water fractions are combined and distributed into the aqueous phase (pore space) of the exchange volume and the melt glass zone according to their relative pore volumes. This approach is consistent with the CAMBRIC HST model.

4.1.4 Sorption

The HST model for CAMBRIC represents sorption of radionuclides using a particle tracking code. In the particle tracking code, surface complexation and ion exchange reactions between radionuclides and reactive minerals in the alluvium are treated with a spatially variable sorption or partitioning model (Pawloski et al., 2001). The particle tracking code is limited to the simple linear isotherm or linear distribution (partitioning) coefficient (K_d) approach and assumes that groundwater chemistry is constant at ambient conditions. The distribution coefficient is defined as:

$$K_d = \frac{\text{Moles of solute per gram of solid phase}}{\text{Moles of solute per milliliter of solution}} \quad (4\text{-}3)$$

Recent analyses of a group of reactive minerals (smectite, calcite, iron oxide, zeolite, and illite/mica) in the Frenchman Flat alluvium (Carle et al., 2002 and Warren et al., 2002) were used to estimate the magnitude and spatial distribution of K_d values for several of the radionuclides included in the RST. Based on the spatial distribution of the reactive minerals, several alluvial layers were identified. K_d values for each of the layers were calculated using a mechanistic surface complexation/ion exchange model. Validation of this mechanistic model for alluvium of both Frenchman Flat and Yucca Flat is presented in Zavarin et al. (2002). A comparison of direct measurements of radionuclide sorption with the mechanistic model is also presented in SNJV (2005).

The distribution coefficients for the CAMBRIC SSM are presented in Table 4-2 for 10 elements (Ca, Cs, Sr, Ni, Am, Eu, Sm, Np, U, and Pu) in two media (the AL3 alluvium layer and the melt glass zone). The values for the average and

standard deviation of the logarithm of the distribution coefficients in Table 4-2 are based on data in Table D2 of (Tompson et al., 2005). Table 4-2 also present values for the mean and standard deviation of the distribution coefficients based on the natural logarithm and for the arithmetic mean and arithmetic standard deviation of the distribution coefficients. These latter values are calculated using the formulas in the note at the bottom of Table 4-2.

The SSM represents near-field transport through multiple one-dimensional pipe pathways. Each pathway samples K_ds from a lognormal distribution defined by the mean and standard deviations shown in Table 4-2. The four exchange volume transport pipes use the K_ds for the AL3 alluvial Layer and compressed zone and the single melt glass zone transport pipe uses the K_ds reported for the melt glass zone (Table 4-2). The SSM approach is similar to that for the particle tracking code in that it is based on a distribution of K_ds and assumes constant groundwater chemistry. The multiple pathways in the SSM, each of which independently samples K_ds from the lognormal distribution, provide a partial representation of the spatially varying permeability and sorption in the particle tracking code.

Table 4-2
Mean and Standard Deviation for the Log Normal Distributions of Kd Values for the CAMBRIC SSM

	Ca	Cs	Sr	Ni	Am	Eu	Sm	Np	U	Pu
AL3 Alluvium Layer and the Upper Compressed Zone										
Expected Value (Log K_d)	2.8	4.1	2.5	3.0	3.8	3.1	3.3	0.4	0.1	1.9
SD (Log K_d)	0.2	0.1	0.2	0.1	0.1	0.1	0.2	0.1	0.2	0.1
Expected Value (Ln K_d)	6.45	9.44	5.76	6.91	8.75	7.14	7.60	0.92	0.23	4.37
SD (Ln K_d)	0.46	0.23	0.46	0.23	0.23	0.23	0.46	0.23	0.46	0.23
Arithmetic Mean (K_d)	701.54	12927.45	351.60	1026.86	6479.07	1292.75	2218.46	2.58	1.40	81.57
Arithmetic SD (K_d)	340.98	3016.55	170.90	239.61	1511.86	301.65	1078.28	0.60	0.68	19.03
Melt Glass Zone										
Expected Value (Log K_d)	2.7	4.0	2.5	3.0	3.7	3.0	3.2	0.4	0.1	1.9
SD (Log K_d)	0.2	0.1	0.2	0.1	0.1	0.1	0.2	0.1	0.2	0.1
Expected Value (Ln K_d)	6.22	9.21	5.76	6.91	8.52	6.91	7.37	0.92	0.23	4.37
SD (Ln K_d)	0.46	0.23	0.46	0.23	0.23	0.23	0.46	0.23	0.46	0.23
Arithmetic Mean (K_d)	557.25	10268.64	351.60	1026.86	5146.51	1026.86	1762.19	2.58	1.40	81.57
Arithmetic SD (K_d)	270.85	2396.13	170.90	239.61	1200.91	239.61	856.51	0.60	0.68	19.03

Note: For a log-normal distribution (see Appendix B of the GoldSim manual), where Ln denotes the natural logarithm:
Expected value $\text{Ln}(K_d)$ = (Expected value $\text{Log}_{10}(K_d)$)/$\log_{10}(e)$ = λ,
Standard Deviation (SD) of Ln(Kd) = (SD $\text{Log}_{10}(K_d)$) /$\log_{10}(e)$ = ζ,
Arithmetic Mean = $\mu = \exp(\lambda + 0.5\zeta^2)$.
Number of significant figures reflect the exact model input

4.1.5 Glass Dissolution

The SSM incorporates the same simplified temperature-dependent glass dissolution model that is used for the particle tracking code in the HST model (Tompson et al., 2005). The following equation is used to calculate the rate of glass dissolution at a specified temperature in the particle tracking code:

$$r(\mathrm{T}) = k_0 \times e^{\frac{E_a}{\mathrm{R}}\left(\frac{\mathrm{T}-\mathrm{T}_0}{\mathrm{TT}_0}\right)} \times A_s \times \prod_i a_i^{n_i} \times \left(1 - \left(\frac{Q}{K}\right)^{1/\sigma}\right)^{\upsilon} + A_s k_f \qquad (4\text{-}4)$$

k_0 = Rate coefficient (mol/m^2/s) at reference temperature T_0, 298.16 K
E_a = Activation Energy, 15,000 cal/mol
R = Gas Constant, 1.98722 cal/Kmol
A_s = Reactive surface area of the glass (m^2/gram [g])
$\prod a_i^n$ = Product Terms of catalytic or inhibitive species (H^+ and OH^-)^i
Q = Activity Product
K = Solubility Product
σ, υ = Saturation Effect Coefficients
k_f = Close to Saturation Term (mol-glass/g sec)

The temperature history in the melt glass is derived from the transient flow model (Tompson et al., 2005). The glass temperature varies between 170ºC at early time to approximately 25ºC at approximately 10 years after the test (Tompson et al., 2005, Figure D5; see also Figure 4-4). Since the dissolution rate from Equation 4-4 is a function of the value of temperature, a lookup table based on the temperature history is included in the SSM. The values for this history are given in Table 4-3. This temperature history data were calculated from the CAMBRIC transient HST model (Tompson et al., 2005).

The rate equation (Equation 4-4) is incorporated into the SSM using the below five terms that are described in the following sections:

1. Arrhenius equation
2. Reactive surface area, A_s
3. Rate coefficient, k_0, and the product terms
4. Saturation terms Q and K
5. Close-to-saturation term, k_f

4.1.5.1 Arrhenius Term

The Arrhenius term, $e^{\frac{E_a}{\mathrm{R}}\left(\frac{\mathrm{T}-\mathrm{T}_0}{\mathrm{TT}_0}\right)}$, in Equation 4-4 is incorporated directly into the SSM; temperature is converted to degrees Kelvin before evaluating the exponential in the SSM. The Arrhenius term is used to establish the temperature dependance of the rate of the melt glass dissolution. The two constants included in this term, E_a and R, are the activation energy and gas constant, respectively. The activation energy describes the amount of energy required for melt glass dissolution to occur. An activation energy of 15,000 cal/mol was used in both the HST model and SSM.

Table 4-3
Temperature Time History in the Melt Glass for the SSM

Time (Years)	Temperature (°C)	Time (Years)	Temperature (°C)
0	170	7.374	27.54
0.00006	169.9	8.374	26.94
0.00019	169.7	9.0	26.63
0.00042	169.3	10.0	26.23
0.00090	168.5	10.4	26.09
0.00183	167.1	11.4	25.80
0.00345	164.7	12.4	25.56
0.00595	161.3	13.4	25.37
0.00939	157.0	14.4	25.20
0.01385	152.1	15.4	25.06
0.01950	146.7	16.4	24.93
0.02665	140.8	17.4	24.83
0.03584	134.4	18.4	24.74
0.04769	127.6	19.4	24.65
0.06269	120.6	20.4	24.58
0.08188	113.5	21.4	24.52
0.1067	106.1	22.4	24.46
0.1378	98.97	23.4	24.41
0.1765	92.04	24.4	24.36
0.2242	85.43	25.4	24.32
0.2828	79.16	26.4	24.28
0.3556	73.19	27.4	24.25
0.4476	67.45	28.4	24.21
0.5662	61.91	29.4	24.18
0.7227	56.56	49.0	23.94
0.9342	51.4	73.8	23.78
1.000	49.96	98.7	23.71
1.293	45.46	100	23.71
1.726	41.05	156	23.66
2.374	36.93	218	23.64
3.374	33.26	280	23.63
4.374	30.95	500	23.63
5.374	29.41	1000	23.63
6.374	28.33		

ºC = Degrees Celsius

4.1.5.2 Reactive Surface Area

A bulk value for the reactive surface area of 0.001 m^2/g was used for the steady state CAMBRIC HST model as well as the SSM. This value accounts for the contribution of brecciated and vesicular glass zones as well as massive glass zones to the reactive surface, and provides for the likelihood that hydrous phases will

precipitate and reduce permeability. This is considered a fairly conservative estimate in the sense that the surface area is not underestimated (Tompson et al., 2005). In the HST model, and the SSM, the surface area of glass was allowed to decrease linearly with the amount of glass dissolved.

4.1.5.3 Rate Coefficient and Product Terms

The rate coefficient and product terms are combined to determine the dissolution rate (mol-glass/m^2 sec) of glass far from saturation. Dacite (63.24 percent silica [SiO_2]) dissolution data, fit to a V-shaped polynomial, is used to account for the effect of pH on the rate of melt glass dissolution (Tompson et al., 2005, Figure D2). The rate at which glass dissolves is greatly affected by its silica content. The dissolution rate was, therefore, adjusted for a glass with 65.1 percent SiO_2. The glass dissolution rate was adjusted by -0.056 log units in mol/m^2/sec (0.03 log units for each percent increase in SiO_2 content). The resulting polynomial is described as the sum of three linear rates, a pH dependant rate at low pHs (a_{pH}), a pH independent rate at intermediate pHs (a_{ind}), and a pOH dependent rate at high pHs (a_{pOH}):

$$\log(a_{pH}) = \log(1.7519\times10^{-9}) - 0.482474(\mathrm{pH(T)}) \tag{4-5}$$

$$\log(a_{ind}) = \log(1.43522\times10^{-11}) \tag{4-6}$$

$$\log(a_{pOH}) = \log(1.59906\times10^{-8}) - 0.551795(\mathrm{pOH(T)}) \tag{4-7}$$

These three rates are combined as follows:

$$a(\mathrm{T}) = 10^{a_{pH}} + 10^{a_{ind}} + 10^{a_{pOH}} \tag{4-8}$$

and substituting from Equations 4-6 through 4-8:

$$a(\mathrm{T}) = 1.7519\times10^{-9}\times10^{-0.482474(\mathrm{pH(T)})} + 1.443552\times10^{-11} + 1.59906\times10^{-8}\times10^{-0.551795(\mathrm{pOH(T)})} \tag{4-9}$$

The units of a(T) are mole/m^2/sec where one mole of glass is defined as 100 g.

The pH and pOH vary as a function of temperature because of water dissociation. The dissociation coefficient of water, K_w, as a function of temperature, was fit to the following polynomial based on K_w data from the EQ3/6 database (Tompson et al., 2005, Appendix C2.1):

$$\log(K_w(\mathrm{T})) = 6.1485\times10^{-10}\mathrm{T}^4 - 4.9425\times10^{-7}\mathrm{T}^3 + 1.9154\times10^{-4}\mathrm{T}^2 - 4.1691\times10^{-2}\mathrm{T} + 14.935 \tag{4-10}$$

Where T is in ºC.

The pH and pOH as a function of temperature are based on the value of K_w of water and a pH of 8.4 at 25ºC as:

$$pH(T) = -\log\left(\frac{1}{2}\left(-2.48\times10^{-6} + \sqrt{(2.48\times10^{-6})^2 + 4K_w(T)}\right)\right) \quad (4\text{-}11)$$

$$pOH(T) = -\log(K_w(T) - pH(T)) \quad (4\text{-}12)$$

4.1.5.4 Glass Saturation Term

The saturation term, $\left(1-\left(\frac{Q}{K}\right)^{1/\sigma}\right)^{\upsilon}$ is used to account for the decrease in the melt glass dissolution rate as the groundwater approaches saturation with respect to the glass. The glass dissolution model is limited to the effect of SiO_2. The value of Q is, therefore, the concentration of SiO_2 in the groundwater and K is the SiO_2 concentration at glass "saturation" for the specific composition of the melt glass (Tompson et al., 2005).

The saturation term was determined by fitting the solubility of β-cristobalite and amorphous silica as a function of temperature to the following polynomial:

$$1-\frac{Q(T)}{K(T)} = 4.1559\times10^{-11}T^4 - 5.8913\times10^{-8}T^3 + 2.1665\times10^{-5}T^2 - 4.1143\times10^{-3}T + 0.58456 \quad (4\text{-}13)$$

Although recent glass dissolution experiments close to saturation suggest that the σ term may be as high as 100 (Zavarin et al., 2004a, b), sufficient evidence was not available to confidently apply this exponent to the CAMBRIC HST model (Tompson et al., 2005). This term may significantly reduce the estimated dissolution. Thus, excluding it would result in a conservative estimate of the saturation term and; therefore, of the rate of glass dissolution. Hence, the SSM assumes that $\sigma = 1$ and $\nu = 1$ in the saturation term.

4.1.5.5 Close-to-Saturation Rate

Glasses exhibit a saturation effect similar to that of crystalline solids where the dissolution rate slows as species build up in solution. However, due to the unstable nature of glasses, dissolution is expected to continue even when solutions are at saturation with amorphous silica. The close-to-saturation rate accounts for this slow rate. Typically, this rate is several orders of magnitude slower than the dissolution rate far from saturation. In the CAMBRIC steady state model, SiO_2 concentrations in solution were not allowed to build up to levels high enough to make the close-to-saturation rate significant, and thus the close-to-saturation rate of glass dissolution is ignored in the particle model (Tompson et al., 2005,

Appendix C1.4). The close-to-saturation term is, therefore, set equal to zero in the SSM.

4.1.5.6 Numerical Comparisons

Figure 4-4 through Figure 4-7 provide comparisons of glass dissolution rates for the CAMBRIC HST and SSM. Figure 4-4 presents a comparison of the glass temperature time histories and confirms that the SSM has the correct temperature history. Figure 4-5 presents a comparison of the glass dissolution rates and indicates that the calculated rates for the HST and SSM are very close. Figure 4-6 presents a comparison of the percent glass dissolved for the HST and SSM. The differences in this figure are probably due to differences in the numerical integration of the glass dissolution differential equation. The information for the HST is based on a first order numerical integration scheme, while the results from the SSM more closely match a third order Runge-Kutta integration scheme (not shown on the plot). These differences are not considered significant, because the releases from the melt glass are a minor contribution to total release, as discussed further in Section 4.3. Finally, the percent of glass dissolved data are replotted on a linear, rather than a logarithmic, scale in Figure 4-7. This figure demonstrates that the dissolution rate is linear except at very early times (less than one year) when the thermal effects on glass dissolution are significant. Approximately 0.3 percent of the melt glass dissolves rapidly over the first month.

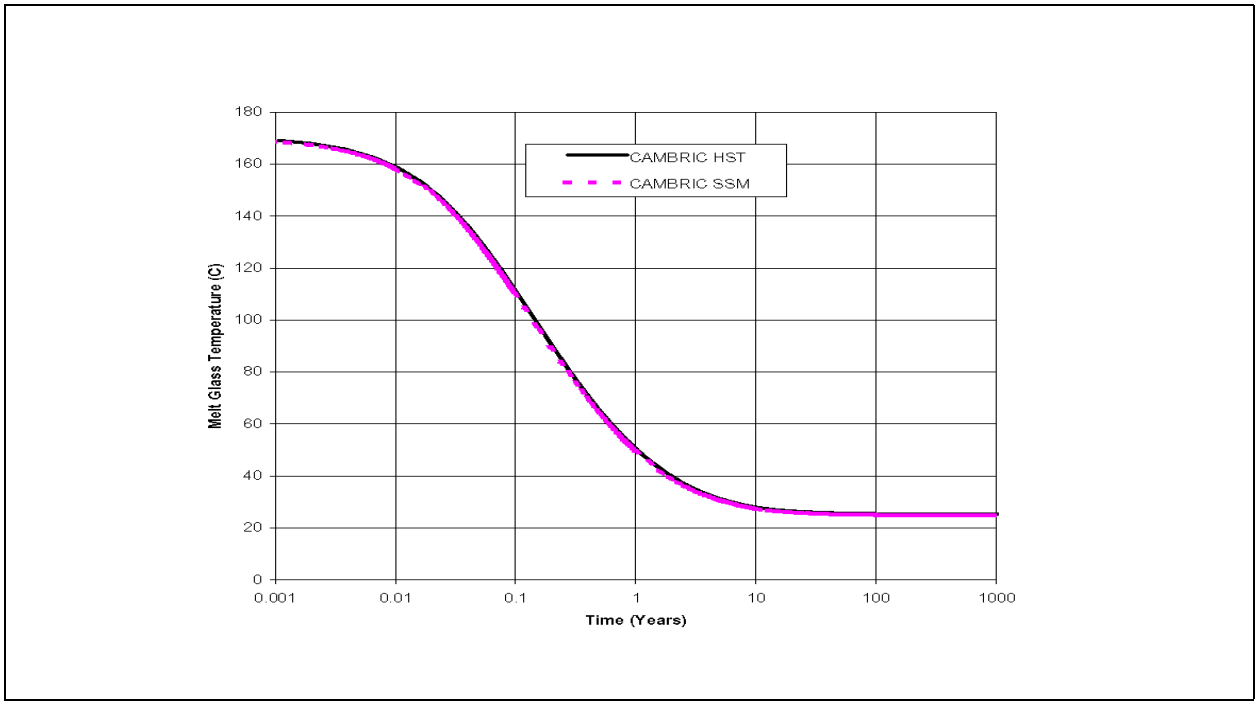

Figure 4-4
Comparison of Melt Glass Temperature Histories

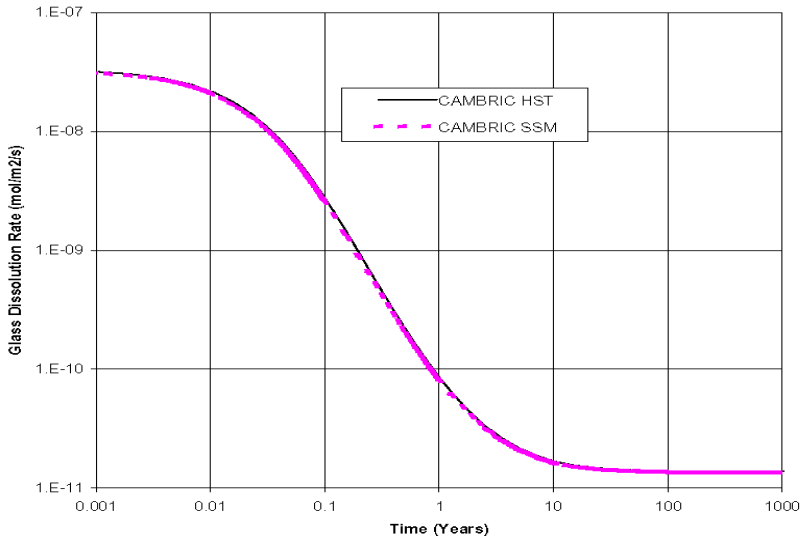

Figure 4-5
Comparison of Glass Dissolution Rate Histories

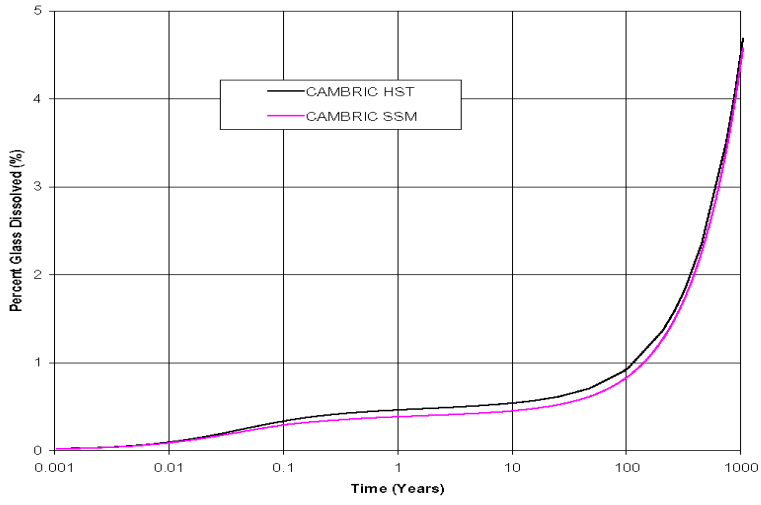

Figure 4-6
Comparison of Percent Melt Glass Dissolved Over Time - Log Scale

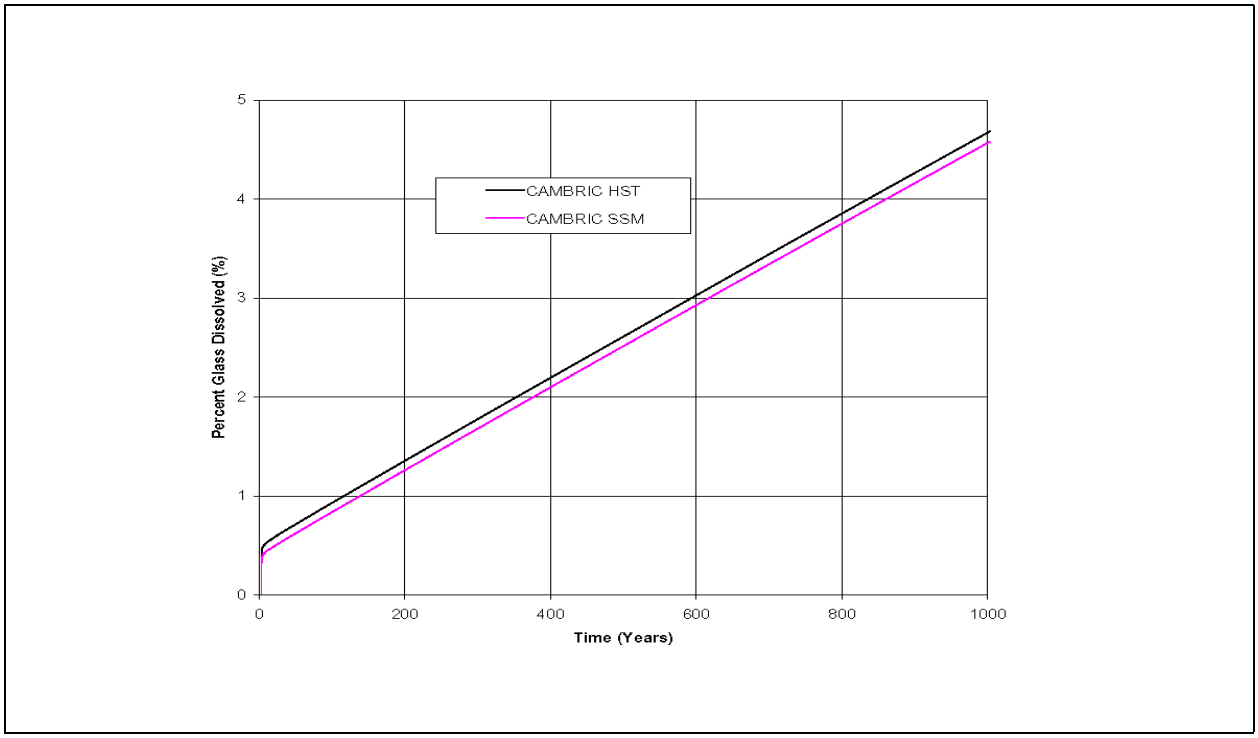

Figure 4-7
Comparison of Percent Melt Glass Dissolved Over Time - Linear Scale

4.2 Simplified Source Term Model Calibration

The initial conceptual model for the tracers in the SSM utilized a single exchange volume cell and a single melt glass zone cell each discharging through a corresponding single flow pathway to the release point at the P1 plane. The free parameters in the conceptual model relate to the pipe pathways, because the properties of the exchange volume and melt glass zone are fixed by the cavity geometry and the porosities of the various cavity units (melt glass zone, cavity zone, and compressed regions).

The free parameters for the pipe pathways are their length, cross-sectional flow area, and the groundwater flow rate through the pipes. Since the SSM will be scaled to other tests at Frenchman Flat, the pipe lengths were initially fixed at 23.03 m, the distance from the center of the CAMBRIC test to the P1 plane. The cross-sectional flow area of the total exchange volume, 807.8 m^2 and the melt glass zone, 152.4 m^2 were initially fixed at the corresponding characteristic areas.

The CT Module is a mass transport model, not a flow model, and does not directly solve for the movement of groundwater through the hydrological system. The cell and pipe pathways in the SSM, therefore, model mass transport. In this situation, the fluxes between the exchange volume and the transport pipe pathway, Q_{EV}, and between the melt glass zone and transport pipe pathway, Q_{MGZ}, must be defined in an appropriate manner. Since the cross-sectional flow area are fixed, the flow rate is the free parameter used for comparison to the results of the HST model.

The flow rate distributions were developed using a three step process:

1. Define the flow rates from the exchange volume based on the groundwater tracers. The groundwater tracers, ^{3}H, ^{14}C, ^{39}Ar, and ^{85}Kr, are radionuclides that are deposited in the pore waters of the exchange volume and melt glass zone and are immediately available for release and transport. The nuclear melt glass has no mass of the groundwater tracers (see Table 3-4) and there is no retardation for these species. These radionuclides arrive relatively quickly at the P1 plane.

2. Define the flow rates from the melt glass zone based on the melt glass tracers. The melt glass tracers are ^{36}Cl, ^{93}Zr, ^{94}Nb, ^{99}Tc, ^{107}Pd, ^{121}Sn, ^{126}Sn, and ^{129}I. These radionuclides are deposited in the pore waters of the exchange volume and the melt glass zone and are also in the nuclear melt glass. The fraction in the pore waters is immediately available for transport and arrives very quickly at the P1 plane, because there is no retardation for these species. The fraction in the nuclear melt glass is released over time as the glass dissolves. The fraction in the melt glass has relatively little impact on releases at the P1 plane, as explained in Section 4.2.3.

3. Examine the breakthrough curves for the retarded radionuclides. The elements Ca, Ni, Sr, Cs, Sm, Eu, Ho, U, Np, Pu, and Am are assigned K_ds in the HST model and the SSM.

It is important to note that several of the radionuclides identified above as tracers (^{93}Zr, ^{94}Nb, ^{107}Pd, ^{121}Sn, and ^{126}Sn) are known to sorb but are treated as tracers in the HST, and thus the SSM, due to the lack of availability of surface complexation/ion exchange data. This is a conservative approach and may be adjusted for the Frenchman Flat CAU transport model.

The three-step process is a reasonable approach, because it allows the effects of the 3-D permeability field as evaluated in Steps 1 and 2 to be separated from the effects of the 3-D K_d field in Step 3. Ideally, the conceptual model and groundwater fluxes determined in Steps 1 and 2 could be directly transferred to Step 3 without change.

The distribution for groundwater flow rates for the transport pipes associated with the melt glass zone and exchange volume are adjusted in an iterative process that provides the best match to the initial arrival times for each tracer, the mass fluxes at 1,000 years, the end of the simulation, and the initial peak mass fluxes. The iterative calibration process first performed individual calculations to determine the groundwater flux that matched the mean, 5^{th} percentile, and 95^{th} percentile breakthrough curves, and then combined these results into a distribution for groundwater flow rate that is sampled stochastically in the SSM. The pipe length and area were initially held constant during the stochastic sampling for groundwater flow rate.

While a single pathway was able to represent the transport and release of tracer radionuclides at the P1 plane, this approach was unable to represent the breakthrough curves for the sorbed radionuclides from the exchange volume.

Extensive testing indicated that a single pathway in the SSM provides too much retardation in comparison to the HST for the radionuclides in the exchange volume. Intuitively, a 3-D transport model has more degrees of freedom than a one-dimensional (1-D) transport model, so a 1-D model like the SSM tends to restrict transport more severely than a 3-D model. The 3-D transport model produces a range of flow pathways, including pathways that are both faster and slower than an average flow path. Depending on the distribution of travel times in the 3-D pathways, the mean breakthrough curve for the 3-D model could be faster or slower than a comparable 1-D model with a given fluid flux.

Several multiple pathway models were created and tested before choosing the conceptual model shown in Figure 4-3. These alternate conceptual models included the following variations:

- A single exchange volume discharging through four pipe pathways. The distribution coefficients for the exchange volume are set to the mean K_d for each radionuclide and the distribution coefficients for the four pipe pathways are independently sampled from the log-normal distributions defined in Table 4-2.

- The exchange volume is divided into four parts, each of which has its own pipe pathway. The distribution coefficients in each of the four exchange volume cells and the four pipe pathways are sampled independently from the log-normal distributions defined in Table 4-2.

- The exchange volume is divided into four parts; each with its own pipe pathway. The distribution coefficients in each pair of exchange volume cell and pipe pathway are equal based on the sampled values from the log-normal distributions in Table 4-2.

The results with these alternate conceptual models were essentially identical; indicating that the multiple pathways are the key difference between the HST and SSM for transport of sorbed radionuclides rather than the detailed sampling scheme for the distribution coefficients. The third option is chosen for the SSM, because it produces incrementally better comparisons with the HST model. The differences are really not significant in comparison to other uncertainties in the SSM, such as the inventory at other sites in Frenchman Flat.

The distribution of flow within the four transport pipes of the exchange volume is based on a random sampling of flow area and flow velocity for each transport pipe. If r_1, r_2, r_3, and r_4 are four independently sampled random numbers between 0 and 1, then the flow area of each transport pipe is calculated as:

$$A_i = \frac{r_i}{r_1 + r_2 + r_3 + r_4} A_{EV} \qquad (4\text{-}14)$$

where A_i is the flow area for the i^{th} pipe pathway and A_{EV} is the characteristic area of the total exchange volume. The flow rate in each pipe connected to the exchange volume is sampled independently from the distribution of flow velocities. This approach results in a different flow velocity in each of the four pipes.

Two additional changes were made to the transport model during this final recalibration. The first change is that the exchange volume is represented as a source of finite length for the transport pathways. This change is appropriate, because the distance to the P1 plane, 23.03 m, is less than the diameter of the compressed zone, 36.2 m. In this situation, the exchange volume is not a point source for releases to the P1 plane. Within GoldSim®, the lengths of the transport pipes from the exchange volume to the P1 plane are increased by the radius of the compressed zone (18.1 m), from 23.03 m to 41.13 m. In addition, the length of the source for each transport pipe increased from 0 (a point source) to the diameter of the compressed zone (36.2 m). Similar changes were not made for the melt glass zone, because it has a relatively small volume and because it has a small contribution to releases over 1,000 years. Dispersivity for all transport pipes was set to 10 percent of the pathlength.

4.2.1 Calibration for Groundwater Tracers

Lognormal distributions of flow velocities (arithmetic mean and standard deviation of 0.020 m/yr) for the exchange volume transport pipes provided the best fit to groundwater tracer results of the HST. These flow velocities are relatively consistent with those of the HST. Mean flow velocities of 0.051 and 0.068 m/yr are estimated as the product of the mean horizontal conductivity (84.7 m/yr for CHM1 and AL3) and the estimated hydraulic gradient for CAMBRIC, 0.0006 to 0.0008 (Tompson et al., 2005, Section 3.1). Similarly, mean flow velocities of 0.002 and 0.003 m/yr are estimated for the compressed zone using the mean horizontal conductivity (3.65 m/yr) reported in Tompson et al. (2005). The range of calibrated flow velocities for the SSM falls well within the range of mean flow velocities estimated for the AL3, CHM1, and compressed zones in the HST.

4.2.2 Comparison of HST and SSM Results for Groundwater Tracers

Comparisons of the HST and SSM for the mean, 5th percentile, and 95th percentile breakthrough curves at the P1 plane for ^{3}H, ^{14}C, ^{39}Ar, and ^{85}Kr are presented in Figure 4-8 through Figure 4-11. The results from the HST are shown as a solid red line (mean flux) and as solid grey lines (5th percentile and 95th percentile fluxes). The results from the SSM are shown as a solid black line (mean flux) and as dashed black lines (5th percentile and 95th percentile fluxes). Computational testing with the SSM demonstrated that 100 realizations and 200 realizations produced essentially identical results for the mean, 5th percentile, and 95th percentile breakthrough curves. The SSM results in Figure 4-8 through Figure 4-11 and throughout this document are based on calculations with 100 realizations.

The agreement between the breakthrough curves for the HST model and the SSM for the groundwater tracer radionuclides is relatively good, as shown in these figures. In general, the shape of the breakthrough curves are quite similar, although the breakthrough over the first approximately 20 to 30 years is greater for

the SSM. Also, the flux at 1,000 years is slightly higher for ^{39}Ar and ^{85}Kr for the SSM. This is considered acceptable since the SSM is predicting greater mass fluxes, which is a conservative estimate.

The correlation coefficient between two variables is a measure of similarity and can be used as a measure of closeness between outputs from the HST model and the SSM. Values close to one represent a good match between the two models. The correlation coefficients for ^{3}H, ^{14}C, ^{39}Ar, and ^{85}Kr are 0.98, 0.96, 0.98, and 1.0, respectively. This indicates a good match between the results of the SSM and the HST for these radionuclides.

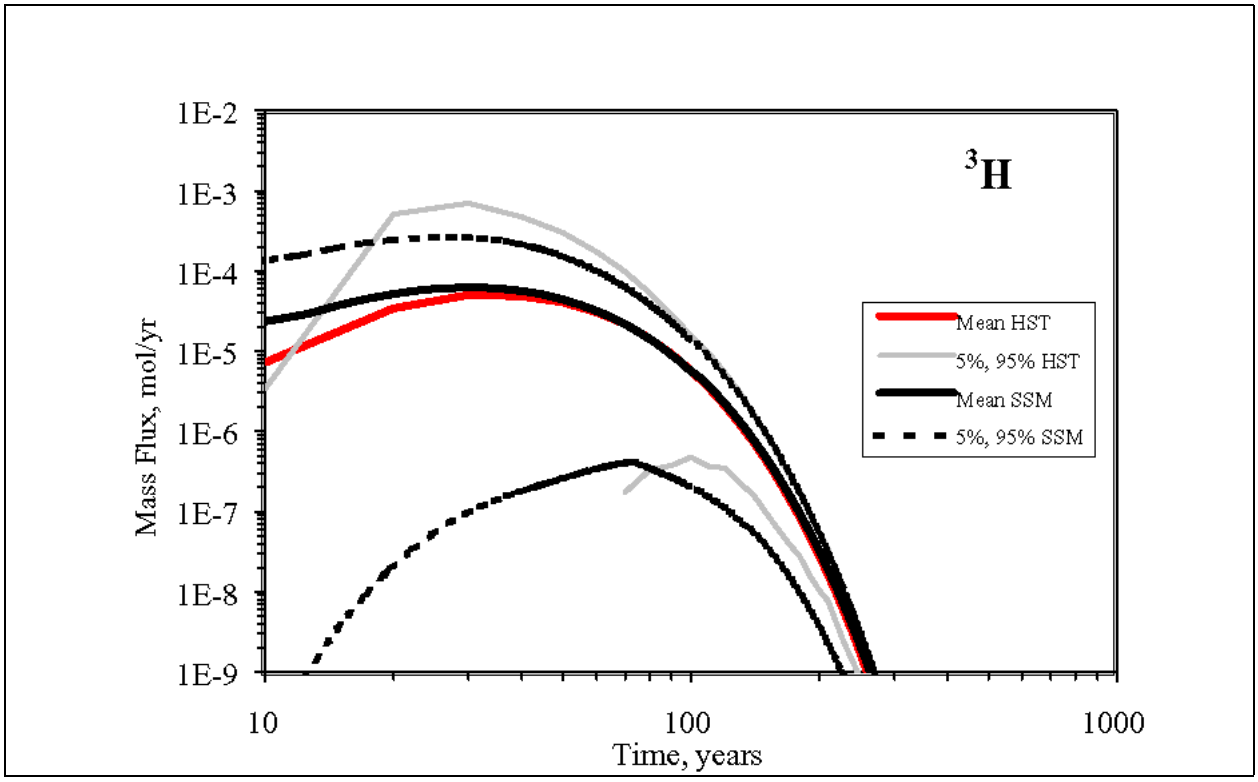

Figure 4-8
Comparison of Mass Fluxes for Tritium from the HST and SSM at the P1 Plane

4.2.3 Calibration for Melt Glass Tracers

The fraction of melt glass tracer in the nuclear melt glass has little impact on total release because only a small fraction of the melt glass dissolves after 1,000 years, thereby limiting the mobilization from this source. Figure 4-6 and Figure 4-7 demonstrate that less than 5 percent of the nuclear melt glass dissolves after 1,000 years, restricting the mobilization of melt glass tracers from the glass. For example, ^{36}Cl has a 50-50 distribution of its initial mass within the nuclear melt glass and the pore water in the exchange volume. The initial mass in the exchange volume is mobilized for immediate transport. However, less than (0.05) (0.50) or 2.5 percent of the initial mass in the nuclear melt glass is mobilized, even after

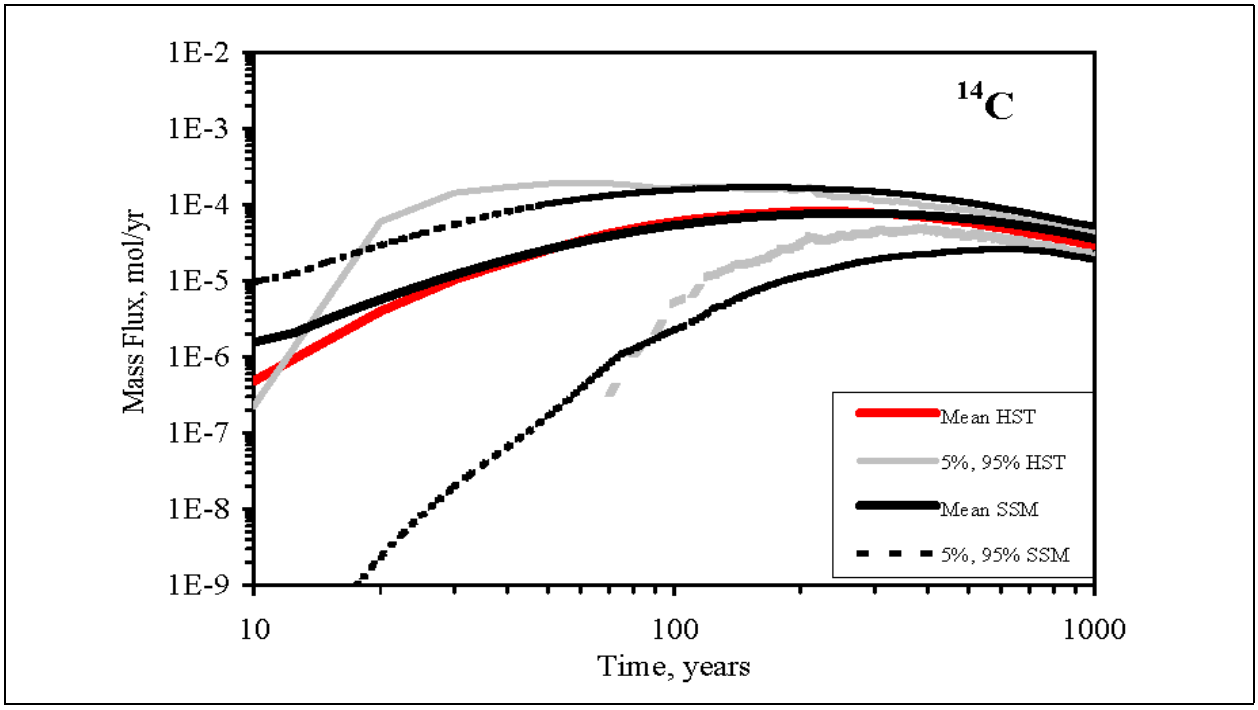

Figure 4-9
Comparison of Mass Fluxes for ^{14}C from the HST and SSM at the P1 Plane

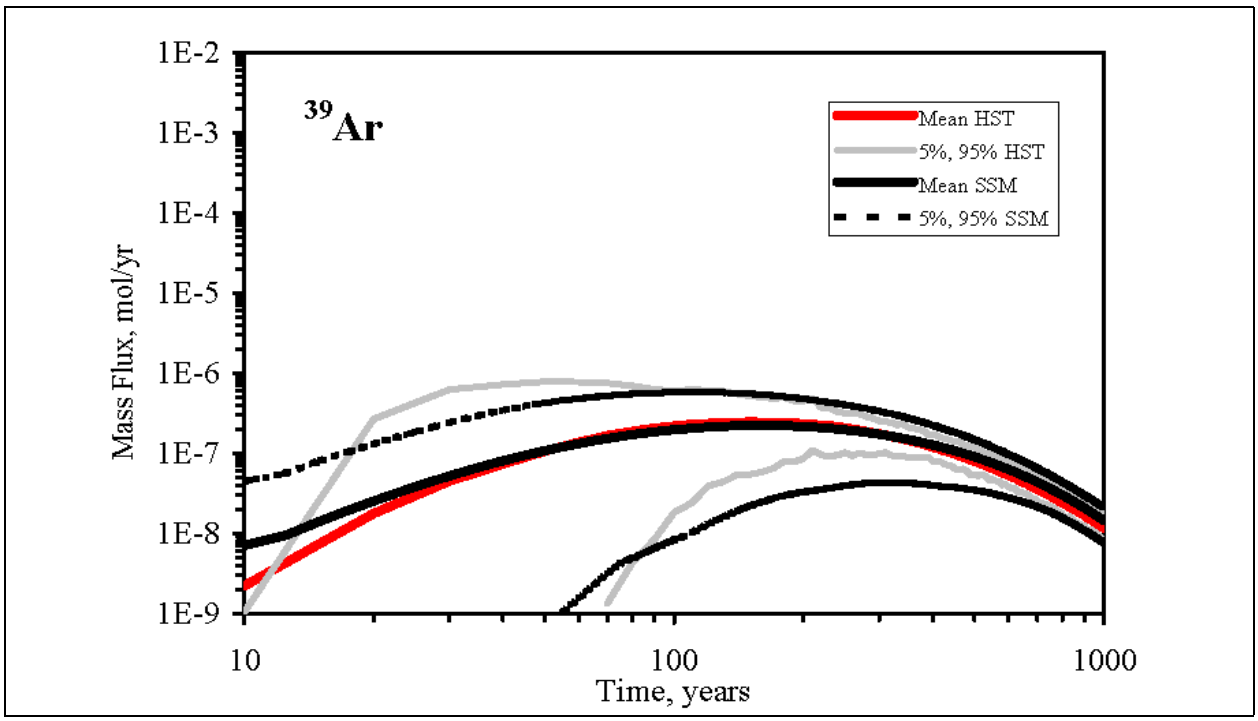

Figure 4-10
Comparison of Mass Fluxes for ^{39}Ar From the HST and SSM at the P1 Plane

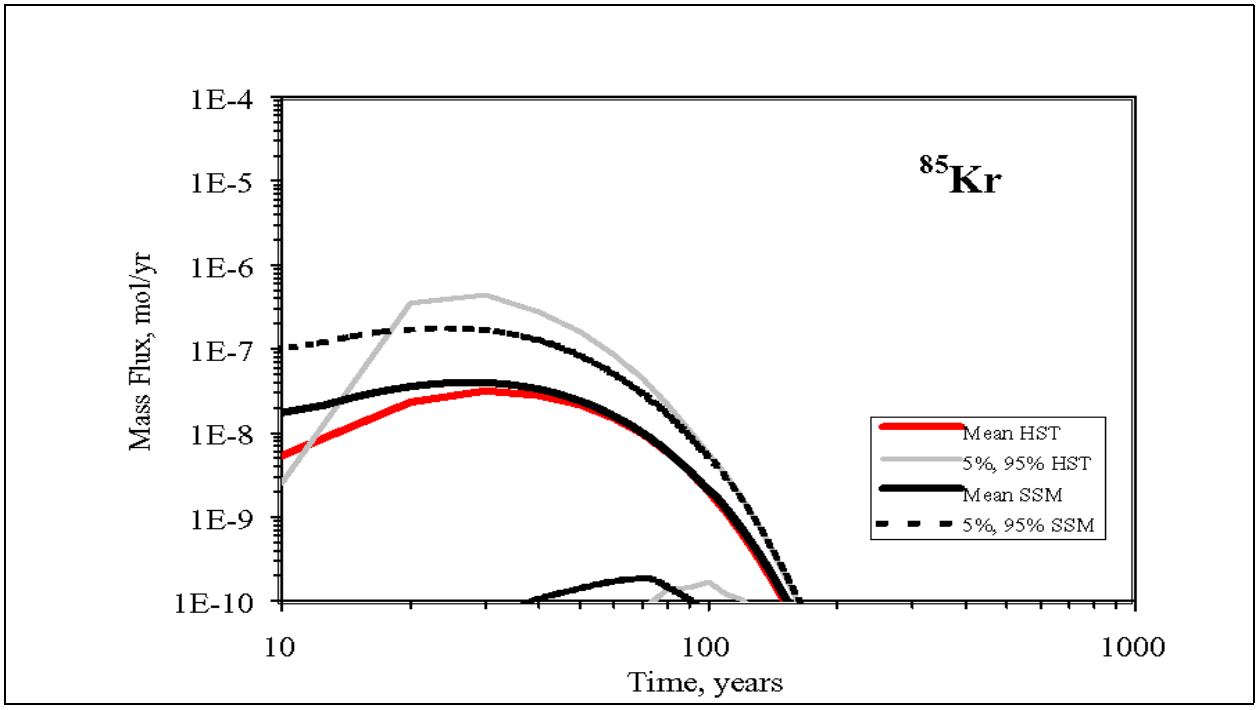

Figure 4-11
Comparison of Mass Fluxes for ^{85}Kr From the HST and SSM at the P1 Plane

1,000 years. Clearly the release from the exchange volume is the major contribution to total release.

The initial distribution of radionuclides with 5 percent of their initial mass in the exchange volume and 95 percent of the initial mass in the nuclear melt glass is more skewed. The initial mass in the exchange volume is mobilized for immediate transport. After 1,000 years, (0.05)(0.95) or 4.75 percent of the initial mass in the nuclear melt glass can be mobilized, comparable to the initial inventory in the pores of the exchange volume. However, the release from the exchange volume is still the major contribution to total release for at least the first few hundred years.

This qualitative argument is confirmed by the results from the HST model for CAMBRIC. The HST model does not calculate release and transport for the individual groundwater and melt glass tracer radionuclides. Instead, it is more computationally efficient to perform a single calculation for the release of a nonradioactive tracer element from the pore water of the exchange volume and to perform a single calculation for the release of a nonradioactive tracer element from the nuclear melt glass. Figure 4-12 and Figure 4-13 present comparisons of the mean breakthrough curves for a nonradioactive tracer from the pore waters of the exchange volume (groundwater flux), and from the melt glass (melt glass flux). Comparisons are presented for a tracer that is distributed 50 percent in the melt glass (Figure 4-12) and one that is distributed 95 percent within the melt glass (Figure 4-13). It is clear from these figures that the groundwater flux, from the

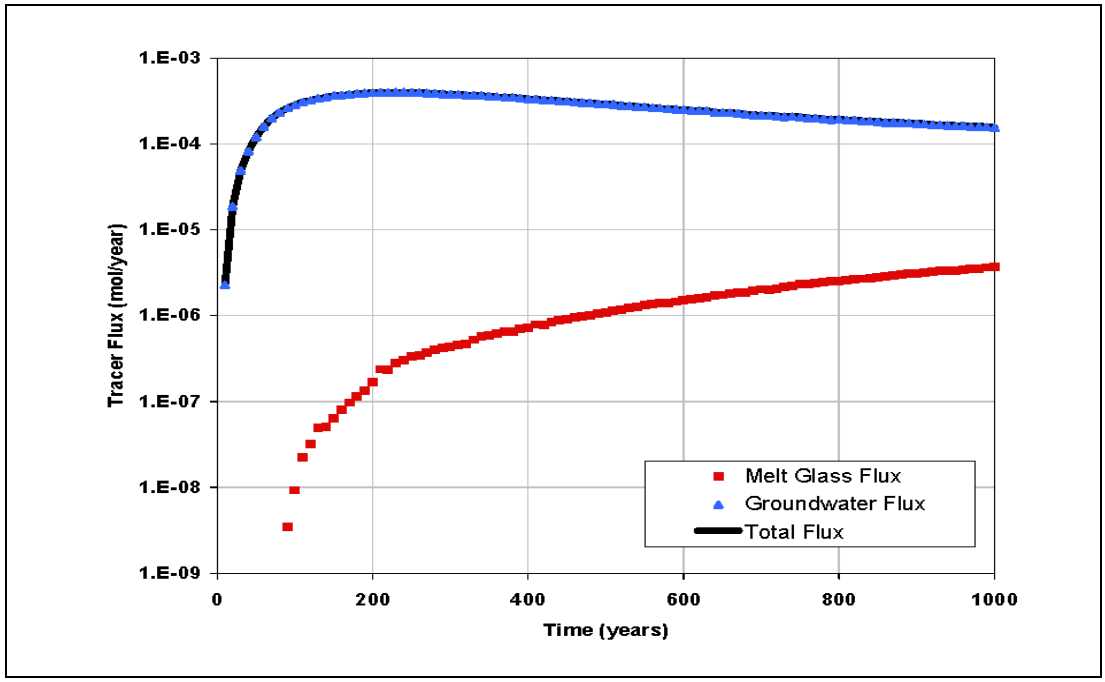

Figure 4-12
Comparison of Mean Fluxes from Groundwater and Melt Glass from the CAMBRIC HST Model for Radionuclides with 50 Percent Distribution in the Melt Glass

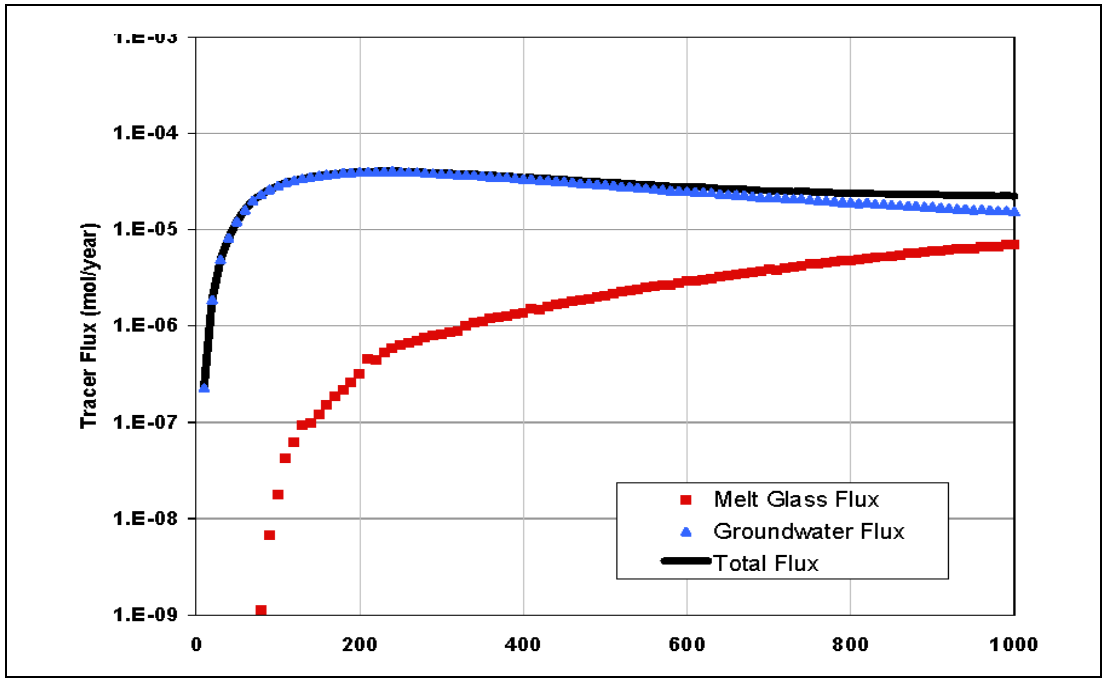

Figure 4-13
Comparison of Mean Fluxes From Groundwater and Melt Glass from the CAMBRIC HST Model for Radionuclides with 95 Percent Distribution in the Melt Glass

pores of the exchange volume, is the dominant contribution to the radionuclide flux at the P1 plane for the HST, particularly for the first few hundred years.

The iterative calibration process for the melt glass zone using the melt glass tracers produced the best results using a lognormal distribution defined with a mean and standard deviation of 0.018 m/yr. Mean flow velocities of 0.033 and 0.044 m/yr are estimated as the product of the mean horizontal conductivity (54.8 m/yr for the melt glass zone) and the estimated hydraulic gradient for CAMBRIC, 0.0006 to 0.0008 (Tompson et al., 2005, Section 3.1). Similar to the flow velocities for the exchange volume, the calibrated flow velocities for the melt glass zone in the SSM are similar, but slightly less, than those of the HST.

4.2.4 Comparison of HST and SSM Results for Melt Glass Tracers

Figure 4-14 presents the comparison of the mean, 5th percentile, and 95th percentile breakthrough curves at the P1 plane for ^{129}I from the HST with the SSM. The mass of ^{129}I is distributed 50:50 between the exchange volume/melt glass zone and the melt glass. The results from the HST are shown as a solid red line (mean flux) and as solid grey lines (5th percentile and 95th percentile fluxes). The results from the SSM, based on a calculation with 100 realizations, are shown as a solid black line (mean flux) and as dashed black lines (5th percentile and 95th percentile fluxes). The agreement between the HST and SSM for ^{129}I is quite good. Figure 4-15 and Figure 4-16 present similar comparisons for ^{36}Cl, with a 50-50 distribution of mass between the exchange volume/melt glass zone and melt glass, and ^{99}Tc**,** with a 80-20 distribution of mass between the exchange volume/melt glass zone and melt glass. The correlation coefficient between the mass flux results of the SSM and the HST model were 0.94, 0.94, and 0.89 for ^{129}I, ^{36}Cl, and ^{99}Tc, respectively. Similar to the groundwater tracers, ^{39}Ar and ^{85}Kr, mass fluxes for the melt glass tracers over approximately the first 20 years, and at 1,000 years, are greater for the SSM than the HST model. Again, this is considered acceptable because this is a conservative estimate.

4.2.5 Comparison of HST and SSM Results for ^{238}U, ^{237}Np, ^{239}Pu, and ^{59}Ni

Four radionuclides, ^{238}U, ^{237}Np, ^{239}Pu, and ^{59}Ni, have been selected to represent the comparisons between the HST model and SSM for the sorbed radionuclides. The comparison for ^{238}U (Figure 4-17) is relatively good. The comparison for ^{237}Np is acceptable (Figure 4-18), although the breakthrough curve for the SSM is delayed in comparison to the breakthrough curve for the HST. Although breakthrough is observed for ^{239}Pu and ^{59}Ni from the HST model (Figure 4-19 and Figure 4-20), no breakthrough is observed using the SSM. Contrary to the HST model results, no breakthrough is observed for the majority of the sorbing radionuclides using the SSM. Small breakthrough fluxes over the 1,000-year period were observed at the P1 plane for the majority of the sorbing radionuclides for the HST model. This is expected to be a result of the molecular diffusivity incorporated in the HST model. Since the RST is distributed throughout the cavity in the HST model, diffusive

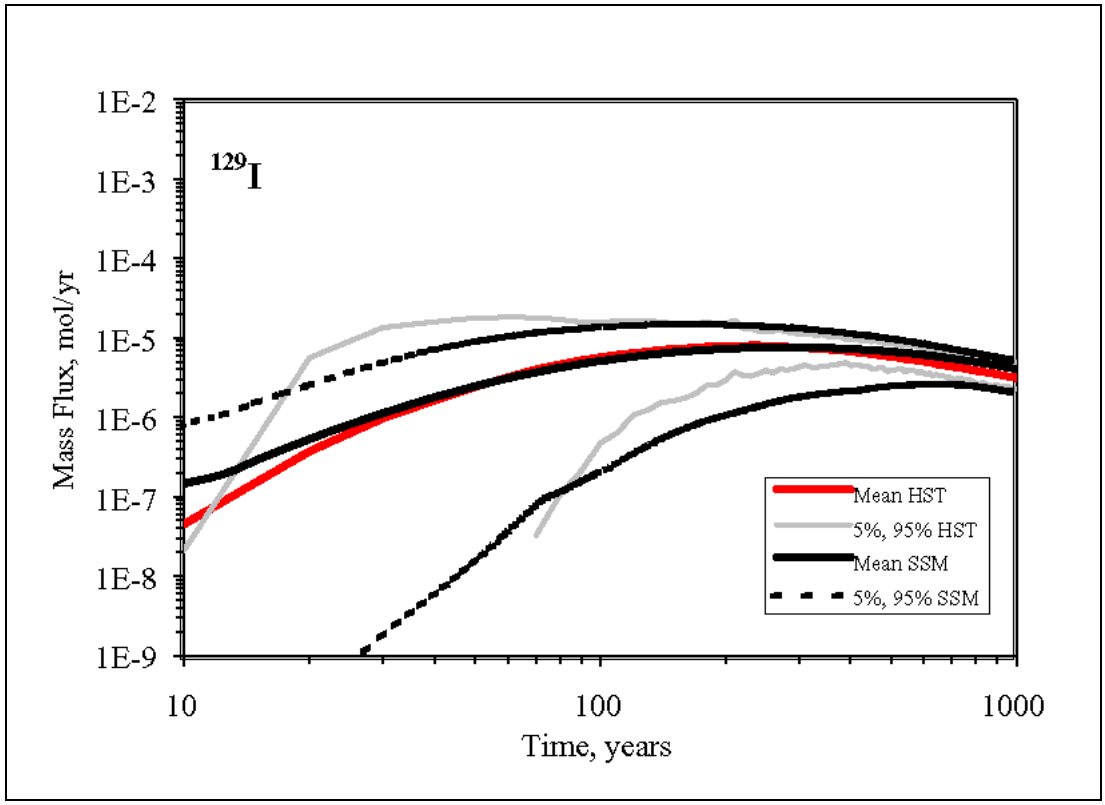

Figure 4-14
Comparison of Mass Fluxes for ^{129}I From the HST and SSM at the P1 Plane

transport to the nearby Pl plane (a distance of less than 10 m from the cavity edge) is likely to occur.

Diffusive transport is less significant for transport to the P2 and P3 planes, which are 80 and 256 m from the cavity edge, respectively. This is clear from the HST breakthrough fluxes presented by Tompson et al. (2005, Figure 8). No breakthrough is observed for the majority of the sorbing radionuclides (Ni, Sr, Cs, Sm, Eu, Ho, Pu, and Am) at the P2 and P3 planes over the 1,000-year time span. Currently, the SSM does not include diffusivity in the same manner as that of the HST model.

Breakthrough curves for all sorbing radionuclides, are shown in Appendix D. These figures demonstrate that the lower 5th percentile of the HST model results for the sorbing radionuclides, consist of zero mass fluxes. This indicates that although the SSM is not matching the mean breakthrough for the majority of the sorbing tracers, the results are within the 95 percent confidence limit of the HST model.

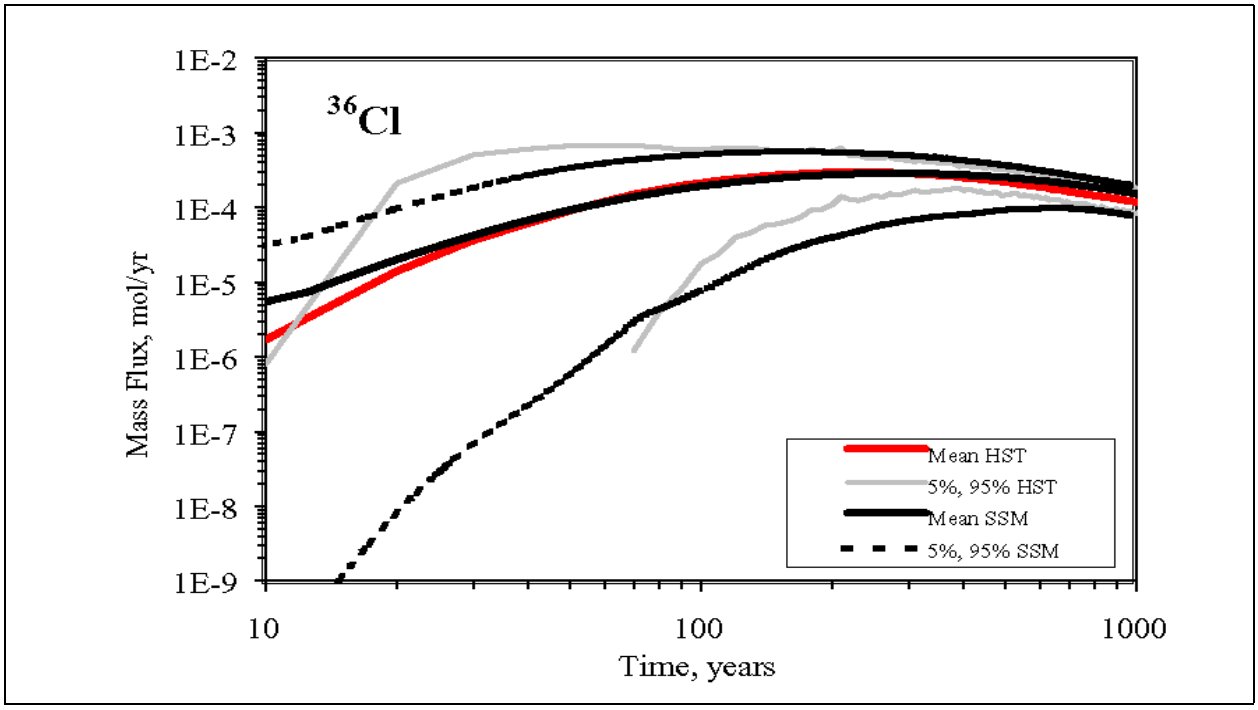

Figure 4-15
Comparison of ^{36}Cl Mass Fluxes from the HST and SSM at the P1 Plane

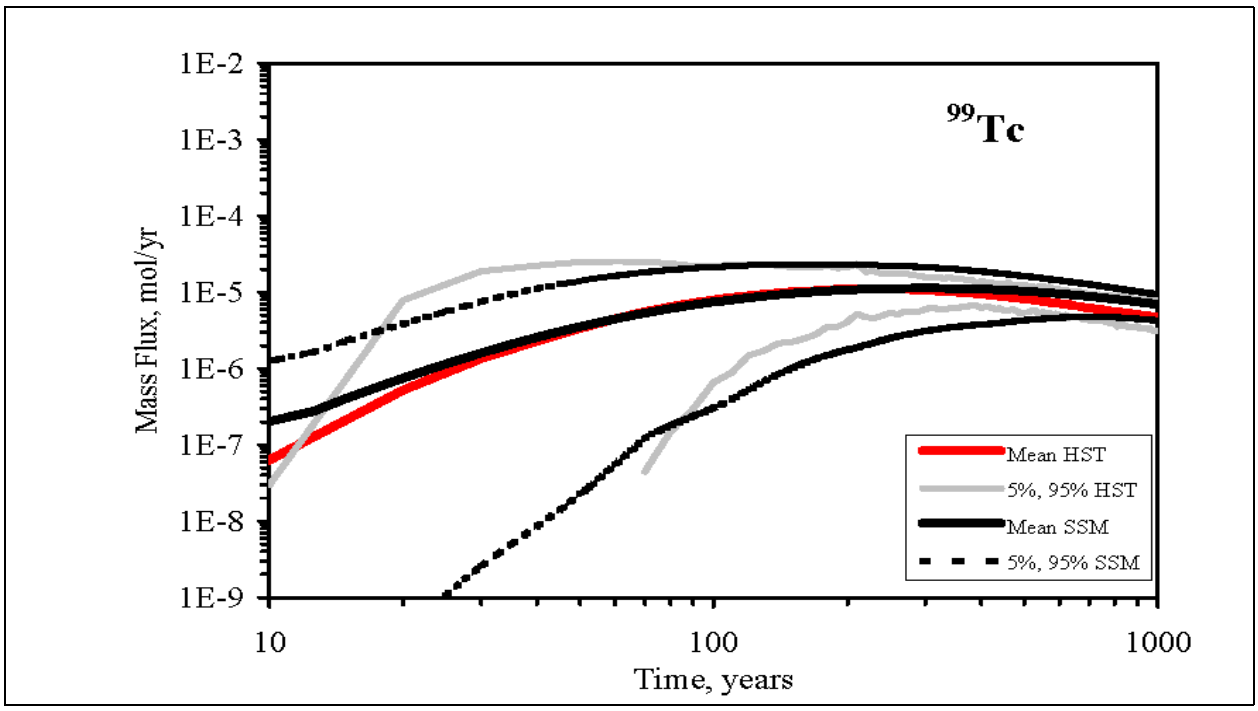

Figure 4-16
Comparison of ^{99}Tc Mass Fluxes from the HST and SSM at the P1 Plane

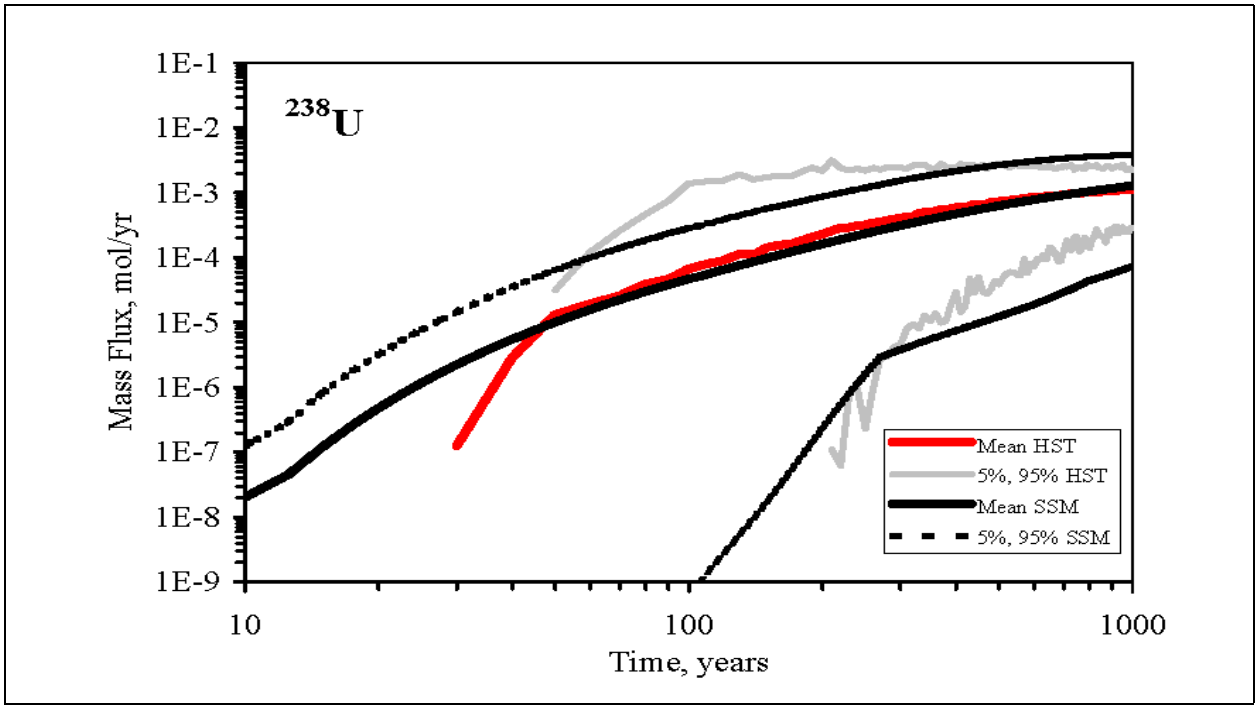

Figure 4-17
Comparison of ^{238}U Mass Fluxes from the HST and SSM at the P1 Plane

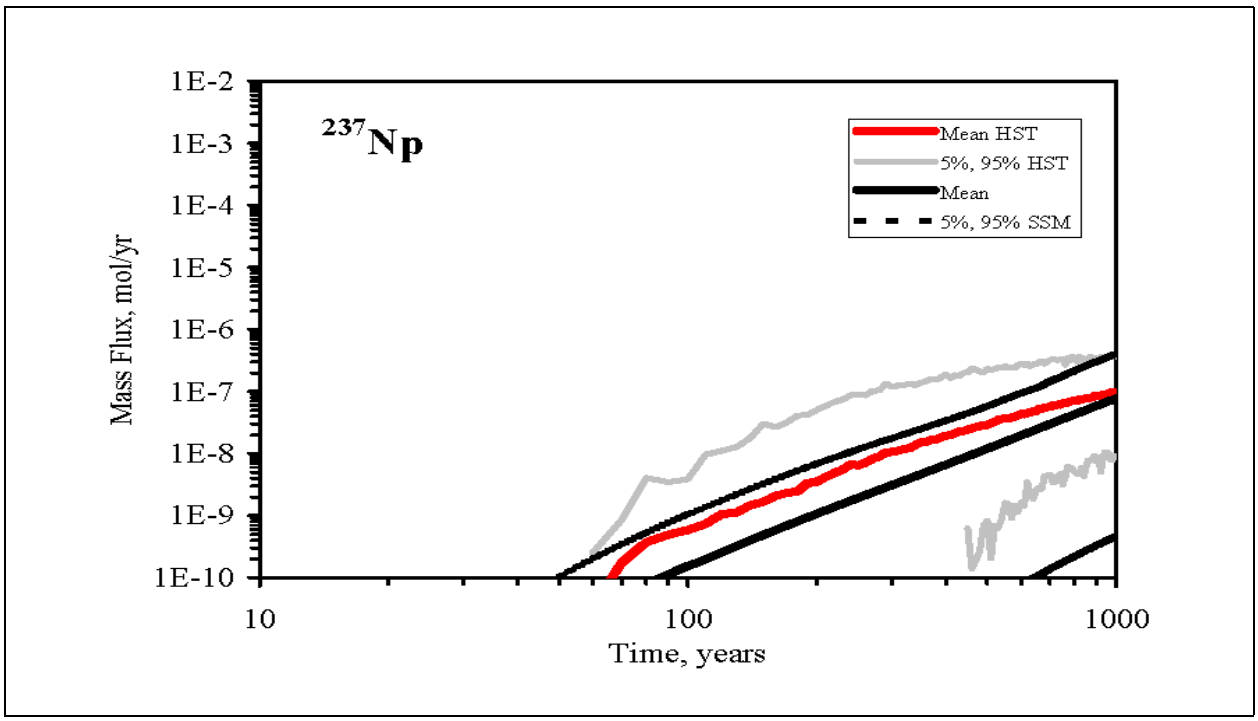

Figure 4-18
Comparison of ^{237}Np Mass Fluxes from the HST and SSM at the P1 Plane

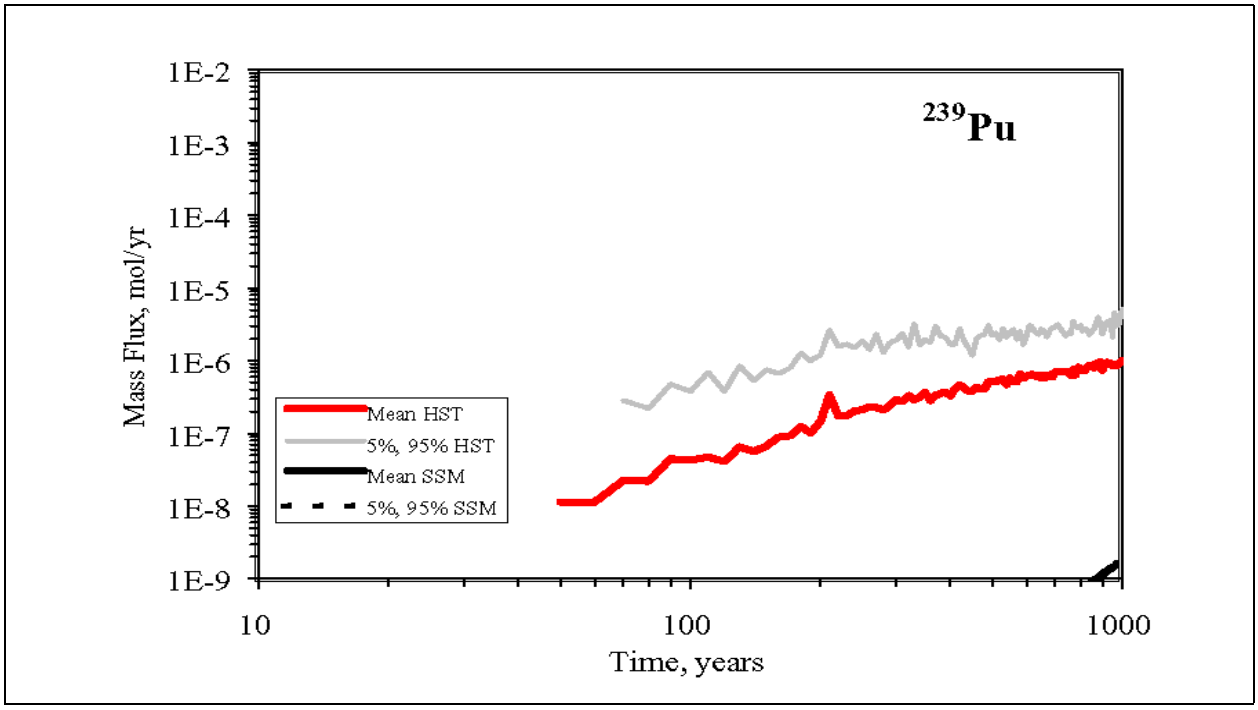

Figure 4-19
Comparison of ^{239}Pu Mass Fluxes from the HST and SSM at the P1 Plane

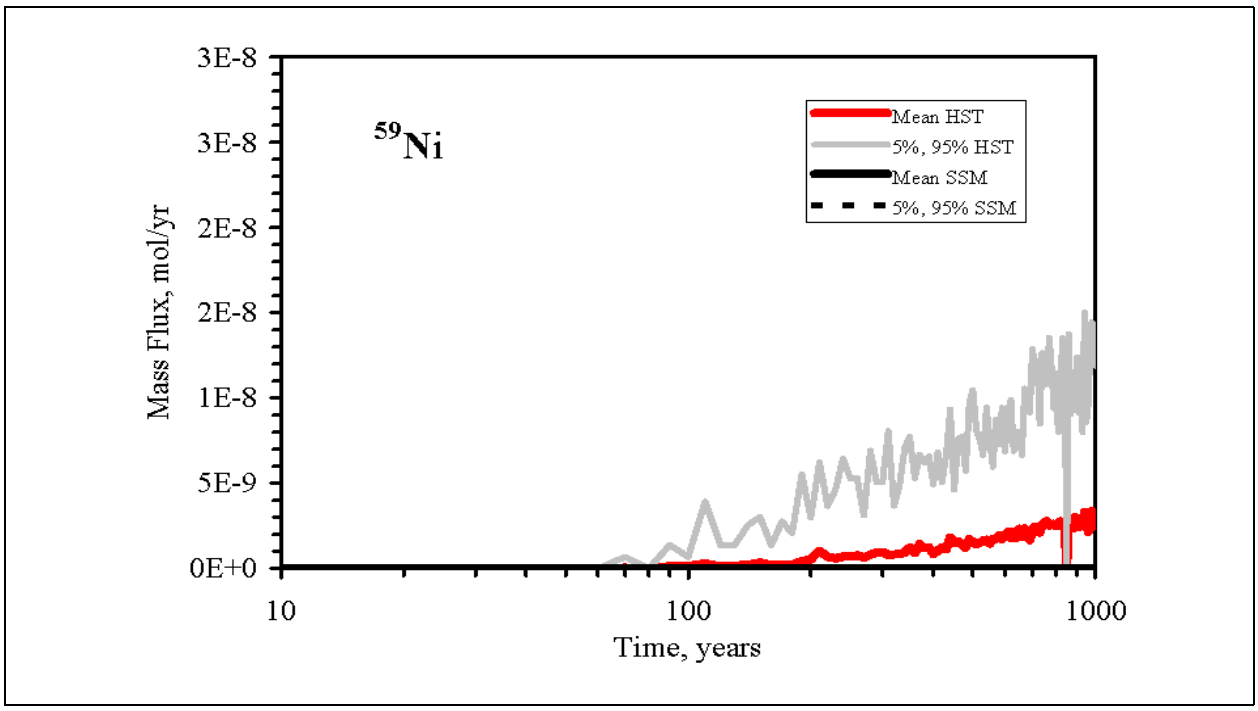

Figure 4-20
Comparison of ^{59}Ni Mass Fluxes from the HST and SSM at the P1 Plane

4.3 Summary of CAMBRIC SSM

An SSM has been developed for the CAMBRIC test using the GoldSim® software platform. The SSM represents the CAMBRIC test as two sources, an exchange volume, and the melt glass zone. The exchange volume encompasses the cavity zone above the melt glass zone and the compressed zones surrounding the central cavity. The melt glass zone represented the alluvium that is melted and fused during the test. The results from the SSM have been calibrated through comparison with the breakthrough curves for CAMBRIC radionuclide inventory based on the 3-D hydrodynamic source term analyses performed by LLNL (Tompson et al., 2005).

The flow/transport model for the SSM has been developed using a three step process:

1. Define the fluxes from the exchange volume for the groundwater tracers: ^{3}H, ^{14}C, ^{39}Ar, and ^{85}Kr. These radionuclides are deposited in the pore waters of the exchange volume and melt glass zone. There is no retardation for these species.

2. Define the fluxes from the melt glass zone for the melt glass tracers: ^{36}Cl, ^{93}Zr, ^{94}Nb, ^{99}Tc, ^{107}Pd, ^{121}Sn, ^{126}Sn, and ^{129}I. These radionuclides are deposited in the pore waters of the exchange volume/melt glass zone and in the nuclear melt glass. The fraction in the nuclear melt glass is released over time as the glass dissolves. There is no retardation for these species.

3. Evaluate the fluxes for the retarded radionuclides. The elements Ca, Ni, Sr, Cs, Sm, Eu, Ho, U, Np, Pu, and Am are assigned distribution coefficients (K_ds) in the HST and the SSM.

The initial conceptual model for the first step represents the exchange volume as a single source (cell pathway) that discharges through a single transport pipe. The pipe pathway had a constant length and constant cross-sectional flow area with variable flow rates. This conceptual model produced excellent comparisons with the breakthrough curves from the HST for the groundwater tracers ^{3}H, ^{14}C, ^{39}Ar, and ^{85}Kr.

The initial conceptual model for the second step represents the melt glass zone as a single source (cell pathway) that discharges through a single transport pipe. The pipe pathway has a constant flow rate and constant cross-sectional flow area with a variable path length. Analysis of the releases from the exchange volume versus the nuclear melt, demonstrates that the exchange volume is the major source for releases, particularly for the first few hundred years after the test. The conceptual model for the nuclear melt glass produced very good to excellent comparisons with the melt glass tracer breakthrough curve for the HST. This conceptual model also produced excellent comparisons with the breakthrough curves from the HST for all of the melt glass tracers: ^{36}Cl, ^{93}Zr, ^{94}Nb, ^{99}Tc, ^{107}Pd, ^{121}Sn, ^{126}Sn, and ^{129}I.

The initial conceptual model for the exchange volume had to be modified during the third step. The SSM with a single transport pipe results in delayed

breakthroughs for the retarded radionuclides in comparison to the 3-D representation in the HST. Intuitively, a 3-D model has more degrees of freedom than the 1-D representation in the SSM, resulting in faster flow pathways and more release than would be predicted by a 1-D representation. This effect is (partly) represented in the SSM by the use of multiple transport pathways from the exchange volume to the release plane. With multiple transport pathways and with log-normal distributions for the distribution coefficients in the HST, the SSM produces good comparisons with the breakthrough curves for the radioisotopes of U but not the other sorbing radionuclides. The poor match for the sorbing radionuclides was attributed to local diffusivity included in the HST model but not the SSM. Since no breakthrough of these radionuclides was observed at the P2 and P3 planes over the 1,000-year time span, the inclusion of local diffusivity in the SSM was not evaluated at this time. Further investigation will take place prior to utilization of the SSMs in the Frenchman Flat contaminant transport model.

5.0 Unclassified Simplified Source Term Calculation Procedure

Development and testing of the SSM for CAMBRIC is described in Section 4.0. To apply the CAMBRIC SSM to the nine other underground tests in Frenchman Flat, several parameters and their associated uncertainties must be modified to better describe each individual site and its test. Uncertainties associated with each parameter must then be captured within each SSM. The general uncertainties described in the SSM include the RST, exchange volume geometry, K_d values, melt glass dissolution parameters, and hydraulic conductivities.

The SSM is a simplification of very complex processes that is necessary to estimate the HSTs for all tests in Frenchman Flat with reasonable computational effort and time. The SSM does not explicitly model spatially-variable parameters within the cavity, although transport pathways in the CAMBRIC SSM is a basic representation of the spatial variability of transport pathways in the HST model. Exhaustive implementation of spatial variability with GoldSim defeats the purpose of the abstraction approach used within the SSM. The SSM also does not simulate convection cells formed (discussed in Section 4.0) by test heat; again, such a feature is best simulated by a detailed process model, which can provide insight into how the complex process can be simplified.

Overall, the purpose of the SSM is to represent major uncertainties in the transport of radionuclides from underground tests in the near-field environment, not to use probabilistic methods as a surrogate for deterministic variability (e.g., different burial depths) across tests. Calculation of the simplified source term (SST) for each test using the SSM is described within this section. The uncertainties considered in computing the unclassified SST are discussed, along with statistical distributions that represent such uncertainties. Finally, the SSTs generated using the SSMs will be presented.

5.1 Approach to Applying the CAMBRIC SSM to Other Frenchman Flat Tests

The CAMBRIC SSM is quite computationally efficient and it is straightforward to define test-specific parameters for the calculation of the SST for each test. Because this is an unclassified analysis, the RST and its distribution cannot be further refined other than as previously described. However, some uncertainty regarding the total RST will be introduced into the SST. The test-specific parameters that are modified for each test include the test cavity geometry, the size of the exchange volume, the RST, melt glass dissolution parameters, and the K_ds. Transport pipe lengths are also adjusted to reflect the distance from the working

point for each individual test to the plane where the SSM intercepts the CAU transport model. These modifications to the CAMBRIC SSM are described in this section.

5.1.1 Radionuclide Inventory

The RST used to develop the SSM for each of the tests within Frenchman Flat was based on the unclassified inventory (see Table 3-1) reported in Bowen et al. (2001). A list of 36 radionuclides, consistent with that used for the CAMBRIC steady state HST model (Tompson et al., 2005) and the CAMBRIC SSM, was selected from the Bowen et al. (2001) inventories as described in Section 3.0. The total mass of radionuclides for any specific underground nuclear test is classified information and not available for this analysis. An estimate of the mass of radionuclides for each underground test was therefore made by calculating the average inventory from the total inventory for all of the tests in Frenchman Flat, as reported in Bowen et al., 2001 (see Table 3-1).

The radionuclide inventory reported in Bowen et al. (2001) is decay-corrected to September 23, 1992, the date of the last underground nuclear test. The averaged radionuclide inventory for each specific test is therefore corrected to the t_0 of each test (Table 5-1). With the exception of ^{237}Np and ^{241}Am, the decay correction for each radionuclide was accomplished using the following formula:

$$N_0 = N/(\exp(-\lambda t)) \quad (5\text{-}1)$$

where:

$\lambda = \ln(2)/T_{1/2}$

N_0 = Number of moles of radionuclide at time t_0 of the test

t = Time elapsed between time of test and September 23, 1992

$T_{1/2}$ = Half life for radionuclide

N = Number of moles of radionuclide reported in Bowen et al. 2001 (decay corrected to September 23, 1992)

This simple approach is not applicable to radioisotopes that are also daughter products in a decay chain for which another radionuclide in the RST is the parent. This is primarily the case when the half life of the radioactive parent is sufficiently short relative to the 1,000-year time simulation period (Tompson et al., 2004). The radionuclides ^{241}Am and ^{237}Np are part of a decay chain ^{241}Pu -> ^{241}Am -> ^{237}Np and cannot be corrected to the t_0 for each test without considering ingrowth (Kersting et al., 2003). The decay-corrected inventories for each of the Frenchman Flat tests, including ingrowth for these two radionuclides, are listed in Table 5-1. Each of the radionuclides within the inventory is individually represented in the inventory for the SSM, including the presence of decay chains.

Uncertainty in the RST is also represented in the SSMs for the nine tests in Frenchman Flat. This uncertainty is represented as a multiplicative factor that

Table 5-1
Radionuclide Inventory for Each Underground Test in Frenchman Flat

Radionuclide	Half-life[a] (years)	Avg. Inventory (mol per Test)	WISHBONE (mol)	CAMBRIC (mol)	DILUTED WATERS (mol)	PIN STRIPE (mol)	DERRINGER (mol)	NEW POINT (mol)	MILK SHAKE (mol)	DIANA MOON (mol)	MINUTE STEAK (mol)	DIAGONAL LINE (mol)
		9/23/1992	**2/18/1965**	**5/14/1965**	**6/16/1965**	**4/25/1966**	**9/12/1966**	**12/13/1966**	**3/25/1968**	**8/27/1968**	**9/12/1969**	**11/24/1971**
^{3}H	12.32	6.01E-01	2.84E+00	2.80E+00	2.79E+00	2.66E+00	2.60E+00	2.65E+00	2.39E+00	2.33E+00	2.20E+00	1.94E+00
^{14}C	5715	1.06E-01	1.07E-01	1.07E-01	1.07E-01	1.07E-01	1.07E-01	1.07E-01	1.07E-01	1.07E-01	1.07E-01	1.07E-01
^{36}Cl	3.01E+05	7.50E-01	7.50E-01	7.50E-01	7.50E-01	7.50E-01	7.50E-01	7.50E-01	7.50E-01	7.50E-01	7.50E-01	7.50E-01
^{39}Ar	269	4.64E-04	4.98E-04	4.98E-04	4.98E-04	4.97E-04	4.96E-04	4.96E-04	4.94E-04	4.94E-04	4.92E-04	4.90E-04
^{41}Ca	1.03E+05	1.88E+00	1.89E+00	1.89E+00	1.89E+00	1.89E+00	1.89E+00	1.89E+00	1.89E+00	1.89E+00	1.89E+00	1.88E+00
^{59}Ni	7.60E+04	3.47E-02	3.47E-02	3.47E-02	3.47E-02	3.47E-02	3.47E-02	3.47E-02	3.47E-02	3.47E-02	3.47E-02	3.47E-02
^{63}Ni	100	4.70E-03	5.69E-03	5.68E-03	5.67E-03	5.64E-03	5.62E-03	5.61E-03	5.57E-03	5.55E-03	5.51E-03	5.43E-03
^{85}Kr	10.76	3.87E-04	2.30E-03	2.25E-03	2.24E-03	2.12E-03	2.07E-03	2.04E-03	1.87E-03	1.82E-03	1.71E-03	1.48E-03
^{90}Sr	28.78	1.51E-02	2.94E-02	2.92E-02	2.92E-02	2.86E-02	2.83E-02	2.81E-02	2.73E-02	2.70E-02	2.63E-02	2.50E-02
^{93}Zr	1.50E+06	4.69E-02	4.69E-02	4.69E-02	4.69E-02	4.69E-02	4.69E-02	4.69E-02	4.69E-02	4.69E-02	4.69E-02	4.69E-02
^{94}Nb	2.00E+04	3.90E-03	3.90E-03	3.90E-03	3.90E-03	3.90E-03	3.90E-03	3.90E-03	3.90E-03	3.90E-03	3.90E-03	3.90E-03
^{99}Tc	2.13E+05	6.96E-02	6.96E-02	6.96E-02	6.96E-02	6.96E-02	6.96E-02	6.96E-02	6.96E-02	6.96E-02	6.96E-02	6.96E-02
^{107}Pd	6.50E+06	3.55E-02	3.55E-02	3.55E-02	3.55E-02	3.55E-02	3.55E-02	3.55E-02	3.55E-02	3.55E-02	3.55E-02	3.55E-02
^{121}Sn	55	2.53E-04	3.59E-04	3.58E-04	3.57E-04	3.53E-04	3.52E-04	3.50E-04	3.45E-04	3.43E-04	3.39E-04	3.29E-04
^{126}Sn	2.50E+05	5.73E-03	5.73E-03	5.73E-03	5.73E-03	5.73E-03	5.73E-03	5.73E-03	5.73E-03	5.73E-03	5.73E-03	5.73E-03
^{129}I	1.57E+07	1.99E-02	1.99E-02	1.99E-02	1.99E-02	1.99E-02	1.99E-02	1.99E-02	1.99E-02	1.99E-02	1.99E-02	1.99E-02
^{135}Cs	2.30E+06	8.76E-02	8.76E-02	8.76E-02	8.76E-02	8.76E-02	8.76E-02	8.76E-02	8.76E-02	8.76E-02	8.76E-02	8.76E-02
^{137}Cs	30.07	4.24E-02	8.01E-02	7.97E-02	7.96E-02	7.80E-02	7.73E-02	7.69E-02	7.46E-02	7.39E-02	7.21E-02	6.86E-02
^{151}Sm	90	7.42E-03	9.18E-03	9.17E-03	9.16E-03	9.10E-03	9.07E-03	9.05E-03	8.97E-03	8.94E-03	8.87E-03	8.72E-03
^{150}Eu	36	9.93E-08	1.69E-07	1.68E-07	1.68E-07	1.65E-07	1.64E-07	1.63E-07	1.59E-07	1.58E-07	1.55E-07	1.48E-07
^{152}Eu	13.54	2.87E-03	1.18E-02	1.16E-02	1.16E-02	1.11E-02	1.09E-02	1.07E-02	1.00E-02	9.83E-03	9.32E-03	8.33E-03
^{154}Eu	8.593	6.30E-04	5.84E-03	5.73E-03	5.69E-03	5.31E-03	5.15E-03	5.04E-03	4.55E-03	4.39E-03	4.04E-03	3.38E-03
^{166}Ho	1.20E+03	6.79E-04	6.90E-04	6.90E-04	6.90E-04	6.90E-04	6.90E-04	6.90E-04	6.89E-04	6.89E-04	6.89E-04	6.88E-04
^{232}U	69.8	2.01E-07	2.64E-07	2.63E-07	2.63E-07	2.61E-07	2.60E-07	2.59E-07	2.56E-07	2.55E-07	2.52E-07	2.47E-07
^{233}U	1.59E+05	5.94E-05	5.94E-05	5.94E-05	5.94E-05	5.94E-05	5.94E-05	5.94E-05	5.94E-05	5.94E-05	5.94E-05	5.94E-05
^{234}U	2.46E+05	2.97E-02	2.97E-02	2.97E-02	2.97E-02	2.97E-02	2.97E-02	2.97E-02	2.97E-02	2.97E-02	2.97E-02	2.97E-02
^{235}U	7.04E+08	1.69E+00	1.69E+00	1.69E+00	1.69E+00	1.69E+00	1.69E+00	1.69E+00	1.69E+00	1.69E+00	1.69E+00	1.69E+00
^{236}U	2.34E+07	1.96E-02	1.96E-02	1.96E-02	1.96E-02	1.96E-02	1.96E-02	1.96E-02	1.96E-02	1.96E-02	1.96E-02	1.96E-02
^{238}U	4.47E+09	1.19E+02	1.19E+02	1.19E+02	1.19E+02	1.19E+02	1.19E+02	1.19E+02	1.19E+02	1.19E+02	1.19E+02	1.19E+02
^{237}Np	2.14E+06	8.25E-03	6.37E-03	6.37E-03	6.38E-03	6.40E-03	6.41E-03	6.42E-03	6.46E-03	6.47E-03	6.52E-03	6.62E-03
^{238}Pu	87.7	7.93E-03	9.86E-03	9.84E-03	9.84E-03	9.77E-03	9.74E-03	9.72E-03	9.62E-03	9.59E-03	9.51E-03	9.35E-03
^{239}Pu	2.41E+04	9.54E+00	9.55E+00	9.55E+00	9.55E+00	9.55E+00	9.55E+00	9.55E+00	9.54E+00	9.54E+00	9.54E+00	9.54E+00
^{240}Pu	6.56E+03	6.40E-01	6.42E-01	6.42E-01	6.42E-01	6.42E-01	6.42E-01	6.42E-01	6.42E-01	6.42E-01	6.42E-01	6.42E-01
^{241}Pu	14.4	1.78E-02	6.70E-02	6.63E-02	6.60E-02	6.33E-02	6.21E-02	6.14E-02	5.77E-02	5.66E-02	5.38E-02	4.84E-02
^{242}Pu	3.75E+05	3.02E-03	3.02E-03	3.02E-03	3.02E-03	3.02E-03	3.02E-03	3.02E-03	3.02E-03	3.02E-03	3.02E-03	3.02E-03
^{241}Am	432.7	6.08E-02	1.34E-02	1.42E-02	1.44E-02	1.71E-02	1.82E-02	1.90E-02	2.26E-02	2.38E-02	2.65E-02	3.18E-02

[a]Source = Bowen et al. (2001)

incorporates the range of inventory uncertainty for the radionuclide types, as shown in Table 5-2. The value for the range of uncertainty factor is sampled from a truncated normal distribution in each realization of the SSM. Uncertainty ranges

Table 5-2
Estimated Accuracies for Groups of Radionuclides

Radionuclide Group[a]	Accuracy[a]	Accuracy Range	Radionuclides[a]	Lower Limit[b]	Upper Limit[b]	Standard Deviation[c]
Fission Products	~10 to 30 percent	0.7 to 1.3 (0.6)	^{85}Kr, ^{90}Sr, ^{93}Zr, ^{99}Tc, ^{107}Pd, ^{121}Sn, ^{126}Sn, ^{129}I, ^{135}Cs, ^{137}Cs, ^{151}Sm	0.7	1.3	0.10
Unspent Fuel Materials	~ 20 percent or better	0.8 to 1.2 (0.4)	^{232}Th, ^{233}U, ^{234}U, ^{235}U, ^{236}U, ^{238}U, ^{243}Am	0.8	1.2	0.067
Fuel Activation Products	~ 50 percent or better	0.5 to 1.5 (1)	^{232}U, ^{237}Np, ^{238}Pu, ^{239}Pu, ^{240}Pu, ^{241}Am, ^{241}Pu, ^{242}Pu	0.5	1.5	0.17
Residual Tritium	~ 300 percent or better	-2 to 4 (6)	^{3}H	0[d]	2[d]	1
Activation Products	~ a factor of 10	-9 to 11 (20)	^{14}C, ^{36}Cl, ^{39}Ar, ^{41}Ca, ^{59}Ni, ^{63}Ni, ^{94}Nb, ^{150}Eu, ^{152}Eu, ^{154}Eu, ^{166}Ho	0[d]	2[d]	3.3

[a]Bowen et al., 2001
[b]Upper and lower limits are based on maximum percent uncertainty
[c]Standard deviation is taken to be the accuracy range divided by 6 (estimate falls within the range of one plus and minus three standard deviations)
[d]Lower limit truncated to be non-negative and upper limit truncated to maintain a mean of one.

~ = Approximately

were associated with each radionuclide, according to Bowen et al. (2001, Table 1) as follows:

- Radionuclide is grouped as a fission product if (1) it is listed solely as a fission product, or (2) it is listed as a fission product and an activation product (with the exception of ^{94}Nb, ^{152}Eu, and ^{166}Ho).
- Radionuclide is grouped as Unspent Fuel Material if (1) it is listed solely as a device component, or (2) it is listed as a device component and as natural or a radiochemical tracer.
- Radionuclide is grouped as a Fuel Activation Product if (1) it is listed both as a device component and an activation component, or (2) it is listed as both a device component and a decay product.
- Radionuclide is grouped as a Activation Product if (1) it is listed solely as an activation product or (2) if it is listed as both an activation product and a fission product and is produced with significantly greater yields as an

activation product than through fission (^{94}Nb, ^{152}Eu, and ^{166}Ho [see text associated with fission products in Bowen et al., 2001]).

For each realization of the SSM, the range uncertainty factor for each radionuclide will be sampled and multiplied by the initial radionuclide mass shown in Table 5-1 to incorporate inventory uncertainty directly into the SST. This approach provides an estimate of the uncertainties associated with the total RST in the SSM, but does not necessarily represent the uncertainties that arise from using the average inventory reported in Bowen et al., 2001 as the RST for each test. For those radionuclides with an accuracy reported as greater than 100 percent (residual tritium and activation products) the lower limit of the normal distribution was truncated at zero, because a negative inventory is not possible. Because of this truncation of the lower limit, truncation of the upper limit was also required. Truncation of the upper limit was required to maintain the mean of this multiplier as one. Without this truncation, the mean multiplier is significantly greater than one and therefore results in a significantly greater average inventory than that reported by Bowen et al. (2001) used for the SSMs. This is considered acceptable because the average unclassified inventory reported by Bowen et al. (2005) is the best estimate available and can not be varied, and the uncertainty reported by Bowen et al. (2001) is an estimate and is somewhat uncertain in itself.

5.1.2 Test-Cavity Geometry

5.1.2.1 Cavity Volume

The cavity radius is calculated from the maximum announced yield, the bulk overburden density, and the depth of burial (Pawloski, 1999):

$$R_C = \frac{70.2(Y)^{1/3}}{(\rho_b DOB)^{1/4}} \qquad (5\text{-}2)$$

where:

R_C = Cavity radius in meters
Y = Yield in kilotons
ρ_b = Overburden density (g/cm^3)
DOB = Depth of burial in meters.

The yield and DOB used to calculate the cavity radius are listed in Table 1-1. The maximum announced yield is used when only this information was available. The overburden density used for this calculation (2.1 g/cm^3) is consistent with Tompson et al. (2004). The cavity radius for each test is reported in Table 5-3. The volume of the cavity is then calculated as $4/3\pi R_c^3$.

The yield is not allowed to vary outside the announced range, and all unclassified calculations must be done with the maximum announced yield. Thus, the only way to introduce uncertainty in the cavity volume is via the bulk overburden density and/or depth of burial. A single value is presented for depth of burial; no

uncertainty is given although some could be assumed to exist from survey or other measurement data. Overburden bulk density also has some uncertainty associated with it. Rather than applying uncertainty to the cavity radius in the SSM, uncertainty is captured in the radius of the exchange volume as described in the following section.

Table 5-3
Cavity Radius and Transport Pipe Pathlength

Parameter	Frenchman Flat Region	Cavity Radius (m)	Pathlength (m)
CAMBRIC	Central	13.4[a]	23.06
DERRINGER	Northern	29	107.1
DIAGONAL LINE	Northern	39	123.8
DIANA MOON	Northern	40	111.3
DILUTED WATERS	Central	42	108.5
MILK SHAKE	Northern	39	107.9
MINUTE STEAK	Northern	39	132.1
NEW POINT	Northern	40	95.7
PIN STRIPE	Northern	38	84.9
WISHBONE	Central	43	124.3

[a] Measured Value (Tompson et al., 2005)
m = meters

5.1.2.2 Exchange Volume

As described in Section 4.0, the source in the SSM is represented as two volumes: the melt glass zone and the exchange volume. The exchange volume consists of the cavity zone (i.e., the cavity above the melt glass zone) and the compressed zones immediately surrounding the cavity. The cavity and exchange volumes used in the CAMBRIC steady state HST model, and subsequently in the SSM, are based on results of the gamma log analyses (Tompson et al., 2005). No data of this kind are available for the other tests within Frenchman Flat.

In this situation, the radius of the exchange volume is estimated as the product of the calculated cavity radius and a multiplier reflecting the potential volume around the cavity that can be immediately affected by the underground test:

$$R_{EV} = MR_C \tag{5-3}$$

where:

R_C = The cavity radius in meters
R_{EV} = The exchange volume radius in meters
M = The value of the multiplicative factor.

A range in the exchange volume multiplier, M, is used to account for the uncertainty in the estimate of the size of the disturbed volume outside the test cavity. A probability distribution reflecting the uncertainty in the exchange volume multiplier is therefore applied in each SSM. A uniform distribution with a lower limit of 1.3 and an upper limit of 2.0 (Borg et al., 1976) is used. During each realization of the SSM, the multiplicative factor is sampled and multiplied by the cavity radii (Table 5-3) to incorporate the uncertainty associated with the exchange volume directly into the SSM.

5.1.2.3 Melt Glass Zone Volume

For CAMBRIC, the melt glass zone is represented as a mixture of the nuclear melt glass and collapsed alluvium in the lower hemisphere of the cavity (i.e., the lower 7.4 m portion of the CAMBRIC cavity). It is assumed that the melt glass zone will occupy a similar proportion of the cavity for the other nine tests in Frenchman Flat. The volume of the melt glass zone will, therefore, be estimated for the nine tests using the relative proportion of cavity and melt glass zone volumes for CAMBRIC. Using the cavity zone and melt glass zone estimates found in Table 4-1 for the CAMBRIC test, this relative proportion is calculated to be 0.18663. As described in Section 4.1.1, the volume of the cavity is calculated as the sum of the volume of the cavity zone (8197.8 m^3) and the melt glass zone (1880.9 m^3). The volume of the cavity for each test is, therefore, multiplied by 0.18663 to estimate the volume of the melt glass zone.

5.1.2.4 Distribution of Radionuclide Source Between the Melt Glass and Exchange Volume

As noted in the work of Pawloski et al. (2001), the partitioning of the RST between the melt glass, rubble, gas, and water are taken primarily from an IAEA report (IAEA, 1998), that describes the distribution of radionuclides underground at the atolls of Mururoa and Fangataufa in the south Pacific Ocean. The extrapolation of the IAEA data to the NTS, and to radionuclides not addressed in the IAEA report means that the percentages shown in Table 3-4 are "best estimates." The distributions reported by IAEA provide conservative estimates of the partitioning for the refractory actinides and lanthanides. One limitation associated with the IAEA data is that it is assumed that the radionuclides are present either in the groundwater or sorbed to mineral surfaces. In actuality, the form of the radionuclides may be more complicated. Some of the radionuclides may be associated with metamorphosed rubble or slightly melted rock, or exist as coprecipitated minerals that are not easily available to groundwater. As a result,

the fraction of radionuclides initially in the cavity groundwater may be overestimated.

As shown in Section 4.2, the SSM reasonably replicates the CAMBRIC HST model results as well as its 5th percentile and 95th percentile breakthrough curves without considering any variation in the RST partitioning. Although a relatively high uncertainty is associated with the distribution of the radionuclides within the cavity and melt glass, no data are available to quantify this. Since there is no reason to assume that the partitioning of the RST is different between the CAMBRIC test and the other nine tests within Frenchman Flat, the partitioning of the RST between the melt glass, rubble, gas, and water is held consistent between the CAMBRIC HST model (Tompson et al., 2005) and all SSMs (Table 3-4). For the SSM analysis, the partitioning is further simplified by combining the percentages from rubble, gas, and water into the exchange volume; the percentage in the glass defines the inventory in the melt glass matrix.

5.1.3 Melt Glass Dissolution

The SSM incorporates the same simplified temperature-dependent glass dissolution model that is used for the steady-state HST model (Tompson et al., 2005). The dissolution rate of glass is estimated as a function of five terms, the Arrhenius term, the reactive surface area, a rate coefficient and product terms, the saturation terms Q and K, and a close-to-saturation term (see Section 4.1.5 for details). It is suggested in Tompson et al. (2005) that uncertainty should be assigned to the reactive surface area, the time temperature history, and also the activation energy for the glass dissolution model used for the SSM.

The reactive surface area is one of the most critical parameters for predicting the radionuclide release rates from melt glass because the reaction rate is proportional to the reactive surface area (Equation 4-4). The reactive surface area refers to the surface area of glass only and does not include the surface areas of the secondary minerals associated with the glass. A bulk value of 0.001 m^2/g was used for both the steady state CAMBRIC HST as well as the CAMBRIC SSM. It was suggested by Tompson et al. (2005) that areas ranging from 0.00005 to 0.4 m^2/g be used to capture the uncertainty associated with this parameter. A uniform distribution describing this range in the reactive surface area (0.00005 to 0.4 m^2/g) was tested to determine the sensitivity of the SSM to this parameter. The CAMBRIC SSM model was used to calculate mass fluxes over 1,000 years for two melt glass tracers, ^{129}I and ^{94}Nb, using this uniform distribution to estimate the reactive surface area. These tracers were selected because of the difference in their relative distribution into the melt glass. Fifty percent of ^{129}I is distributed into the melt glass, whereas 95 percent of ^{94}Nb is distributed in the melt glass. During each realization, the reactive surface area is sampled from the uniform distribution and glass dissolution calculated according to Equation 4-4. Figure 5-1 illustrates the large impact on the mass fluxes for these radionuclides. The mean for this distribution, 0.2 m^2/g, is significantly greater than the 0.001 m^2/g area used for the CAMBRIC HST model and the SSM. It is stated in Tompson et al. (2005) that the surface area of 0.001 m^2/g is considered a conservative estimate. Increasing the

mean to 0.2 m^2/g is therefore unreasonable. Instead, a normal distribution with a mean of 0.001 m^2/g and standard deviation of 0.0001 m^2/g, truncated at the lower end at 0.00005 m^2/g and at the upper end at 0.4 m^2/g was used to estimate the

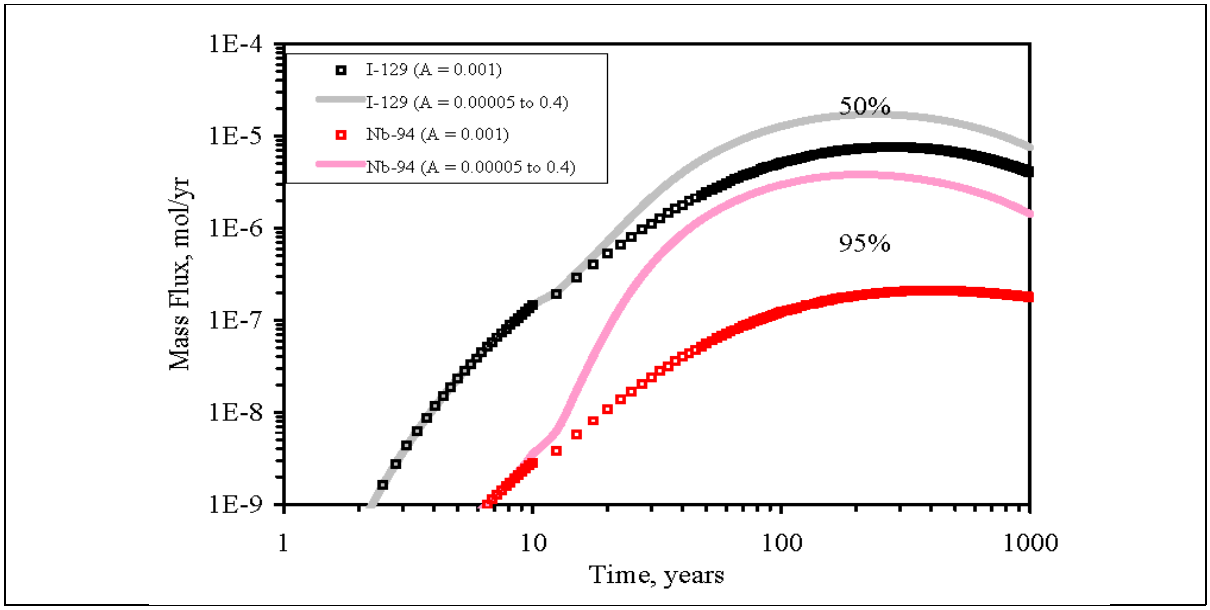

Figure 5-1
Mass Fluxes for ^{129}I and ^{94}Nb From the SSM Using a Uniform Distribution to Estimate Reactive Surface Area in the Glass Dissolution Model

uncertainty associated with this parameter. This allows a mean of 0.001 m^2/g, similar to the CAMBRIC HST model and SSM, to be used for all SSMs.

The temperature history for the melt glass is simulated from the transient flow model; two temperature histories are presented (Tompson et al., 2005). The first one is based on an initial temperature of 170ºC and the other on an initial temperature of 120ºC. The 170ºC result was used for both the HST model and is based on an initial temperature just below the boiling point of water when water pressure is hydrostatic. The 120ºC result is based on an initial temperature below the boiling point of water when the water pressure is below hydrostatic (Tompson et al., 2005). A comparison was performed to determine the sensitivity of the results of the SSM to the two glass temperature histories. The results in Figure 5-2 demonstrate that the temperature history does not significantly impact the results of the SSM and therefore the same 170ºC temperature history will be used for all of the SSMs, consistent with the CAMBRIC SSM. This is considered a conservative estimate.

Tompson et al. (2005) suggested that the activation energy is another parameter used in the glass dissolution model for which uncertainty should be applied. A plausible range of activation energies from 10 Kilocalories per mole (Kcal/mol) to 20 Kcal/mol was suggested (Tompson et al., 2005). The impact of the activation

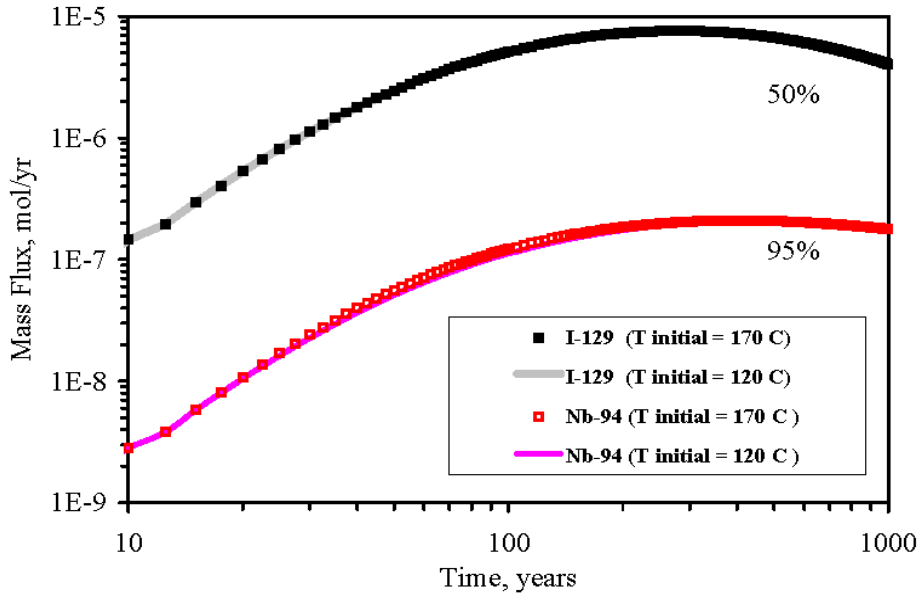

Figure 5-2
Mass Fluxes for ^{129}I and ^{94}Nb From the SSM Using Two Temperature Histories in the Glass Dissolution Model

energy was tested using the two melt glass tracers, ^{129}I and ^{94}Nb. The SSM was tested using three activation energies, 10, 15, and 20 Kcal/mol. The results are presented in Figure 5-3. Although no significant difference in the results is observed for activation energies of 10 and 15 Kcal/mol, an increased mass flux is observed when an activation energy of 20 Kcal/mol is used. A uniform distribution, ranging from 10 to 20 Kcal/mol for activation energy was included in the SSM for all tests.

5.1.4 Flow and Transport Parameters

5.1.4.1 Sorption

The CAMBRIC HST model is based on a mechanistic surface complexation/ion exchange model to account for radionuclide sorption. In the mechanistic model, radionuclide sorption is a function of the groundwater chemistry, sorbing mineral properties (e.g., cation exchange capacity, surface area, reactive site density), and the surface complexation/ion exchange constants that govern radionuclide sorption affinities. Ion exchange reactions are represented for Ca, Cs, and Sr for the minerals zeolite, illite/mica, and smectite. Surface complexation reactions are represented for Am, Eu, Np, U, and Pu for the minerals smectite, iron oxide, and calcite. Surface complexation reactions are also represented for Sr for iron oxide

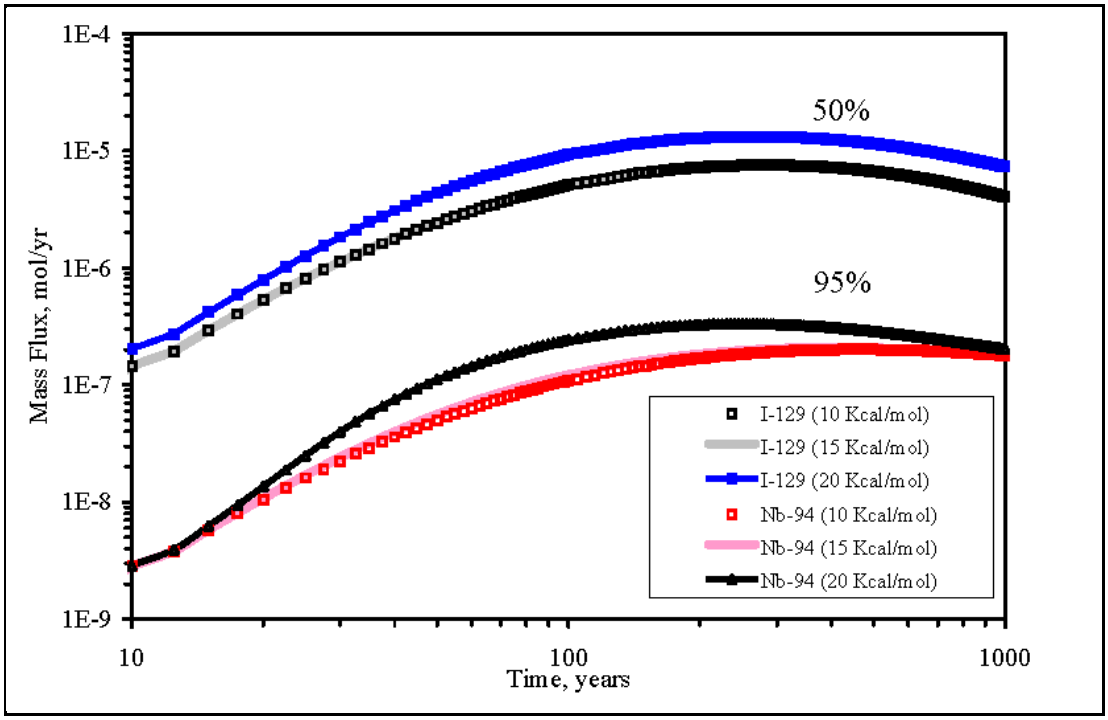

Figure 5-3
Mass Fluxes for ^{129}I and ^{94}Nb From the SSM Using Three Activation Energies in the Glass Dissolution Model

and calcite and also for Ca and calcite. The surface complexation/ion exchange constants that govern radionuclide sorption affinities were developed based on electrostatic surface complexation and Vanselow ion exchange (Zavarin and Bruton, 2004a, b). The sorbing mineral properties are based on published data and the recent model validation experiments performed on Yucca Flat and Frenchman Flat (Zavarin et al., 2002).

The mechanistic model generates a K_d for each radionuclide-mineral pair. A component additivity approach is then used to predict radionuclide K_ds as a function of the mineral abundances:

$$K_d = \sum_{i=1}^{n} K_{d,i}\phi_{m,i} \qquad (5\text{-}4)$$

where:

$K_{d,i}$ = Distribution coefficient for the individual mineral, i, under specified groundwater chemistry conditions

ϕ = Mass of the fraction of mineral, i, with respect to the total bulk medium

Recent X-Ray Diffraction (XRD) data on mineral distributions and abundances from core samples collected primarily from drill hole ER-5-4 were evaluated and alluvial zones with relatively uniform mean values of sorbing minerals (iron oxide, smectite, illite/mica, zeolite, and calcite) were identified (Warren et al., 2002 and Carle et al., 2002). K_ds for each radionuclide were estimated using the mechanistic model for each of the alluvial layers (see Table 5-4). The oxygen (O_2) fugacity was set to 10^{-20} bars for the K_d calculations (Tompson et al., 2005). This ensured that the Pu(IV) and P(V) oxidation states were the dominate species for this calculation. All other radionuclides remain in their oxidized form under these conditions (Tompson et al., 2005). These K_ds were used for both the steady state CAMBRIC HST model as well as the CAMBRIC SSM.

Table 5-4
Mean and Standard Deviation of Log Distribution Coefficients (mL/g) for the Frenchman Flat Tests

	Ca	Cs	Sr	Ni	Am	Eu	Sm	Np	U	Pu
Central Frenchman Flat[a]										
Expected Value (Log K_d)	2.22	3.98	1.94	3.18	3.97	3.26	3.52	0.63	0.27	2.09
SD (Log K_d)	0.31	0.21	0.34	0.21	0.21	0.23	0.27	0.23	0.16	0.20
Expected Value (Ln K_d)	5.11	9.16	4.47	7.32	9.14	7.51	8.11	1.45	0.62	4.81
SD (Ln K_d)	0.71	0.48	0.78	0.48	0.48	0.53	0.62	0.53	0.37	0.46
Arithmetic Mean (K_d)	214.11	10734	118.33	1701.3	10489	2093.7	4017.3	4.91	1.99	136.79
Arithmetic SD (K_d)	174.53	5509.2	108.82	873.15	5383.8	1191.3	2759.5	2.79	0.76	66.49
Northern Frenchman Flat[b]										
Expected Value (Log K_d)	2.77	3.81	2.53	2.97	3.84	3.29	3.67	0.68	0.14	2.05
SD (Log K_d)	0.27	0.28	0.28	0.27	0.23	0.23	0.26	0.25	0.21	0.21
Expected Value (Ln K_d)	6.38	8.77	5.83	6.84	8.84	7.58	8.45	1.57	0.32	4.72
SD (Ln K_d)	0.62	0.64	0.64	0.62	0.53	0.53	0.60	0.58	0.48	0.48
Arithmetic Mean (K_d)	714.38	7948.1	417.12	1132.2	7959.8	2243.4	5595.4	5.65	1.55	126.12
Arithmetic SD (K_d)	490.71	5705.9	299.45	777.72	4529.1	1276.5	3673.6	3.54	0.80	64.73

[a] Calculated based on mineralogy of alluvium in well ER-5-4 and water chemistry of RNM-1, RNM-2S, and UE-5n
[b] Calculated based on mineralogy of alluvium in well ER-5-3 and water chemistry of ER-5-3 (composite)

Carle et al. (2002) evaluated the K_ds for nine radionuclides (Am, Ca, Cs, Eu, Np, Pu, Sm, Sr, and U) in drill holes ER-5-4 and Ue-5n, in central Frenchman Flat, and ER-5-3 and U-11g-1, in northern Frenchman Flat, to determine whether the K_ds vary laterally as a result of changes in sorbing mineral abundances. No significant lateral variation was identified in the K_d values for Am, Eu, Np, Pu, Sm, and U. The K_ds for these radionuclides appeared to be well characterized by a log normal distribution. This was not the case for Ca, Cs, and Sr. Higher K_ds for Ca and Sr

tended to occur in northern Frenchman Flat and lower values in central Frenchman Flat. This differences was attributed primarily to the greater relative abundance of zeolite in the older alluvial aquifer (OAA) present in northern Frenchman Flat (Carle et al., 2002).

Separate K_ds will be used to describe sorption in the northern and central Frenchman Flat alluvium. Using the approach described above, along with XRD mineral abundance data (Warren et al., 2002) and groundwater chemistry data (SNJV, 2005, Table A.2-1) from wells within Frenchman Flat, the K_ds listed in Table 5-4 were calculated. K_ds for the tests in the Central Frenchman Flat alluvium were calculated using mineral abundance data from the alluvium in the ER-5-4 drill hole and those for the northern tests were based on mineral abundance data in the ER-5-3 drill hole. The mean groundwater chemistry from wells RNM-1, RNM-2S, and UE-5n, and the composite groundwater chemistry in well, ER-5-3 were used to calculate the K_ds for central and northern Frenchman Flat, respectively (SNJV, 2005, Table A.2-1). A composite sample from ER-5-3 represents groundwater sampled from two intervals that sample both the OAA and TM-WTA HSUs (SNJV, 2005). Only one sample is available from the alluvium in the northern area of Frenchman Flat (ER-5-3 upper). Because of the unusually high pH (9.25) in this sample, the composite sample was used to represent the water of the alluvium in northern Frenchman Flat. The XRD analysis has been performed on only two samples from the TM-LVTA within Frenchman Flat. Although, the volcanic rocks have a somewhat different mineralogy than those of the alluvial aquifer (SNJV, 2005), the K_ds used for the alluvium within northern Frenchman Flat were also used for the TM-LVTA (e.g., PIN STRIPE test). The K_ds, reported in Table 5-4, are used for the exchange volume transport cell and four transport pipes of the SSM. The K_ds for the melt glass zone, reported in Table 4-2 are used for the melt glass zone transport cell and transport pipes of the SSM for all tests.

Colloidal-facilitated transport is not considered significant at CAMBRIC and is not represented in the HST model (Tompson et al., 2005) nor the CAMBRIC SSM. Colloid concentrations comparable to those associated with the sampling and measurement methods (e.g., background levels) were observed in samples from RNM-25 (Abdel-Fattah, 2004, SNJV, 2005). Colloid transport is also not considered for the other tests in Frenchman Flat.

5.1.5 Transport Pathways

The length of the transport pathways in the SSM are based on the distances from the working point to the plane where the SSM intersects the Frenchman Flat contaminant transport model. The pathlengths used for the SSM for each test are based on the flow directions and distances to the nearest node in the preliminary Phase II Frenchman Flat flow model. The flow velocities used in the SSM for each test are the same as those used for the CAMBRIC SSM. The pathlengths and flow velocities may be updated for each site based on the final CAU flow model.

The alluvium porosities used for the SSM for all tests within the alluvium will be consistent with those used for the CAMBRIC HST and SSM (Table 4-1). The

mean porosity of 0.35 for the TM-LVTA (see SNJV, 2005, Table 5-4) will be used for the PIN STRIPE test.

Sensitivity studies will be performed during the Phase II Frenchman Flat contaminant transport modeling. This work will be described in the document associated with the contaminant transport modelling.

5.2 Results of Simplified Source Term Models

Mean mass flux curves for ^{3}H, ^{36}Cl, and ^{238}U at the planes described in Table 5-3, for each of the Frenchman Flat tests, are shown in Figure 5-4 through Figure 5-6, respectively. Breakthrough curves for each test, including the mean, 5th percentile, and 95th percentile of the mass fluxes are presented for the same radionuclides in Appendix E. The mass fluxes for all radionuclides for the nine tests, in electronic format (Excel), are included in Appendix F. In general, the shapes of the mean mass flux curves are consistent for each of the radionuclides for each of the tests in Frenchman Flat. This suggests a successful abstraction for these SSMs.

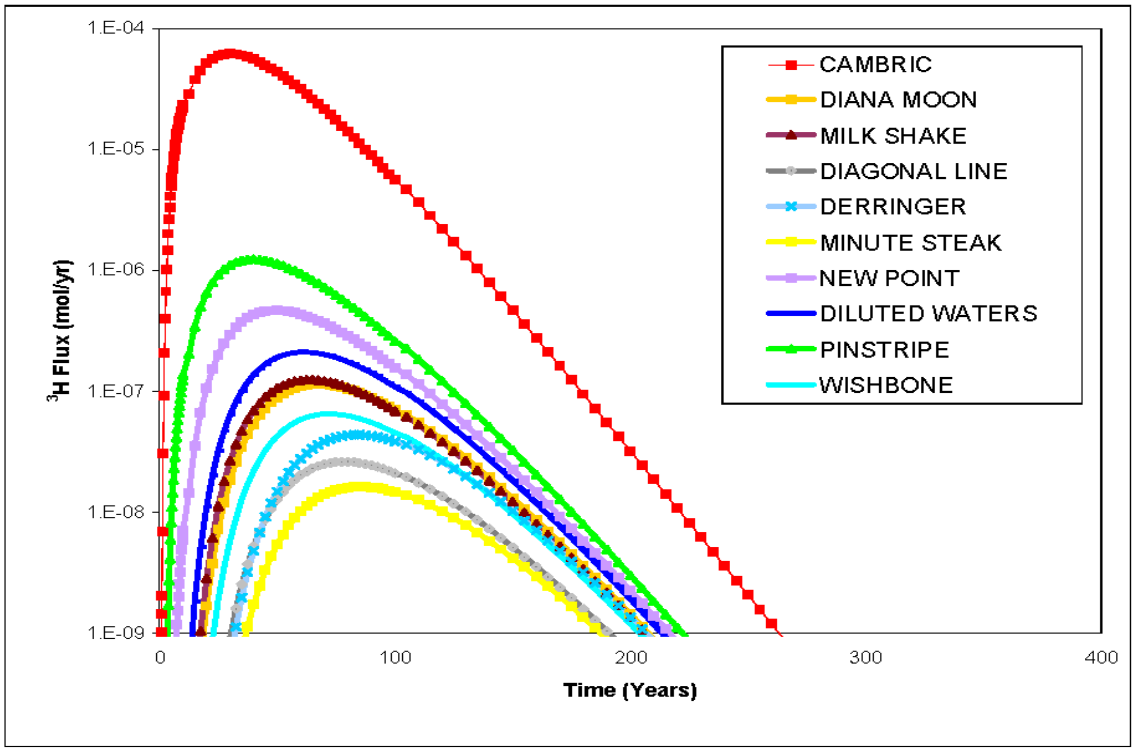

Figure 5-4
Mass Fluxes for ^{3}H From the SSM for Each Frenchman Flat Test

Mean mass flux curves for ^{3}H, for the ten tests in Frenchman Flat, are shown in Figure 5-4. As described earlier, ^{3}H is a groundwater tracer. It does not partition into the melt glass nor does it absorb unto the aquifer material. Therefore, the melt glass dissolution model and K_d distributions will not impact the mass flux results for ^{3}H. The announced yield for these tests, with the exception of CAMBRIC and DERRINGER, are the same, less than 20 kt. The larger yields for the tests, relative to CAMBRIC, translate to larger cavity radii and thus larger cavity and exchange volumes. In addition, the pathlengths are much larger for the nine tests (84.9 m to 124.3 m) than that for CAMBRIC (23.06 m). It is clear from Figure 5-4 that lower mean mass fluxes are observed for the nine tests in Frenchman Flat when compared to CAMBRIC. The differences between the ^{3}H mass flux curves reflect the different RST, exchange volume and cavity sizes, as well as the pathlengths (see Table 5-3) used in the SSMs. Interestingly, the trend in decreasing mass flux peak maxima is not as correlated with the size of the cavity and exchange volume sizes as much as it is with the pathlengths. For instance, the second greatest peak maxima is observed for the PINSTRIPE test, with a cavity radius of 38 m, and not for DERRINGER, with a cavity radius of 29 m. In general, the decreasing trend correlates well with increasing pathlengths. The pathlength for PINSTRIPE is the lowest, other than that for CAMBRIC, and the peak mass flux is the greatest. The path lengths for MINUTE STEAK is the greatest and the peak mass flux is the lowest. This trend is slightly offset due to the differences in the initial inventory as well as the sizes of the cavity and exchange volumes. This is not unexpected. The larger pathlengths allow for more travel time which is further compounded by the increased level of decay for ^{3}H (half-life = 12.32 years).

The mean mass flux curves for ^{36}Cl, at the planes described in Table 5-3, are shown in Figure 5-5 for each of the Frenchman Flat tests. The radionuclide, ^{36}Cl, is a melt glass tracer; 50 percent of this radionuclide is initially partitioned into the melt glass (see Table 3-4). No adsorption to the aquifer material is assumed for ^{36}Cl, and its large half-life (3.01×10^{5} years) ensures that decay is not a significant process over the 1,000 year span of the SSM. In addition, the initial inventory for ^{36}Cl is identical for all tests within Frenchman Flat (Table 5-1). The maxima observed for each of the mass flux curves is again correlated with the pathlength (Figure 5-5). This trend is not as pronounced as that observed for ^{3}H because radionuclide decay is not as significant for ^{36}Cl as it is for ^{3}H. The relative decrease in the mean mass fluxes for ^{36}Cl are primarily due to the increased travel times resulting from the greater pathlengths. Again, the differences in the size of the cavity and exchange volume somewhat offset this trend.

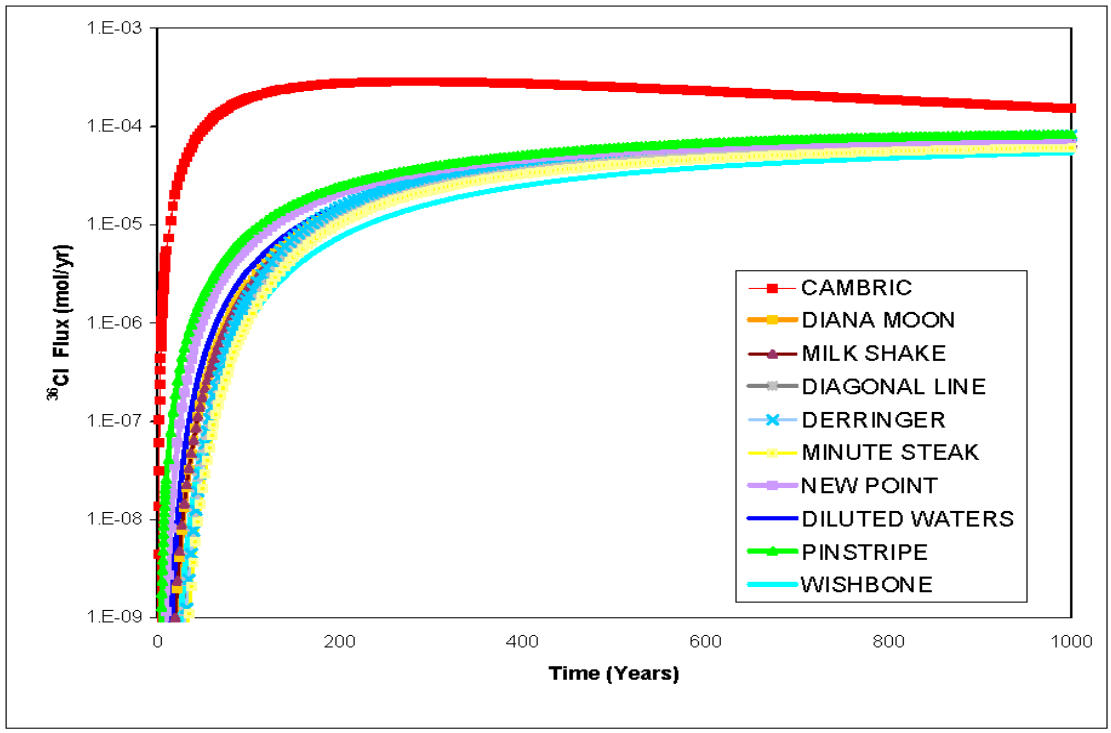

Figure 5-5
Mass Fluxes for ^{36}Cl From the SSM for Each Frenchman Flat Test

The mean mass flux curves for ^{238}U, at the planes described in Table 5-3, are shown in Figure 5-6 for each of Frenchman Flat tests. The large half-life for ^{238}U (4.47×10^9 years) ensures that decay is not a significant process over the 1,000-year span of the SSM. Since ^{238}U is a sorbing radionuclide, trends observed between the mean mass flux curves for the different tests will reflect the pathlength, the sizes of the cavity and exchange volume, and the K_d distributions used to estimate sorption along the flow path. Lower mass fluxes are observed for the tests that took place in central Frenchman Flat (DILUTED WATERS and WISHBONE) when compared to those tests that took place in the northern testing area. This is expected because the K_d for ^{238}U is greater (log K_d = 0.27 mL/g) for central Frenchman Flat when compared to that of the alluvium of northern Frenchman Flat (log K_d = 0.14 mL/g). Similar to ^{36}Cl and ^{3}H, the mass flux curves again correlate to the pathlength (Figure 5-5) when separating the tests in the northern and central testing areas of Frenchman Flat.

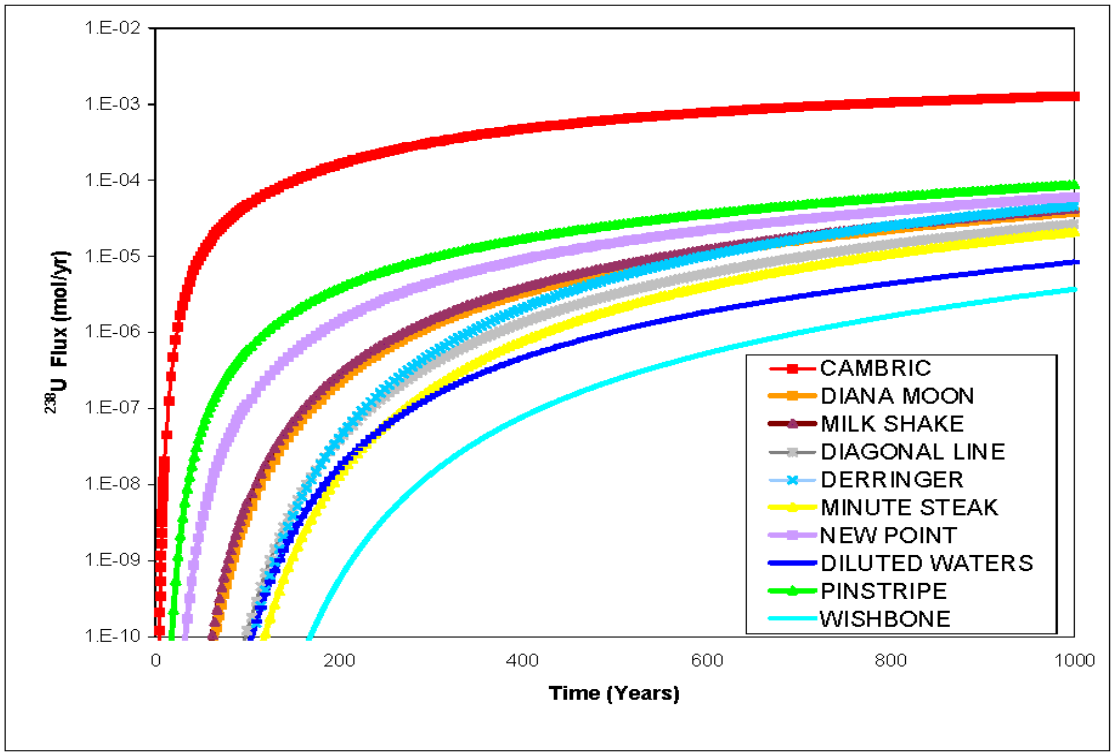

Figure 5-6
Mass Fluxes for ^{238}U From the SSM for Each Frenchman Flat Test

6.0 Summary and Limitations

The Frenchman Flat CAU transport model requires that the sources of contamination be defined as input to the model. The sources are generally accepted to be the radionuclides released into groundwater from underground nuclear test cavities. A method for estimating the unclassified hydrologic source terms for nuclear tests conducted in the Frenchman Flat area was developed. In this method, a simplified version of an HST process model was developed using GoldSim®. This simplified method was tested against the detailed process model calculations for the CAMBRIC test. A procedure is presented for estimating the source term for the underground nuclear tests of Frenchman Flat using estimates of the unclassified radiologic source terms published by Bowen et al. (2001), hydrologic information from the Frenchman Flat hydrologic data document (SNJV, 2004d) and the Frenchman Flat Transport Parameter document (SNJV, 2005), and test-specific characteristics.

The radionuclide data available for groundwater sampling sites located within the the Frenchman Flat area were compiled and assessed. These data will be used to attempt to constrain the simulation results of the CAU radionuclide transport model. In general, groundwater radionuclide concentrations are low (most likely background) at well locations other than those associated with the CAMBRIC RNM project. Radionuclide contamination was observed in the near-field well associated with the CAMBRIC RNM project. During the RNM project, an artificial gradient was applied that accelerated radionuclide transport.

The simplified hydrologic source term model presented in this document is based on simplifying assumptions that may place limitations on the results. The assumptions or simplifications and associated limitations are identified in Table 6-1.

Table 6-1
Source Model Assumptions or Simplifications
and Associated Limitations

Assumption or Simplification	Limitation
Total mass of each radionuclide in the study area is based on the unclassified inventory of Bowen et al. (2001). Bowen et al. (2001) also provides estimates of associated accuracies.	The total mass of radionuclides in Frenchman Flat as provided by Bowen et al. (2001) is an adequate unclassified estimate and is not considered a significant limitation.
The initial mass of each radionuclide for each underground test is calculated as the total inventory for the corresponding NTS area averaged by the number of tests in that area.	The initial mass of any radionuclide at a particular test may be significantly in error as a result of this simplification. To overcome this limitation, classified, test-specific data would be required.
Radionuclides are assumed to be uniformly distributed in the exchange volume and melt glass. The form of the radionuclide may be more complicated. For instance the radionuclide may be associated with metamorphosed rubble or slightly melted rock, or may exist as coprecipitated minerals that may not be easily available to groundwater.	The spatial variability of radionuclide mass in the cavity region could lead to errors when compared to measured data from cavities, even if classified source inventories are used. Disregard of the form of the radionuclide may tend to overestimate the fraction of the radionuclides that is initially in the cavity water.
The chemical reactions are based on assumed linear adsorption isotherms.	The work of Tompson et al. (1999) and Pawloski et al. (2001) clearly show that near-field heterogeneity in reactive mineral distribution controls the near-field migration of radionuclides. At larger distances, the linear isotherm approach is expected to have greater validity, if K_d values can be defined.
Saturation limits on melt glass dissolution are ignored in this analysis.	The radionuclide flux due to melt glass dissolution may be overestimated by ignoring the effect of saturation of silica that might limit dissolution.
Distribution coefficients (K_ds) for the radionuclides at the PIN STRIPE test are based on mineralogy of the alluvium deposits within the northern Frenchman Flat testing area.	Volcanic deposits have different mineralogy which could result in significantly different K_ds. This could effect the retardation of the sorbing radionuclides and the time of their estimated arrival and relative concentrations at the breakthrough plane.
Test holes located above the water table are projected downward to the water table for purposes of simulating transport of radionuclides.	Travel velocities in the vadose zone, where these tests are located, are likely to be significantly slower than in the saturated groundwater aquifers.
Travel velocities, distances, and orientations to the breakthrough planes are based on the preliminary evaluation of the ground water flow field under test areas 5 and 11.	A Phase II flow model is being calibrated for Frenchman Flat. Results of this model will be used when the final models are used for transport analyses. Therefore, the results provided herein are the current best estimate of radionuclide transport and may be revised once the flow model is finalized.

7.0 References

Abdel-Fattah, A., P.W. Reimus, and M.J. Haga. 2003. *Colloid Concentration and Size Distribution Analyses of Groundwater Samples from Different Wells at the Nevada Test Site*. Letter report to R. Bangerter, U.S. Department of Energy, Nevada Operations Office. Los Alamos, NM: Los Alamos National Laboratory. BN, see Bechtel Nevada.

Bechtel Nevada. 2003. *Nevada Test Site Radiological Environmental Monitoring Plan,* DOE/NV/11718-804. Las Vegas, NV.

Bechtel Nevada. 2004a. *A Hydrostratigraphic Model and Alternatives for the Groundwater Flow and Contaminant Transport Model of Corrective Action Unit 98: Frenchman Flat, Clark, Lincoln and, Nye Counties, Nevada*. Prepared for U.S. Department of Energy, National Nuclear Security Administration Nevada Operations Office. Las Vegas, NV.

Bechtel Nevada. 2004b. *Nevada Test Site Environmental Report 2003,* DOE/NV/11718-971. Las Vegas, NV.

Bethke, C.M. 1996. *Geochemical Reaction Modeling*. Oxford University Press, New York.

Borg, I.Y., R. Stone, H.B. Levy, and L.D. Ramspott. 1976. *Information Pertinent to the Migration of Radionuclides in Ground Water at the Nevada Test Site, Part 1: Review and Analysis of Existing Information,* UCRL-52078. Livermore, CA: Lawrence Livermore National Laboratory.

Bowen, S.M., D.L. Finnegan, J.L. Thompson, C.M. Miller, P.L. Baca, L.F. Olivas, C.G. Geoffrion, D.K. Smith, W. Goishi, B.K. Esser, J.W. Meadows, N. Namboodiri, and J.F. Wild. 2001. *Nevada Test Site Radionuclide Inventory, 1951-1992,* LA-13859-MS. Los Alamos, NM: Los Alamos National Laboratory.

Bryant, E.A. 1992. *The Cambric Migration Experiment*, A Summary Report, LA-12335-MS. Los Alamos, NM: Los Alamos National Laboratory.

Buddemeier, R.W., and D. Isherwood. 1985. *Radionuclide Migration Project 1984 Progress Report*, UCRL-53628. Livermore, CA: Lawrence Livermore National Laboratory.

Burbey, T.J., and S.W. Wheatcraft. 1986. *Tritium and Chlorine-36 Migration from a Nuclear Explosion Cavity,* Publication No. 45050. Las Vegas, NV: Desert Research Institute.

Carle, S.F., M. Zavarin, and G.A. Pawloski. 2002. *Geostatistical Analysis of Spatial Variability of Mineral Abundance and K_d in Frenchman Flat, NTS, Alluvium*, UCRL-ID-150200. Livermore, CA: Lawrence Livermore National Laboratory.

DOE, see U.S. Department of Energy.

DOE/NV, see U.S. Department of Energy, Nevada Operations Office.

FFACO, *see Federal Facility Agreement and Consent Order.*

Federal Facility Agreement and Consent Order. 1996 (as amended). Agreed to by the State of Nevada, the U.S. Department of Energy, and the U.S. Department of Defense.

Finnegan, D.L., and J.L. Thompson. 2001. *Laboratory and Field Studies Related to Radionuclide Migration at the Nevada Test Site in Support of the Underground Test Area and Hydrologic Resources Management Projects October 1, 1999-September 30, 2000,* LA-13787-PR. Los Alamos, NM: Los Alamos National Laboratory.

Finnegan, D.L., and J.L. Thompson, 2002. *Laboratory and Field Studies Related to Radionuclide Migration at the Nevada Test Site in Support of the Underground Test Area and Hydrologic Resources Management Projects,* LA-13919-MS. Los Alamos, NM: Los Alamos National Laboratory.

Finnegan, D.L., and J.L. Thompson. 2004. *Laboratory and Field Studies Related to Radionuclide Migration at the Nevada Test Site in Support of the Underground Test Area and Hydrologic Resources Management Projects October 1, 2002-September 30, 2003,* LA-14151-PR. Los Alamos, NM: Los Alamos National Laboratory.

Golder Associates. 2002a. User's Guide: GoldSim Contaminant Transport Module, Version 1.30. Redmond, WA: Golder Associates, Inc.

Golder Associates. 2002b. User's Guide: GoldSim Graphical Simulation Environment, Version 7.40. Redmond, WA: Golder Associates, Inc.

Hoffman, D.C., R. Stone, W.W. Dudley, Jr. 1977. *Radioactivity in the Underground Environment of the Cambric Nuclear Explosion at the Nevada Test*, LA-6877-MS. Los Alamos, NM: Los Alamos National Laboratory.

IAEA, see International Atomic Energy Agency.

IT, see IT Corporation.

International Atomic Energy Agency. 1998. *The Radiological Situation at the Atolls of Mururoa and Fangataufa, Technical Report, Volume 3: Inventory of Radionuclides Underground at the Atolls*, IAEA-MFTR-3. Proceedings of an IAEA Conference, Vienna, 30 June - 3 July 1998, to present the results of the International Study. Vienna, Austria.

IT Corporation. 1998. *Underground Test Area Subproject Corrective Action Unit 98: Frenchman Flat Data Analysis Task: Vol. I - Hydrostratigraphic Model Documentation Package*, Rev.0, DOE/NV/13052-044. Prepared for U.S. Department of Energy, Nevada Operations Office. Las Vegas, NV.

IT Corporation. 1999a. *External Peer Review Group Report on Frenchman Flat Data Analysis and Modeling Task, Underground Test Area Project*, *Revision No. 0*, ITLV/13052-077. Las Vegas, NV.

IT Corporation. 1999b. *Underground Test Area Project Corrective Action Unit 98: Frenchman Flat, Vol. II - Groundwater Data Documentation Package,* Rev. 0, DOE/NV/13052-044-V2. Prepared for U.S. Department of Energy, Nevada Operations Office. Las Vegas, NV.

IT Corporation. 1999c. *Underground Test Area Project Corrective Action Unit 98: Frenchman Flat, Vol. III - Groundwater Flow and Contaminant Transport Model Documentation Package*. Prepared for U.S. Department of Energy, Nevada Operations Office. Las Vegas, NV.

IT Corporation. 2000a. *Lessons Learned from the Frenchman Flat Corrective Action Groundwater Flow and Radionuclide Transport Model*. Las Vegas, NV.

IT Corporation. 2000b. *Frenchman Flat Well Cluster ER-5-3 Data Report for Development and Hydraulic Testing*. Las Vegas, NV.

IT Corporation. 2001. *Frenchman Flat Well Cluster ER-5-3 Data Report for Development and Hydraulic Testing*. Las Vegas, NV.

IT Corporation. 2001b. *Frenchman Flat Well ER-5-4 Data Report for Development and Hydraulic Testing*. Las Vegas, NV.

Kersting, A.B. 1996. *The State of the Hydrologic Source Term.* UCRL-ID-126557. Livermore, CA: Lawrence Livermore National Laboratory.

Kersting, A.B., and P.W. Reimus. 2003. *Colloid-Facilitated Transport of Low-Solubility Radionuclides: A Field, Experimental, and Modeling Investigation*, UCRL-ID-149688. Livermore, CA: Lawrence Livermore National Laboratory and Los Alamos, NM: Los Alamos National Laboratory.

Kersting, A.B., D. L. Finnegan, A.F.B. Tompson, B.K. Esser, D.K. Smith, M. Zavarin, C.J. Bruton, and G.A. Pawloski. 2003. *Radionuclide Decay and In-growth Technical Basis Document,* UCRL-ID-153798. Livermore, CA: Lawrence Livermore National Laboratory.

Laczniak, R.J., J.C. Cole, D.A. Sawyer, and D.A. Trudeau. 1996. *Summary of Hydrogeologic Controls on Ground-Water Flow at the Nevada Test Site, Nye County, Nevada,* USGS-WRIR-96-4109. Denver, CO: U.S. Geological Survey.

LANL, see Los Alamos National Laboratory.

LLNL, see Lawrence Livermore National Laboratory.

Marsh, K.V. comp. 1991. *Hydrology and Radionuclide Migration Program, 1987 Progress Report,* UCRL-53779-87. Livermore, CA: Lawrence Livermore National Laboratory.

Nimz, G.J., and J.L. Thompson. 1992. *Underground Radionuclide Migration at the Nevada Test Site*, DOE/NV-346. Las Vegas, NV: Reynolds Electrical & Engineering Co., Inc.

Nitao, J.J. 1988. Reference Manual for the NUFT Flow and Transport Code, Version 2.0, UCRL-MA-130651. Livermore, CA: Lawrence Livermore National Laboratory.

Ogard, A.E., J.L. Thompson, R.S. Rundberg, K. Wolfsberg, P.W. Kubic, D. Eklmore, and H.W. Bentley. 1988. "Migration of Chlorine-36 and Tritium from an Underground Nuclear Test." In *Radiochim. Acta,* Vol. 44/45: 213-217. Munich, Germany: R. Oldenburg.

Olsen, C.W. 1967. *Time History of Cavity Pressure and Temperature Following a Nuclear Detonation in Alluvium,* UCRL-70379. Livermore, CA: Lawrence Livermore National Laboratory.

Papelis, C., and W. Um. 2003a. *Evaluation of Cesium, Strontium, and Lead Sorption, Desorption, and Diffusion in Volcanic Tuffs from Frenchman Flat, Nevada Test Site: Macroscopic and Spectroscopic Investigations*, DOE/NV/13609-18, DRI Publication No. 45189. Las Vegas, NV.

Pawloski, G.A. 1999. *Development of Phenomenological Models of Underground Nuclear Tests on Pahute Mesa, Nevada Test Site–BENHAM and TYBO,* UCRL-ID-136003. Livermore, CA: Lawrence Livermore National Laboratory.

Pawloski, G.A., A.F.B. Tompson, and S.F. Carle, eds. 2001. *Evaluation of the Hydrologic Source Term from Underground Nuclear Test on Pahute Mesa at the Nevada Test Site:* the CHESHIRE Test, UCRL-ID-147023. Livermore, CA: Lawrence Livermore National Laboratory.

Rose, T.P. 2003a. *Isotopic Analyses: Environmental Monitoring Well ER-5-3*. Livermore, CA: Lawrence Livermore National Laboratory.

Rose, T.P. 2003b. *Isotopic Analyses: Environmental Monitoring Well ER-5-3#2*. Livermore, CA: Lawrence Livermore National Laboratory.

Rose, T.P. 2003c. *Isotopic Analyses: Environmental Monitoring Well ER-5-4*. Livermore, CA: Lawrence Livermore National Laboratory.

Rose, T.P. 2003d. *Isotopic Analyses: Environmental Monitoring Well ER-5-4#2*. Livermore, CA: Lawrence Livermore National Laboratory.

Rose, T.P., D.K. Smith, and D.L. Phinney. 2000. "Secondary Ion Mass Spectrometry Measurements of Volcanic Tuffs Containing Radionuclides from Underground Nuclear Tests." In *Radiochim*. Acta, Vol. 88: 465 - 473. Munich, Germany: R. Oldenberg.

Rose, T.P., G.F. Eaton, and A.B. Kersting, eds. 2003. *Hydrologic Resources Management Program and Underground Test Area Project FY2001-2002 Progress Report,* UCRL-ID-154357. Livermore, CA: Lawrence Livermore National Laboratory.

Rose, T.P., G.F. Eaton, and A.B. Kersting, eds. 2004. *Hydrologic Resources Management Program and Underground Test Area Project FY2003 Progress Report,* UCRL-ID-206661. Livermore, CA: Lawrence Livermore National Laboratory.

Shaw, see Shaw Environmental, Inc.

Shaw Environmental, Inc. 2003. *Frenchman Flat Well ER-5-4 # 2 Data Report for Development and Hydraulic Testing*.

SNJV, see Stoller-Navarro Joint Venture

Smith, D.K. 1993. *Review of Literature Pertaining to the Leaching and Sorption of Radionuclides Associated with Nuclear Explosive Melt Glasses,* UCRL-ID-113370. Livermore, CA: Lawrence Livermore National Laboratory.

Smith, D.K. 1995a. *Challenges in Defining a Radiologic and Hydrologic Source Term for Underground Nuclear Test Centers, Nevada Test Site, Nye County, Nevada,* UCRL-JC-120389. Livermore, CA: Lawrence Livermore National Laboratory.

Smith, D.K. 1995b. *Phenomenology of Underground Nuclear Explosions Conducted at the Nevada Test Site with Emphasis on Recent Experience at BASEBALL (U7ba) and INGOT (U2gg).* Prepared for the U.S. Department of Energy, Nevada Operations Office. Livermore, CA: Lawrence Livermore National Laboratory.

Smith, D.K. 2001. *Unclassified Radiologic Source Term for Nevada Test Site Areas 19 and 20,* UCRL-ID-141706. Livermore, CA: Lawrence Livermore National Laboratory.

Smith, D.K. 2002. *Evaluation of the Radiochemistry of Near-Field Water Samples at the Nevada Test Site Applied to the Definition of a Hydrologic Source Term*, UCRL-ID-149049. Livermore, CA: Lawrence Livermore National Laboratory.

Smith, D.K., B.K. Esser, and J.L. Thompson. 1995. *Uncertainties Associated with the Definition of a Hydrologic Source Term for the Nevada Test Site,* UCRL-ID-120322. Livermore, CA: Lawrence Livermore National Laboratory.

Smith, D.K., R.J. Nagle, and J.M. Kenneally. 1996. "Migration of Fission Products at the Nevada Test Site: Detection with an Isotopic Tracer." In *Radiochim*. *Acta*, 52/53: 229 – 231. Munich, Germany: R. Oldenberg.

Stoller-Navarro Joint Venture. 2004a. *Assessment of Radionuclide Migration from Underground Nuclear Tests in Northern Frenchman Flat, Nevada Test Site*. Prepared for U.S. Department of Energy. Las Vegas, NV.

Stoller-Navarro Joint Venture. 2004b. *Integrated Analysis Report for Single and Multiple-Well Aquifer Testing at Frenchman Flat Well Cluster RNM-2s, Nevada Test Site, Nevada*, S-N/99205-029, Rev. 0. Las Vegas, NV.

Stoller-Navarro Joint Venture. 2004c. *Interpretation of Hydraulic Test and Multiple-Well Aquifer Test Data at Frenchman Flat Well Cluster ER-5-3.* Las Vegas, NV.

Stoller-Navarro Joint Venture. 2004d. *Phase II Hydrologic Data for the Groundwater Flow and Contaminant Transport Model of Corrective Action Unit 98:Frenchman Flat, Nye County, Nevada*, S-N/99205-032. Prepared for U.S. Department of Energy. Las Vegas, NV.

Stoller-Navarro Joint Venture. 2004e. *A User's Guide to the Comprehensive Water Quality Database for Groundwater in the Vicinity of the Nevada Test Site.* S-N/99205-026, Rev. 7. Las Vegas, NV.

Stoller-Navarro Joint Venture. 2005. *Phase II Contaminant Transport Parameters for the Groundwater Flow and Contaminant Transport Model of Corrective Action Unit 98: Frenchman Flat, Nye County, Nevada*. Las Vegas, NV.

Thompson, J.L., and J.S. Gilmore. 1991. "Migration of Fission Products at the Nevada Test Site: Detection with an Isotopic Tracer." In *Radiochim. Acta,* Vol. 52/53: 229-231. Munich, Germany: R. Oldengerg.

Tompson, A.F.B., C.J. Bruton, and G.A. Pawloski (eds.). 1999. *Evaluation of the Hydrologic Source Term from Underground Nuclear Tests in Frenchman Flat at the Nevada Test Site: The CAMBRIC Test,* UCRL-ID-132300. Livermore, CA: Lawrence Livermore National Laboratory.

Tompson, A.F.B., D.K. Smith, and G.B. Hudson. 2002. *Analysis of Radionuclide Migration Through a 200-m Vadose Zone Following a 16-year Infiltration Event,* UCRL-ID-146979. Livermore, CA: Lawrence Livermore National Laboratory.

Tompson, A.F.B., M. Zavarin, C.J. Bruton, and G.A. Pawloski. 2004. *Method for Calculating a Simplified Hydrologic Source Term for Frenchman Flat Sensitivity Studies of Radionuclide Transport Away From Underground Nuclear Tests,* UCRL-TR-201817. Livermore, CA: Lawrence Livermore National Laboratory.

Tompson, A.F.B., S.F. Carle, R.M. Maxwell, G. Pawloski, and M. Zavarin. 2005. Evaluation of the Non-Transient Hydrologic Source Term from the CAMBRIC Underground Nuclear Test in Frenchman Flat, Nevada Test Site. August 5, 2005, Livermore, CA. Lawrence Livermore National Laboratory.

U.S. Congress, Office of Technology Assessment. 1989. *The Containment of Underground Explosions.* Washington, DC: U.S. Government Printing Office. OTA-ISC-414.

U.S. Department of Energy, Nevada Operations Office. 1997a. *Regional Groundwater Flow and Tritium Transport Modeling and Risk Assessment of the Underground Test Area, Nevada Test Site, Nevada,* DOE/NV–477. Las Vegas, NV.

U.S. Department of Energy, Nevada Operations Office. 1997b. *Shaft and Tunnel Nuclear Detonations at the Nevada Test Site: Development of a Primary Database for the Estimation of Potential Interactions with the Regional Groundwater System,* DOE/NV–464. Las Vegas, NV.

U.S. Department of Energy, Nevada Operations Office. 1999. *Corrective Action Investigation Plan for Corrective Action Unit 98: Frenchman Flat, Nevada Test Site, Nevada*, DOE/NV--478-Rev. 1. Las Vegas, NV.

U.S. Department of Energy, Nevada Operations Office. 2000a. *Underground Test Area Quality Assurance Project Plan, Nevada Test Site, Nevada,* DOE/NV--341, Rev. 3. Las Vegas, NV.

U.S. Department of Energy, Nevada Operations Office. 2000b. *United States Nuclear Tests, July 1945 through September 1992,* DOE/NV--209, Rev. 15. Las Vegas, NV.

U.S. Department of Energy, Nevada Operations Office. 2001. *Addendum to Revision 1 of the Corrective Action Investigation Plan for Corrective Action Unit 98: Frenchman Flat, Nevada Test Site, Nevada,* Rev. 1, DOE/NV--478 REV. 1-ADD. Las Vegas, NV.

Warren, R.G., F.C. Benedict Jr., T.P. Rose, D.K. Smith, S.J. Chipera, E.C. Kluk, and K.M. Raven. 2002. *Alluvial Layering and Distribution of Reactive Phases within Drill Holes ER-5-4 and UE-5n of Frenchman Flat,* LA-UR-02-6206. Los Alamos, MN: Los Alamos National Laboratory.

Zavarin, M., S.K. Roberts, T.P. Rose, D.L. Phinney. 2002. *Validating Mechanistic Sorption Model Parameters and Process for Reactive Transport In Alluvium,* UCRL-ID-149728. Livermore, CA: Lawrence Livermore National Laboratory.

Zavarin, M., and C.J. Bruton. 2004a. *A Non-Electrostatic Surface Complexation Approach to Modeling Radionuclide Migration at the Nevada Test Site: II. Aluminosilicates,* UCRL-TR-208672. June 6. Livermore, CA: Lawrence Livermore National Laboratory.

Zavarin, M., and C.J. Bruton. 2004b. *A Non-Electrostatic Surface Complexation Approach to Modeling Radionuclide Migration at the Nevada Test Site: I. Iron Oxides and Calcite,* UCRL-TR-208673. June 6. Livermore, CA: Lawrence Livermore National Laboratory.

Zavarin, M., S.K. Roberts, P. Zhao, R. W. Williams, T. P. Rose, A. Rainer, and G.A. Pawloski. 2004c. *High -Temperature Studies of Glass Dissolution Rates Close to Saturation.,* UCRL-TR-204874. Livermore, CA: Lawrence Livermore National Laboratory.

Zavarin, M., S.K. Roberts, B.E. Viani, G.A. Pawloski, and T.P. Rose. 2004d. *Nuclear Melt Glass Dissolution and Secondary Mineral Precipitation at 40 to 200C.,* UCRL-TR-204870. Livermore, CA: Lawrence Livermore National Laboratory.

Zavarin, M., S.F. Carle, and R.M. Maxwell. 2004e. *Upscaling Radionuclide Retardation - Linking the Surface Complexation and Ion Exchange Mechanistic Approach to a Linera K_d Approach,* UCRL-TR-204713. Livermore, CA: Lawrence Livermore National Laboratory.

Appendix A

Hydrostratigraphic Model Supporting Information

A.1.0 Description of the Frenchman Flat Model Hydrogeologic and Hydrostratigraphic Units

The hydrogeologic framework used in the NTS regional model, which is adapted to create the CAU-scale Frenchman Flat hydrogeologic framework, is based on a conceptual hydrologic system established for the NTS area by Winograd and Thordarson (1975) and Blankennagel and Weir (1973). The rocks of the NTS have been classified for hydrologic modeling using a two-level classification scheme in which hydrogeologic units (HGUs) are grouped to form hydrostratigraphic units [HSUs] IT, 1996b). Rocks of the NTS and vicinity were classified as one of eight HGUs, which include the alluvial aquifer, four volcanic HGUs, an intrusive HGU, and two HGUs that represent the pre-Tertiary sedimentary and metasedimentary rocks (Table A.2-1). The nine HSUs defined for the NTS regional HSU model that are within the Frenchman Flat model area are listed in Table A.2-2. New HGUs and HSUs, along with additional detail, have been added to this basic framework definition.

The Frenchman Flat hydrostratigraphic framework model (BN, 2004) includes considerable structural detail and stratigraphic enhancement over the NTS regional HSU model (IT, 1996b). The total number of HSUs increased from 9 to 17. Brief descriptions of the HSUs and HGUs used to construct the Frenchman Flat geologic model are provided in Table A.2-3. They are listed in approximate order from surface to basement, although some are laterally rather than vertically contiguous, and not all units are present in all parts of the model area. Table A.2-4 shows the correlation of Frenchman Flat HSUs with HSUs from earlier hydrostratigraphic models for this region. These correlated units have been updated and revised to include mineralogy, a necessary component for generalizations between units when assessing transport parameters (BN, 2004).

A.2.0 References

Bechtel Nevada. 2002. *Hydrostratigraphic Model and Alternatives for the Groundwater Flow and Contaminant Transport Model of Corrective Action Units 101 and 102: Central and Western Pahute Mesa, Nye County, Nevada*, DOE/NV/11718-706, Prepared for U.S. Department of Energy, National Nuclear Security Administration Nevada Operations Office. Las Vegas, NV.

Bechtel Nevada. 2004. *Hydrostratigraphic Model of the Frenchman Flat Area, Nye County, Nevada,* DOE/NV/11718-XXX. Prepared for U.S. Department of Energy, National Nuclear Security Administration Nevada Operations Office. Las Vegas, NV.

Blankennagel, R.K., and J.E. Weir, Jr. 1973. *Geohydrology of the Eastern Part of Pahute Mesa, Nevada Test Site, Nye County, Nevada*, USGS Professional Paper 712-B. Denver, CO: U.S. Geological Survey.

Ferguson, J.F., A.H. Cogbill, and R.G. Warren. 1994. "A Geophysical-Geological Transect of the Silent Canyon Caldera Complex, Pahute Mesa, Nevada." In *Groundwater*, Vol. 99 (B3): 4323-4339. Columbus, OH: Groundwater Publishing Company.

Gonzales, J.L., S.L. Drellack, Jr., and M.T. Townsend. 1998. *Descriptive Narrative for the Hydrogeologic Model of the Yucca Flat Corrective Action Unit: An Interim Report. U.S. Department of Energy, Nevada Operations Office.* Las Vegas, NV: Bechtel Nevada, Geology/Hydrology Group.

IT Corporation. 1996a. *Groundwater Recharge and Discharge Data Documentation Package (Phase I Data Analysis Documentation,* Volume III). Prepared for the U.S. Department of Energy, Nevada Operations Office. Las Vegas, NV.

IT Corporation. 1996b. *Regional Geologic Model Data Documentation Package (Phase 1 Data Analysis Documentation, Volume I)*. Prepared for the U.S. Department of Energy, Nevada Operations Office. Las Vegas, NV.

IT Corporation. 1998. *Underground Test Area Project Corrective Action Unit 98: Frenchman Flat Data Analysis Task: Vol. I - Hydrostratigraphic Model Documentation Package*, DOE/NV/13052-044. Prepared for U.S. Department of Energy, Nevada Operations Office. Las Vegas, NV.

Slate, J.L., M.E. Berry, P.D. Rowley, C.J. Fridrich, K.S. Morgan, J.B. Workman, O.D. Young, G.L. Dixon, V.S. Williams, E.H. McKee, D.A. Ponce, T.G. Hildenbrand, W.C. Swadley, S.C. Lundstrom, E.B. Ekren, R.G. Warren, J.C. Cole, R.J. Fleck, M.A. Lanphere, D.A. Sawyer, S.A. Minor, D.J. Grunwald, R.J. Laczniak, C.M. Menges, J.C. Yount, and A.S. Jayko. 1999. *Digital Geologic Map of the Nevada Test Site and Vicinity, Nye, Lincoln, and Clark Counties, Nevada, and Inyo County, California,* USGS-OFR-99-554-A. Denver, CO: U.S. Geological Survey.

Winograd, I.J., and W. Thordarson. 1975. *Hydrogeologic and Hydrochemical Framework, South-Central Great Basin, Nevada-California, with Special Reference to the Nevada Test Site,* USGS-PP-712-C. Denver, CO: U.S. Geological Survey.

Table A.2-1
Hydrogeologic Units of the NTS Regional Model

Hydrogeologic Unit	Typical Lithologies	Hydrologic Significance
Alluvial Aquifer (AA) (AA is also an HSU in hydrogeologic models)	Unconsolidated to partially consolidated gravelly sand, aeolian sand, and colluvium; thin, basalt flows of limited extent.	Has characteristics of a highly conductive aquifer, but less where lenses of clay-rich paleocolluvium or playa deposits are present.
Welded Tuff Aquifer (WTA)	Welded ash-flow tuff, vitric to devitrified	Degree of welding greatly affects interstitial porosity (less porosity as degree of welding increases) and permeability (greater fracture permeability as degree of welding increases).
Vitric Tuff Aquifer (VTA)	Bedded tuff, ash-fall and reworked tuff; vitric	Constitutes a volumetrically minor HGU; generally does not extend far below the static water level due to tendency of tuffs to become zeolitic (which drastically reduces permeability) under saturated conditions; significant interstitial porosity (20 to 40 percent); generally insignificant fracture permeability.
Lava Flow Aquifer (LFA)	Rhyolite lava flows; includes flow breccias (commonly at base) and pumiceous zones (commonly at top)	Generally a caldera-filling unit and/or of local extent; hydrogeologically complex; wide range of transmissivities; fracture density and interstitial porosity differ with lithologic variations.
Tuff Confining Unit (TCU)	Zeolitic bedded tuff with interbedded, but less significant, zeolitic, nonwelded to partially welded ash-flow tuff	May be saturated but measured transmissivities are very low; may cause accumulation of perched and/or semi-perched water in overlying units.
Intrusive Confining Unit (ICU)	Granodiorite, quartz monzonite	Relatively impermeable; forms local bulbous stocks; north of Rainier Mesa, Yucca Flat, and scattered elsewhere in the NTS regional model area; may contain perched water.
Clastic Confining Unit (CCU)	Argillite, siltstone, quartzite	Clay-rich rocks are relatively impermeable; more siliceous rocks are fractured, but with fracture porosity generally sealed due to secondary mineralization.
Carbonate Aquifer (CA)	Dolomite, limestone	Transmissivity values vary greatly and are directly dependent on fracture frequency.

Source: Adapted from IT (1996b) and BN (2004)

Table A.2-2
Hydrostratigraphic Units of the Frenchman Flat Area Included in the NTS Regional Hydrostratigraphic Framework Model

HSU Layer Number[a]	Hydrostratigraphic Unit (Symbol)	Dominant Hydrogeologic Unit(s)[b]	Stratigraphic Unit Map Symbols[c]	General Description
20	Alluvial Aquifer (AA) (this term is also used to designate a hydrogeologic unit)	AA	Qay, QTc, Qam, QTa, Qtu, Tybf, Tt	Consists mainly of alluvium that fills extensional basins such as Gold Flat, Crater Flat, Kawich Valley, and Sarcobatus Flat. Also includes generally older Tertiary gravels, tuffaceous sediments, and nonwelded tuffs (where thin) that partially fill other basins such as Oasis Valley and the moat of the Timber Mountain caldera complex.
19	Timber Mountain Aquifer (TMA)	Mostly WTA, minor VTA; TCU within the Tm caldera complex	Tm, Tp	"The uppermost welded tuffs" in the Frenchman Flat model area consists mainly of extra-caldera welded ash-flow tuffs (aquifer-like lithologies). However, the altered intra-caldera equivalent rocks within the Timber Mountain caldera are modeled as confining units.
15	Tuff Confining Unit (TCU)	TCU	Th, Tw, Tc, Tn, To	Mostly zeolitized nonwelded tuffs.
14	Volcanic Aquifer (VA)	WTA, VTA, LFA	Tm, Tp, Tw, Tc	Imprecisely known grouping of volcanic rocks; generally with aquifer-like qualities. Also used as a lumping unit away from the more data-rich NTS.
12	Volcaniclastic Confining Unit (VCCU)	TCU, minor AA, lesser CA	Tgp, Tgw	Complex three-dimensional distribution of zeolitic nonwelded tuff, gravels, mudstones, and limestones. Present in the southern portion of the Frenchman Flat model area.
11	Volcanics undifferentiated (VU)	WTA,TCU, lesser LFA	Potentially includes all Tertiary volcanic units	All Quaternary and Tertiary volcanics outside the NTS proper and the proximal NTS caldera complex.
8	Upper Clastic Confining Unit (UCCU)	CCU	MDc, MDe	Late Devonian through Mississippian siliciclastic rocks. Present in the northeastern corner (CP basin) of the Frenchman Flat model area.
7	Lower Carbonate Aquifer (LCA)	CA	Dg through Cc	Cambrian through Devonian mostly limestone and dolomite. Widespread throughout the Frenchman Flat model area.
6	Lower Clastic Confining Unit (LCCU)	CCU	Cc, Cz, Czw, Zs, Zj	Late Proterozoic through Early Cambrian siliciclastic rocks. Widespread throughout the Frenchman Flat model area.

[a]NTS UGTA regional model (IT, 1996b)
[b]See Table A-1-1 for definitions of HGUs
[c]Refer to Slate et al. (1999) and Ferguson et al. (1994) for definitions of stratigraphic unit map symbols

Table A.2-3
Hydrostratigraphic Units of the Frenchman Flat Hydrostratigraphic Framework Model
(Page 1 of 2)

Hydrostratigraphic Unit (Symbol)	Dominant Hydrogeologic Unit(s) [a]	Stratigraphic Unit Map Symbols [b]	General Description
Alluvial Aquifer (AA, AA3, AA2, AA1) (this term is also used to designate a hydrogeologic unit)	AA	Qay, QTc, Qai, QTa, Tt	Consists mainly of alluvium that fills extensional basins. Also includes generally older Tertiary gravels, and very thin air-fall tuffs (e.g. Tt). AA, AA1, AA2, and AA3 are equivalent hydrogeologically except for position relative to other HSUs embedded within the alluvial section.
Playa Confining Unit (PCU2T)	PCU	Qp	Clayey silt and sandy silt forms the Frenchman Flat playa (dry lake).
Basalt Lava Flow Aquifer (BLFA)	LFA	Tybf	Several (possibly dissected) basalt flows recognized in the middle of the alluvial section of the northeastern Frenchman Flat. Possibly related to other basalt flows in Nye Canyon.
Older Alluvial Aquifer (OAA, and OAA1)	AA	QTa	Older, denser, zeolitized alluvium recognized only in northern Frenchman Flat. OAA and OAA1 are equivalent except for position; the OAA is above the BLFA and the OAA1 is stratigraphically beneath the BLFA.
Older Playa Confining Unit (PCU1U and PCU1L)	PCU	QTp	Deep, subsurface playa deposits in the deepest portion of Frenchman Flat. Recognized in Well ER-5-4#2 and with 3-D seismic data. The PCU1U and PCU1L are similar except for position.
Timber Mountain Welded Tuff Aquifer (TM-WTA)	Mostly WTA, minor VTA	Tma, Tmab, Tmr	Consists mainly of extra-caldera welded ash-flow tuffs of Ammonia Tanks Tuff and Rainier Mesa Tuff. Unit occurs mostly in north and central Frenchman Flat. Prolific aquifer when saturated.
Timber Mountain Lower Vitric Tuff Aquifer (TM-LVTA)	VTA	Tma, Tmab, Tmr, Tmrh, Tp, Th	Defined to include all unaltered (non-zeolitic) nonwelded and bedded tuffs below the welded Tmr and above the level of pervasive zeolitization. The presence of the welded Tpt (see TSA) complicates this general description.
Upper Tuff Confining Unit (UTCU)	TCU	Tmr (lower most), Tmrh, Tp	Relatively thin TCU above the TSA. Grouped with the LTCU where the TSA is not present.
Topopah Spring Aquifer (TSA)	WTA	Tpt	The welded ash-flow lithofacies of the Topopah Spring Tuff in Massachusetts Mtn/French Peak area and north-central Frenchman Flat.
Lower Vitric Tuff Aquifer (LVTA)	VTA	Th	Relatively thin VTA unit below the TSA. Grouped with the TM-LVTA where TSA is not present.
Lower Tuff Confining Unit (LTCU and LTCU1)	TCU, minor WTA	Th, Tw, Tc, Tn, To	Generally includes all the zeolitic nonwelded and bedded tuffs in southeastern NTS. May include all units from base of Tmr to top of Paleozoic-age rocks. The Tw stratigraphic interval grades/interfingers laterally (westward) into the WCU (see below). Zeolitic bedded tuffs stratigraphically below the WCU (e.g. Tc, Tn, and To) are classified as the LTCU1 in order to address the operation requirements of the EarthVision® modeling software.
Wahmonie Confining Unit (WCU)	TCU, minor LFA	Tw (Twu, Twm, Twl, Twis)	Mixture of lava flows, debris flows, lahars, ash-flows, and air-falls. Typically zeolitic, argillic, or hydrothermally altered. Grades/interfingers laterally with the LTCU.
Volcaniclastic Confining Unit (VCU)	TCU, minor AA and CA	Tgp, Tgw	Older Tertiary sedimentary rocks of variable lithologies including silts, clays, limestones, gravels and tuffaceous units. Present in southeastern half of Frenchman Flat.

Table A.2-3
Hydrostratigraphic Units of the Frenchman Flat Hydrostratigraphic Framework Model
(Page 2 of 2)

Hydrostratigraphic Unit (Symbol)	Dominant Hydrogeologic Unit(s) [a]	Stratigraphic Unit Map Symbols [b]	General Description
Lower Carbonate Aquifer-Thrust Plate (LCA3)	CA	Dg through Cc	Cambrian through Devonian, mostly limestone and dolomite, rocks that occur in the hanging wall of the Belted Range thrust fault. Present only in the northwest corner (CP basin) of the model area.
Upper Clastic Confining Unit (UCCU)	CCU	Mc, MDe	Late Devonian through Mississippian siliciclastic rocks. Present only in the northwest corner (CP basin) of the model area, northwest of the Cane Spring fault and southwest of the Topgallant fault.
Lower Carbonate Aquifer (LCA)	CA	Dg through Cc	Cambrian through Devonian mostly limestone and dolomite. Regional carbonate aquifer present throughout the model area.
Lower Vitric Tuff Aquifer (LVTA)	VTA	Th	Relatively thin VTA unit below the TSA. Grouped with the TM-LVTA where TSA is not present.
Lower Clastic Confining Unit (LCCU)	CCU	Cc, Cz, CZw, Zs, Zj	Late Proterozoic through Early Cambrian siliciclastic rocks. Hydrologic "basement" present at great depth in the model area.

[a]Hydrogeologic units: See Table 4-3 in BN (2004) for definition of hydrogeologic units.
[b]Stratigraphic units: See Tables 4-1 and 4-2 in BN (2004) for definition of stratigraphic units.

3-D = Three dimensional
HSU = Hydrostratigraphic

Table A.2-4
Correlation of Hydrostratigraphic Units of the Frenchman Flat Model and Earlier UGTA Models

Hydrostratigraphic Unit[a]	Symbol This Report	Correlation with Phase I Frenchman Flat HSU Model[b]	Correlation with NTS Phase I Regional Model[c]	Correlation with Yucca Flat Model[d]	Correlation with Pahute Mesa/ Oasis Valley Model[e]
Playa Confining Unit	PCU2	AA[f]	AA[f]	PCU	NP
Alluvial Aquifer	AA			AA	AA
Basalt Lava Flow Aquifer	BLFA			BLFA	YVCM
Older Alluvial Aquifer	OAA and OAA1			NP[g]	NP
Older Playa Confining Unit	PCU1			NP, PCU	NP
Timber Mountain-Welded Tuff Aquifer	TM-WTA	TMA[f]	TMA, TC, VA[f]	TM-WTA	TMA
Timber Mountain-Lower Vitric Tuff Aquifer	TM-LVTA			TM-LVTA	PVTA, CHVTA
Upper Tuff Confining Unit	UTCU			UTCU[d] (YF-UCU)[h]	UPCU, LPCU
Topopah Spring Aquifer	TSA			TSA	TSA
Lower Vitric Tuff Aquifer	LVTA			LVTA	PVTA, CHVTA
Lower Tuff Confining Unit	LTCU	TCU	BCU, VCCU	LTCU[d] (YF-LCU)[h]	CHCU, CFCU, BFCU, PBRCM[i]
Wahmonie Confining Unit	WCU	WCU		NP	NP
Volcaniclastic Confining Unit	VCU	VCCU	VCCU	NP	NP
Lower Carbonate Aquifer-Thrust Plate	LCA3	NP	LCA3	LCA3	LCA3
Upper Clastic Confining Unit	UCCU	NP	UCCU	UCCU	UCCU
Lower Carbonate Aquifer	LCA	PreT[f]	LCA	LCA	LCA
Lower Clastic Confining Unit	LCCU		LCCU	LCCU	LCCU

[a]If correlative to more than one HSU, all HSUs are listed.
[b]See IT (1998) for explanation of initial Frenchman Flat model nomenclature.
[c]See IT (1996a) for explanation of the UGTA Phase I HSU nomenclature.
[d]Documentation for final Yucca Flat model is in progress.
[e]See BN (2002) for explanation of Pahute Mesa/Oasis Valley HSU nomenclature.
[f]Not subdivided.
[g]NP = Not present.
[h]See Gonzales et al. (1998) for explanation of the Yucca Flat HSU nomenclature.
[i]Minor embedded ash-flow tuffs may have better aquifer properties than the bulk of this HSU.

UGTA = Underground Test Area
HSU = Hydrostratigraphic Unit
NTS = Nevada Test Site

Appendix B

Summary Description of GoldSim® Software

B.1.0 GoldSim® Overview

GoldSim® is a general-purpose simulation software program designed to simulate complex systems in support of better decision making. GoldSim® is currently being used to support the investigation of radionuclide migration in groundwater as part of the UGTA Project. GoldSim® models constitute a major departure from the other models. Rather than simulating detailed processes at small scales and integrating those impacts for larger scales, the GoldSim® approach uses 1-D transport simulations to simultaneously assess broad groupings of processes that influence the contaminant boundary. GoldSim® relies on the detailed process models developed for the source of contamination, groundwater flow, and contaminant transport to constrain the possible range of outcomes. The advantage of GoldSim® is speed of simulation and flexibility to incorporate almost any process. As a result, GoldSim® is a convenient method to assess the full range of uncertainty inherent in the system without having to link and simulate numerous detailed process models.

GoldSim® key capabilities include the following:

- The variability and uncertainty present in real-world systems maybe quantitatively addressed using Monte Carlo simulations.
- The occurrence and consequences of discrete events may be superposed onto continuously varying systems.
- Top-down models may be constructed using hierarchical containers which facilitate the simulation of large and complex systems.
- External programs or spreadsheets may be directly and dynamically linked into GoldSim® models.
- Data may be directly exchanged between a GoldSim® model and any Open Database Connectivity-compliant database.

More information about the GoldSim® software may be found in the users guides (Golder, 2002a, b).

B.2.0 References

Golder. 2002a. Users Guide: GoldSim® Contaminant Transport Module, Version 1.30, (April).

Golder. 2002b. Users Guide: GoldSim® Graphical Simulation Environment, Version 7.40, (April).

Appendix C

Description of GeoChem Database

C.1.0 Description of GEOCHEM Database

The *GEOCHEM* database has been developed as part of the UGTA Program with the cooperation of several agencies actively participating in ongoing evaluation and characterization activities under contract to the NNSA/NSO. The database has been constructed to provide up-to-date, comprehensive, and quality-controlled data in a uniform format for the support of current and future projects. The *GEOCHEM* database is updated and distributed on an annual basis. The title of each version contains two digits that indicate the release year (e.g., *GEOCHEM04* for the version released during FY 2004).

Chemistry data have been compiled for groundwater within the NTS and the surrounding region. These data include major ions, organic compounds, trace elements, radionuclides, various field parameters, and environmental isotopes. The area covered by the *GEOCHEM* database extends from approximately 35.6 to 39.7° north latitude and from 114.1 to 117.6° west longitude. Types of sampling sites include precipitation stations, surface water, springs, and wells. Analyses from over 13,000 samples, collected since 1901 from approximately 1,800 springs and wells, are included in the database.

The majority of the data originate from the USGS, LLNL, DRI, BN, EPA, LANL, Reynolds Electrical & Engineering Co., Inc., and the Harry Reid Center for Environmental Studies. Other data sources include published literature and a variety of programs and projects in support of the NNSA/NSO programs. These include the Hydrologic Resources Management Program, the RREMP, and UGTA.

The *GEOCHEM* database is documented in a user's guide (SNJV, 2004) which provides an explanation of the database configuration and summarizes the general content and utility of the individual data tables. The user's guide also provides a description of the quality assurance/quality control protocols for this database. The user's guide also includes full citations of the published data sources in the reference section.

C.2.0 Reference

Stoller-Navarro Joint Venture. 2004. *A User's Guide to the Comprehensive Water Quality Database for Groundwater in the Vicinity of the Nevada Test Site.* S-N/99205-026, Rev. 7. Las Vegas, NV.

Appendix D

Comparison of Mass Fluxes from the SSM and HST Model for 36 Radionuclides in the CAMBRIC Inventory

D.1.0 Comparison of Mass Flux from the SSM and HST Model for Tracer Radionuclides

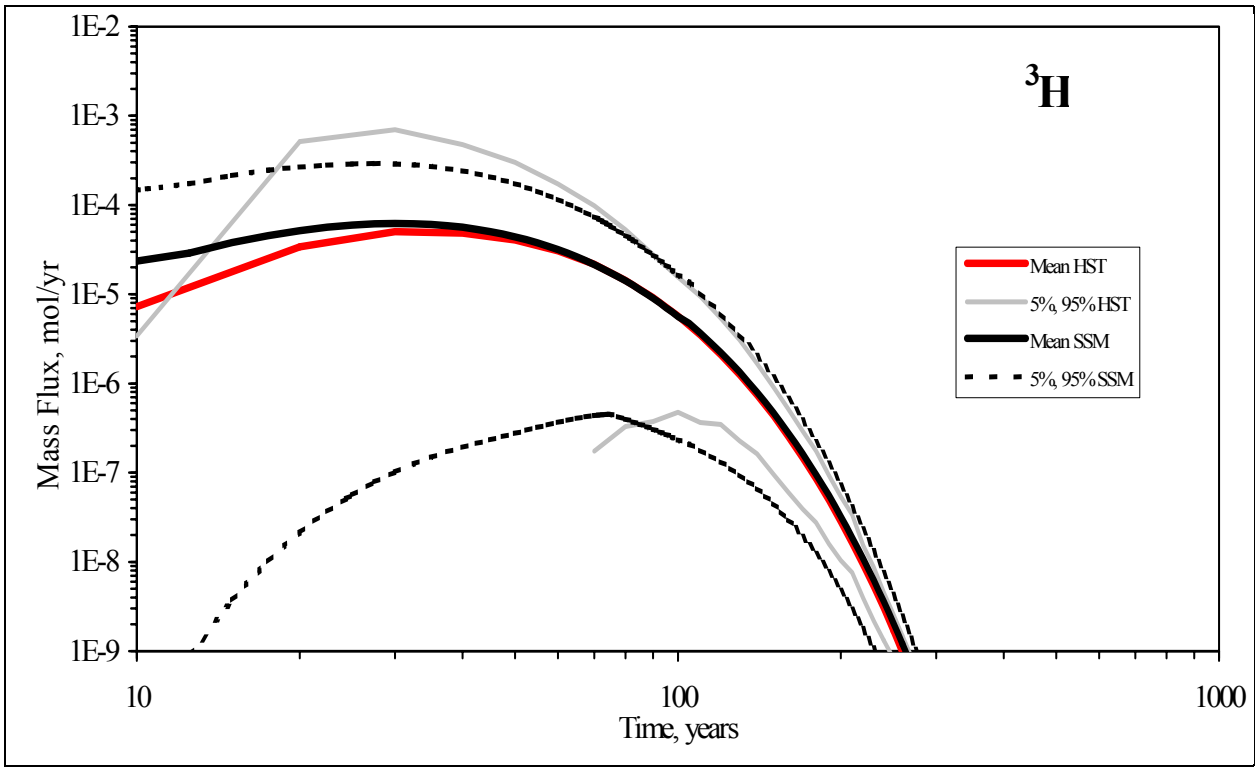

Figure D.1-1
Comparison of ^{3}H Exit Mass Fluxes from the HST Model with the SSM.

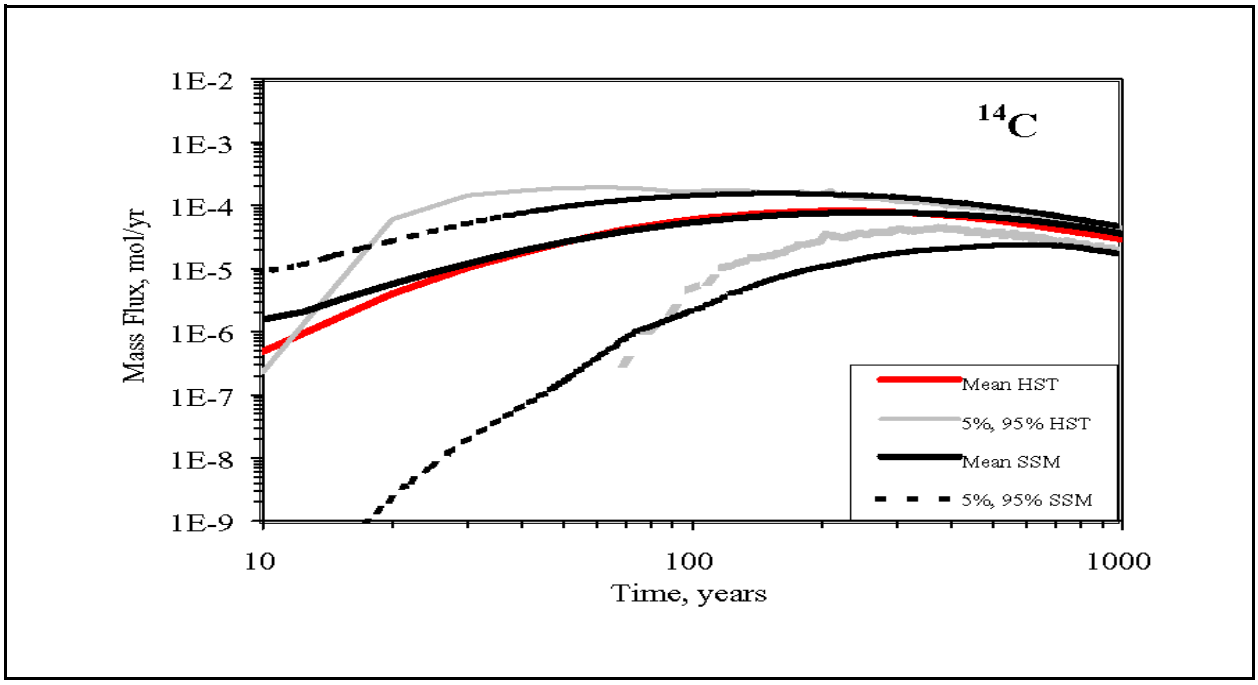

Figure D.1-2
Comparison of ^{14}C Exit Mass Fluxes from the HST Model with the SSM.

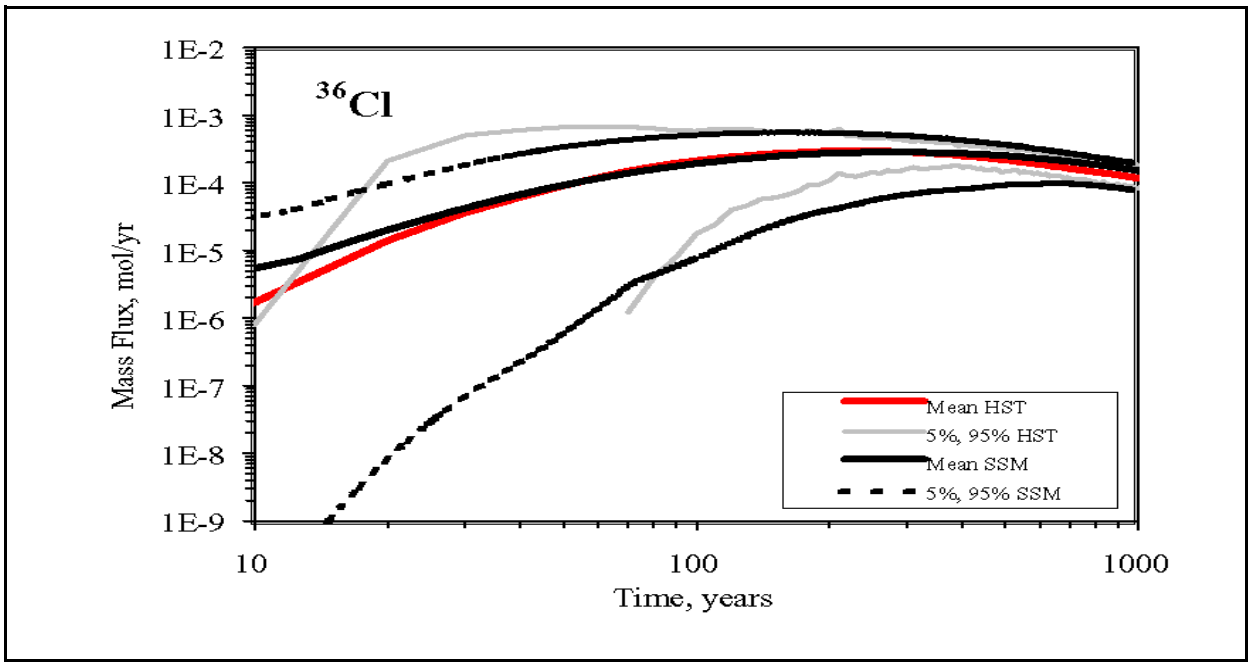

Figure D.1-3
Comparison of ^{36}Cl Exit Mass Fluxes from the HST Model with the SSM.

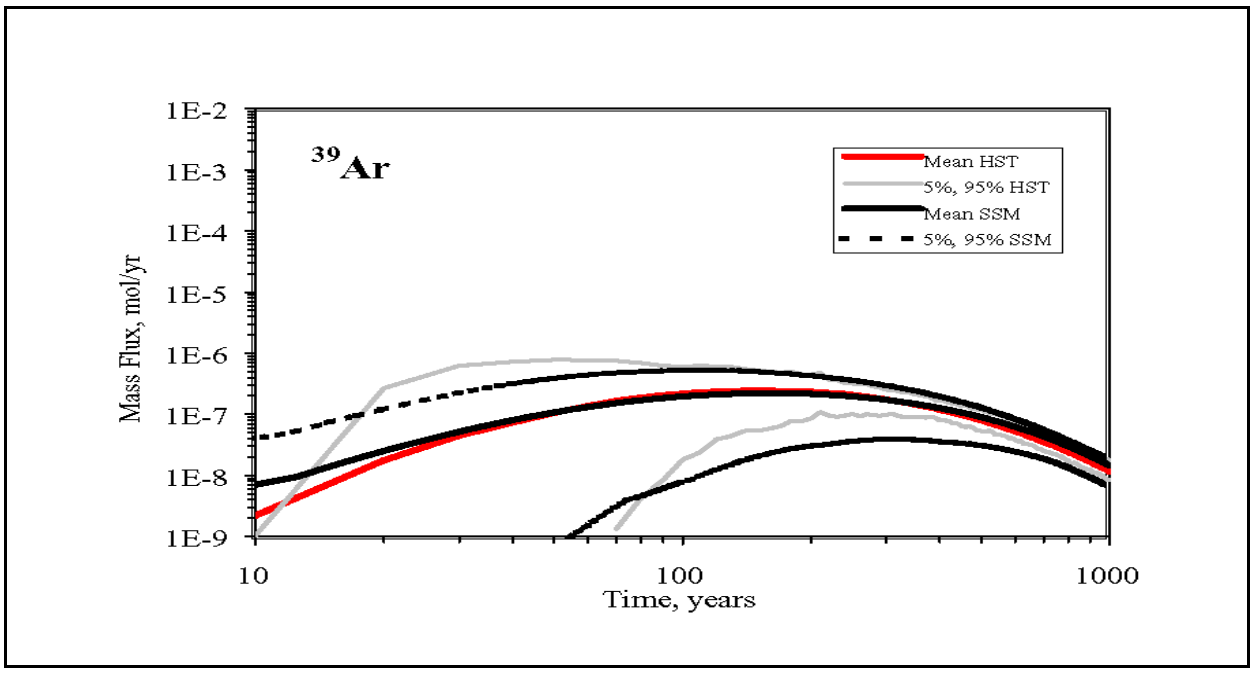

Figure D.1-4
Comparison of ^{39}Ar Exit Mass Fluxes from the HST Model with the SSM.

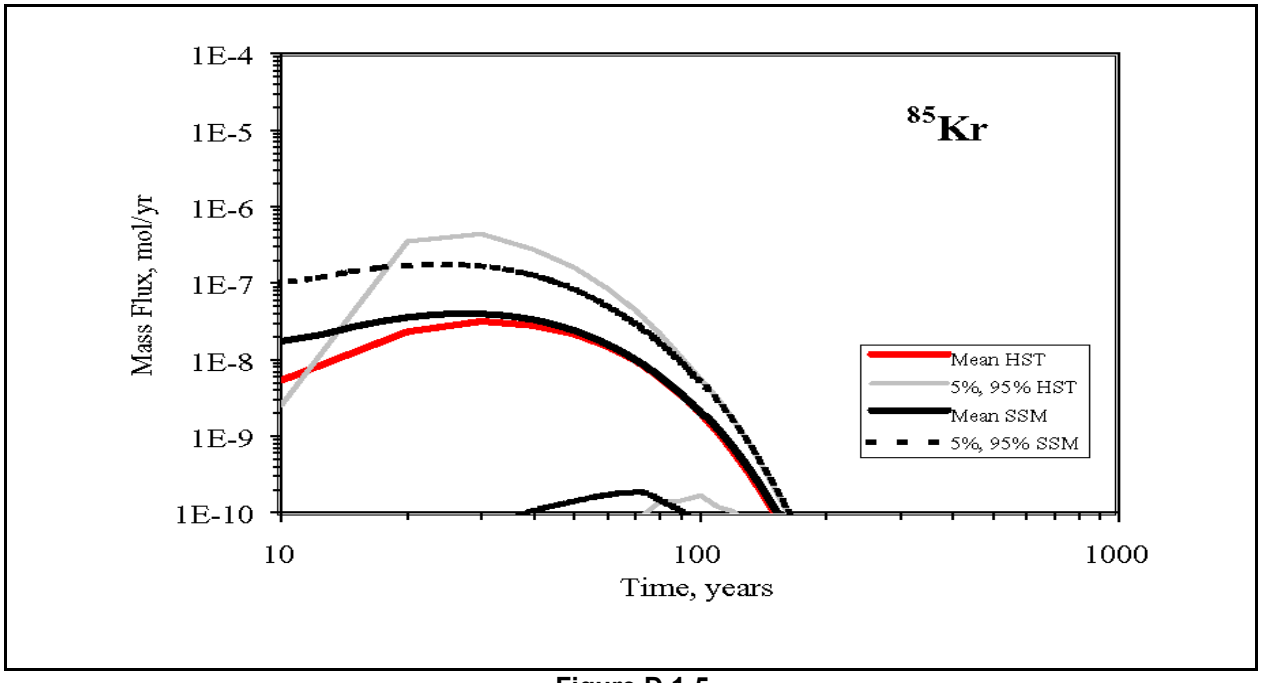

Figure D.1-5
Comparison of ^{85}Kr Exit Mass Fluxes from the HST Model with the SSM.

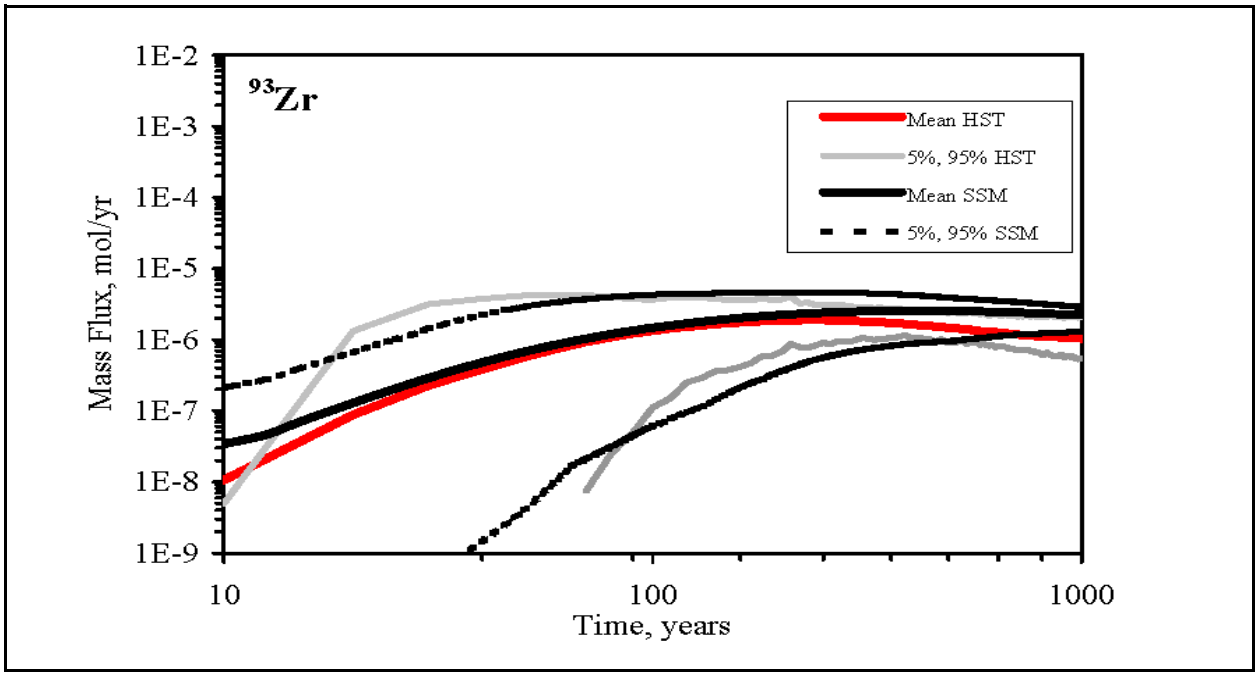

Figure D.1-6
Comparison of ^{93}Zr Exit Mass Fluxes from the HST Model with the SSM.

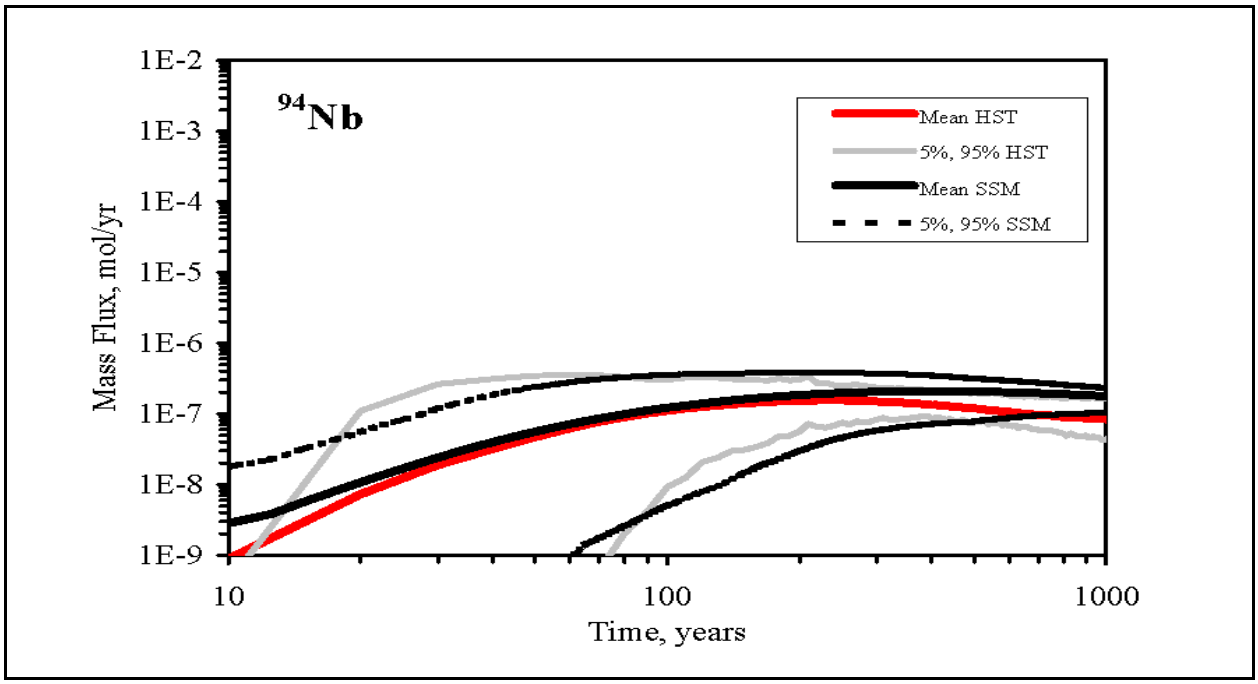

Figure D.1-7
Comparison of ^{94}Nb Exit Mass Fluxes from the HST with the SSM.

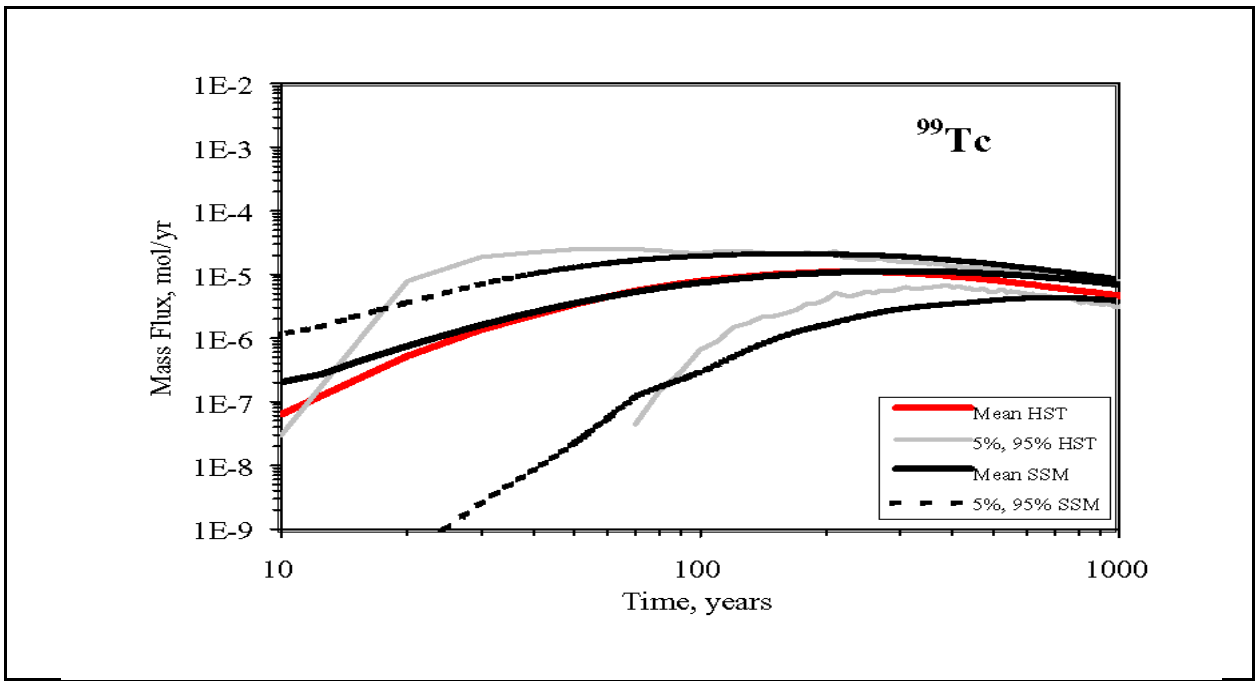

Figure D.1-8
Comparison of ^{99}Tc Exit Mass Fluxes from the HST Model with the SSM.

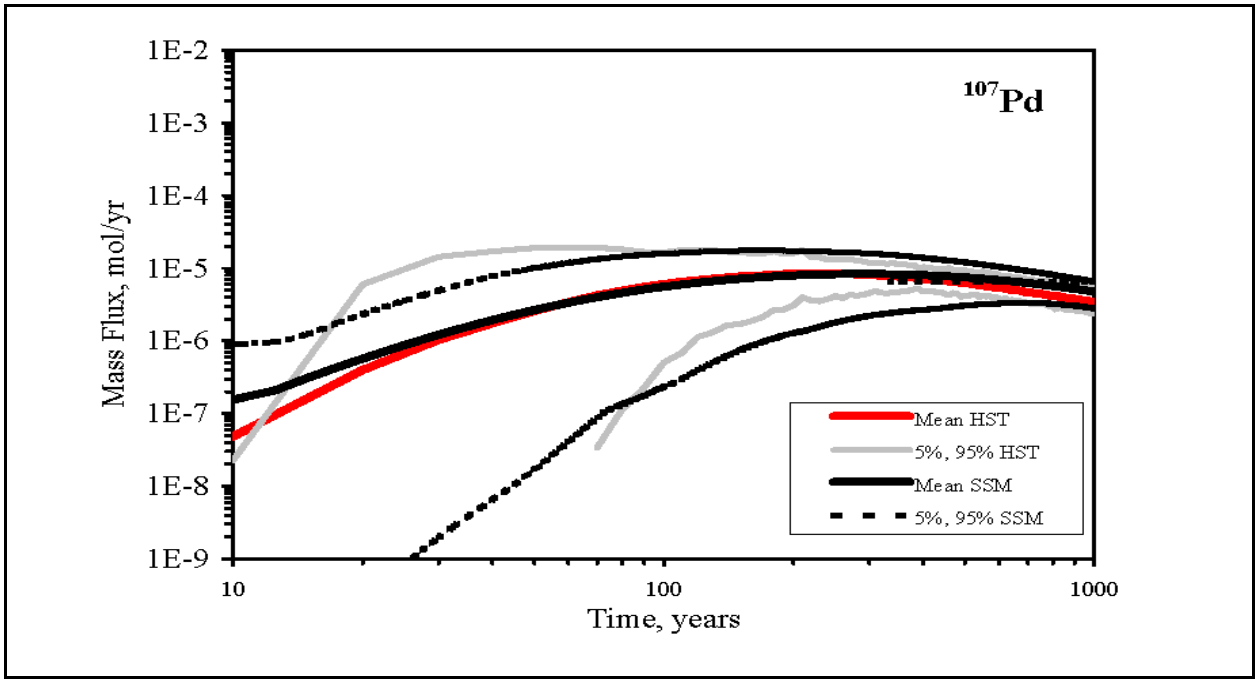

Figure D.1-9
Comparison of ^{107}Pd Exit Mass Fluxes from the Model with the SSM.

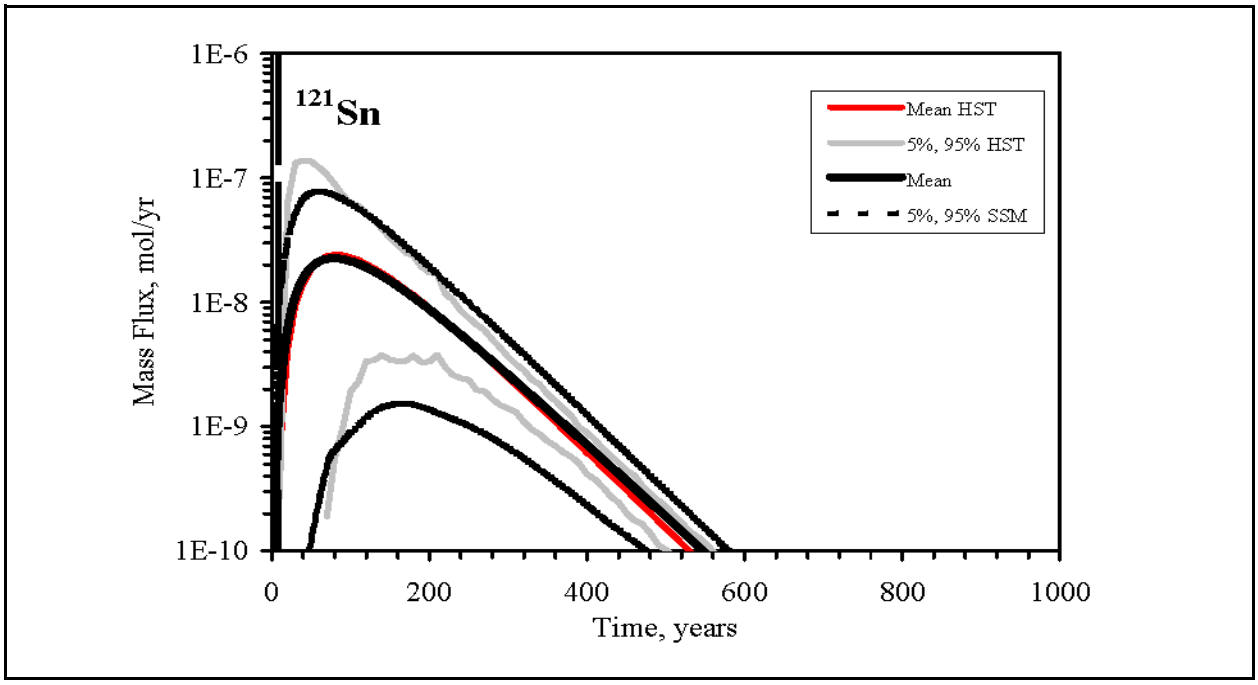

Figure D.1-10
Comparison of ^{121}Sn Exit Mass Fluxes from the HST Model with the SSM.

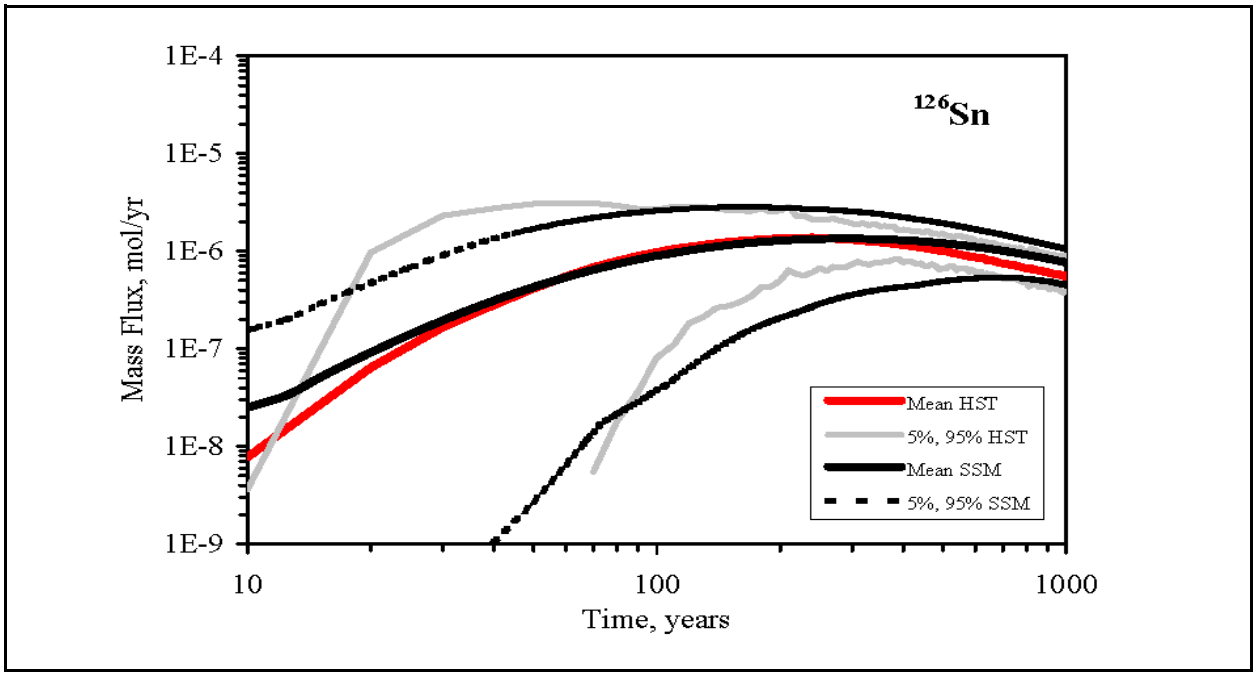

Figure D.1-11
Comparison of ^{126}Sn Exit Mass Fluxes from the HST Model with the SSM.

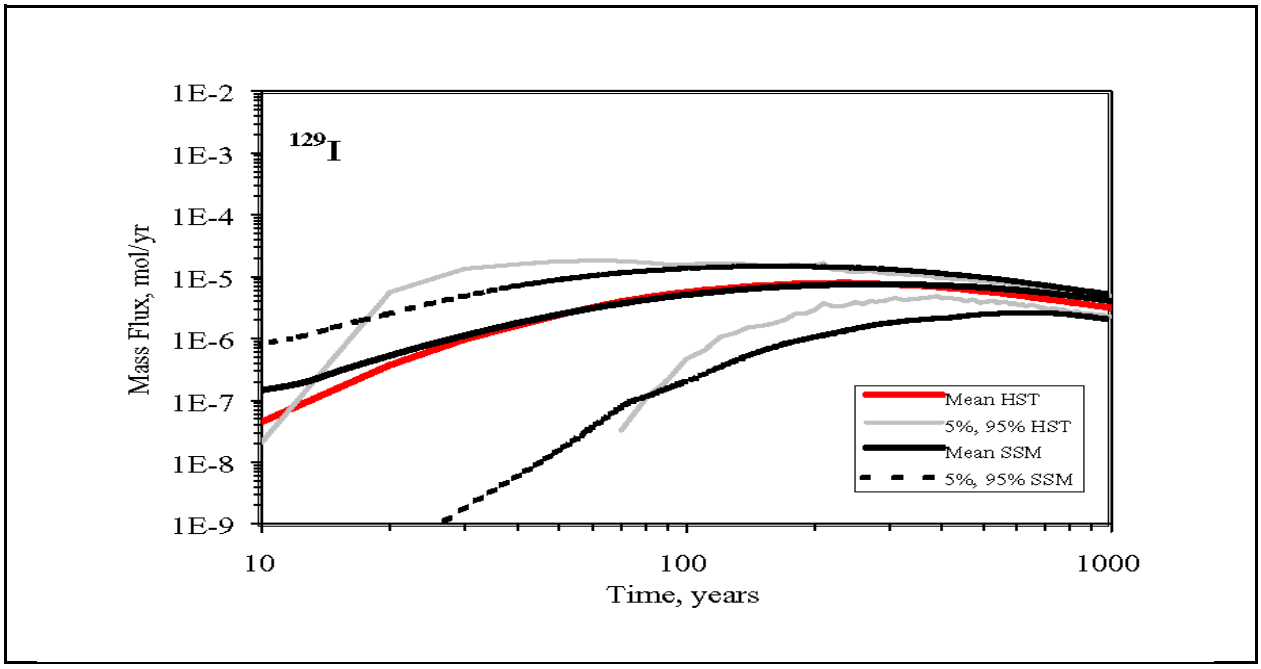

Figure D.1-12
Comparison of ^{129}I Exit Mass Fluxes from the HST Model with the SSM.

D.2.0 Comparisons of Mass Flux from the SSM and HST Model for Sorbing Radionuclides

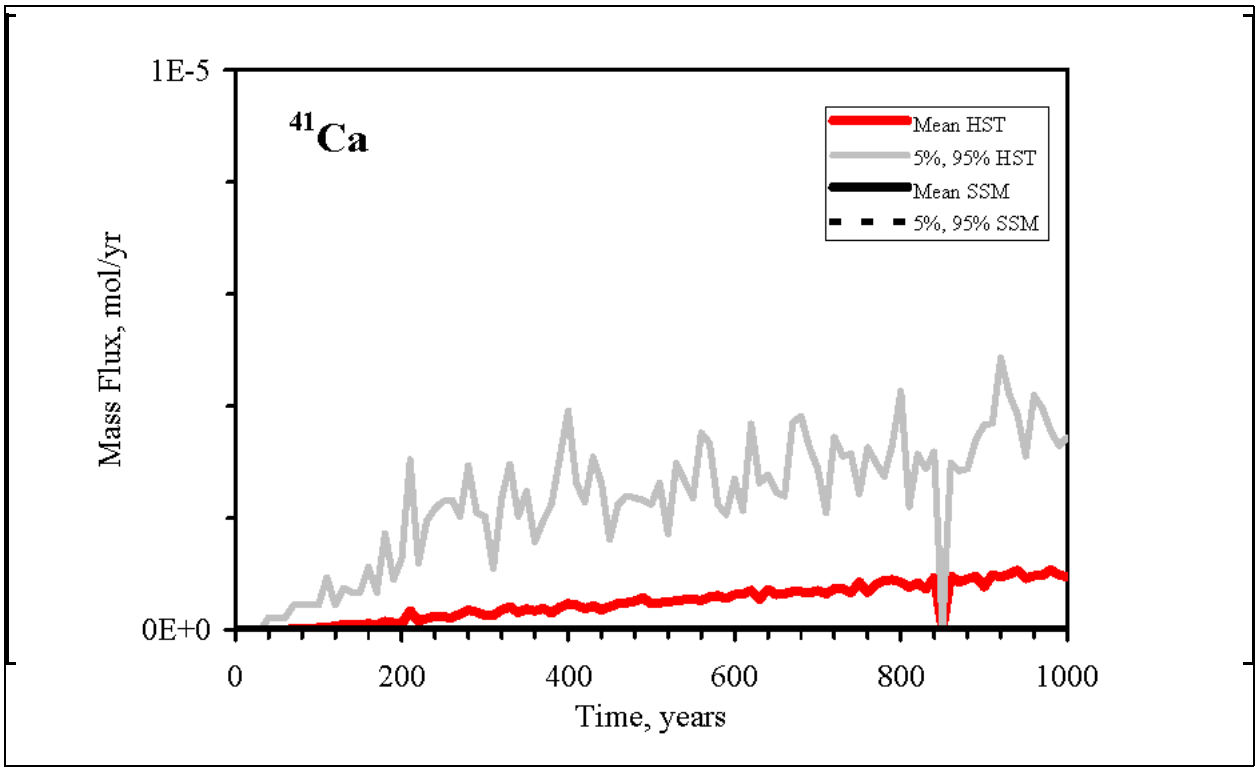

Figure D.2-1
Comparison of ^{41}Ca Exit Mass Fluxes from the HST Model with the SSM.

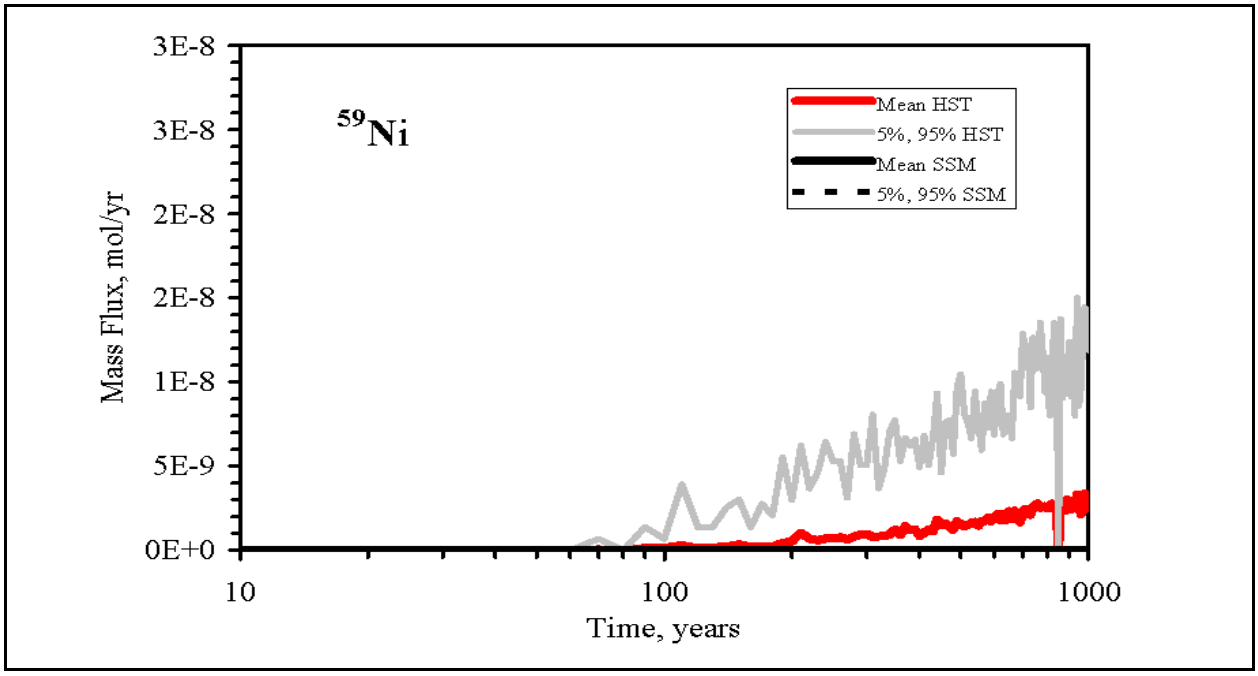

Figure D.2-2
Comparison of ^{59}Ni Exit Mass Fluxes from the HST Model with the SSM.

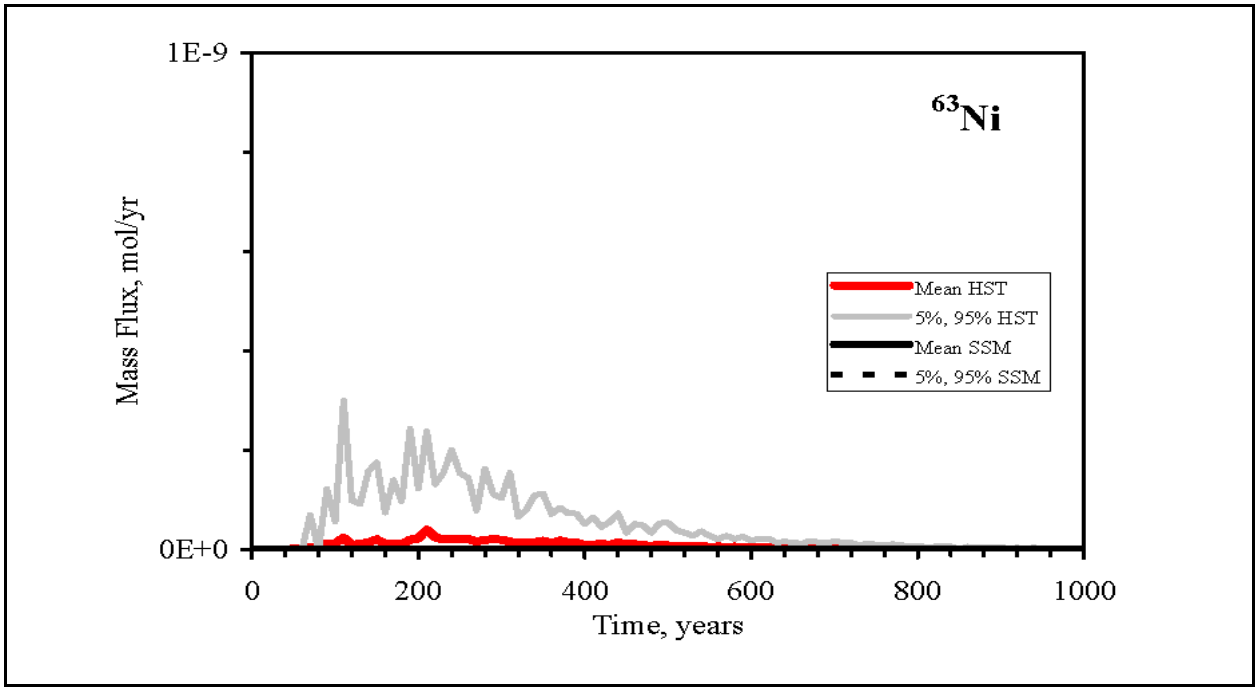

Figure D.2-3
Comparison of ^{63}Ni Exit Mass Fluxes from the HST Model with the SSM.

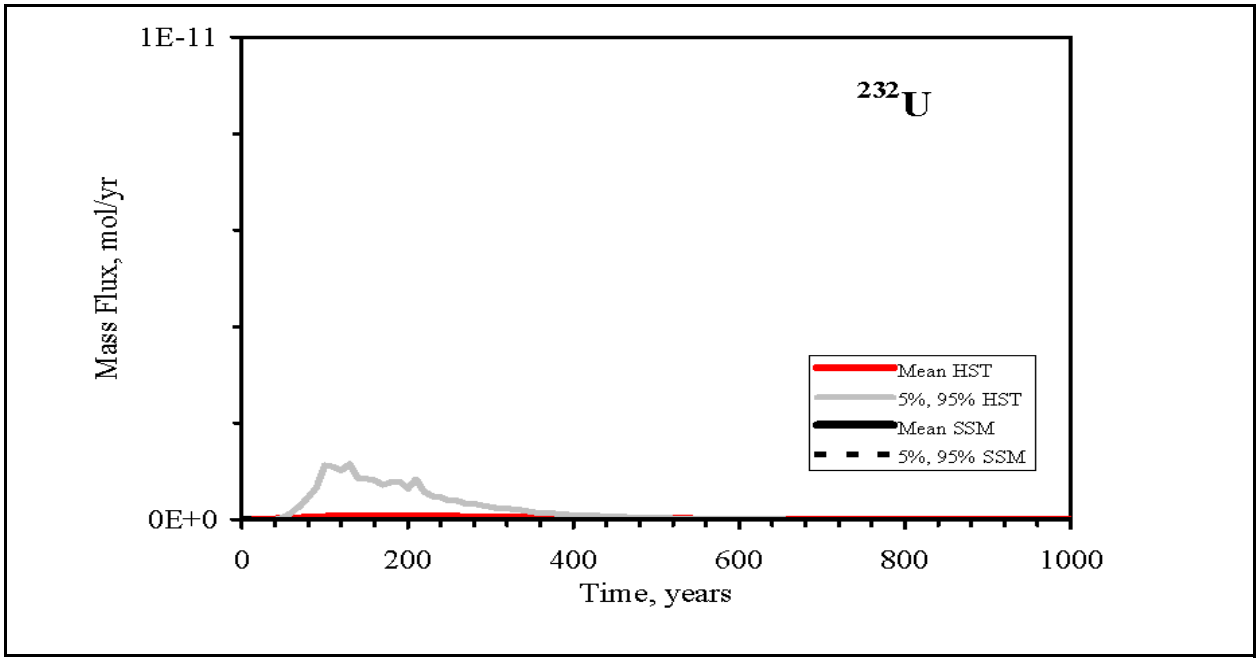

Figure D.2-4
Comparison of ^{232}U Exit Mass Fluxes from the HST Model with the SSMI

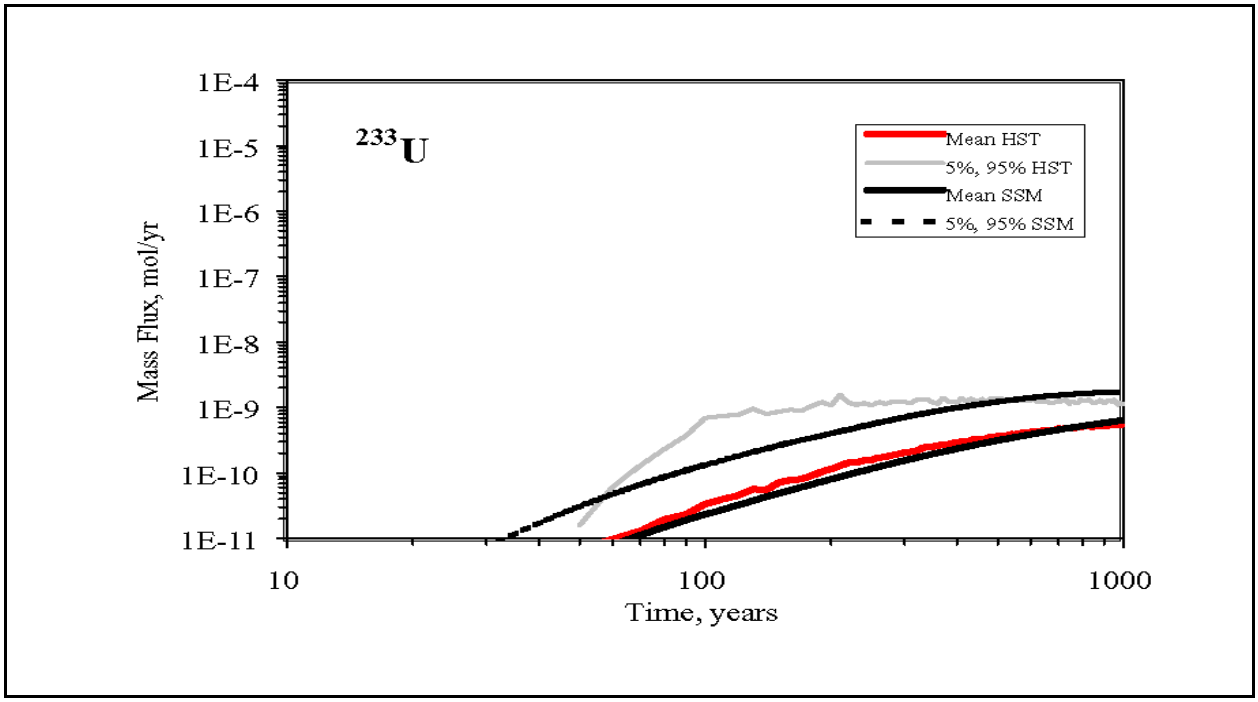

Figure D.2-5
Comparison of ^{233}U Exit Mass Fluxes from the HST Model with the SSM.

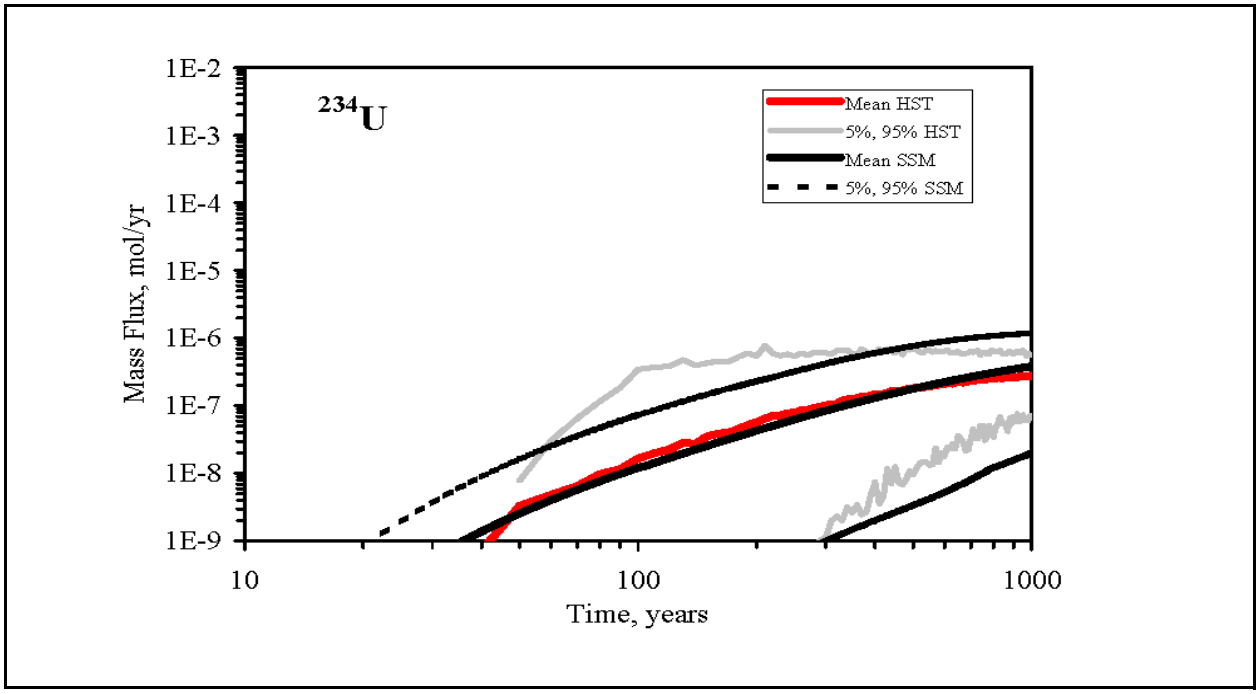

Figure D.2-6
Comparison of ^{234}U Exit Mass Fluxes from the HST Model with the SSM.

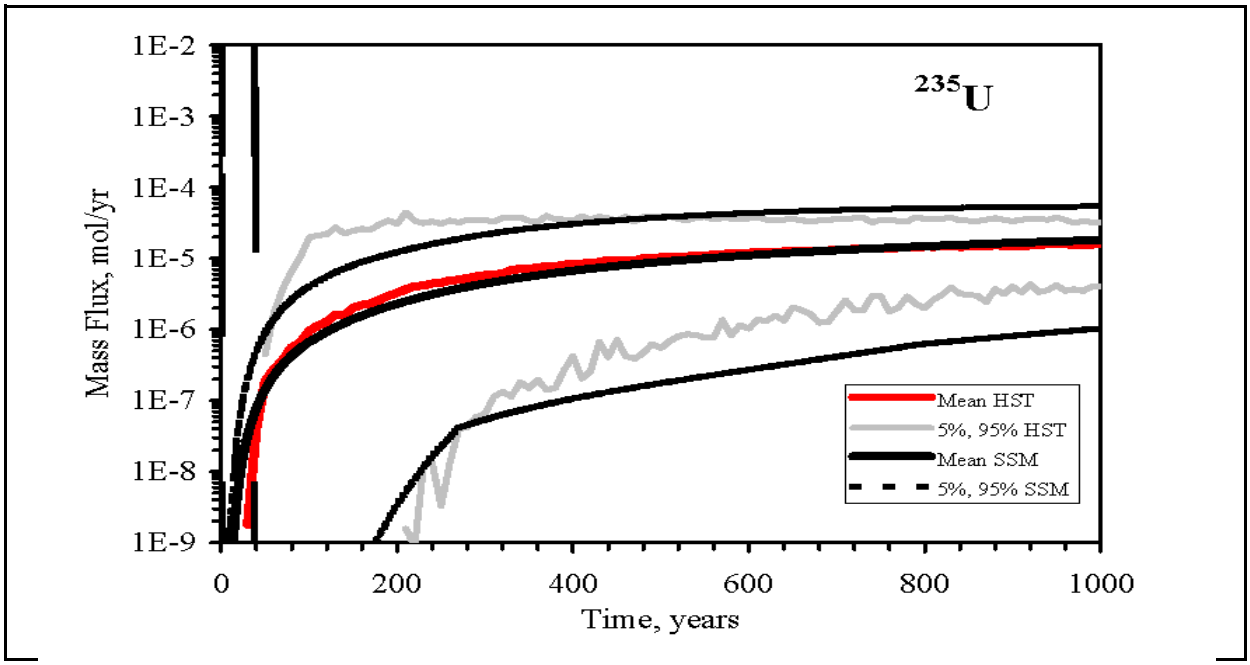

Figure D.2-7
Comparison of ^{235}U Exit Mass Fluxes from the HST Model with the SSM.

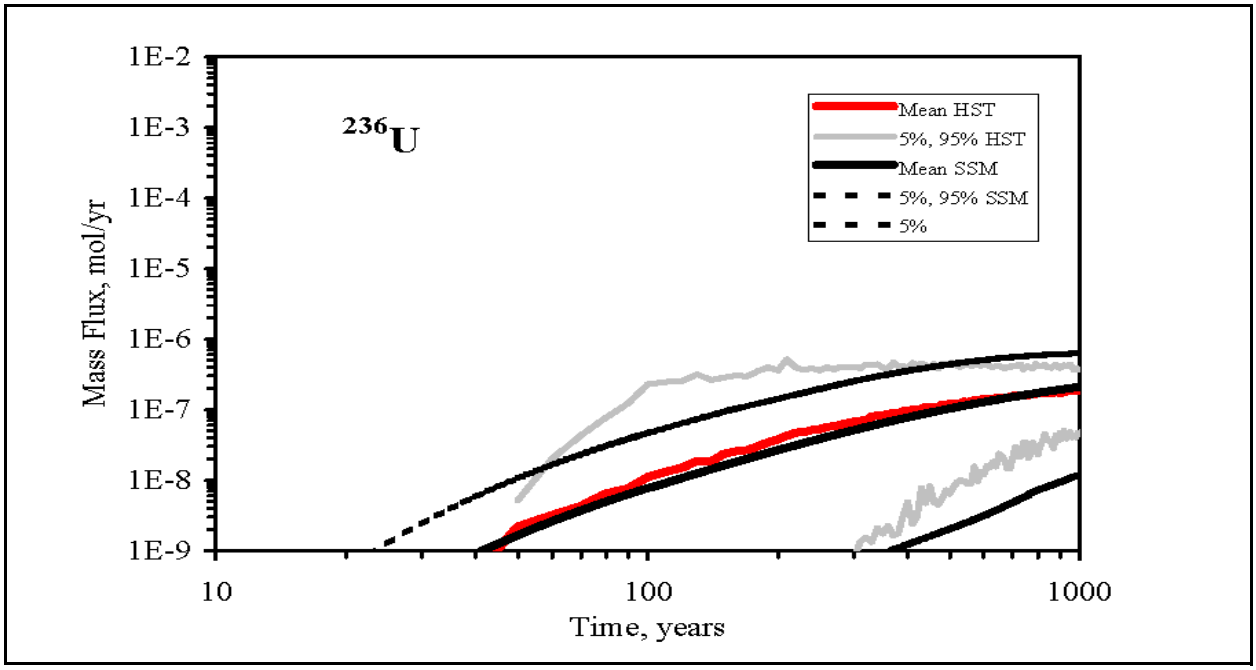

Figure D.2-8
Comparison of ^{236}U Exit Mass Fluxes from the HST Model with the SSM.

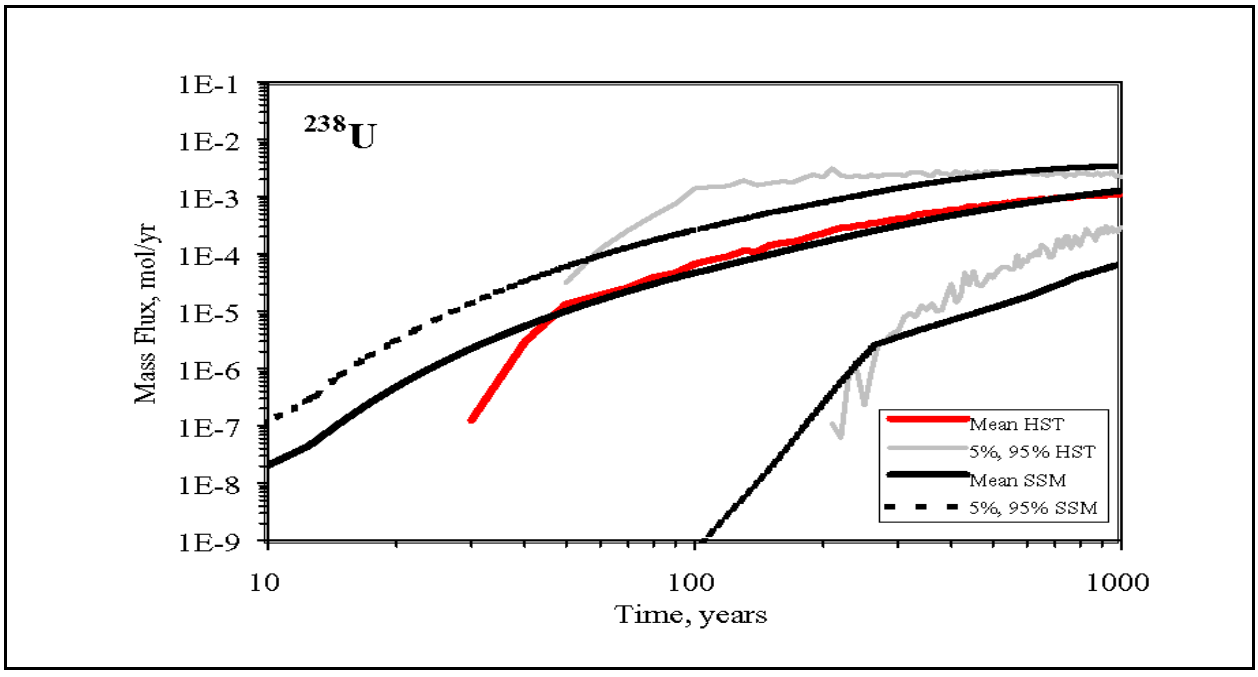

Figure D.2-9
Comparison of ^{238}U Exit Mass Fluxes from the HST Model with the SSM.

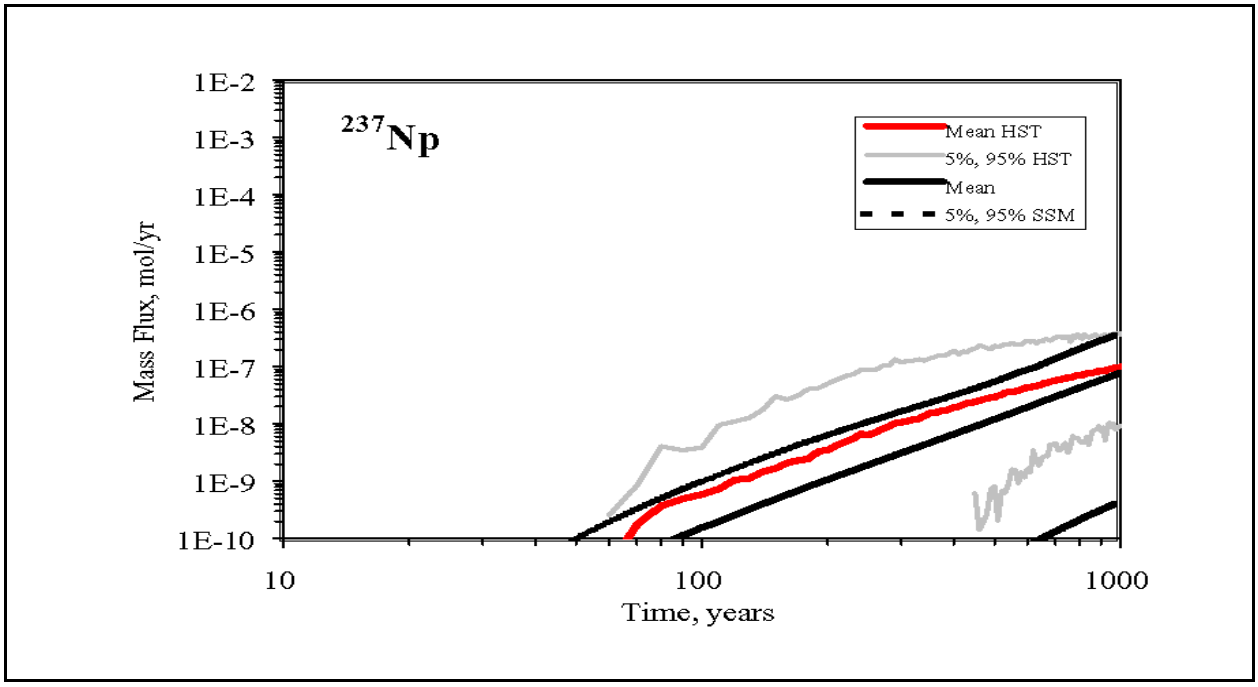

Figure D.2-10
Comparison of ^{237}Np Exit Mass Fluxes from the HST Model with the SSM.

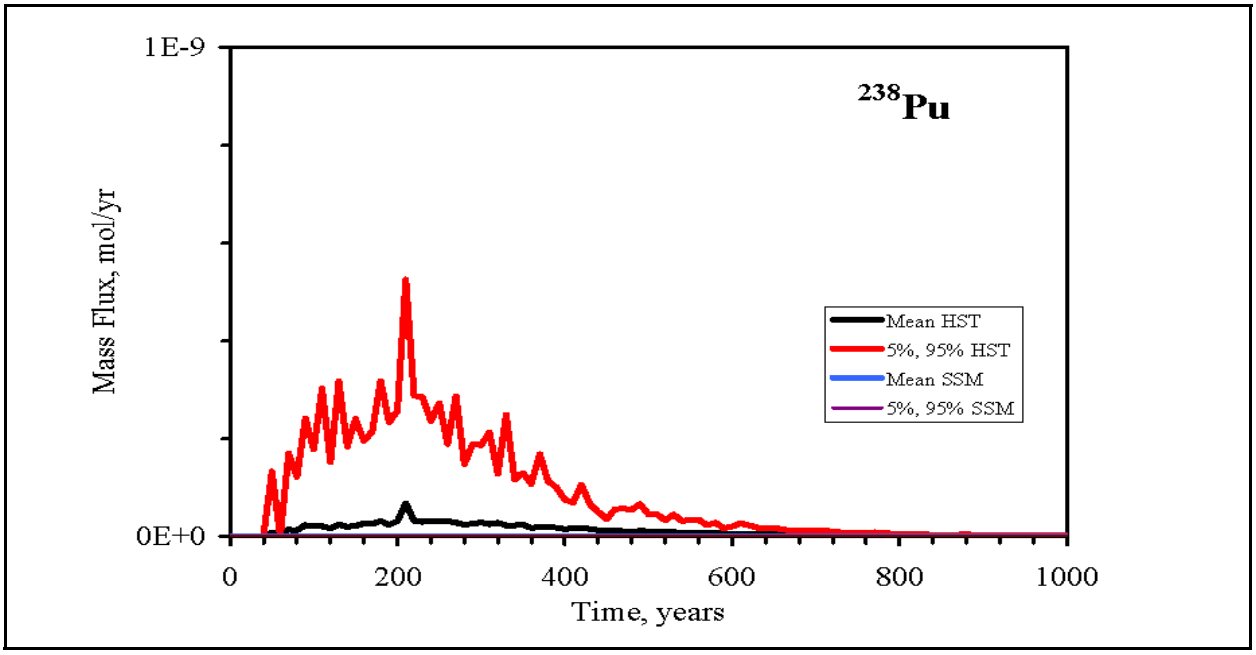

Figure D.2-11
Comparison of ^{238}Pu Exit Mass Fluxes from the HST Model with the SSM.

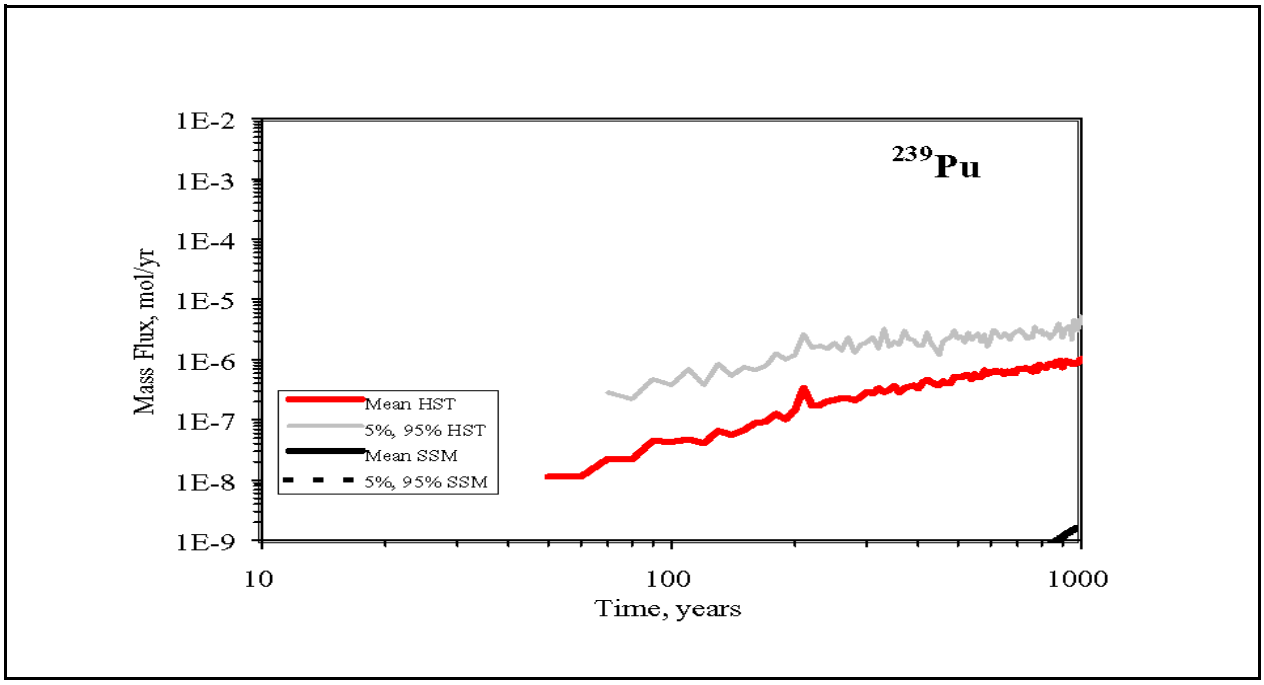

Figure D.2-12
Comparison of ^{239}Pu Exit Mass Fluxes from the HST Model with the SSM.

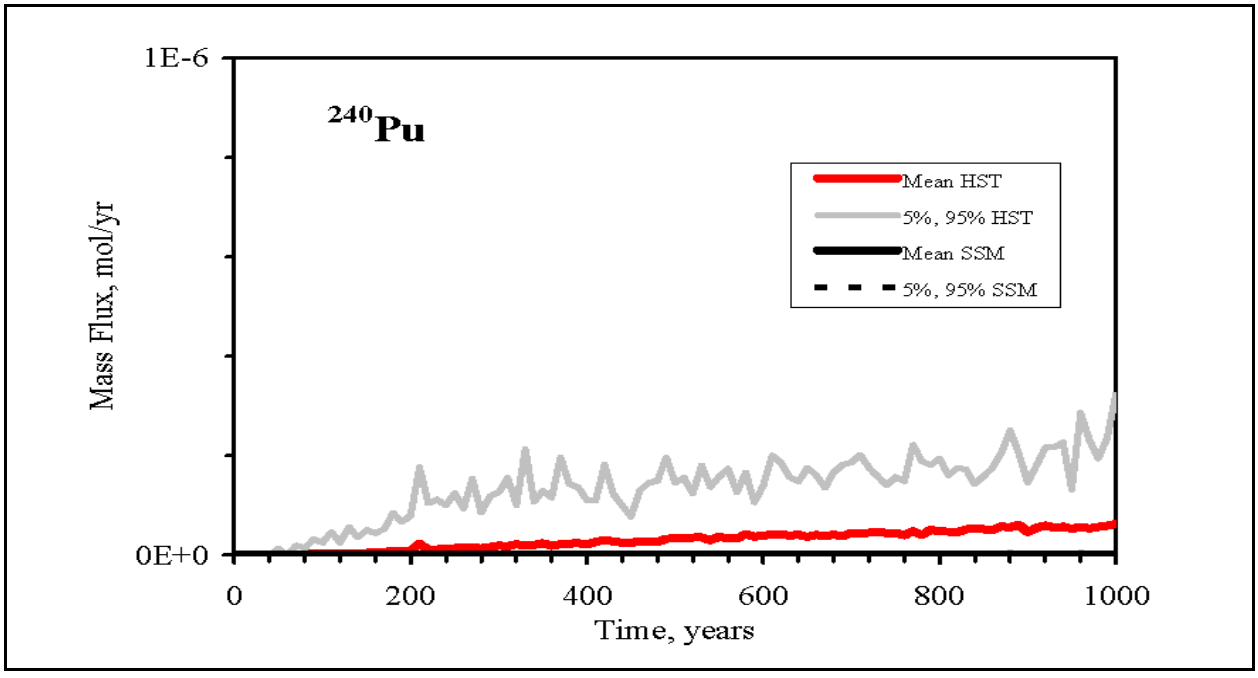

Figure D.2-13
Comparison of ^{240}Pu Exit Mass Fluxes from the HST Model with the SSM.

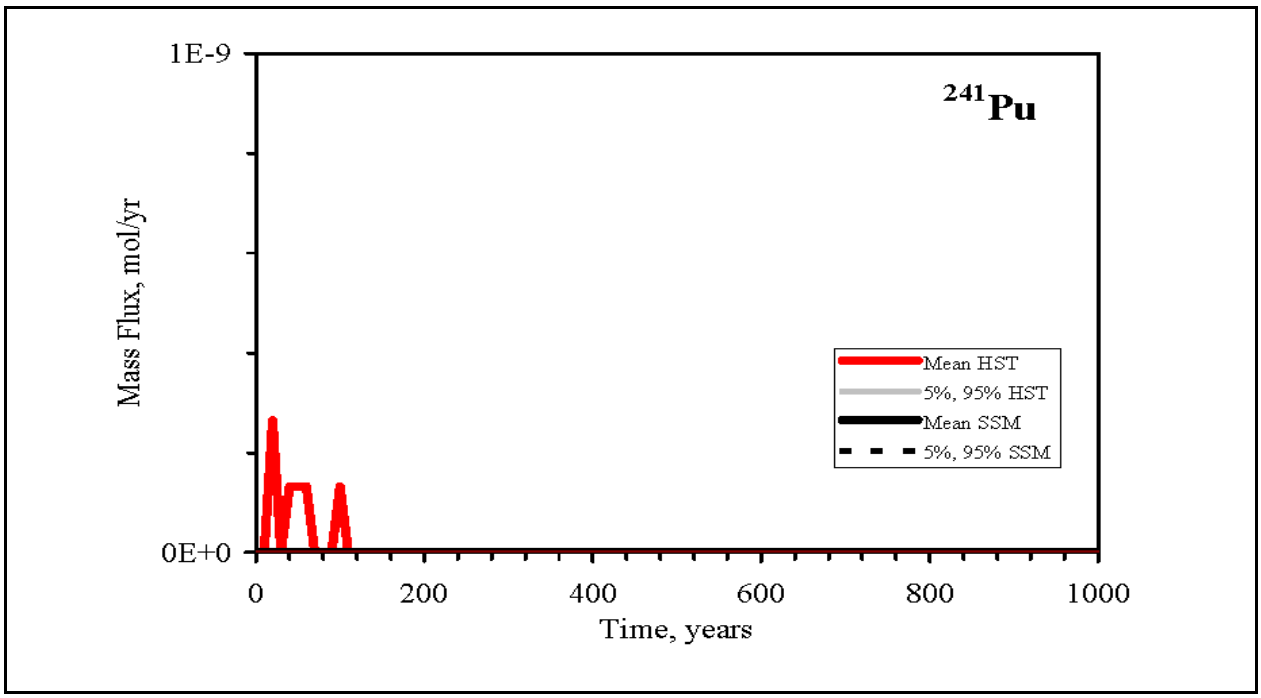

Figure D.2-14
Comparison of ^{241}Pu Exit Mass Fluxes from the HST Model with the SSM.

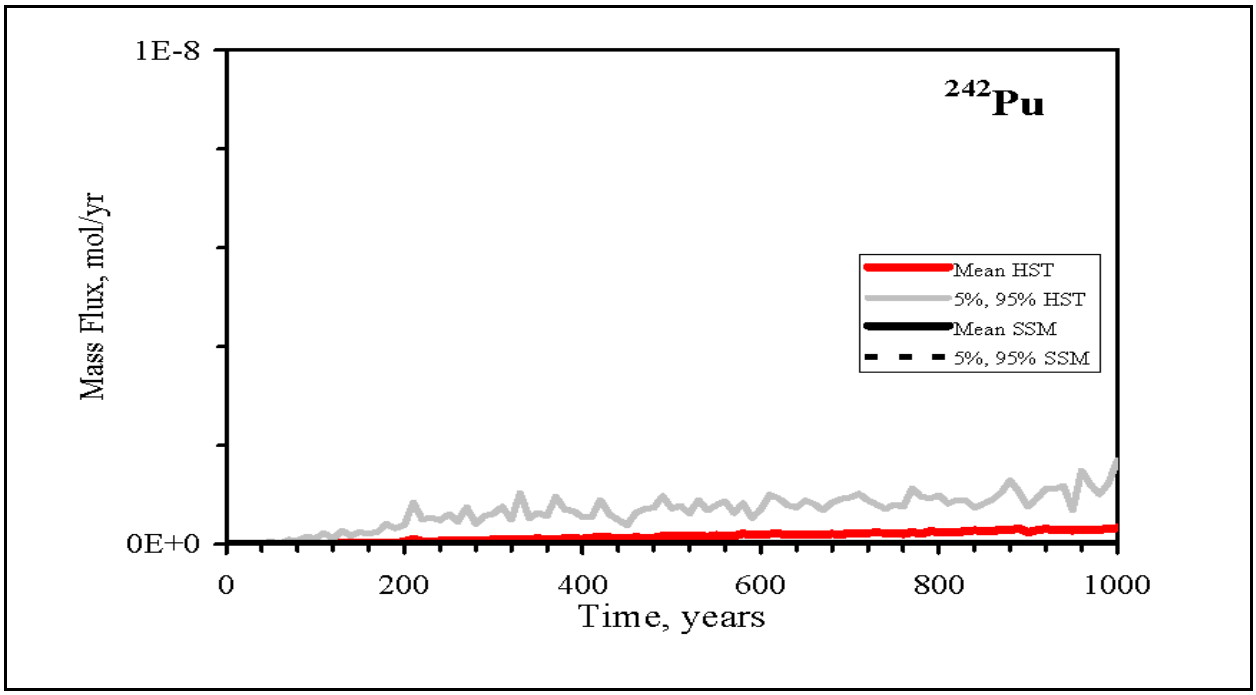

Figure D.2-15
Comparison of ^{242}Pu Exit Mass Fluxes from the HST Model with the SSM.

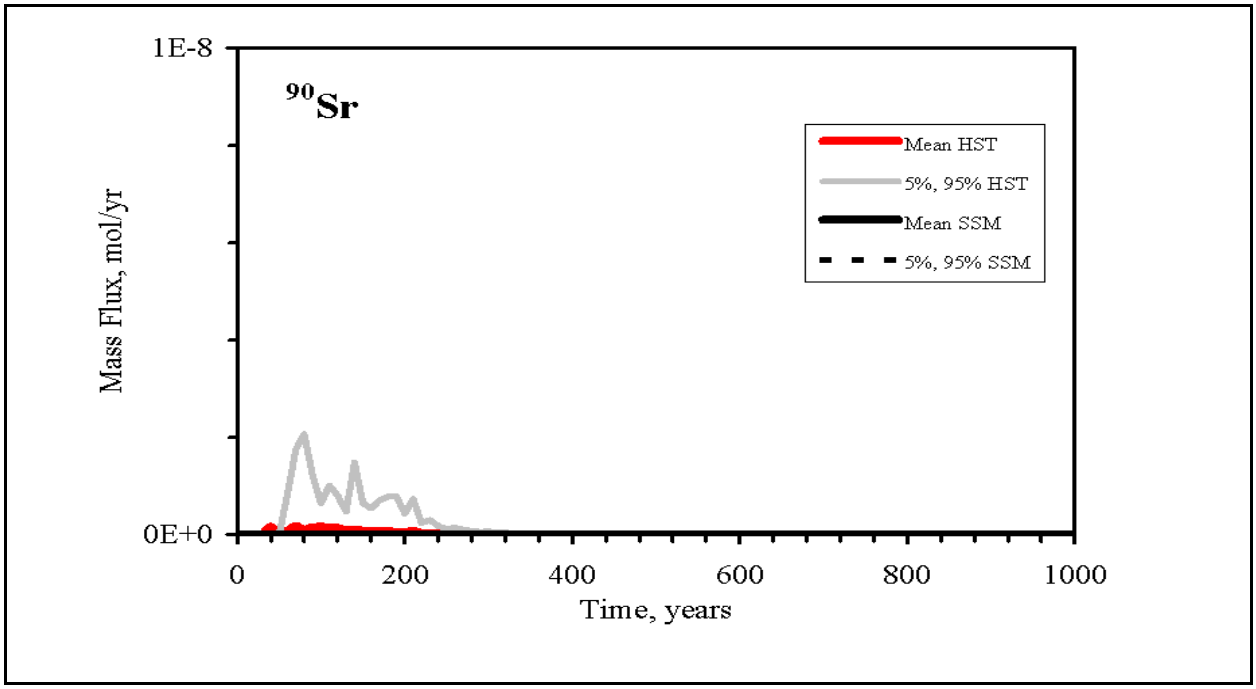

Figure D.2-16
Comparison of ^{90}Sr Exit Mass Fluxes from the HST Model with the SSM.

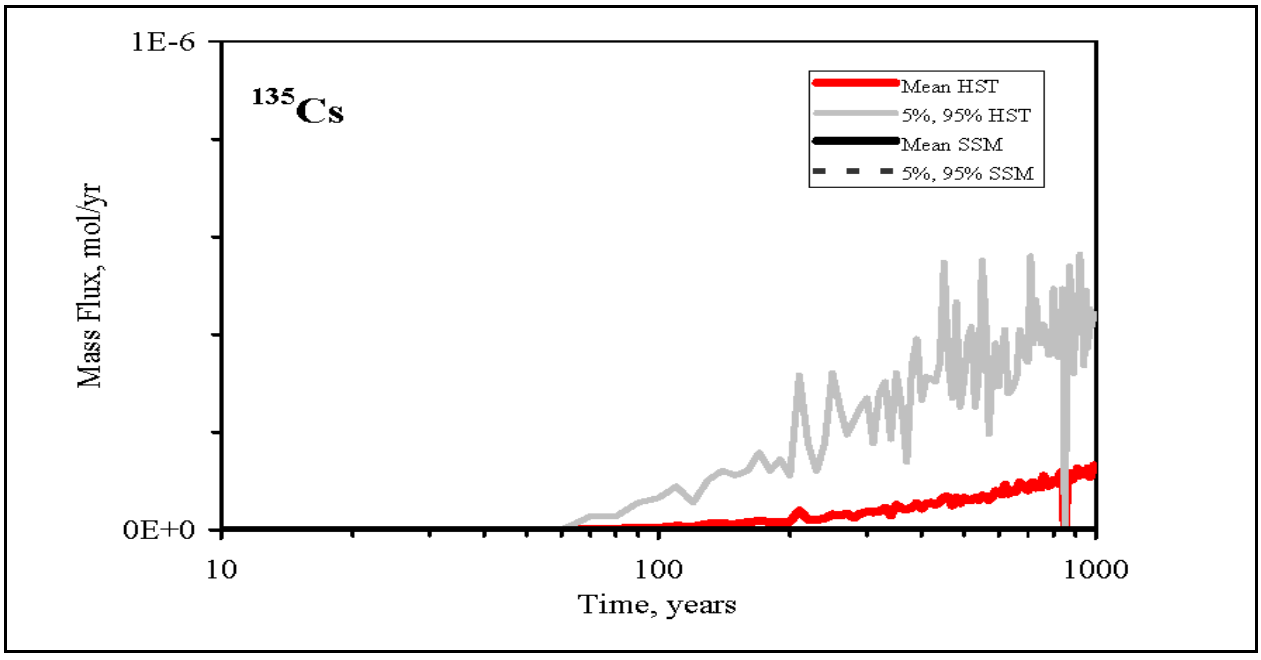

Figure D.2-17
Comparison of ^{135}Cs Exit Mass Fluxes from the HST Model with the SSM.

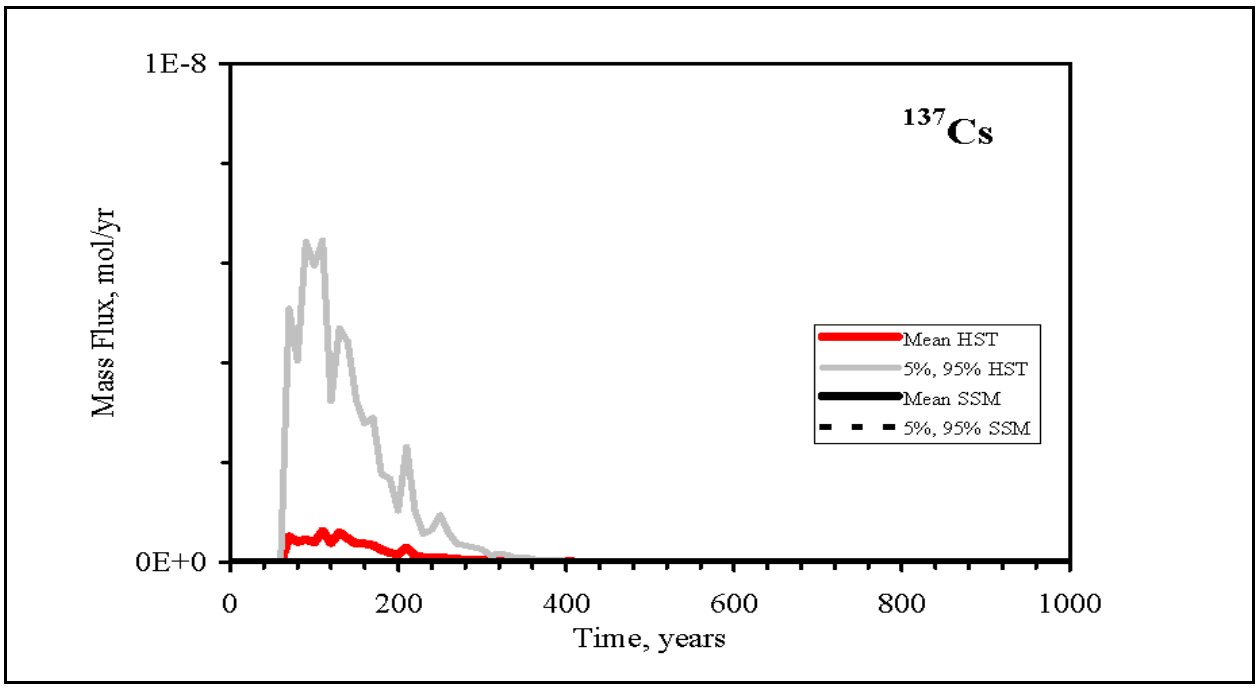

Figure D.2-18
Comparison of ^{137}Cs Exit Mass Fluxes from the HST Model with the SSM.

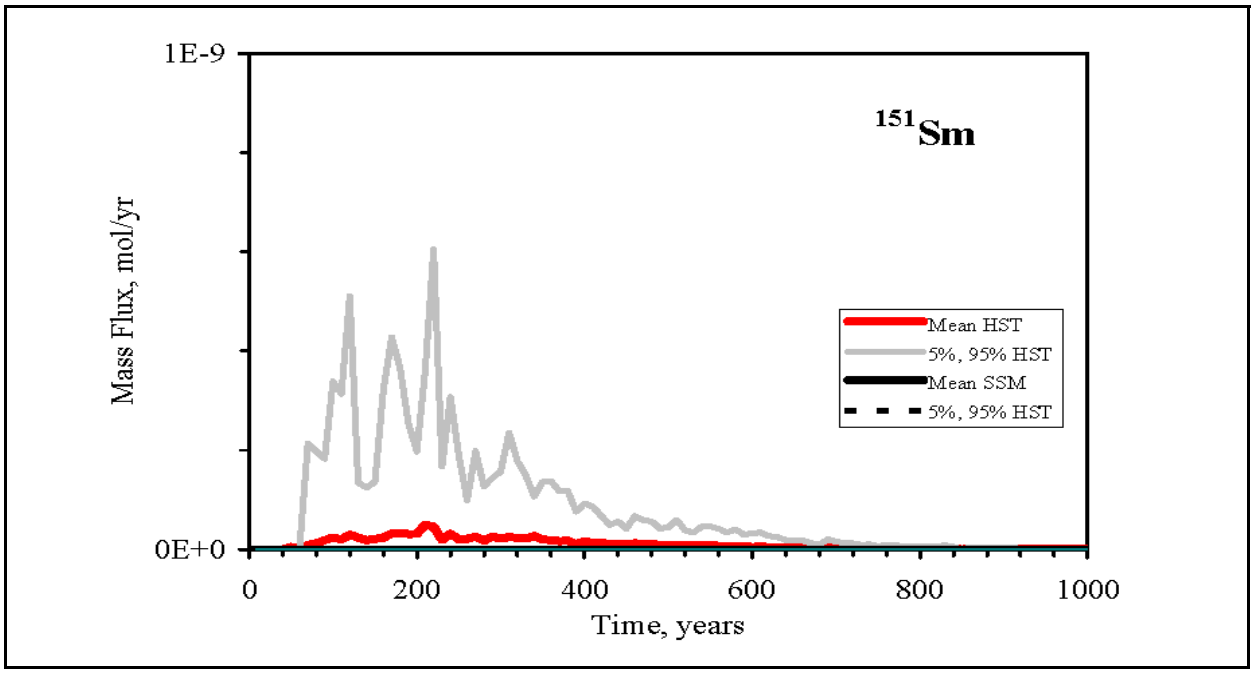

Figure D.2-19
Comparison of ^{151}Sm Exit Mass Fluxes from the HST Model with the SSM.

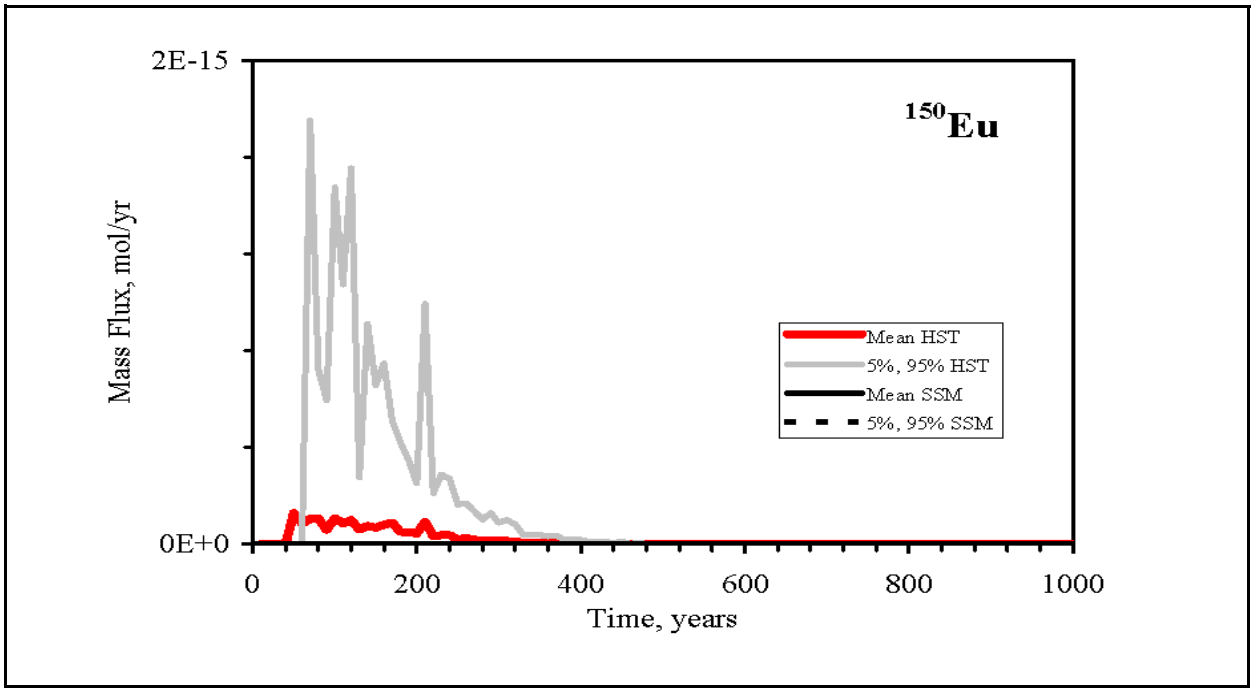

Figure D.2-20
Comparison of ^{150}Eu Exit Mass Fluxes from the HST Model with the SSM.

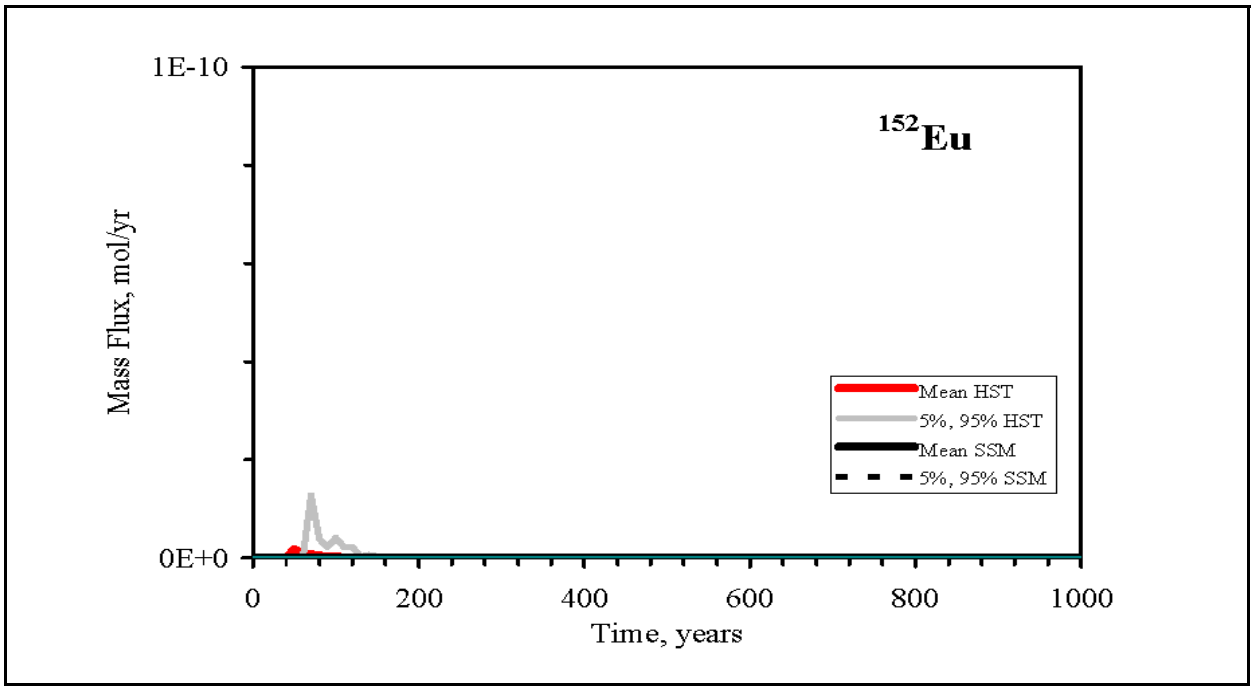

Figure D.2-21
Comparison of ^{152}Eu Exit Mass Fluxes from the HST Model with the SSM.

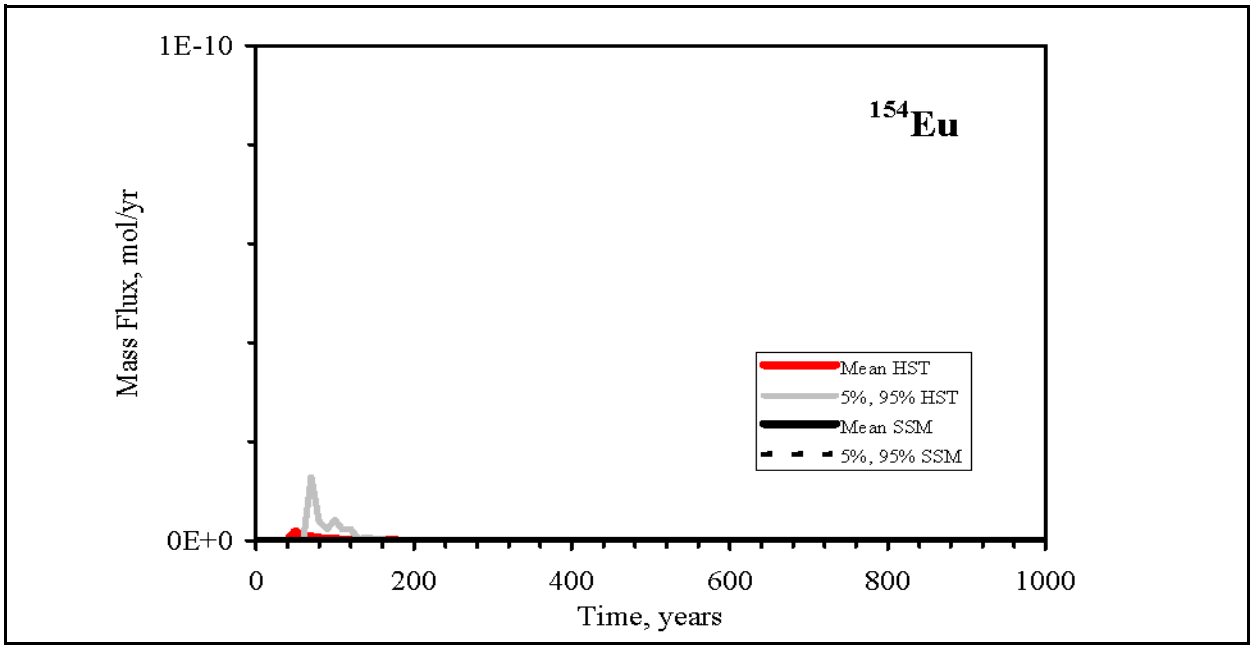

Figure D.2-22
Comparison of ^{154}Eu Exit Mass Fluxes from the HST Model with the SSM.

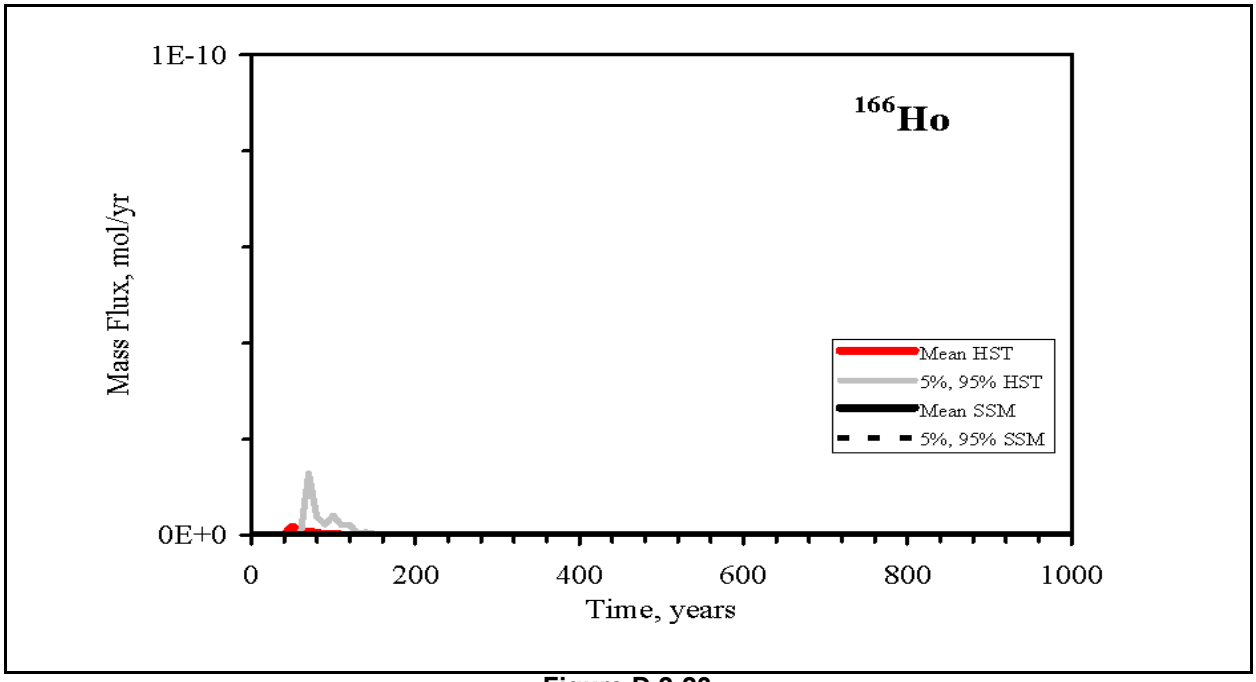

Figure D.2-23
Comparison of ^{166}Ho Exit Mass Fluxes from the HST Model with the SSM.

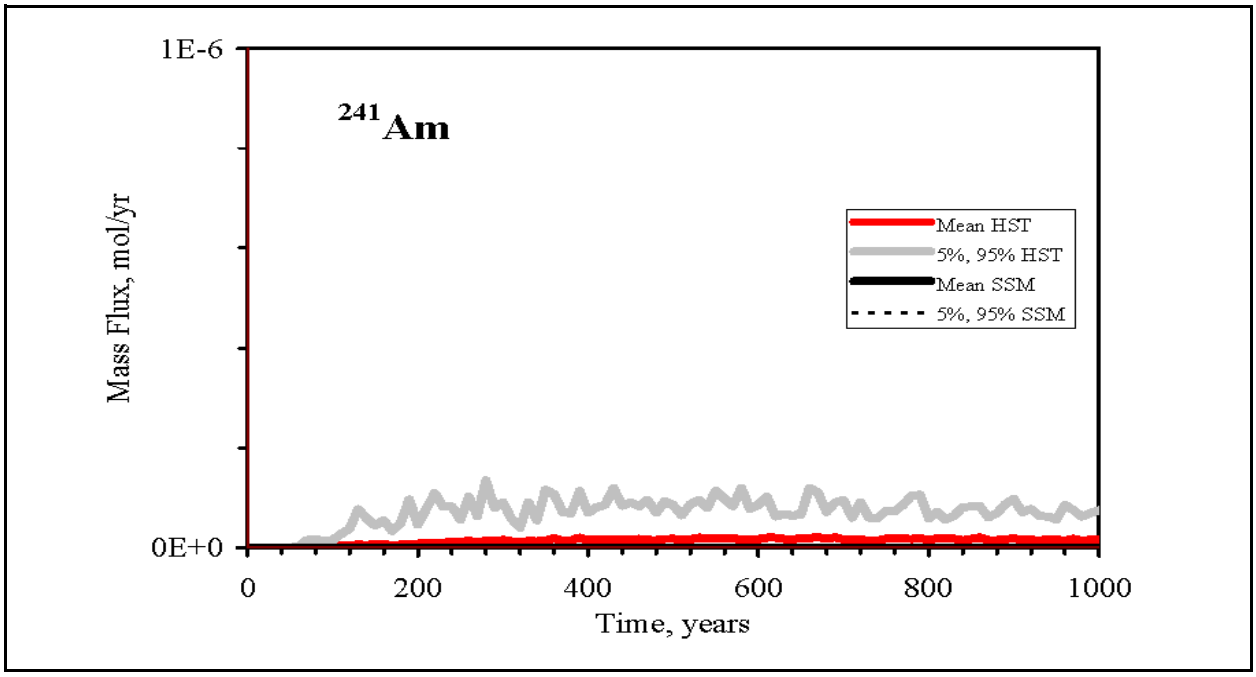

Figure D.2-24
Comparison of ^{241}Am Exit Mass Fluxes from the HST Model with the SSM.

Appendix E

Mean Mass Fluxes for a Groundwater Tracer (^{3}H), a Melt Glass Tracer (^{36}Cl), and a Sorbing Radionuclide (^{238}U) from Simplified Source Term Models Generated for Nine Tests in Frenchman Flat

E.1.0 Mean Mass Fluxes for a Groundwater Tracer (^{3}H), a Melt Glass Tracer (^{36}Cl), and a Sorbing Radionuclide (^{238}U) from Simplified Source Term Models Generated for Nine Tests in Frenchman Flat

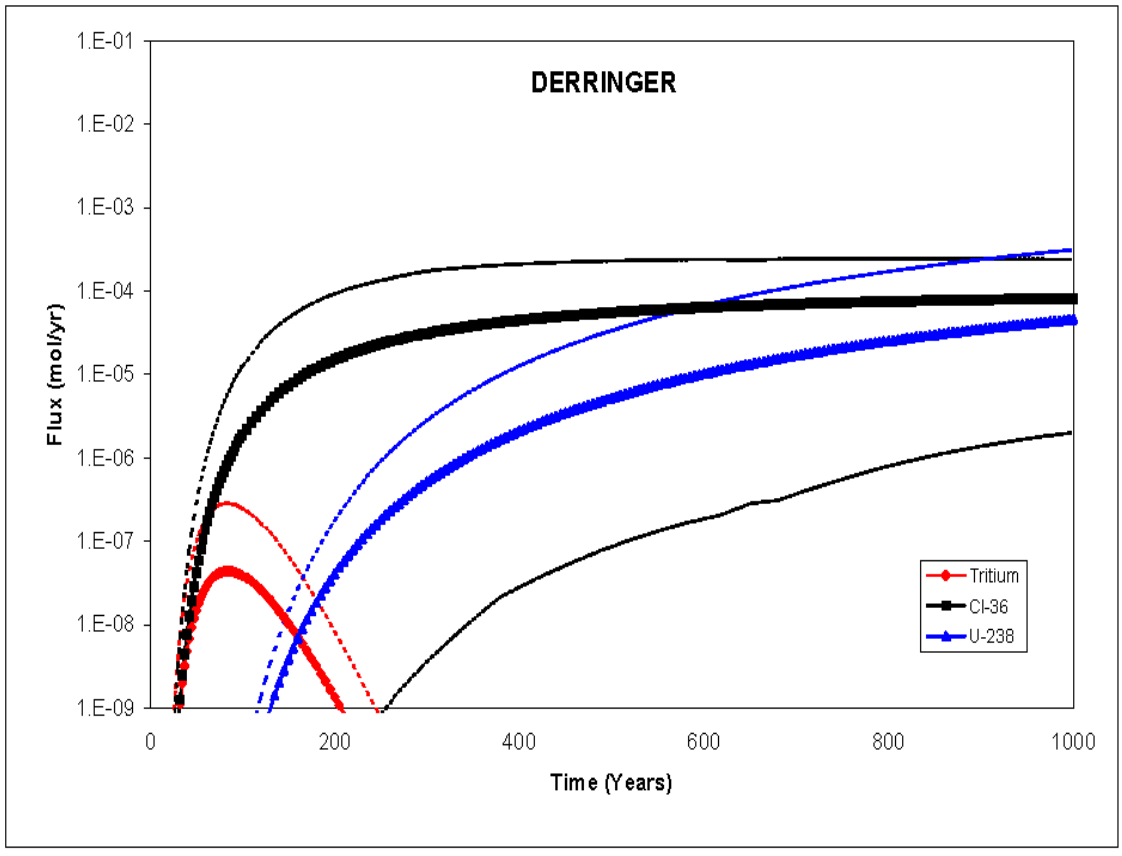

Figure E.1-1
^{3}H, ^{36}Cl, and ^{238}U Exit Mass Fluxes from the SSM for the DERRINGER test. Solid lines represent mean values and dashed lines represent the 5th and 95th percentiles

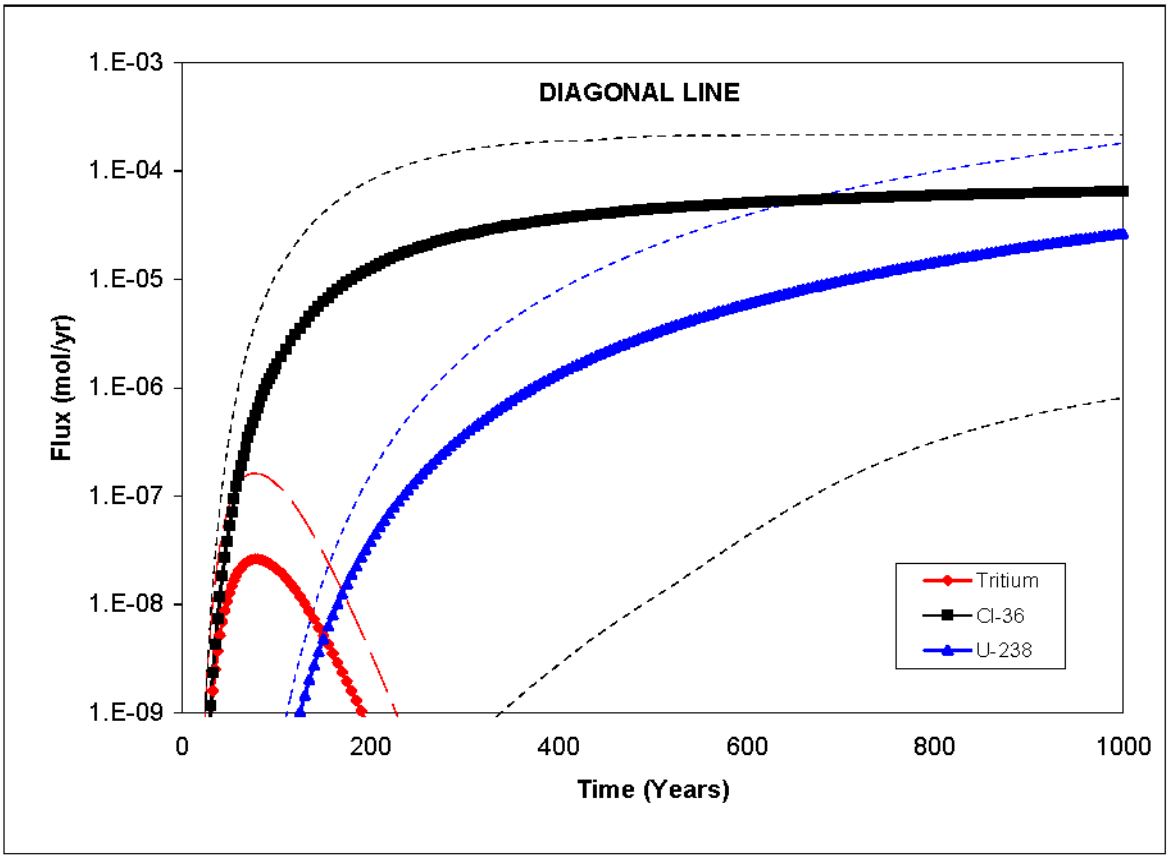

Figure E.1-2
^{3}H, ^{36}Cl, and ^{238}U Exit Mass Fluxes from the SSM for the DIAGONAL LINE test. Solid lines represent mean values and dashed lines represent the 5th and 95th percentiles

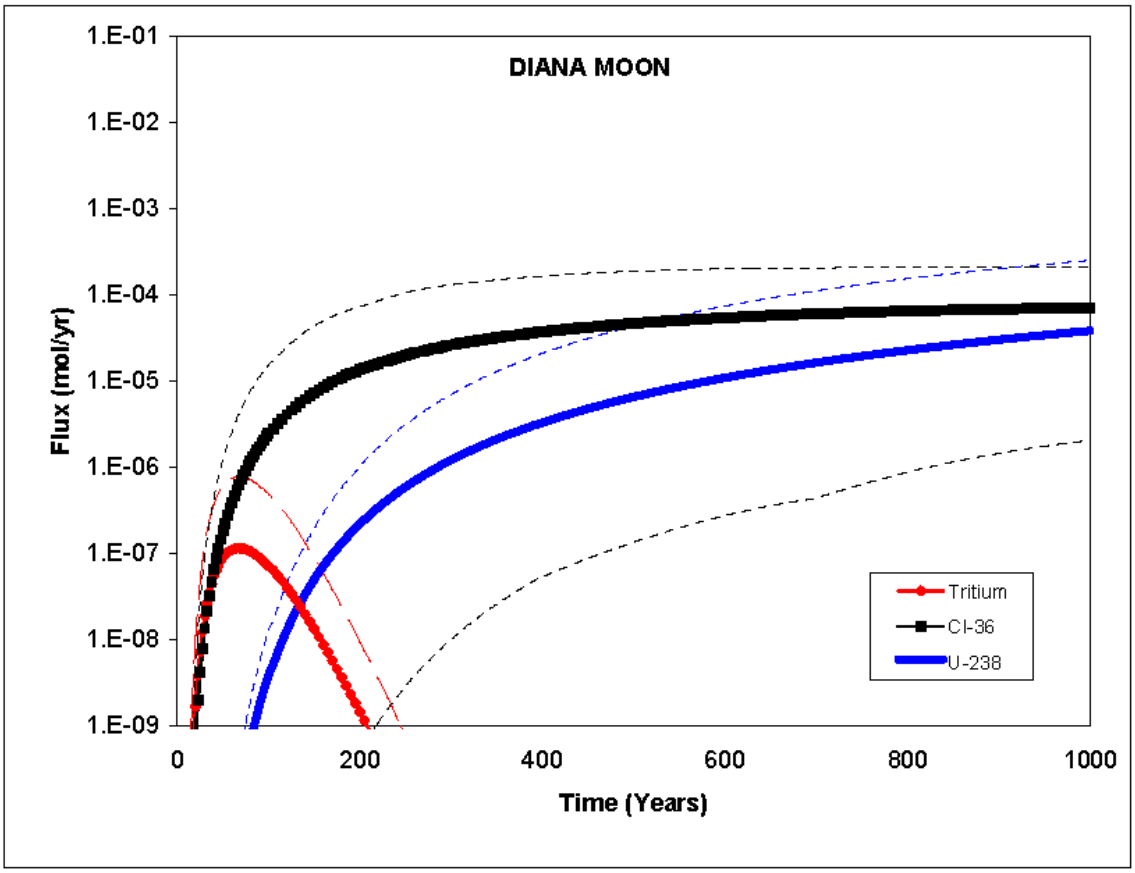

Figure E.1-3
^{3}H, ^{36}Cl, and ^{238}U Exit Mass Fluxes from the SSM for the DIANA MOON test. Solid lines represent mean values and dashed lines represent the 5th and 95th percentiles

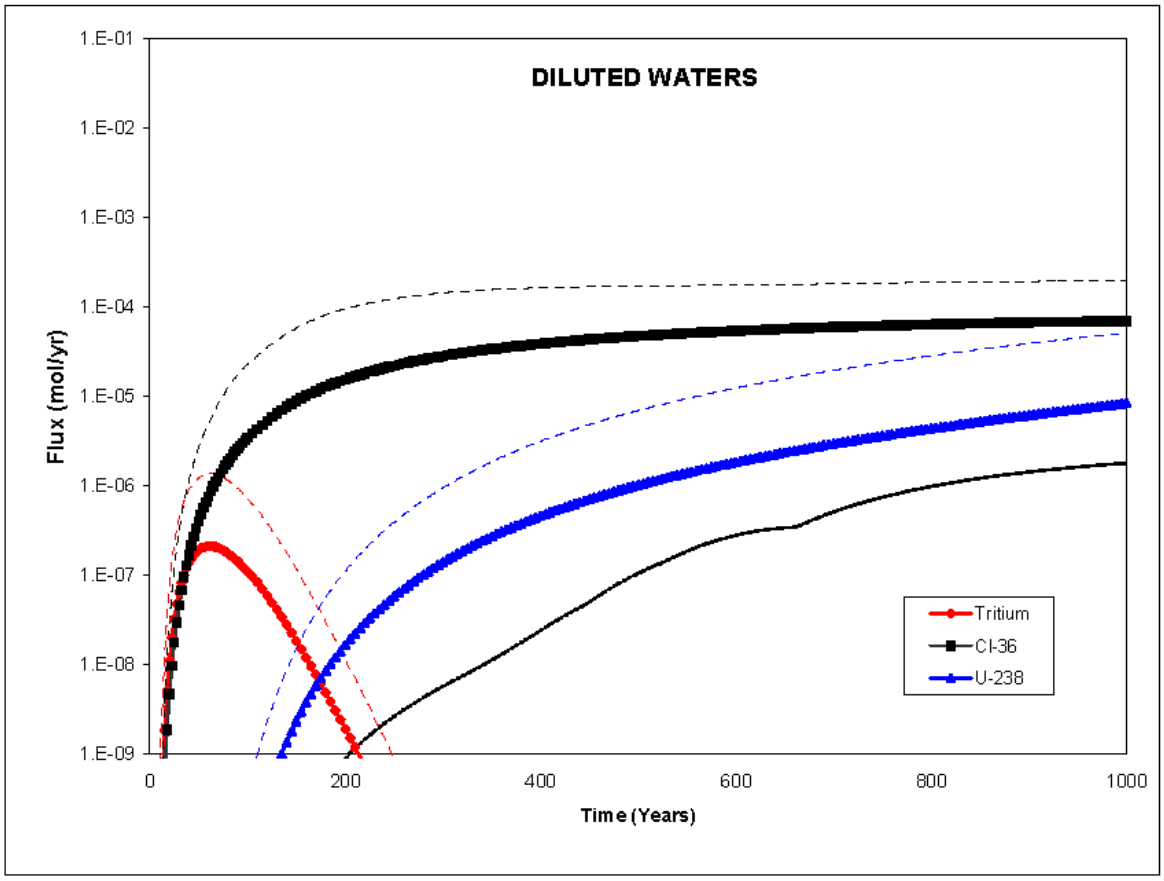

Figure E.1-4
^{3}H, ^{36}Cl, and ^{238}U Exit Mass Fluxes from the SSM for the DILUTED WATERS test. Solid lines represent mean values and dashed lines represent the 5th and 95th percentiles

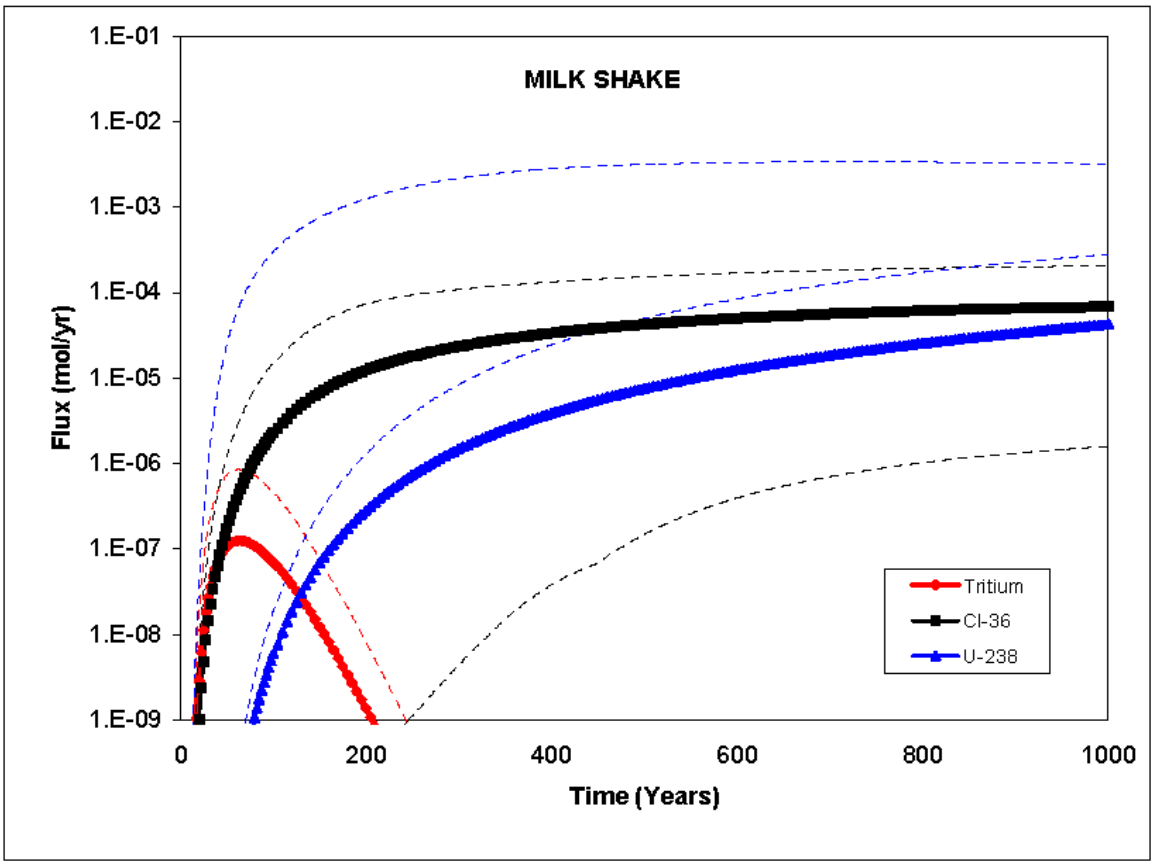

Figure E.1-5
^{3}H, ^{36}Cl, and ^{238}U Exit Mass Fluxes from the SSM for the MILK SHAKE test. Solid lines represent mean values and dashed lines represent the 5th and 95th percentiles

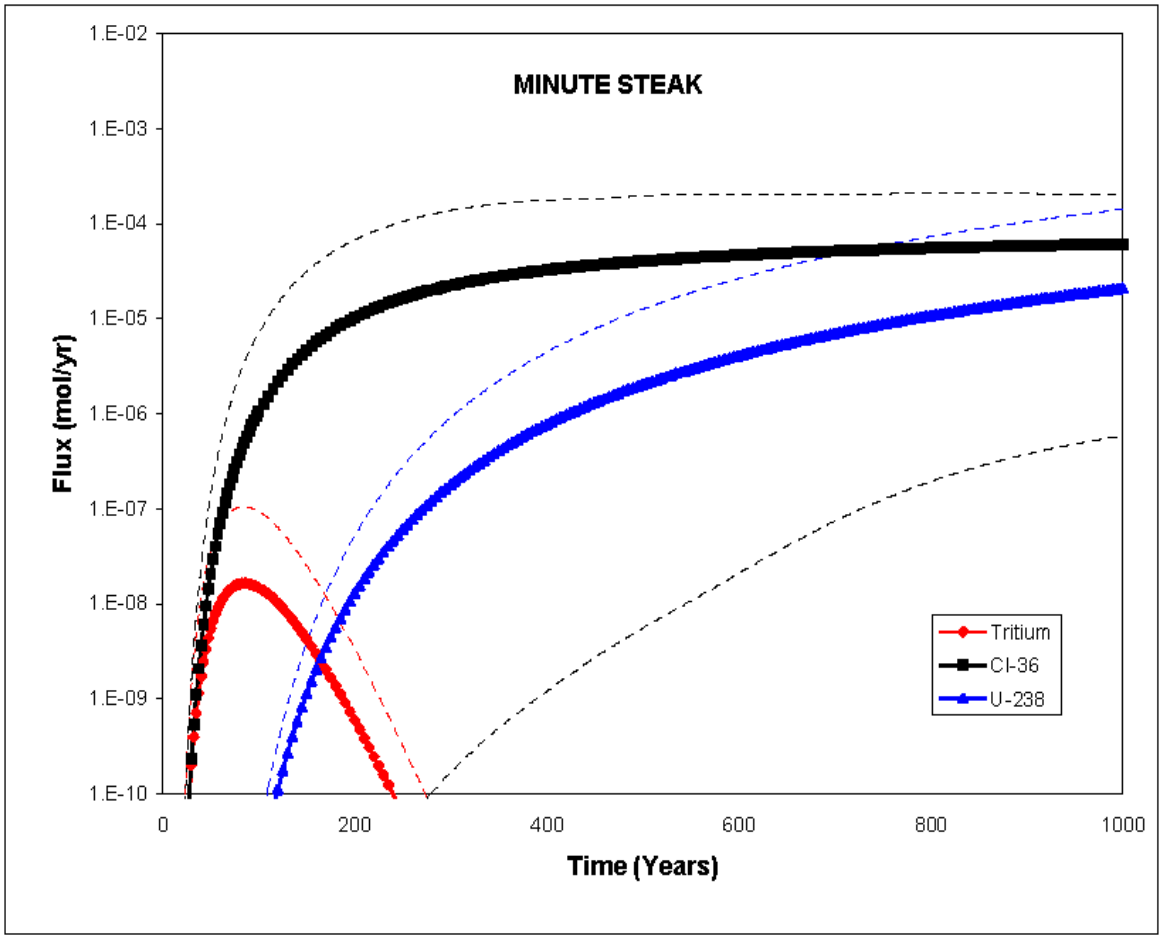

Figure E.1-6
^{3}H, ^{36}Cl, and ^{238}U Exit Mass Fluxes from the SSM for the MINUTE STEAK test. Solid lines represent mean values and dashed lines represent the 5th and 95th percentiles

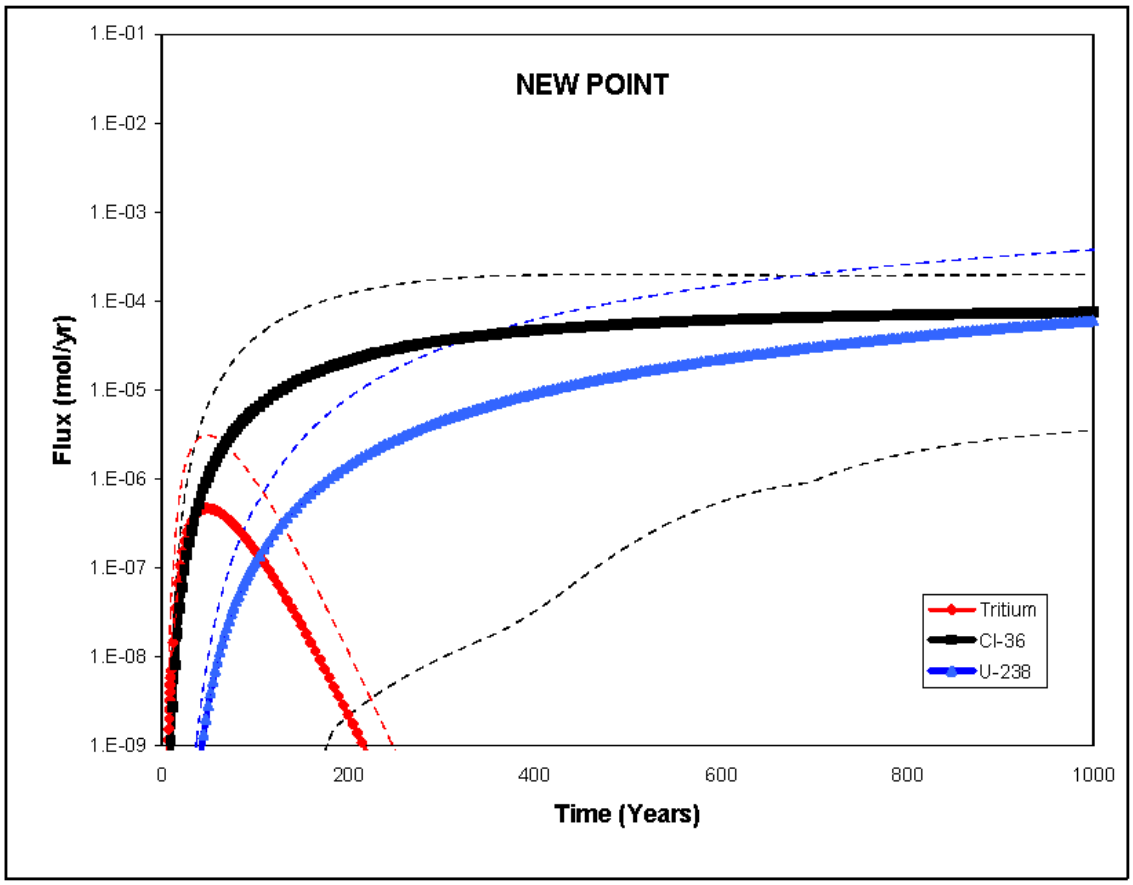

Figure E.1-7
^{3}H, ^{36}Cl, and ^{238}U Exit Mass Fluxes from the SSM for the NEW POINT test. Solid lines represent mean values and dashed lines represent the 5th and 95th percentiles

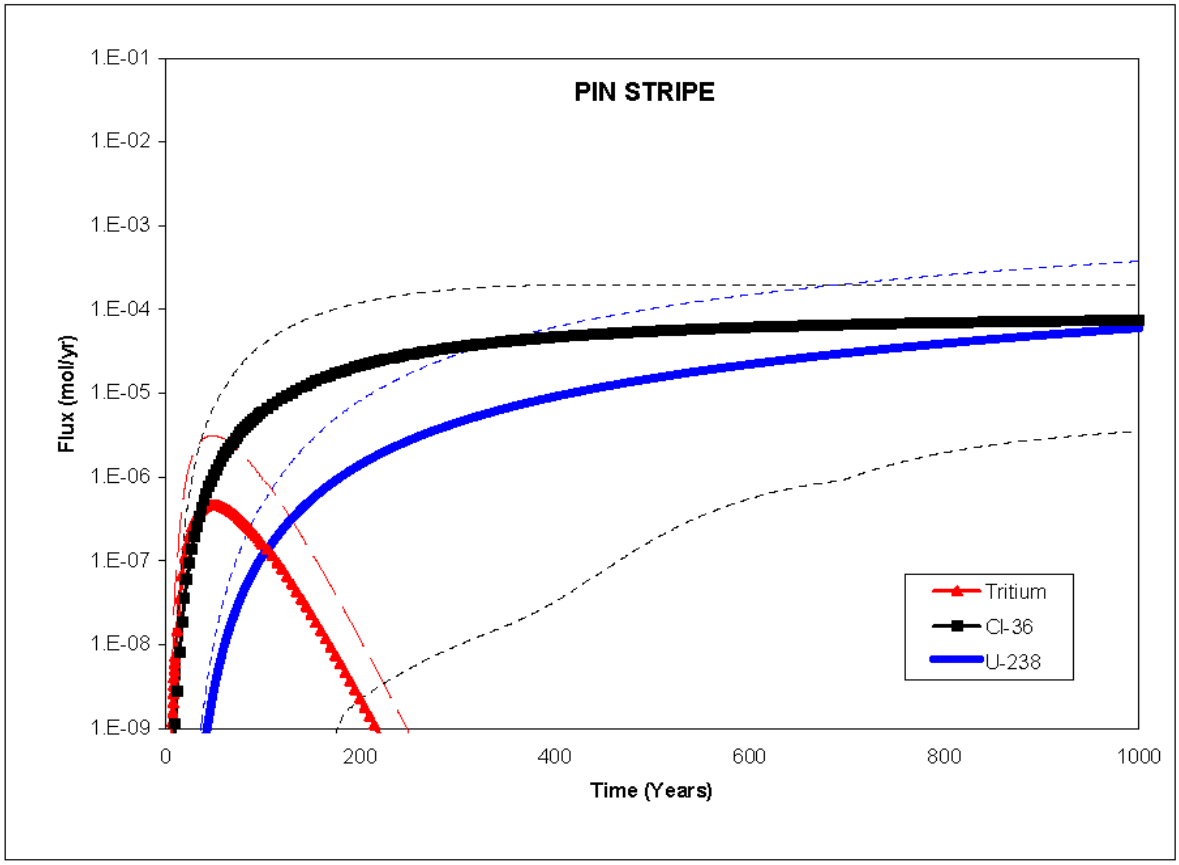

Figure E.1-8
^{3}H, ^{36}Cl, and ^{238}U Exit Mass Fluxes from the SSM for the PIN STRIPE test. Solid lines represent mean values and dashed lines represent the 5th and 95th percentiles

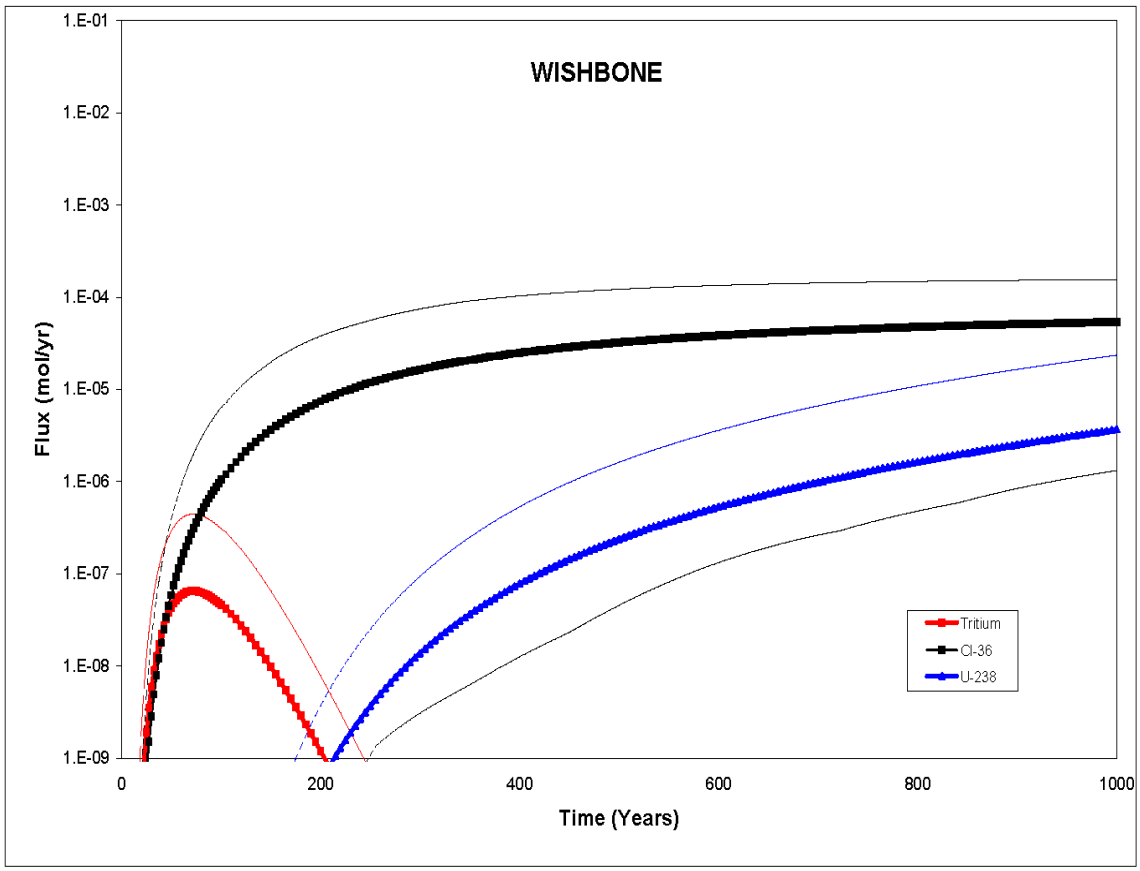

Figure E.1-9
^{3}H, ^{36}Cl, and ^{238}U Exit Mass Fluxes from the SSM for the WISHBONE test. Solid lines represent mean values and dashed lines represent the 5th and 95th percentiles

Appendix F

Electronic Files Containing Mass Fluxes of Thirty-Six Radionuclides for Nine Tests in Frenchman Flat

Electronic Files Containing Mass Fluxes of Thirty-six Radionuclides for Nine Tests in Frenchman Flat

This appendix contains the Excel Files that describe mass flux as a function of time for each of the 36 radionuclides included in the RST for the Frenchman Flat tests. Mass flux distributions for nine tests in Frenchman Flat were generated using the SSMs described in Section 5.0. Each file included in this appendix represents an individual test and each worksheet within the file describes the mass flux for a given radionuclide. For instance, the mass flux values for the DERRINGER test are reported in the spreadsheet, Derringer.xls. The H-3 page within the Derringer.xls file reports the ^{3}H mass fluxes for this test. The following spreadsheets are included in this appendix:

- Derringer.xls
- DiagonalLine.xls
- DianaMoon.xls
- DilutedWaters.xls
- MilkShake.xls
- MinuteSteak.xls
- NewPoint.xls
- PinStripe.xls
- WishBone.xls

Distribution

W.R. Wilborn — 4 Hard Copies and 3 CDs
Environmental Restoration Division
U.S. Department of Energy
National Nuclear Security Administration
Nevada Site Office
P.O. Box 98518, M/S 505
Las Vegas, NV 89193-8518

TIRC — 1 Hard Copy and 1 CD
U.S. Department of Energy
National Nuclear Security Administration
Nevada Site Office
P.O. Box 98518, M/S 505
Las Vegas, NV 89193-8518

J.P. McCord — 1 Hard Copy and 1 CD
Stoller-Navarro Joint Venture
7710 W. Cheyenne Ave. Bldg. 3
Las Vegas, NV 89129

G.J. Ruskauff — 1 Hard Copy and 1 CD
Stoller-Navarro Joint Venture
7710 W. Cheyenne Ave. Bldg. 3
Las Vegas, NV 89129

I.M. Farnham — 1 Hard Copy and 1 CD
Stoller-Navarro Joint Venture
7710 W. Cheyenne Ave. Bldg. 3
Las Vegas, NV 89129

N.M. DeNovio — 1 Hard Copy and 1 CD
Stoller-Navarro Joint Venture
7710 W. Cheyenne Ave. Bldg. 3
Las Vegas, NV 89129

M. Gross — 1 Hard Copy and 1 CD
MG Enterprises
415 Riviera Drive
San Rafael, CA 94901

T.P. Rose — 1 Hard Copy and 1 CD
Lawrence Livermore National Laboratory
P.O. Box 808, L-221
Livermore, CA 94551

Mavrik Zavarin — 1 Hard Copy and 1 CD
Lawrence Livermore National Laboratory
P.O. Box 808, L-221
Livermore, CA 94551

A. Tompson
Lawrence Livermore National Laboratory
P.O. Box 808, L-204
Livermore, CA 94551
1 Hard Copy and 1 CD)

G.A. Pawloski
Lawrence Livermore National Laboratory
P.O. Box 808, L-221
Livermore, CA 94551
1 Hard Copy and 1 CD

D.L. Finnegan
Los Alamos National Laboratory
P.O. Box 1663, M/S J514
Los Alamos, NM 87545
1 Hard Copy and 1 CD

E.M. Kwicklis
Los Alamos National Laboratory
P.O. Box 1663, M/S F665
Los Alamos, NM 87545
1 Hard Copy and 1 CD

B.K. Thompson
U.S. Geological Survey
160 N. Stephanie St.
Henderson, NV 89074
1 Hard Copy and 1 CD

Central Files
Stoller-Navarro Joint Venture
7710 W. Cheyenne Ave. M/S 439
Las Vegas, NV 89129
1 Hard Copy and 1 CD